University of Southampton
Faculty of Engineering, Science & Mathematics
School of Engineering Sciences

Thermal Management of Multifunctional Spacecraft Power Structures

James A Foster MEng ARAeS

Thesis for the degree of Doctor of Philosophy
January 2011

UNIVERSITY OF SOUTHAMPTON

ABSTRACT

FACULTY OF ENGINEERING, SCIENCE & MATHEMATICS

SCHOOL OF ENGINEERING SCIENCES

Doctor of Philosophy

THERMAL MANAGEMENT OF MULTIFUNCTIONAL SPACECRAFT POWER STRUCTURES

by James Abbott Foster

Multifunctional power structures (MFPS) are fully integrated sub-assemblies that perform both structural and power functions for spacecraft. By combining functions across subsystems into single units, mass and volume savings can be achieved. Focusing on battery based MFPS in Earth orbiting spacecraft, the imbedded lithium ion batteries used have strict temperature limits, outside of which efficiency and safety is compromised.

To investigate what constraints these temperature limits would place on the use of MFPS, two applications are proposed; that of a MFPS used as part of a deployed wing solar array and that of a MFPS panel forming a body mounted solar array. Isothermal models were developed and used to show that there exists a range of orbits in which there are no thermal constraints on the use of MFPS.

In order for the thermal control systems found to be applicable to the scenario to be assessed, lumped parameter models of the applications were developed. Using these it was found that for the wing application, solutions exist provided that a proportion of the MFPS saving can be sacrificed. The best performing method was to optimise the emittance of the coatings used. For the body application the smaller MFPS saving reduced the range of the solutions which could be considered viable. It was found that the addition of heaters to prevent overcooling was a viable solution as it required little extra mass.

This thesis concludes by showing how the results of the example numerical models can be used to determine the viable orbits of the whole range of potential MFPS applications and discusses of the quality of the numerical modelling performed.

Contents

Table of Contents . . . iii
List of Figures . . . ix
List of Tables . . . xiv
Nomenclature . . . xvii
Declaration of Authorship . . . xix
Acknowledgements . . . xx

1 Introduction 1
1.1 Multifunctional Power Structures . . . 1
1.2 Benefits of Multifunctional Power Structures . . . 2
1.3 Risks of Multifunctional Power Structures . . . 3
1.4 Objective of Work . . . 3
1.5 Thesis Summary . . . 4

2 Literature Review 7
2.1 Current Multifunctional Power Structures . . . 7
2.1.1 Structural Battery Cells . . . 7
2.1.2 Batteries on Structures . . . 9
2.1.3 Commercial Off the Shelf Assemblies . . . 11
2.2 Technical Issues of Multifunctional Power Structure Use . . . 12
2.3 Thermal Control Relating to Multifunctional Structures . . . 13
2.3.1 Multifunctional Thermal Structures . . . 13
2.3.2 Thermal Control of Multifunctional Structures . . . 13
2.4 Conclusions of Literature Review . . . 14

3 Thermal Environment 15
3.1 The Sun . . . 15
3.2 Earth Albedo . . . 16
3.3 Earth Infrared Radiation . . . 19

3.4 Free Molecular Heating . . . 20
3.5 Internal Heat Output . . . 20
3.5.1 Battery Cell Heat Output . . . 20
3.6 Dark Space . . . 21
3.7 Heat Emission . . . 21
3.8 Summary of the Environment . . . 21

4 The COTS MFPS 23
4.1 Spacecraft Orientation . . . 23
4.1.1 Earth Inputs of the Body Mounted System . . . 24
4.2 The Panel Components . . . 25
4.3 Material Thermal Properties . . . 27
4.4 Wing Mounting . . . 28
4.5 Body Mounting . . . 28
4.6 Number of Battery Cells . . . 30
4.7 Multifunctional Saving . . . 32

5 Isothermal Model 33
5.1 Model Definition . . . 33
5.1.1 Equilibrium Method . . . 33
5.1.2 Transient Response Method . . . 34
5.1.3 Model Assumptions . . . 34
5.1.4 Orbits Considered . . . 35
5.2 Wing Mounting Results . . . 35
5.2.1 Equilibrium Results . . . 35
5.2.2 Transient Results . . . 38
5.3 Body Mounted Results . . . 40
5.3.1 Equilibrium Results . . . 41
5.3.2 Transient Results . . . 43
5.3.3 Variations of the Body Mounting . . . 44
5.4 Recommendations from the Isothermal Model . . . 44

6 Lumped Parameter Model 47
6.1 ThermXL . . . 47
6.1.1 Global Assumptions . . . 48

6.2 Wing Mounting Model . . . 49
6.2.1 Steady State Results . . . 50
6.2.2 Transient Results . . . 51
6.3 Body Mounting Model . . . 55
6.3.1 Steady State Results . . . 56
6.3.2 Transient Results . . . 57
6.3.3 Body Mounted Variations . . . 61
6.4 Summary of Lumped Parameter Model . . . 62

7 Review of Thermal Control 63
7.1 Thermal Control Requirements . . . 63
7.2 Thermal Control Technologies . . . 65
7.2.1 Optical Properties . . . 65
7.2.1.1 Coatings . . . 65
7.2.1.2 Louvres . . . 66
7.2.1.3 Multi-Layer Insulation . . . 66
7.2.2 Conduction Modifiers . . . 67
7.2.2.1 Thermal Links . . . 67
7.2.2.2 Insulation . . . 68
7.2.2.3 Thermal Switches . . . 68
7.2.2.4 Heat Pipes . . . 69
7.2.3 Phase Change Materials . . . 69
7.2.4 Active Systems . . . 70
7.2.4.1 Heaters . . . 71
7.2.4.2 Thermoelectric Heat Pump . . . 71
7.2.4.3 Pumped Fluid Loops . . . 71
7.3 Thermal Control Technologies Summary . . . 71

8 Thermal Control of the Wing Mounted Array 73
8.1 Optical Properties . . . 73
8.1.1 Coatings . . . 73
8.1.1.1 Emittance . . . 73
8.1.1.2 Absorptance . . . 76
8.1.1.3 Coating Viability . . . 76

8.1.2 Louvres . . . 77
8.2 Insulation . . . 81
8.3 Thermal Switches . . . 85
8.4 Heaters . . . 85
8.5 Phase Change Materials . . . 87
8.5.1 Viability of Phase Change Material Use . . . 91
8.6 Summary of Viability for Wing Mounted Panel . . . 97

9 Thermal Control of the Body Mounted Panels 99
9.1 Coatings . . . 99
9.2 Louvres . . . 100
9.3 Insulation . . . 102
9.4 Thermal Switches . . . 105
9.5 Thermal Links . . . 105
9.5.1 Defining Linear Conductance Requirement . . . 105
9.5.2 Linear Conductance Requirement . . . 109
9.5.3 Viability of Thermal Links . . . 111
9.6 Phase Change Materials . . . 113
9.7 Heaters . . . 114
9.8 Summary of Viability for Body Mounted Panel . . . 114
9.9 Effect of Configuration Variations . . . 115

10 Discussion 117
10.1 Effect of Battery Cell Thermal Envelope . . . 117
10.2 Effect of the Application Design . . . 120
10.2.1 Estimated Values . . . 120
10.2.2 Design Values . . . 121
10.3 Assessment of Model Assumptions and Methods . . . 125
10.3.1 Assumptions and Simplifications . . . 125
10.3.2 Numerical Methods . . . 127

11 Conclusion 129
11.1 Contribution to Viability by the Orbit . . . 130
11.2 Contribution to Viability by the MFPS Design . . . 131
11.3 Orbit Viability . . . 133

11.4 Case Studies . . . 135
11.5 Summary . . . 139
11.6 Further Work . . . 140

A Publications 141
A.1 Conferences . . . 141
A.2 Journals . . . 141

B Variations of the Body Mounting 143
B.1 Isothermal Model of the Variations . . . 143
B.1.1 Three Panel Variation . . . 143
B.1.2 Sun Pointing Variation . . . 144
B.1.3 Space Pointing Variation . . . 144
B.2 Lumped Parameter Modelling of the Variations . . . 148
B.2.1 Earth Pointing with Three Panels . . . 148
B.2.2 Sun Pointing . . . 150
B.2.3 Space Pointing . . . 152
B.3 Thermal Control of the Variations . . . 155
B.3.1 Three Panel Earth Pointing . . . 155
B.3.1.1 Optics . . . 155
B.3.1.2 Insulation . . . 156
B.3.1.3 Thermal Links . . . 157
B.3.1.4 Phase Change Material . . . 157
B.3.1.5 Heaters . . . 158
B.3.2 Sun Pointing . . . 158
B.3.2.1 Optics . . . 158
B.3.2.2 Insulation . . . 159
B.3.2.3 Thermal Links . . . 159
B.3.2.4 Phase Change Material . . . 160
B.3.2.5 Heaters . . . 161
B.3.3 Space Pointing . . . 161
B.3.3.1 Optics . . . 161
B.3.3.2 Insulation . . . 162
B.3.3.3 Thermal Links . . . 162

B.3.3.4 Phase Change Material 163
B.3.3.5 Heaters 164

C Validation of Modelling 165
C.1 Confidence in Accuracy of Software 165
C.1.1 Modelling Techniques 166
C.1.1.1 Isothermal Model 166
C.1.1.2 Lumped Parameter Model 167
C.1.1.3 Finite Element Model - Patran/Nastran 167
C.1.2 Results 167
C.1.3 Conclusion 169
C.2 Transition Range of Phase Change Material 169
C.3 Comparison of Conduction and Radiation 172
C.4 Cell Heat Output 172

D Material Properties 175
D.1 CFRP Facesheet 175
D.2 Battery Cell 176
D.3 Honeycomb Core 177

References 178

List of Figures

1.1 System level mass saving of MFPS 2

3.1 The modelling reference frame 15
3.2 The definition of the Earth's shadow. 16
3.3 Albedo models 17
3.4 Energy predicted by albedo models at 200 km altitude 18
3.5 Energy predicted by albedo models at GEO altitude 19
3.6 Heat inputs in the hot environment. 22
3.7 Heat inputs in the cold environment. 22

4.1 MFPS application orientations. 25
4.2 Details of the proposed applications. 27
4.3 Connector for the body mounting. 29
4.4 The body mounting 30

5.1 Hot environment wing mounting equilibrium temperatures . . 36
5.2 Cold environment wing mounting equilibrium temperatures . 37
5.3 The transient response of the wing mounting. 38
5.4 Maximum temperature of the wing mounting with altitude . . 40
5.5 Hot body mounting equilibrium temperatures 42
5.6 Cold body mounting equilibrium temperatures 42
5.7 Transient response of the Earth pointing body mounting. . . . 43

6.1 Finite difference model of the wing mounted panel 49
6.2 Diagram of the arrangement of the cells in the panel. 50
6.3 Lumped parameter transient results of the wing panel in a hot LEO case. 53
6.4 Lumped parameter transient results of the wing panel in a cold LEO case. 53

6.5 Lumped parameter transient results of the wing panel in a hot GEO case. 54
6.6 Lumped parameter transient results of the wing panel in a cold GEO case. 54
6.7 Finite difference model of the body mounting 55
6.8 Lumped parameter transient results of the Earth pointing body mounting in a hot LEO case. 58
6.9 Lumped parameter transient results of the Earth pointing body mounting in a cold LEO case. 59
6.10 Lumped parameter transient results of the Earth pointing body mounting in a hot GEO case. 59
6.11 Lumped parameter transient results of the Earth pointing body mounting in a cold GEO case. 60

8.1 Emittance of the wing model effecting battery temperature in 200 km LEO 74
8.2 Emittance of the wing model effecting battery temperature in GEO 75
8.3 Absorptance of the wing model effecting battery temperature in 200 km LEO 76
8.4 The effect of switching temperature on louvre performance in a hot LEO. 77
8.5 The effect of switching temperature on louvre performance in a cold LEO. 78
8.6 Envelope of the theoretical louvre solution. 79
8.7 Effect of switch temperature on louvre performance for a switch between 0.25 and 0.66. 80
8.8 Effect of switch temperature on louvre performance for a switch between 0.04 and 0.94. 80
8.9 Wing insulation in a cold 200 km LEO 81
8.10 Wing insulation in a hot 200 km LEO 82
8.11 Wing insulation in a cold GEO 82
8.12 Wing insulation in a hot GEO 83
8.13 Illustration of PCM freezing options 88

8.14 Pause energy vs PCM transition temperature in 200 km LEO 89
8.15 Pause energy vs PCM transition temperature in GEO 90
8.16 The time taken to freeze a selection of PCMs. 92

9.1 The effect of a louvre on the body mounting Earth pointing system in a hot LEO case. 101
9.2 The effect of a louvre on the body mounting Earth pointing system in a hot GEO case. 101
9.3 Effect of insulating the Earth pointing system in a 200 km cold LEO. 102
9.4 Effect of insulating the Earth pointing system in a 200 km hot LEO. 103
9.5 Effect of insulating the Earth pointing system in a cold GEO. 103
9.6 Effect of insulating the Earth pointing system in a hot GEO. 104
9.7 Effect of increasing emittance on the insulated Earth pointing system in a 200 km hot LEO. 105
9.8 The effect of varying linear conductance on the body mounted panels in a hot 200 km LEO. 108
9.9 Minimum and maximum temperatures for ten orbits in hot 200 km LEO. 108
9.10 Illustration of the minimum linear conductance determination.109
9.11 Variation of required linear conductance to prevent overcooling with altitude in the cold environment. 110
9.12 Variation of required linear conductance to prevent overcooling with altitude in the hot environment. 110
9.13 An example of a thermal strap 111

11.1 Battery temperature of the MFPS panel in a Molniya orbit. . 136
11.2 Battery temperature of the MFPS panel in an ISS orbit. . . . 137
11.3 Battery temperature of the MFPS panel in a Galileo GPS orbit.138
11.4 Battery temperature of the MFPS panel in a Dawn-Dusk orbit.139

B.1 Equilibrium temperatures of the three panel variation. 144
B.2 Transient temperatures of the three panel variation. 145
B.3 Equilibrium temperatures of the Sun pointing variation. 145

B.4 Transient temperatures of the Sun pointing variation. 146
B.5 Equilibrium temperatures of the space pointing variation. . . . 146
B.6 Transient temperatures of the space pointing variation. 147
B.7 Lumped parameter transient results of the three panel body mounting in a hot 200 km LEO case. 148
B.8 Lumped parameter transient results of the three panel body mounting in a cold 200 km LEO case. 149
B.9 Lumped parameter transient results of the three panel body mounting in a hot 3200 km LEO case. 149
B.10 Lumped parameter transient results of the three panel body mounting in a cold 3200 km LEO case. 150
B.11 Lumped parameter transient results of the Sun pointing body mounting in a hot 200 km LEO case. 151
B.12 Lumped parameter transient results of the Sun pointing body mounting in a cold 200 km LEO case. 151
B.13 Lumped parameter transient results of the Sun pointing body mounting in a hot GEO case. 152
B.14 Lumped parameter transient results of the Sun pointing body mounting in a cold GEO case. 152
B.15 Lumped parameter transient results of the space pointing body mounting in a hot 200 km LEO case. 153
B.16 Lumped parameter transient results of the space pointing body mounting in a cold 200 km LEO case. 154
B.17 Lumped parameter transient results of the space pointing body mounting in a hot GEO case. 154
B.18 Lumped parameter transient results of the space pointing body mounting in a cold GEO case. 155
B.19 The effect of using an aerogel core on the three panel Earth pointing body mounting. 156
B.20 The effect of using an aerogel core on the Sun pointing body mounting. 159
B.21 The effect of PCM use on the Sun pointing body mounting in LEO. 161

B.22 The variation of temperatures with emittance in the space pointing orientation. 162
B.23 The effect of using an aerogel core on the space pointing body mounting. 163

C.1 The validation model. 165
C.2 Patran finite element model. 167
C.3 Transient results of isothermal model validation. 168
C.4 Transient results of lumped parameter model validation. . . . 168
C.5 Transient results of finite element model validation. 169
C.6 An example of varying heat capacity during PCM transition . 170
C.7 Possible models of heat capacity distribution of a PCM. 170
C.8 Temperature profiles in eclipse caused by the heat capacity distribution models. 171

List of Tables

3.1 Summary of the environment limits. 21

4.1 The properties of the sample panel. 26
4.2 Temperature limits of the Varta PoLiFlex cell. 27
4.3 Thermal properties of the materials used 28
4.4 Properties of the wing version of the MFPS panel. 28
4.5 Properties of the body mounted version of the MFPS panel. . 29
4.6 Composition of the spacecraft with body mounted panels. . . 30

5.1 Overcooling of wing mounted panel. 39

6.1 Equilibrium results of the finite difference model of the wing . 51
6.2 Comparison of predicted equilibrium temperatures of the wing 52
6.3 Equilibrium results of the lumped parameter model of the Earth pointing body in LEO 57
6.4 Equilibrium results of the lumped parameter model of the Earth pointing body in GEO 58
6.5 Maximum and minimum temperatures encountered in the transient lumped parameter model. 62

7.1 Summary of potential thermal control applications. 72

8.1 The minimum and maximum values of emittance to prevent overheating and overcooling. 75
8.2 Times to overcool for emittance to prevent overheating. 75
8.3 Variation of battery temperature with core conductivity for a cold 200 km LEO. 84
8.4 Variation of battery temperature with core conductivity for a cold GEO orbit. 84
8.5 Times to overcool for aerogel core. 85

8.6 Heater power required to maintain battery temperature during eclipse for the wing mounting. 86
8.7 Effect of increasing the temperature below which the heater activates. 87
8.8 The mass of phase change material required for the worst case orbits, part 1. 95
8.9 The mass of phase change material required for the worst case orbits, part 2. 96
8.10 The efficiency of each thermal control system 98
8.11 The maximum eclipse time in seconds each TCS can make safe. 98

9.1 The minimum and maximum emittances of the spacecraft. . . 99
9.2 Effect of altering the body to panel connector material 112
9.3 Effect of altering the body to panel connector area 113
9.4 Mass of PCM required to maintain battery temperature in the Earth pointing body mounting. 114

10.1 Effect of the stricter battery thermal envelope on coating emittance requirement. 118
10.2 Effect of stricter battery thermal envelope on the time to overcool offered by insulation. 119
10.3 Effect of stricter battery thermal envelope on the required linear conductance. Baseline values are in parentheses. 120
10.4 The effect of errors in the estimated properties 121
10.5 Effect of altering the MFPS design on the wing mounted panel in a hot 200 km LEO 122
10.6 Effect of altering the MFPS design on the body mounted panel in a hot 200 km LEO 123

11.1 The orbital elements of orbits used in the case study 135

B.1 Emittance values for the three panel body mounting. 156
B.2 Minimum linear conductance for the three panelled Earth pointing orientation. 157

B.3 Mass of PCM required to maintain battery temperature in the three panel Earth pointing body mounting. 158
B.4 Minimum linear conductance for the Sun pointing orientation. 160
B.5 Minimum linear conductance for the space pointing orientation. 163

C.1 Equilibrium temperatures tended to by the cell 173

D.1 The properties of the components of a lithium polymer cell. . 176

Nomenclature

Acronyms

- CFRP - Carbon Fibre Reinforced Polymer
- CIGS - Copper-Indium-Gallium Selenium
- COTS - Commercial off the Shelf
- FIPP - Flexible Integrated Power Pack
- GEO - Geosynchronous Earth Orbit
- LEO - Low Earth Orbit
- LP - Lumped Parameter
- MAV - Micro Air Vehicle
- MEMS - Micro-Electro-Mechanical Systems
- MFPS - Multifunctional Power Structures
- MFS - Multifunctional Structures
- MFTS - Multifunctional Thermal Structure
- MLI - Multi-Layer Insulation
- NASA - National Aeronautics and Space Administration
- NiCd - Nickel Cadmium
- NiMH - Nickel Metal Hydride
- PCM - Phase Change Material
- PEG - Poly(Ethylene Glycol)
- PVDF - Poly(Vinylindene Fluoride)
- SER - Specific Energy Requirement
- SMA - Shape Memory Alloy
- TCS - Thermal Control System

Symbols

- α - Absorptance
- α_{η} - Solar cell effective absorptance
- α_{kt} - Absorptance of kapton tape
- α_{sc} - Solar cell absorptance
- α_{wp} - Absorptance of wing coating
- ΔT - Temperature difference
- ϵ - Emittance
- ϵ_{bp} - Emittance of black paint
- ϵ_{kt} - Emittance of kapton tape
- ϵ_{MLI} - Emittance of MLI
- ϵ_{sc} - Solar cell emittance
- ϵ_{wp} - Emittance of wing coating
- η_{sc} - Solar cell efficiency
- η_T - Solar cell temperature co-efficient
- ρ_k - Density of conductor
- ν - Frequency
- σ - Stefan-Boltzmann constant
- τ - Time constant
- $_{Eab}$ - Subscript denoting the Earth albedo
- $_{Eir}$ - Subscript denoting the Earth heat radiation
- $_{rad}$ - Subscript denoting heat emission

- $_{sun}$ - Subscript denoting the Sun
- A_B - Surface area of battery cell
- A_b - Area of body panel
- A_s - Surface area
- A_w - Area of wing panel
- A_x - Cross sectional area of conductor
- a - Major axis of fibre cross section
- b - Minor axis of fibre cross section
- C - Specific heat capacity
- F - View factor
- F_p - Perpendicular view factor
- G_l - Linear conductance
- H - Heat capacity
- H_b - Heat capacity of body panel
- H_{pcm} - Heat capacity of a PCM
- H_w - Heat capacity of wing panel
- h - Orbit Radius
- h_{air} - Convection co-efficient
- k - Thermal conduction
- k_f - Thermal conductivity of fibre
- k_l - Thermal conductivity longitudinal
- k_m - Thermal conductivity of matrix
- k_t - Thermal conductivity transverse
- M - Mass
- M_B - Mass of Battery
- M_b - Mass of body panel
- M_s - Mass of spacecraft
- M_w - Mass of wing panel
- P - Power per unit area from source
- P_ρ - Power density of battery
- Q - Power flux
- Q_B - heat output of a single cell
- Q_p - Power per unit area on a surface perpendicular to the Earth
- Q_r - Radiation heat flow
- R - Power per unit area emitted by a surface
- r - Reference radius
- T - Temperature
- T_B - Battery cell temperature
- T_{air} - Air temperature
- T_{eq} - Equilibrium temperature
- t - Time
- V_f - Volume fraction of fibre
- X - Cartesian co-ordinate
- x_c - Core thickness
- x_f - Facesheet thickness
- x_k - Length of conductor
- x_{ply} - Ply thickness
- X_B, Y_B, Z_B - Size of Battery Cell
- X_s, Y_s, Z_s - Size of spacecraft
- Y - Cartesian co-ordinate
- Z - Cartesian co-ordinate

Declaration of Authorship

I, **James Abbott Foster** declare that the thesis entitled **Thermal Management of Multifunctional Spacecraft Power Structures** and the work presented in the thesis are both my own, and have been generated by me as the result of my own original research. I confirm that:

- this work was done wholly or mainly while in candidature for a research degree at this University;
- where any part of this thesis has previously been submitted for a degree or any other qualification at this University or any other institution, this has been clearly stated;
- where I have consulted the published work of others, this is always clearly attributed;
- where I have quoted from the work of others, the source is always given. With the exception of such quotations, this thesis is entirely my own work;
- I have acknowledged all main sources of help;
- where the thesis is based on work done by myself or jointly with others, I have made clear exactly what was done by others and what I have contributed myself;
- parts of this work have been published as detailed in Appendix A.

Signed:.....

Date:.....

"There is something fascinating about science. One gets such wholesale returns of conjecture out of such a trifling investment of fact."

Mark Twain

Acknowledgements

This thesis of 44134 words on 204 pages would not have been successfully completed without the welcome support of family, friends and academic staff. Thank you to you all.

Chapter 1

Introduction

Mass and volume are key factors in determining the viability of a spacecraft's mission, as they directly affect the cost of the spacecraft, particularly the cost of launch [1]. Multifunctional structures (MFS) are a technology for improving the efficiency of spacecraft, by reducing mass and volume. A structure is multifunctional when it performs spacecraft functions in addition to its structural functions. This is a removal of discrete components that have singular purpose in favour of amalgamated components with multiple purposes. This allows the functionality of the spacecraft to be optimised by reducing structural redundancies in the design. This primarily takes the form of reduced mass. Multifunctional structures have been identified as a key technology for the development of spacecraft technology by Das and Obal [2], Sercel et al. [3], Moore [4], Rossoni and Panetta [5] and this thesis focuses on enabling this technology through assessment of the technical issues of its use.

1.1 Multifunctional Power Structures

A Multifunctional Power Structure (MFPS) is a multifunctional structure that incorporates functions associated with the Electrical Power System, namely the generation, storage and control of electrical power. Typically, this will involve solar cells, batteries and a power control and distribution unit. At about 20 % of the total spacecraft mass [6] the electrical power system makes up a substantial part of the spacecraft. Reducing the mass of this subsystem would clearly benefit the spacecraft.

1.2 Benefits of Multifunctional Power Structures

Roberts and Aglietti [7] have developed a detailed method for calculating the system level mass savings that can be achieved from using a MFPS based on power storage. The amount of mass that can be saved is developed in terms of the Specific Energy Requirement (SER) of the spacecraft; the total energy storage required (in terms of the battery capacity in Watt-Hours) by the spacecraft divided by the total mass (in kg) of the spacecraft. Figure 1.1 shows the savings achieved when two of the benefits of using MFPS are considered; the removal of parasitic mass and a reduction in the spacecraft bus volume (described below). A smaller mass saving is possible in the situation where the battery directly replaces part of the structure as the structural mass removed can then be counted towards the mass saving of the MFPS.

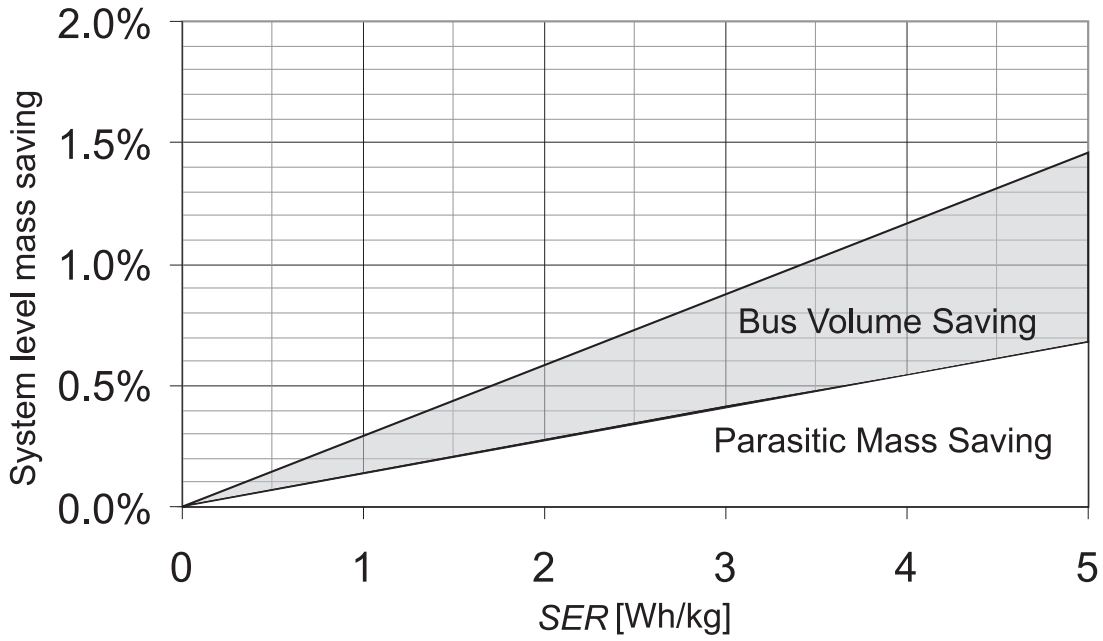

Figure 1.1: *The system level mass saving achievable through the use of a MFPS [7]. SER is the Specific Energy Requirement of the spacecraft (Whr/kg).*

The traditional method of including a battery on a spacecraft involves the use of extra structures to mount the battery in the spacecraft. Many battery cells are used to meet the capacity and voltage requirements and these cells require a casing to hold them together. This casing then needs to be mounted to the structure. The casing and the mounting are termed parasitic as they add no functionality to the spacecraft directly. By adding power storage capability to the structure itself these parasitic structures are no longer required: a mass saving.

For the battery to be inside the spacecraft bus, the bus has to have sufficient internal

volume. With power storage now a function within the structure, the space in the bus is no longer required. Thus the spacecraft can be made smaller which has benefits. A smaller spacecraft is not only a lower mass spacecraft, it will also now fit a wider range of launchers, though such a drastic effect is unlikely.

Multifunctional structures present an advance over traditional lightweighting methods. As described by Jackson and Epstein [8] the process of repackaging components will not eliminate cases and mountings, only make them lighter. A similar argument applies to solely using improved battery chemistry to reduce battery mass, as while the smaller battery has less parasitic structure, it still has a parasitic mass associated with it.

1.3 Risks of Multifunctional Power Structures

The overall risk of using MFPS is that of increased costs associated with design and complexity, Roberts and Aglietti [7]. By its definition it involves a multi-subsystem approach that will require extensive co-operation between design teams during the development of the spacecraft. Failures in communication will result in a slower design process and mistakes will have a wider impact as more systems will be effected. The use of concurrent design, as outlined by Bandecchi et al. [9] should be effectively used to minimise this. Coupled with this is the increased complexity of the design of combining the functions which slows the design process.

An important risk associated with MFPS is that of component failure. As the component now has multiple functions there is more that can potentially go wrong with it. This issue is compounded by the difficultly in repairing any faults found while the spacecraft is tested as the embedding of the power storage function into the structure will make it more efficient to manufacture a new part than to try to prise the MFPS apart to replace the faulty power storage.

1.4 Objective of Work

Work by Roberts and Aglietti [7] has assessed the mechanical issues and Wang et al. [10], Choquette and Lessard-Deziel [11] have shown that the radiation environment is not a threat. The greatest remaining technical issue is that of thermal control. Thus the objective of this work is to assess how the potential need for thermal control affects the

use of MFPS on modern spacecraft. The pursuit of this objective has led to the following contributions to the state of the art:

- That an exploration of the concept space has revealed that there exists a great many orbits for which the unaltered properties of the MFPS are sufficient as the equilibrium temperatures of the MFPS are always within the temperature envelope of the battery. These orbits are defined by how the MFPS exchanges heat with its environment.
- That further to this, a range of orbits is determined for which the battery temperatures remain safe, despite the equilibrium temperatures not being so. These orbits are defined by the thermal inertia of the MFPS.
- That the range of orbits can be extended by the use of simple thermal control systems. The limits of this range are defined by the viability of the thermal control systems, as defined by the feasibility and mass of the system.
- And that there exists a range of orbits in which the MFPS as defined cannot be used as there are no viable thermal control solutions. These orbits show how the thermal control need limits MFPS use.

1.5 Thesis Summary

Chapter 2 contains a literature review of current MFPS technologies. This starts with a general review of the different approaches to MFPS. From this the concept of a commercial off the shelf MFPS is explored. The knowledge gap in the state of the art that this work intends to fill is identified here: the thermal control of MFPS. Chapter 3 details the thermal environment that an MFPS will encounter in Earth orbit. The MFPS applications that are looked at are defined as being a deployed wing array panel and a panel mounted to the spacecraft body. Chapter 4 is the design specification of a MFPS that has been developed for the purpose of numerical modelling. The design is used as an example of MFPS and conclusions can be drawn for the wider technological scope.

Chapter 5 is the first modelling of the example, in which the MFPS is modelled as a point mass node with a single degree of freedom. From this the orbits where a thermal control solution is needed are determined. Chapter 6 develops a multi-node finite difference model of the MFPS. These models are developed to allow for the modelling of

possible thermal control solutions. This chapter also refines the work of the previous chapter, clarifying in which orbits thermal control is needed.
With the orbits requiring thermal control defined, chapter 7 establishes the requirements a thermal control solution must meet in order to be considered viable. The key requirement is that the mass of the solution is less than the MFPS saving. The chapter also reviews the current state of the art of thermal control and briefly discusses how they may be applied. Chapters 8 and 9 are the analysis of these technologies for the MFPS applications considered. Chapter 10 shows how variation in the design affects the results and evaluates the potential sources of error in the model. Chapter 11 is the conclusion of this thesis and draws conclusions from the results as to the viability of thermal control for MFPS.

Chapter 2

Literature Review

Spacecraft structures have an inherent amount of multifunctionality in that they form part of the thermal control and radiation protection systems. A review of current MFS technology where the extra functionality was a leading part of the structure's design has been carried out by Aglietti et al. [12]. This chapter presents a more specific overview, focusing on the current state of the art of just multifunctional structures for power storage. From this, existing work on the technical issues of MFPS use is reviewed and the focus of the thesis defined.

2.1 Current Multifunctional Power Structures

Battery based MFPS take three forms. While all of these forms enable the benefits of multifunctional structures to be reaped, the methodologies have distinct differences.

2.1.1 Structural Battery Cells

Firstly, there are structural battery cells which are cells that have been designed to carry structural loads. They can be normal cell materials that have been shaped to form part of a structure and/or batteries whose materials have be developed so that they can carry load and store charge. Such batteries can easily be optimised for their roles, but by the same token, the key downfall of this, as noted by Thomas and Qidwai [13], is that such cells would have to be custom made for each and every application. The cost of such custom cells will be very high to support a small market, tooling and hand labour. The use of hand labour raises the issue of quality control, an issue that large scale manufacturing would not face.

A good example of a structural cell is the work by Thomas and Qidwai [13]. Here a polymer lithium ion battery is used as a key structural component in the Wasp Micro Air Vehicle (MAV). The Wasp has a wing span of 32 cm and 98 g of its 171 g is taken up by the battery. The lithium ion cells were specially made by Telcordia Technologies. The Wasp flew successfully for 107 minutes on one charge and Thomas et al. [14] go on to state that when compared to using a battery of the same specific energy in a conventional unifunctional arrangement, the multifunctional structure would have 26% better endurance. The use of MFPS was further explored using the Black Widow MAV where the polystyrene of the structure was replaced with a lithium polymer battery [15]. While demonstrating that the battery could survive being part of a structure, limited conclusions can be drawn from this for the application to spacecraft due to the radically different loading conditions. The batteries used here have limited structural properties.

Qidwai et al. [16] have also looked at the use of lithium polymer bicells to form struts, using an optimisation routine they developed. While able to achieve high energy densities, the mechanical properties of the battery are not sufficient for the strut to be used for high loadings.

Liu et al. [17] have developed a cell that has structural properties. By mixing Poly(Vinylindene Fluoride) (PVDF) with the relevant materials they we able to create composites for each of the cell's parts for a $LiCoO_2$/carbon chemistry. Elastic polymer binders are used to bind the cell chemistry together and carbon fibres can be added to improve the strength further. While this creates a cell with an elastic modulus of 3.1 GPa the cost is that the added structure does not contribute power storage and thus the specific capacity of the cell drops to 35 Whr/kg, comparable to nickel-cadmium (NiCd) batteries.

Snyder et al. [18] of the Army Research Lab have worked on the creation of an electrolyte with both high ionic conductivity and good mechanical properties. Their work focuses on the use of vinyl ester derivatives of Poly(Ethylene Glycol) (PEG) complexed with lithium trifluoromethanesulfonate to form the electrolyte, wherein the PEG transported the salt ions and the cross linked vinyl esters provide the structural properties. The effects of the salt concentration, polymer chemistry and polymer architecture where analysed in an attempt to optimise the chemistry for multifunctional performance. Unfortunately, the study concluded that the structural and electrical properties opposed each other and that the resulting properties were an order of

magnitude lower than wanted.

The work of the Army Research Lab, Wong et al. [19], has continued by looking at creating structural electrodes to create a complete cell. The design utilizes a carbon fibre anode, cathode material cast on a metal substrate, glass fibre separator, and the polymer electrolyte matrix as previously described. The carbon fibre anode consists of either a plain-woven or non-woven layer of carbon fibres with no polymer matrix. The cathode is formed by the active ingredient, $LiFePO_4$, being mixed with acetylene black and PEG which is then solvent cast using acetonitrile onto a porous stainless steel foil. The separator is a 4-harness satin weave glass fibre. The resulting battery suffered badly due to flaws in the manufacturing process of the composite. As such, neither its mechanical nor electrical properties were found to be sufficient.

The implication is that while these approaches are potentially optimal, as one component performs both functions, the technology is not mature enough for a single component to meet the exacting requirements; the specific energy is too low and/or the mechanical properties are not sufficient.

2.1.2 Batteries on Structures

In this approach the cell chemistry is bonded onto a structural component and the MFPS are characterised either by a component that performs no charge storage or structural function. This option provides better structural performance than just a battery, however it is less efficient as the there is now a clear division of function between parts of the MFPS; separate masses perform the two functions with an overlap as the battery can carry some loading. They suffer from the same custom build problems as structural batteries.

There have been several studies into the attachment of cell chemistry to the core material of a sandwich panel. Marcelli et al. [20] have developed a product they call LiBaCore^{TM}. The product is made up of a thin film lithium chemistry cell that is attached to the ribbons that make up a honeycomb. In this application, the load carried by the battery is minimal as it is a very small proportion of the component. LiBaCore was planned to fly on the MightySat II.2 spacecraft, but the mission was cancelled [21].

The Boundless Corp have developed Powercore^{TM}, Lyman and Feaver [22], which exploits the properties of NiH_2 cell chemistry. By using nickel foam, a laminate can be formed of the cell components that can then be used corrugated and bonded to form a

honeycomb structure. This has an advantage over LiBaCore in that the structural component (the nickel foam) is active in the chemistry of the cell. The foam however has poorer mechanical properties than solid aluminium and the use of stronger nickel alloys is limited by cell chemistry. In an advancement on Powercore, Boundless have developed a lithium polymer bi-cell that they have used to form core structures, Olson et al. [23], by using a pitch based carbon fabric composite to form the anode. This takes advantage of the better properties of the cell chemistry and structural material for improved performance.

Boundless have also carried out a feasibility study of using nickel foam as a substrate for the electrodes of a NiMH, Metzger et al. [24]. For the negative electrode, a slurry consisting of a hydriding alloy mixed with nickel powder was pasted and then sintered onto nickel foam substrates. For the positive electrode, NiOH and CoOH was electrochemically impregnated into the foam by using the Pickett method. These two nickel foam strips are then bonded with a polypropylene separator. The resulting cell could be used as a foam core in bulk or as strips to form a honeycomb. The cell properties are limited by the chemistry and the nickel foam is not as strong as aluminium and the capacity is poor compared to newer cell chemistries.

Considering sandwich panels, another option is to bind the cell within the facesheet. Pereira et al. [25] have looked at the lamination of thin film lithium ion energy cells into carbon fibre reinforced polymer (CFRP). Having determined the limits of flexure and the surface pressure the thin film cell can withstand, the cells are manufactured into the panels and are shown to survive the process. Mechanical testing reveals that the properties of the laminate have not been adversely affected with the cell performing near baseline when subjected to 450 MPa uniaxial loading with a maximum of 50% of the tensile strength of the CFRP.

The idea of blending the cell into the facesheet can also be done at a smaller scale. Neudecker et al. [26] have developed the concept of Power Fibres^{TM}. Thin film lithium ion material is wrapped around individual carbon fibres. These fibres can then be used as normal carbon fibres to create CFRP facesheets. As the cell chemistry is wrapped around each fibre, the surface area of the cell is greatly increased and thus the capacity increased. While this method avoids putting discontinuities into the laminate, the paper does not state what effect the cell layers have on the binding between fibre and matrix nor other mechanical properties.

Such MFPS are effectively parasitic batteries, in that the batteries are attached to an existing structure, exploiting their properties in such as way as to enable the benefits of MFPS. The downfall of this approach is that the amount of capacity available is limited by the available structure to attach it to. They have a poor capacity density and thus for a given volume of structure, they may not be able to fulfill the required capacity and clearly the structure cannot be expanded to include extra capacity.

2.1.3 Commercial Off the Shelf Assemblies

A commercial off the shelf (COTS) assembly is a set of COTS components that are assembled together to form a MFPS. Typically these COTS components are mass manufactured and are of traditional design. This eliminates the cost associated with custom manufacture of the previous types of MFPS. The trade off is that in a COTS assembly the component parts are effectively unifunctional; the battery's contribution to the structure is minimal and the structure stores no charge; thus the MFPS is not optimal in terms of mass.

An example would be the Flexible Integrated Power Pack (FIPP) as presented by Clark et al. [27] that is produced by ITN Energy Systems. It is a MFPS that consists of thin film Copper-Indium-Gallium Selenium (CIGS) photovoltaic cells, flex circuitry and thin film lithium ion cells laminated onto a flexible substrate of titanium foil. The resulting component has the flexibility of 0.05 mm polyimide film or 0.025 mm steel. This commercially available product could easily be mounted to the face of a structure to create a MFPS assembly. However, the CIGS cells have poor efficiency (9%) and thus a large area would be required to meet spacecraft power demands. This area requirement also affects the potential battery capacity as the film is only one cell thick.

A MFPS consisting of more widely available components is proposed by Roberts and Aglietti [7]. Lithium polymer cells are imbedded into the core of a sandwich panel in place of a section of core. This places the battery inside a structure to support it, thus realising the benefits of MFPS in a simple and effective way. While this MFPS is the least optimal solution as functions are carried out by very separate components, it is the least expensive solution and does not involve any immature technology. As such, this concept could fly once the technical issues have been assessed.

2.2 Technical Issues of Multifunctional Power Structure Use

These are defined as issues with the use of MFPS that are required to be solved before they can be used. Taking the structural properties as an example, Schwingshackl et al. [28] have looked at the structural properties of various sandwich panel core geometries that are made up of lithium bi-cells [23] and aluminium corrugations. With numerical modelling and experimental work, Schwingshackl et al. [29] have shown that such a MFPS is structurally sound, resolving the technical issue of can an MFPS be an adequate structure.

For a COTS assembly MFPS, Roberts and Aglietti [30] have subjected a Varta PoLiFlex cell [31] to a variety of experiments. A lithium polymer chemistry was selected as they have a high specific energy, are prismatic (allowing for efficient packing) and are all solid chemistries (they required only sealing). The cell was put through a vibration regime to show that they would survive the launch environment. The cell showed no noticeable change in electrical properties after repeated shaking. The cell was also shown to survive the manufacturing process, though a low curing temperature is required to not adversely effect the battery performance, Roberts and Aglietti [32]. Finally, the shear modulus of the cell was determined by dynamic experiment, Roberts et al. [33]. It was found that while the cells have poor stiffness, it is sufficient that with careful design, the panel will not be structurally compromised. Thus it has been shown that a COTS assembly MFPS can be mechanically sound.

Wang et al. [10] have also tested commercial lithium polymer cells for their use in spacecraft. The cells were subjected to a vacuum and showed no outgassing. The cells were also subjected to γ-ray radiation and vibration testing and showed no noticeable reduction on performance. Choquette and Lessard-Deziel [11] have assessed the lithium polymer cells for the effects of proton and electron radiation and concluded that over the course of a 5 year mission the battery would suffer no significant loss of performance.

As noted above, a lower curing temperature during manufacture is required as the cells have thermal limits. For example the Varta PoLiFlex cell operates between 273 K and 318 K. When too cold, the ionic conductivity of the electrolyte reduces, lowering the output of the cell, Xing and Sugiyama [34]. At temperatures that are too high, the resistance of components increases causing losses. In moderate cases, these effects are

reversible, however, if the temperature of a lithium polymer cell becomes too high, thermal runaway ensues and the cell suffers permanent damage, Mohamedi et al. [35]. With this in mind, it is thus important to determine if a local thermal control solution for the battery in a COTS assembly is required. If the COTS assembly is located in the middle of the spacecraft, then it falls within the remit of the spacecraft's thermal control system (TCS). However, if the COTS assembly is at the extremities of the spacecraft, then it maybe outside the 'reach' of the TCS and the local thermal control requirement has to be assessed. An example is given by Li et al. [36] who have shown that the temperatures of a solar array can go outside the operating temperature envelope of lithium polymer cells.

2.3 Thermal Control Relating to Multifunctional Structures

2.3.1 Multifunctional Thermal Structures

A multifunctional thermal structure (MFTS) is a spacecraft component that in addition to meeting structural requirements, has adaptations that enhance or add new thermal control functions. At the simplest level is the MFTS presented by Marcos et al. [37], John et al. [38] where to improve the flow of heat away from a high energy emitting electronic, high conductivity pitch fibres were mixed into a CFRP laminate structure. To improve heat flow in the sandwich core, Queheillalt et al. [39] have shaped a nickel foam so that the pores can act as a heat pipe when a suitable wicking fluid is introduced. Electron beam directed vapour deposition was used by Queheillalt et al. [40] to deposit copper onto polyurethane foam, creating micro heat pipe paths. Wirtz et al. [41] have created millimetre scale channels in aluminium panels which will be filled with phase change materials to create a heat storing structure. As shown by the examples, MFTS tend to concern themselves with improving either the conductivity or heat storage of the structure so that separate thermal control components are not required.

2.3.2 Thermal Control of Multifunctional Structures

As part of the New Millennium Project, NASA launched the Deep Space 1 spacecraft, Rayman et al. [42]. Part of this mission was a payload to test the feasibility of an

electronic based multifunctional structure, Barnett and Rawal [43], Barnett et al. [44]. The electronics used were of small size and had a small contact area with the structure. As they still outputted heat at rates similar to traditional components, there was a risk of them overheating due to the limited contact conduction. Rawal [45] addressed this by using a high conductivity face sheet, a thermal doubler[2.1] and a high conductivity core fill to dissipate the 14 W/cm^2 produced by the electronics.

2.4 Conclusions of Literature Review

To date, no work has been published on the thermal control of a COTS assembly MFPS. During spacecraft design, work is indeed carried out on the thermal control of the battery, for example Megahed and El-Dib [46], but this is a battery mounted to the spacecraft structure inside the spacecraft, i.e. in the conventional manner. Thermal control of the battery in this situation can take advantage of the surrounding spacecraft to regulate heat flow and provide thermal inertia. It is envisioned that the most efficient interpretation of MFPS would be one where the functions of the electrical power system could be brought together into a single structure that would be faced with solar cells and also contain the control electronics, possibly through the use of thin film circuitry and multi-chip modules, Clark et al. [27]. Such a solar array would either be mounted to the body of the spacecraft or form part of a deployed wing array. In both cases, the COTS assembly MFPS would be at the extremities of the spacecraft.
It is thus important to determine if a thermal control system is required and what authority is needed to maintain a safe battery temperature. This is important as it will determine the mass required to overcome the thermal obstacle for COTS assembly MFPS use. How much this mass outweighs the benefits of using the MFPS concept will determine the viability of COTS assembly use and this forms the core contribution of this work.

[2.1] A spacer between the component and the structure to increase the 'footprint' of the component.

Chapter 3

Thermal Environment

The majority of spacecraft are satellites in Earth orbit. Any COTS MFPS that is used on a satellite will encounter the thermal environment of Earth orbit, an environment that is not specific to the application. This chapter contains the description of this thermal environment. The environment is described in an Earth centred reference frame, as shown in fig. 3.1. No other bodies in the solar system nor stars are considered in the model as their thermal input is negligible.

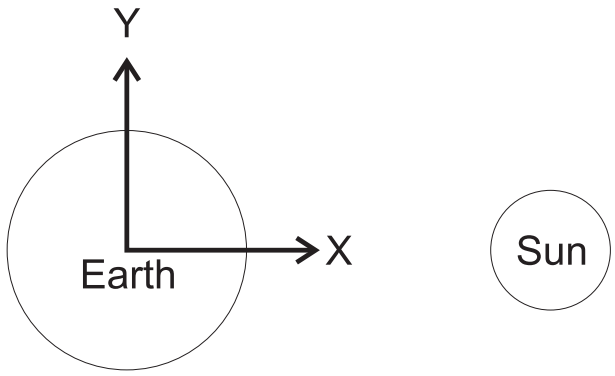

Figure 3.1: *The modelling reference frame, which is Earth centric. X is defined as pointing towards the Sun, Z as along the Earth's direction of travel and Y as upwards from the plane of the ecliptic.*

3.1 The Sun

The Sun could be modelled as a constant 1367 W/m^2 with no variation over the course of the spacecraft orbit as the effect of moving up to 35786 km closer to or further from the Sun is negligible. However, the orbit of the Earth is elliptical and thus the power does vary. The Sun is thus modelled as the extremes of input; 1414 W/m^2 and 1322

W/m^2. The Sun's input is considered to be parallel to the Earth-Sun vector for the calculation of angles of incidence. The shadow cast by the Earth is modelled as a cylinder with a radius equal to that of the Earth, as illustrated in fig. 3.2.

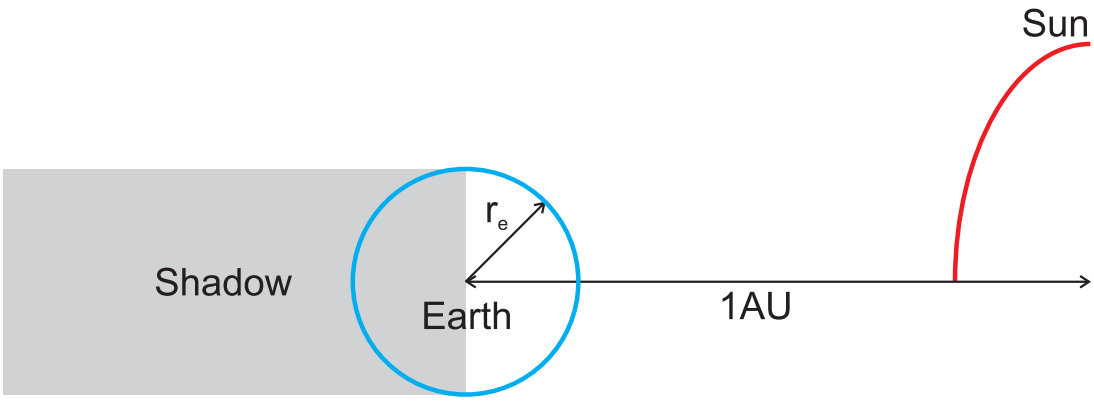

Figure 3.2: *The definition of the Earth's shadow. The radius of the Earth (r_e) used is the mean radius 6371 km.*

3.2 Earth Albedo

Of the models available to represent the reflection of the Sun's light by the Earth, three were considered. All three models use an inverse square law to propagate the reflected power to the spacecraft's orbit. The first model, selected for its simplicity, assumes that the reflection of light by the Earth is at a constant 0.3, as used by Yang et al. [47] and Li et al. [36], and that it reduces with distance from the sub-solar point by a cosine law, becoming zero at the terminator. The result is propagated from the Kärmän Line Sanz Fernandez de Cordoba [48]. The most complex model Bhanderi and Bak [49], selected for its level of detail, discretises the Earth's surface into a matrix of cells each having a reflection co-efficient calculated from experimental data. The method determines which of the cells is illuminated by the Sun and which are visible by the spacecraft and calculates the contribution of each cell to the total albedo at the spacecraft's location, propagated from the Earth's surface. The model takes into account the angles of incidence between Sun, surface cell and the spacecraft.

The third model, as presented in Gilmore [50] and originally reported by Anderson et al. [51], Justus et al. [52] for NASA, was selected for the authority of its authors and as a compromise between the other models. It takes satellite measurements of the reflection and normalises them for an altitude of 30 km with an additional factor added to account

for the solar zenith angle[3.1], which is used as recommended for time dependant modelling. A cosine of the solar zenith angle is used to model the Sun's angle of incidence to the local Earth surface. The data is presented in look up tables where statistical probabilities, time constant and susceptibility of the surfaces to albedo and infrared affect the recommended value to use for the reflection co-efficient. For this numerical modelling, the solar cells have a high absorptance to both, the surface coating may have a high absorptance to both and the time constant of the panel is of the order of hundreds of seconds. Using the tables for the 3.3 σ case (tables 2.1 and 2.2 from [50]), the albedo at the sub-solar point is 0.28 for the hot environment and 0.14 for the cold environment. 3.3 σ indicates that the values will only be exceeded 0.04% of the time and these values are thus the extremes of the orbit environment.

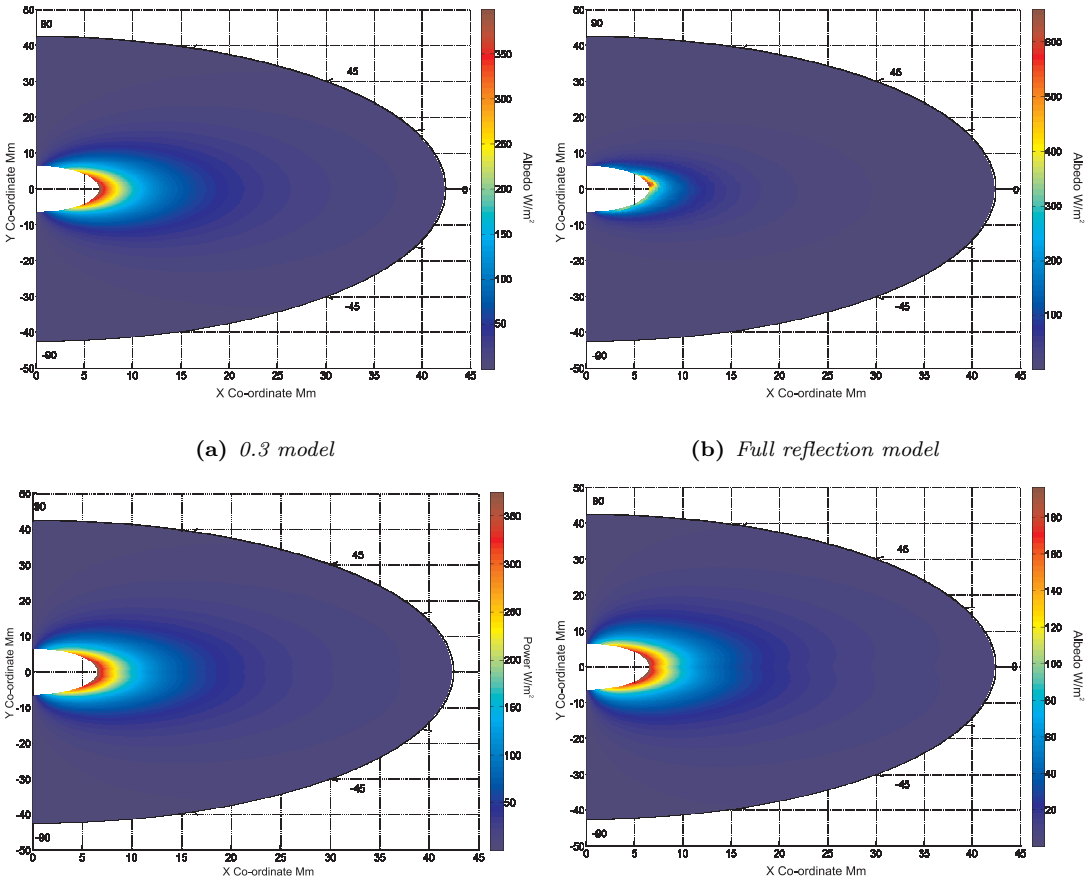

(a) *0.3 model*

(b) *Full reflection model*

(c) *Hot NASA model*

(d) *Cold NASA model*

Figure 3.3: *Surface plots of the power per area predicted by each model, from 200 km to geosynchronous altitude. The unit of the axes is Mm, megameters.*

These models are compared in figs. 3.3 to 3.5. These results are in the plane of the solar ecliptic. Figure 3.3 shows surface plots of the predicted power per area, comparing how

[3.1] The angle at the Earth's surface measured between the Sun and an observers zenith.

the power changes with altitude and distance from the sub-solar point. Figures 3.4 and 3.5 compare the total energy input at 200 km LEO and GEO altitude. These plots are for one west to east pass over the Earth along plane of the solar ecliptic. It should be noted that the output of the full reflection model is dependent on the orientation of the Earth and that the other models are not.

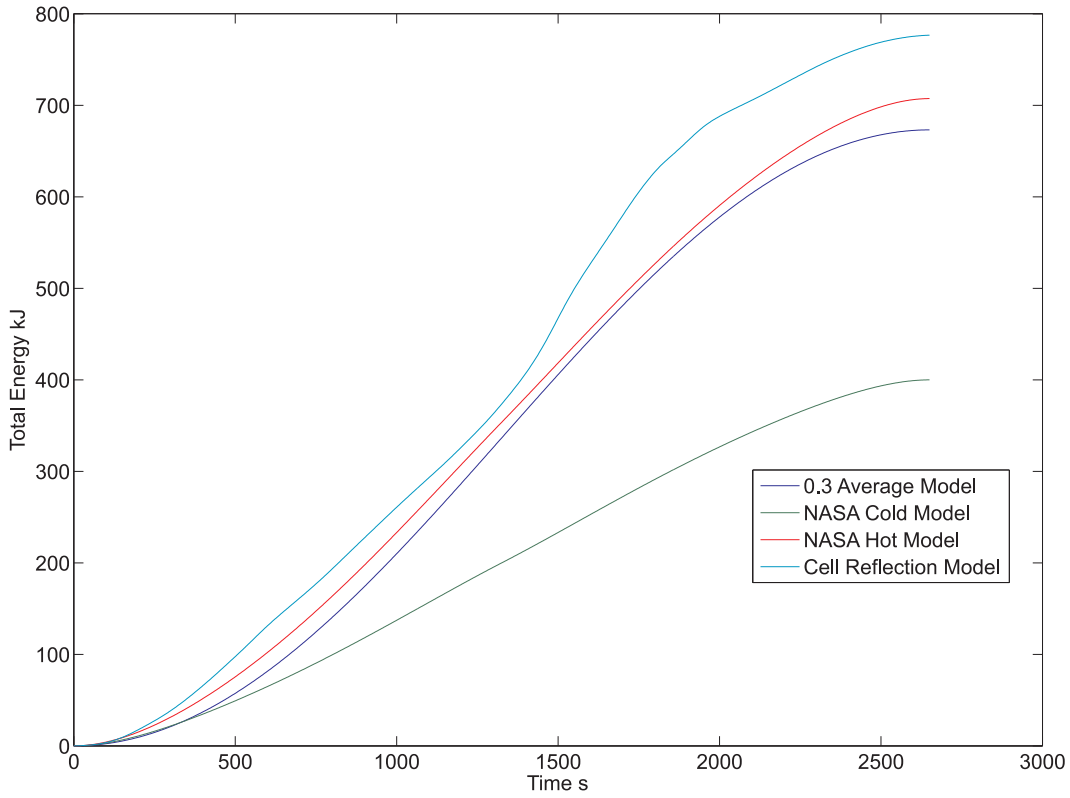

Figure 3.4: *The total energy predicted by each of the albedo models for one pass over the illuminated Earth surface at 200 km altitude.*

The NASA and 0.3 models present a smooth surface plot. The full reflection model shows rapid and large variations as the spacecraft passes over surfaces with different reflections. In low Earth orbit (LEO), the models show larger differences than at higher altitudes as at higher altitudes the local reflection properties of the Earth are averaged out as more of the surface is visible to the satellite. The energy plots illustrate further the differences between the models at different altitudes. In LEO, the 0.3 model and the NASA hot model better match the full reflection model due to high localised reflection of the Earth causing a high albedo, whereas the NASA cold model matches better at geosynchronous altitude where there variations are damped by the large amount of Earth reflection to the point at this distance.

The full reflection model is considered to be the most accurate model as it models an

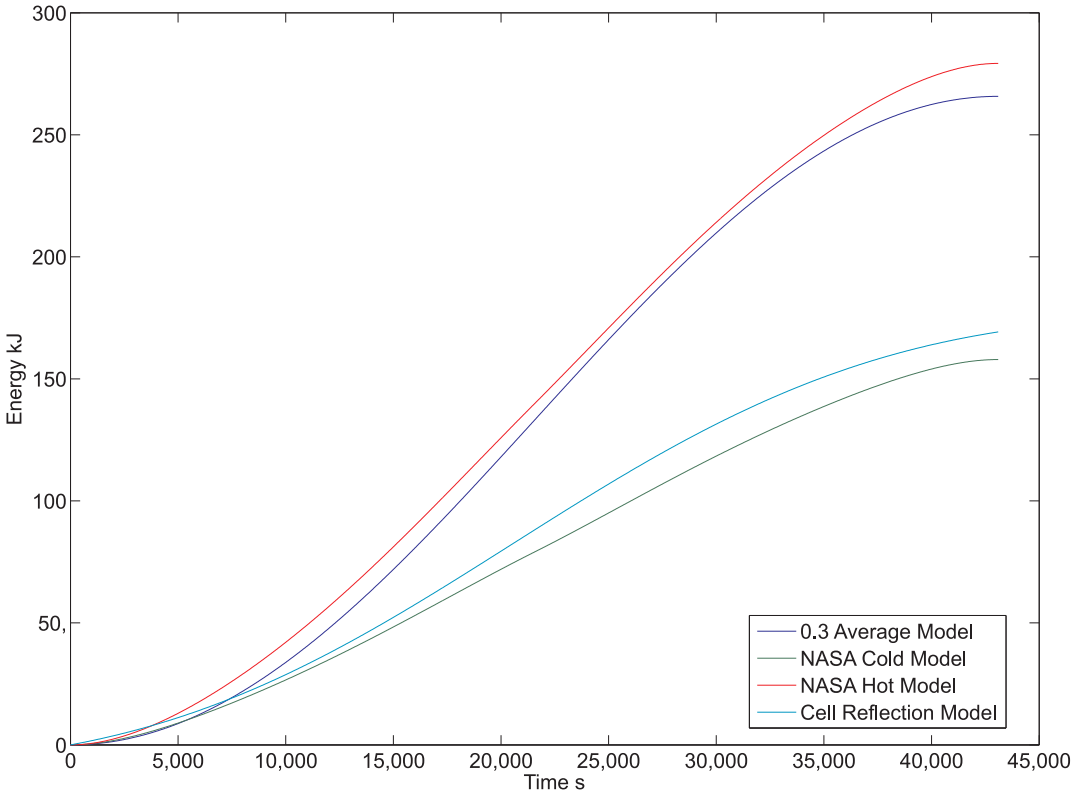

Figure 3.5: *The total energy predicted by each of the albedo models for one pass over the illuminated Earth surface at a geosynchronous altitude.*

Earth with varying reflection properties, however it requires a large amount of calculation to be undertaken for every point considered during the orbit and requires the orientation of the Earth to be defined, an added complexity, and thus its use is avoided. As the 0.3 model lacks scientific review, the NASA model is used. The NASA hot model is a better match for the full reflection model than the NASA cold model, implying that the full reflection data is based on maximum likely albedo. Both hot and cold NASA models are used to provide a range of possible thermal environments.

3.3 Earth Infrared Radiation

The model used is from the same study as the selected albedo model [50] and using the same properties, a power output of 232 W/m^2 (cold environment) or 275 W/m^2 (hot environment) is propagated from an altitude of 30 km using an inverse square law. This model assumes a constant heat output from the Earth, whereas it will be greater in sunlit areas, cooler on the night side and vary with surface temperature; such as cooler arctic regions and warmer topical regions. The hot and cold environment values

accommodate for this by providing the limits of the environment.

3.4 Free Molecular Heating

Free molecular heating is considered to have an effect on spacecraft temperatures in orbits below 180 km, Gilmore [50]. As no orbits below this altitude are considered, free molecular heating is not modelled.

3.5 Internal Heat Output

For the wing mounting, the majority of the electrical power generated by the solar cells is directed to the main body of the spacecraft, with a small amount to trickle charge the cells. As such, there are very few electrical components in the MFPS panel beyond the solar cells and the batteries. The heat output of the wiring carrying power to the spacecraft is considered negligible and is not modelled. The body mounting includes the spacecraft in the model and all power absorbed by the solar cells is re-emitted here, representing heat loss from the electrical system, preserving conservation of energy.

3.5.1 Battery Cell Heat Output

When charging and discharging, cells produce a small heat output. Current research into the heat output of cells has focused on understanding the heat output of Lithium based cells when they are being overcharged, Pals and Newman [53, 54], and when used in difficult charge/discharge regimes, Chen and Evans [55]. The work is undertaken to understand more about the process that result in thermal runaway. The results of these works indicated that a thermal output of the order of milliwatts is to be expected under these hostile regimes. In the applications considered in this work, the charging of the cells takes place over long periods of time and does not involve any overcharging. It is thus safe to assume that the charge rates will be low and that the thermal output of the cells will be correspondingly low and therefore a negligible input[3.2].

[3.2] For an estimate of the heat output of the cells used, please see appendix C.4.

3.6 Dark Space

Space is modelled as a black body, which has a constant temperature of 4 K. It is considered to be uniform in every direction and have no angles on incidence nor view factor corrections.

3.7 Heat Emission

Heat emission as radiation per unit area (R) from a surface is modelled using the grey body equation, where ϵ is the emittance of the surface, σ is the StefanBoltzmann constant of 5.67E-08 W/m^{2}K^4 and T is the temperature of the surface;

$$R = \epsilon \sigma T^4 \tag{3.1}$$

3.8 Summary of the Environment

Two environmental extremes are defined. The hot environment is the maximum of each variable and the cold environment is the minimum of all variables, shown in table 3.1. These cases represent the extremes of the environment in Earth orbit. Figures 3.6 and 3.7 show these two environments in the specific example of a 200 km low Earth orbit that passes over the sub-solar point and thus experiences the longest eclipse. The figures show how the inputs varies over the course of one orbit and include the net power input per m^2 on an object in this orbit. In LEO, the inputs from the Earth will increase the difference between the environments beyond the 92 W/m^2 difference in the Sun's input seen at higher altitudes.

Table 3.1: *Summary of the environment limits.*

Environment	Hot	Cold
Solar Input	1414 W/m^2	1322 W/m^2
Earth Albedo (at 30 km)	0.28	0.14
Earth IR Heat (at 30 km)	275 W/m^2	232 W/m^2

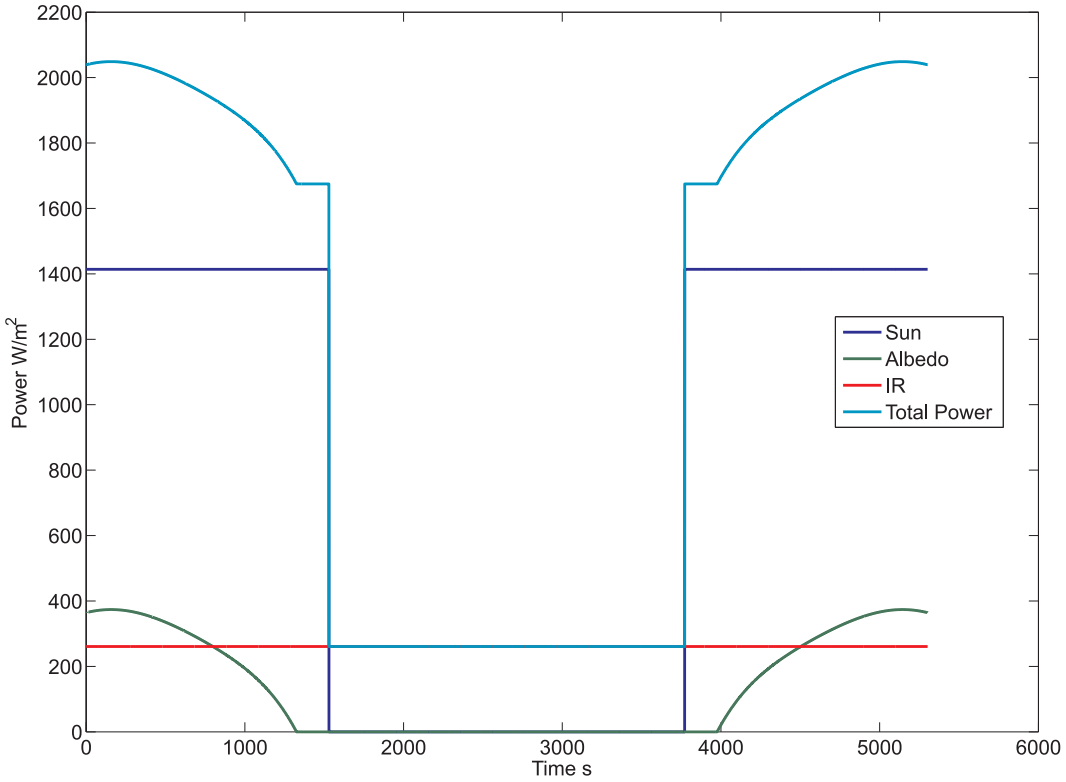

Figure 3.6: *Heat inputs in the hot environment.*

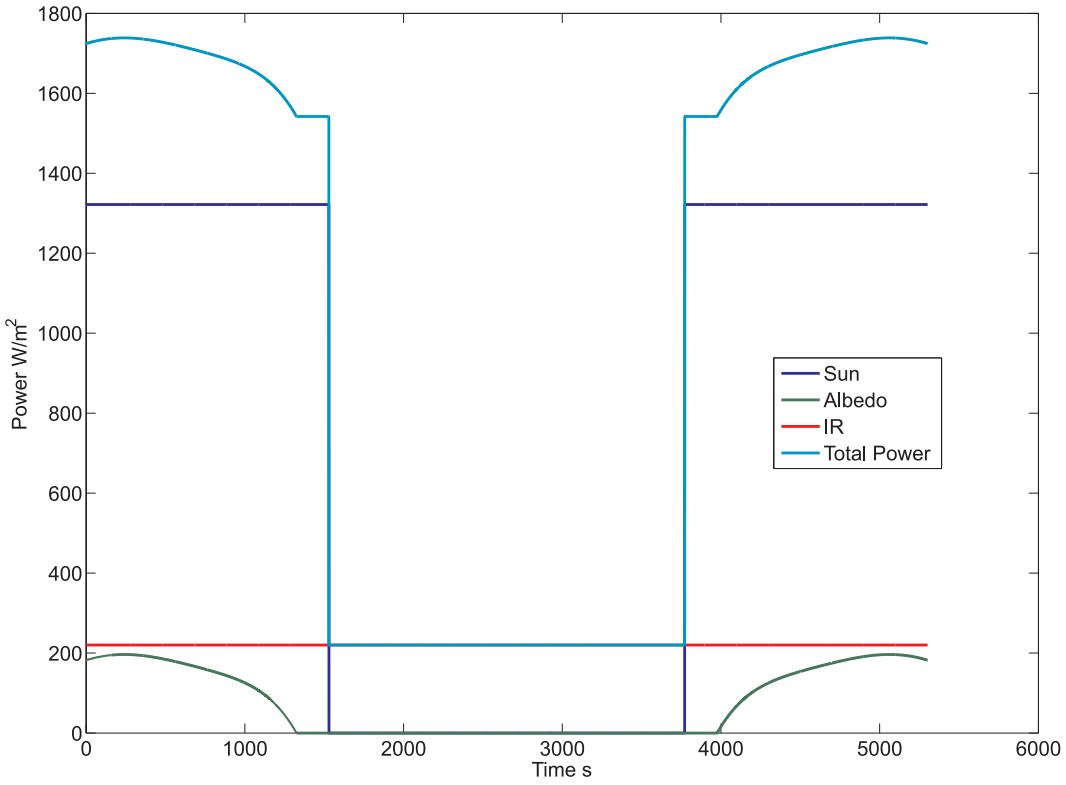

Figure 3.7: *Heat inputs in the cold environment.*

Chapter 4

The Commercial Off the Shelf Assembly Multifunctional Power Structure

The environment defined in chapter 3 is consistent for all MFPS panels that are placed in Earth orbit. For the thermal control requirement to be assessed by a numerical simulation, the MFPS must be further defined. This chapter presents the components of the MFPS and the numerical values used, which have been selected to be realistic. The results of this specific sample model can be used to draw interpretations about the general application.

Two applications are considered: one where the battery is embedded into the structure of a panel in the deployed wing solar array; the other where the battery is embedded into structure of a panel that forms part of a body mounted solar array.

4.1 Spacecraft Orientation

The orientations of the applications are shown in fig. 4.1. The wing mounted spacecraft is orientated so that the solar cells are always perpendicular to the Sun's input, as is standard to maximise the power from the cells. The spacecraft is also orientated so that the axis of the wing array is parallel with the Earth's surface, pointing the spacecraft at the Earth's surface which results in no shadowing of the input from the Earth, fig. 4.1(a). The body mounted system is orientated so that one panel is always parallel to and facing the Earth's surface, fig. 4.1(b). Thus the input from the Earth will only ever fall

on to this panel. As the spacecraft orbits the Earth, the Sun will illuminate each panel in turn as the spacecraft rotates to keep one panel facing the Earth, with each panel thus experiencing being in the spacecraft's shadow. This is consistent with an Earth pointing payload. The orientation is such that the non MFPS panel surfaces face perpendicular to the solar ecliptic.

Three variations on the body mounting orientation are considered. In the first, the Earth facing panel is removed in orbits below 3200 km. This is because in these low Earth orbits, the panel is only illuminated by the Sun for a very short period of time before eclipse and it is not worth carrying an extra panel. The two other variations considered reflect the requirements of a space pointing payload where the spacecraft's attitude is fixed with respect to the Sun. The Sun pointing orientation is with one panel perpendicular to the Sun, fig. 4.1(c). The space pointing orientation is with two panels both at 45 degrees to the Sun, fig. 4.1(d). The Sun pointing orientation represents the colder scenario and the space pointing orientation the hotter scenario, due the difference in the area illuminated by the sun. These orientations are maintained throughout an orbit; the spacecraft not undergoing attitude changes so that the illumination of the panels is constant. These variations are considered to evaluate how the body mounting responds when the inputs are perpetually uneven between the panels; i.e. unvarying illumination and shadowing.

4.1.1 Earth Inputs of the Body Mounted System

Chapter 3 has detailed the environment that the body mounted system will encounter. When the body mounted system is in LEO (below 3000 km) an extra input has to be considered, that of the illumination of the panels that are perpendicular to the Earth's surface. As the Earth is much larger than the spacecraft there will be illumination of these surfaces by both Earth Albedo and Earth Heat Infra-red. This is calculated using the following:

$$Q_p = PF_p \tag{4.1}$$

$$F = \frac{1}{\pi}\left(\arctan\frac{1}{\sqrt{L^2-1}} - \frac{\sqrt{L^2-1}}{L^2}\right) \tag{4.2}$$

$$L = \frac{h}{r} \tag{4.3}$$

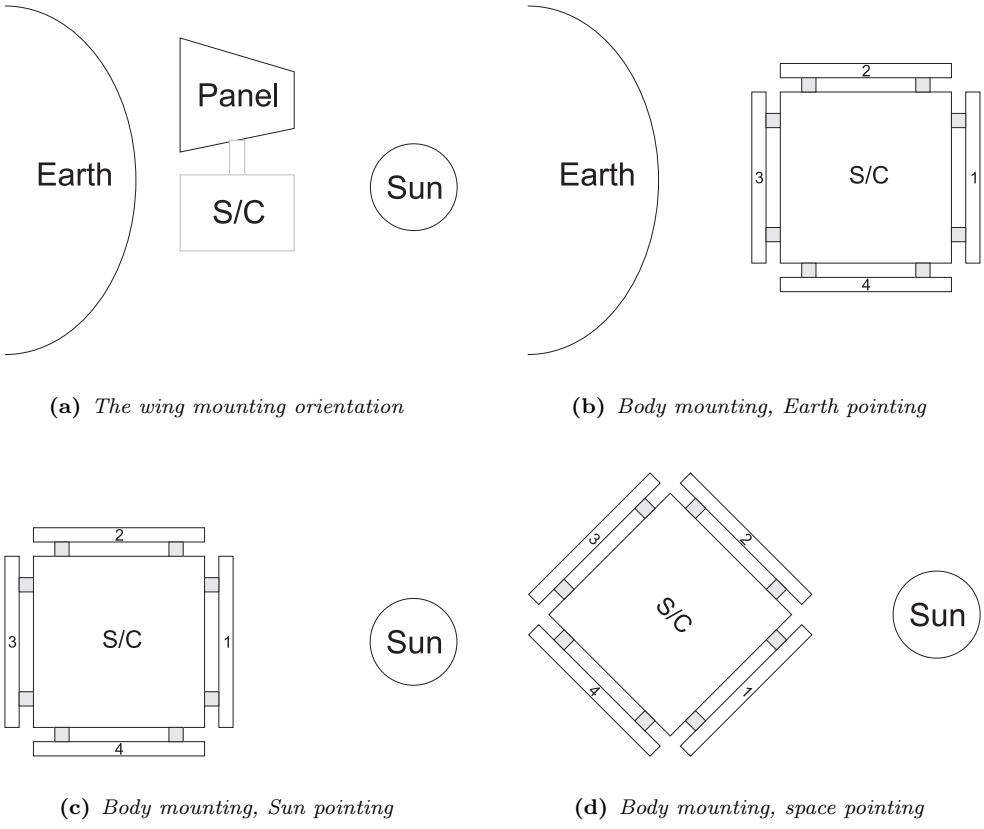

(a) *The wing mounting orientation*

(b) *Body mounting, Earth pointing*

(c) *Body mounting, Sun pointing*

(d) *Body mounting, space pointing*

Figure 4.1: *MFPS application orientations.*

Where Q_p is the power per square metre on the surface, P is the value of the input at the reference radius, F_p is the view factor, h is the orbit radius and r is the reference radius [4.1]. The equation for the view factor is taken from appendix C of Siegel and Howell [56].

4.2 The Panel Components

In the simplest most general terms, the panel is composed of a facesheet and a core with a battery embedded in the core and solar cells on one face, fig. 4.2(a), as proposed by Roberts and Aglietti [7]. Table 4.1 shows the details of the panel and the variables assigned to the properties. The components used are typical of the current state of the art, ensuring that the sample models are relevant. The panel is assumed to have been manufactured without error, preserving its nominal properties. As such, no gaps exist and contact conduction is not considered to be a factor in the flow of heat. As the panel is manufactured under pressure with an adhesive and it is an important structural requirement that the core is bound to the facesheet, this is deemed a reasonable assumption. A 100% packing factor for the solar cells is used to simplify the model; the

[4.1] 30km above the Earth's surface.

entire Sun facing surface is solar cell. It also represents the worst case design scenario where there are fewer design options as the surface properties of gaps between solar cells cannot now be optimised. The core geometry is shown in fig. 4.2(b). The tape added to the edges of the panel reduces the emitted heat of this very small area to negligible amounts.

Table 4.1: *The properties of the sample panel.*

Property	Variable	Value	Unit
Facesheet Material		CFRP	
Fibres		M55J	
Resin		Epoxy	
Volume Fraction	V_f	0.6	
Bi-Weave Ply Thickness	x_{ply}	0.3	mm
Facesheet Thickness	x_f	1.8	mm
Core Type		Honeycomb	
Core Material		Aluminium 5052	
Core Thickness	x_c	12	mm
Solar Cells		Triple Junction	
Solar Cell Efficiency	η_{sc}	28 % at 28 °C	
Solar Cell Temperature Co-efficient [57]	η_T	0.07	% /K
Solar Cell Absorptance	α_{sc}	0.91	
Solar Cell Effective Absorptance	$alpha_\eta$	0.63	
Solar Cell Emittance	ϵ_{sc}	0.8	
Battery Cell		PLF263441 D [31]	
Battery Cell Power Density	P_ρ	166	Whr/kg
Battery Cell Mass	M_B	6	g
Battery Cell Size	X_B Y_B Z_B	41, 34, 2.6	mm
Kapton Tape Absorptance	α_{kt} [50]	0.12	
Kapton Tape Emittance	ϵ_{kt} [50]	0.03	

The cell used was selected for its superior properties, Ilic et al. [58]. The temperature envelope of the cell [31] is given in table 4.2. The tighter limits of 0°C- 45°C(273 K - 318 K) are selected for a conservative model. This is potentially a wide temperature range, as Gilmore [50] notes that it is preferential for NiCd and NiMH batteries to be kept

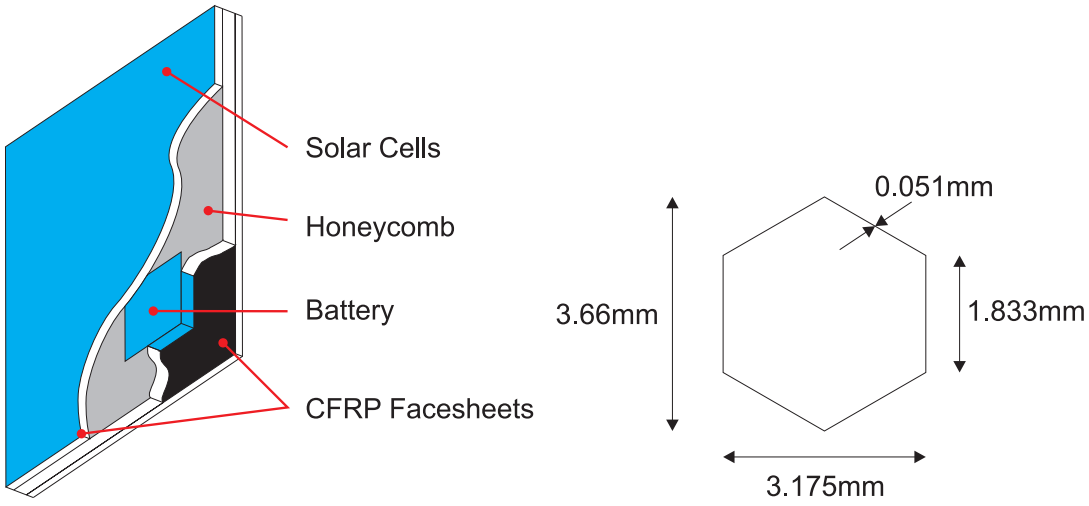

(a) *Representation of the COTS assembly MFPS* **(b)** *The geometry of the honeycomb*

Figure 4.2: *Details of the proposed applications.*

between 273 K and 298 K for better efficiency. The potential effects of this are discussed in section 10.1.

Table 4.2: *Temperature limits of the Varta PoLiFlex cell.*

Cell Condition	Charge	Discharge
Upper Limit	45°C	60°C
Lower Limit	0°C	-20°C

Potting foam is used for structural inserts to ensure that the insert is properly bonded to the structure. Inserts are typically shaped so the expanding foam holds it in place and transfers loads to reduce stress concentrations. The adhesives used to bond the materials together are considered to be sub-millimetre in thickness and are therefore considered to have no effect. The surface of the reverse side of the panel is given a paint coating or surfacing, the optical properties of which can be altered.

4.3 Material Thermal Properties

The thermal properties of the materials used are given in table 4.3 and details of their calculation are given in appendix D.

Table 4.3: *Thermal properties of the materials used. X is defined as through the thickness of the panel with Y and Z orthogonal to X.*

Material	Conductivity X W/mK	Conductivity Y W/mK	Conductivity Z W/mK	Density kg/m^3	Specific Heat Capacity J/kgK
Solar Cells	58.6	58.6	58.6	5324	322
CFRP	0.49	93.5	93.5	1570	1048
Battery Cell	0.72	62.7	62.7	1655	803
Aluminium Alloy [59]	138	138	138	2680	880

4.4 Wing Mounting

The panel would form part of a deployed wing array. To avoid over constraining the model, the spacecraft is not modelled. As the connection to the spacecraft would increase the heat capacity of the model, not modelling it will increase the reaction of the system to the environment, causing larger temperature changes. This is considered a conservative modelling. In this mounting, the dark surface is initially given a white paint coating to reflect albedo and promote high heat loss. Table 4.4 shows the properties of the wing panel.

Table 4.4: *Properties of the wing version of the MFPS panel.*

Property	Variable	Value	Unit
Area	A_w	1	m^2
Coating Absorptance	α_{wp}	0.09	
Coating Emittance	ϵ_{wp}	0.92	
Mass	M_w	8.4	kg
Heat Capacity	H_w	7.86	kJ/K

4.5 Body Mounting

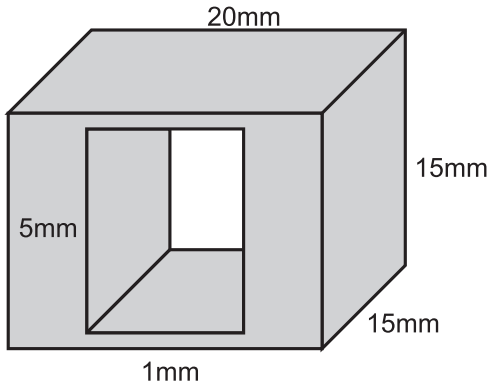

Figure 4.3: *Connector for the body mounting.*

The second mounting considered is when the panel is mounted to the side of the spacecraft by a set of connectors, typically called brackets or flexures in practice. This is similar to the manner in which the solar array is mounted to the micro-satellite described by Rossoni and Panetta [5]. In this instance, four panels of the same composition as used for the wing mounting are mounted around a central spacecraft, as shown in fig. 4.4. This is a 170 kg micro-satellite, the composition of which is shown in table 4.6. Four connectors are used for each panel and are made of aluminium with dimensions as shown in fig. 4.3. The connectors are designed to allow for differences in thermal expansion of the various components due to differences in temperature and co-efficients of thermal expansion. The properties of the body panel are shown in table 4.5.

The panels are mounted to the larger surfaces of the spacecraft. The faces of the spacecraft that do not have a panel are covered with Multi-Layer Insulation (MLI) to minimise heat loss from the spacecraft. A black paint is used as a surface coating on the surfaces of the spacecraft and panel that face each other. This is to maximise the radiative heat exchange between the spacecraft and panels. The radiation exchange between these surfaces and space is considered to be negligible as the distance between them is so small that the surface area visible to space is tiny.

Table 4.5: *Properties of the body mounted version of the MFPS panel.*

Property	Variable	Value	Unit
Spacecraft Mass	M_s	170	kg
Spacecraft Size	X_s,Y_s,Z_s	0.6,0.6,0.8	m
Panel Area	A_b	0.48	m^2
Panel Mass	M_b	4.25	kg
Panel Heat Capacity	H_b	3795	J/K
MLI Absorptance	α_{MLI}	0.25	
MLI Emittance	ϵ_{MLI}	0.02	
Black Paint Emittance	ϵ_{bp}	0.94	

Table 4.6: *Composition of the spacecraft with body mounted panels.*

Material	Specific Heat Capacity	Mass Fraction	Heat Capacity
	J/kgK		J/K
Aluminium Alloy	880	0.5	74800
Copper Alloy	385	0.05	3273
Silicon	702	0.1	11934
Glass Fibre	1260	0.1	21420
Titanium	524	0.15	13362
Nylon	2200	0.05	18700
Fuel	4000	0.05	34000
		Total	177488

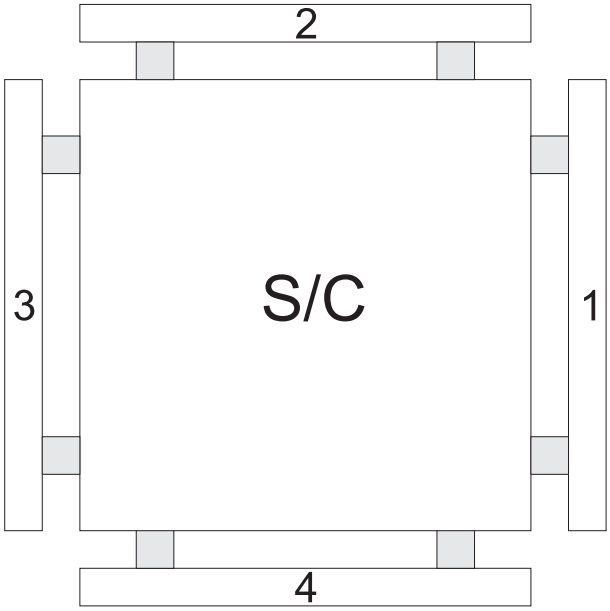

Figure 4.4: *The body mounting with the 4 panels numbered.*

4.6 Number of Battery Cells

In order to meet the power storage requirement, a number of battery cells is required. It is safe to assume that the solar cell area of a spacecraft is the minimum required as extra solar cells would not improve the performance of the spacecraft. Thus the solar cell area can be used to calculate the amount of power the spacecraft requires. In order

to avoid having to recalculate for each altitude the number of cells, a geosynchronous eclipse was considered as it is the longest. The following were assumed as realistic for both mountings:

- Power use in eclipse = 80 %
- Charging efficiency = 80 %
- Eclipse time = 1.12 hours
- Eclipse fraction = 0.047
- Depth of discharge = 40 %

For the wing mounting the amount of solar area for the entire spacecraft is unknown as the system around the isolated panel has not been described. However, the minimum solar cell area would be the panel by itself. This gives a solar power requirement of 271 Watts and an eclipse power of 217 Watts. This gives a required capacity of 821 Whr. This is 740 cells. For a level of redundancy (degradation with age, faults), 900 cells are used to give 1 kWhr of capacity. This is a mass of 5.4 kg and a heat capacity of 4335 J/K. For the body mounting, the minimum solar and eclipse powers are 176 W and 140 W. To survive the eclipse, a capacity of 394 Whr is needed. Dividing this equally over the four panels (to reduce the number of cells in each panel and their effects on the structure) gives 89 cells per panel. For redundancy, 100 cells per panel are used for a total capacity of 444 Whr for 0.6 kg and 481 J/K.

When the Earth pointing panel is removed (as detailed in section 4.1) the amount of sunlight on the solar cells will reduce as the spacecraft rotates over its orbit, thus the time the spacecraft goes without sunlight is now increased. The battery capacity requirement also increases and with the removal of a panel the cells are now distributed over 3 panels. As the battery provides 80 % of the sunlit power demand, they begin discharging when the amount of power received by the solar arrays falls to 80 %. For orbits below 1545 km in altitude, the spacecraft goes into eclipse before this occurs and thus no extra battery capacity is required. At an altitude of 3200 km, which is the highest considered for the three panel orientation and thus the worst case, an extra 610 seconds of battery power is required. This is 422 Whr over 127 cells in each of the 3 panels, rounded to 140 cells for redundancy, giving an extra capacity of 22.2 Whr as 20 extra cells.

4.7 Multifunctional Saving

Roberts and Aglietti [7] have defined the saving from using MFPS, as aforementioned. For the body mounting, the spacecraft is a known quantity and thus the specific energy requirement is calculated to be 2.34 Whr/kg. Using fig. 1.1 [7], when just considering the removal of parasitic mass a saving of 0.6 kg is made and with the bus volume reduction the saving is 1.3 kg, mass saving of 0.68 %. For the wing mounting the spacecraft is undefined and thus calculation of the SER is difficult. However, supposing the spacecraft is 250 kg, 500 kg or 1000 kg, gives SERs of 4, 2 and 1. This is turn gives a saving of 1.18 %, 0.59 % and 0.3 % which is a mass saving of 2.95 kg is all three cases. These mass savings are dependent on energy capacity of the multifunctional structure, with smaller capacities leading to smaller savings.

Chapter 5

Isothermal Model

An isothermal model with a single degree of freedom was used to determine the equilibrium temperatures of the proposed MFPS applications and the transient response of the MFPS panel to the environment. The model is limited in scope as it consists of a single node with surfaces that interact with the environment. As such, it does not model temperature differences that may exist across the panel or spacecraft, nor does it model heat flow. This modelling is limited to giving a first indication of the thermal control requirement, as it is possible the model may predict a safe average temperature when a battery temperature is unsafe. Safe is defined as where the temperature of the battery is within its envelope.

5.1 Model Definition

5.1.1 Equilibrium Method

Mapping the equilibrium temperature of the panel in Earth orbit allows orbits to be defined where the equilibrium temperature is always safe and thus orbits where the panel can be used without thermal control. Such orbits are valuable as the lack of extra mass allows the MFPS benefits to be fully realised. The equilibrium temperature is determined by the inputs from the environment and the grey body radiation of the model to space. The inputs on the model are;

$$Q_{Sun} = A_{Sun}\alpha P_{Sun} \tag{5.1}$$

$$Q_{Eab} = A_{Eab}\alpha P_{Eab} \tag{5.2}$$

$$Q_{Eir} = A_{Eir}\alpha P_{Eir} \tag{5.3}$$

The heat emission by each surface is modelled, as described in section 3.7;

$$Q_{rad} = A_{rad}\epsilon\sigma T^4 \tag{5.4}$$

Where, Q is the power flux, A is the area of the surface effected by the heat flow, α is the absorptance of the surface, ϵ is the emittance of the surface, P is the power per unit area from the source with view factors and angles of incidence accounted for, sun is the Sun, Eab is Earth albedo, Eir is Earth heat radiation and rad is heat loss. Equilibrium occurs when

$$Q_{Sun} + Q_{Eab} + Q_{Eir} = Q_{rad} \tag{5.5}$$

which can be solved for the temperature of the system.

5.1.2 Transient Response Method

For locations where the equilibrium temperature is not within the envelope acceptable for the battery, the response of the panel to the changing environment in Earth orbit is assessed. Orbits that pass through these locations can be declared safe if the battery temperature does not leave the envelope, which will occur if the panel does not spend enough time in the unsafe region to be too adversely affected.
The orbital paths are modelled as a set of discrete points that are spaced with a constant time step. The panel passes from one point to another, with the environment being a function of position. A fourth order Runge-Kutta method is used to calculate the temperature at each point from the previous point.

5.1.3 Model Assumptions

- Kirchoff's law[60], $\alpha(\nu) = \epsilon(\nu)$, states that for a given frequency (ν), the absorptance (α) and emittance (ϵ) of a surface are equal. It is used for radiation in the infrared range and it is assumed that the heat radiation given off by both the Earth and panel is in the infrared range. As such, when considering infrared radiation, the emittance of the panel is equivalent to the absorptance.
- No heat flow across the panels edges is considered, as aforementioned in section 4.2.
- The background radiation emitted by space is not considered as it is several orders of magnitude smaller than the other inputs.

- No orbit perturbation is modelled as its effect is indirect (the thermal inputs are a function of position) and it would add unnecessary complexity
- Celestial bodies (ie the Earth and the Sun) are considered fixed to reduce complexity.

5.1.4 Orbits Considered

A range of orbits from 200 km LEO to Geosynchronous Earth Orbit (GEO) are considered. A 200 km LEO has the largest eclipse proportion of the orbit, the shortest time in the Sun and the shortest orbit period. Geosynchronous has the longest eclipse time, the smallest eclipse proportion, the longest sunlit period and the longest orbit period. These orbits represent the extremes the panel will encounter. Equilibrium plots are in the plane of the solar ecliptic with the X-axis orientated towards the Sun with the Earth at the centre. These plots are symmetrical about the X-axis and may be rotated about the X-axis to produce a three dimensional map. For the transient cases, circular orbits at the spring equinox with the ascending node under the sub-solar point are used for maximum eclipse time.

5.2 Wing Mounting Results

The isothermal model for the wing mounting represents a two dimensional panel of no thickness in space, effectively with two surfaces. As heat flow and temperature difference across the thickness of the panel are not modelled, both surfaces of the panel will radiate at the same temperature. In actuality, the solar cells would be warmer as they have a greater heat input. As the panel is thin compared to its area, the effect should be small[5.1].

5.2.1 Equilibrium Results

Figures 5.1 and 5.2 show a surface plot of the equilibrium temperatures of the wing mounting in Earth orbit in the two environments considered. The plot is generated in the plane of the ecliptic with the X-axis pointing towards the Sun. The distance unit is megameters, Mm. As the heat inputs (as modelled) from the Sun and the Earth IR are uniform and the albedo variation is only a function of solar zenith angle, the results may

[5.1] Section 6.2.1 shows this is true.

be rotated about the X-axis to from a complete picture for all locations within geosynchronous altitude. The equilibrium surface plot shows the equilibrium temperature of the panel in Earth orbit that the panel would tend to if that position was maintained. Thus, any orbit where the equilibrium temperature at all locations along it are within the battery temperature envelope can be considered safe. The locations can be grouped into regions where the temperature is too cold, too hot or safe. Figures 5.1 and 5.2 are annotated to indicate these regions.

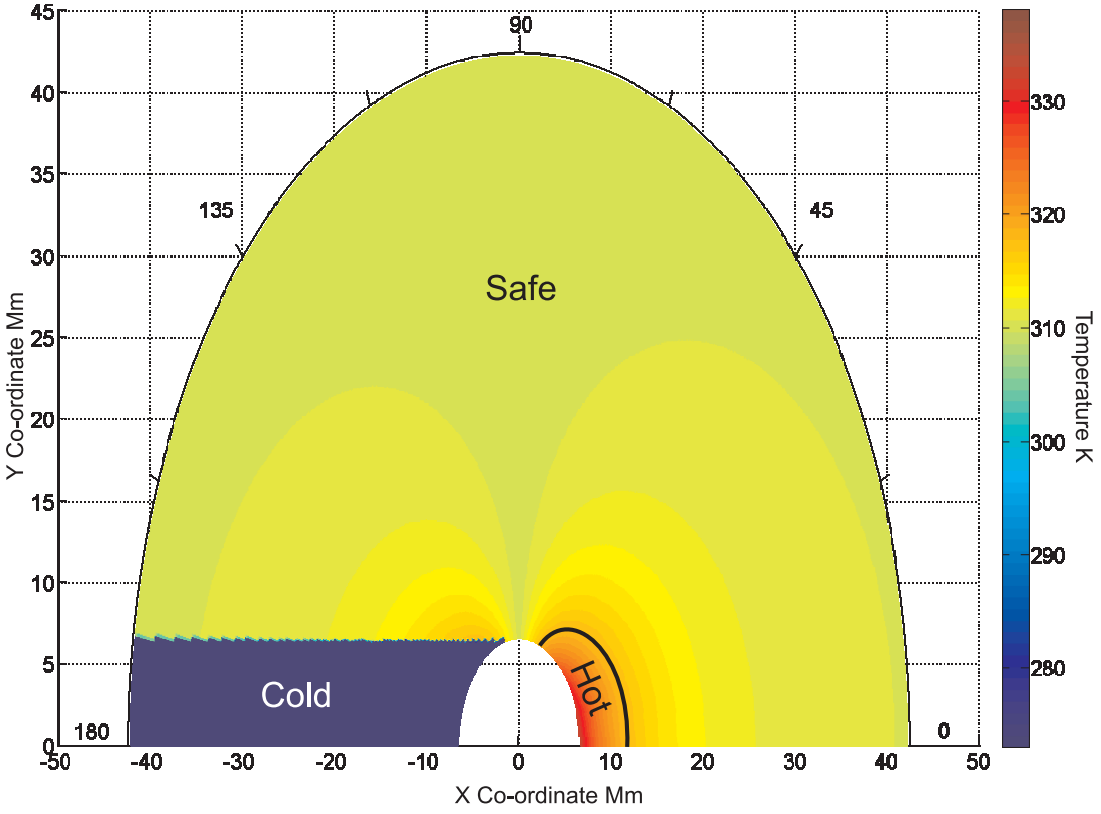

Figure 5.1: *Surface plot of the hot wing mounting equilibrium temperatures. The colour map is in kelvin, with a lower limit of 273 to preserve the detail of the sunlit temperatures.*

The surfaces results for both environments show the same pattern of regions that are too cold and too hot. In both cases eclipse is too cold, caused by the lack of sunlight. The temperature in eclipse decreases with distance from the Earth as the heat from the Earth IR reduces. The boundary of it is unaltered by the use of either hot or cold environment as it is determined solely by the Earth's shadow. An overheating region exists about the sub-solar point where the heat from the Earth is at a maximum and which fades towards the terminator. In the hot environment the region is much larger and extends out to 5000 km with a maximum temperature of 332 K compared to an extent of 1600 km and 323 K maximum temperature in the cold environment. The

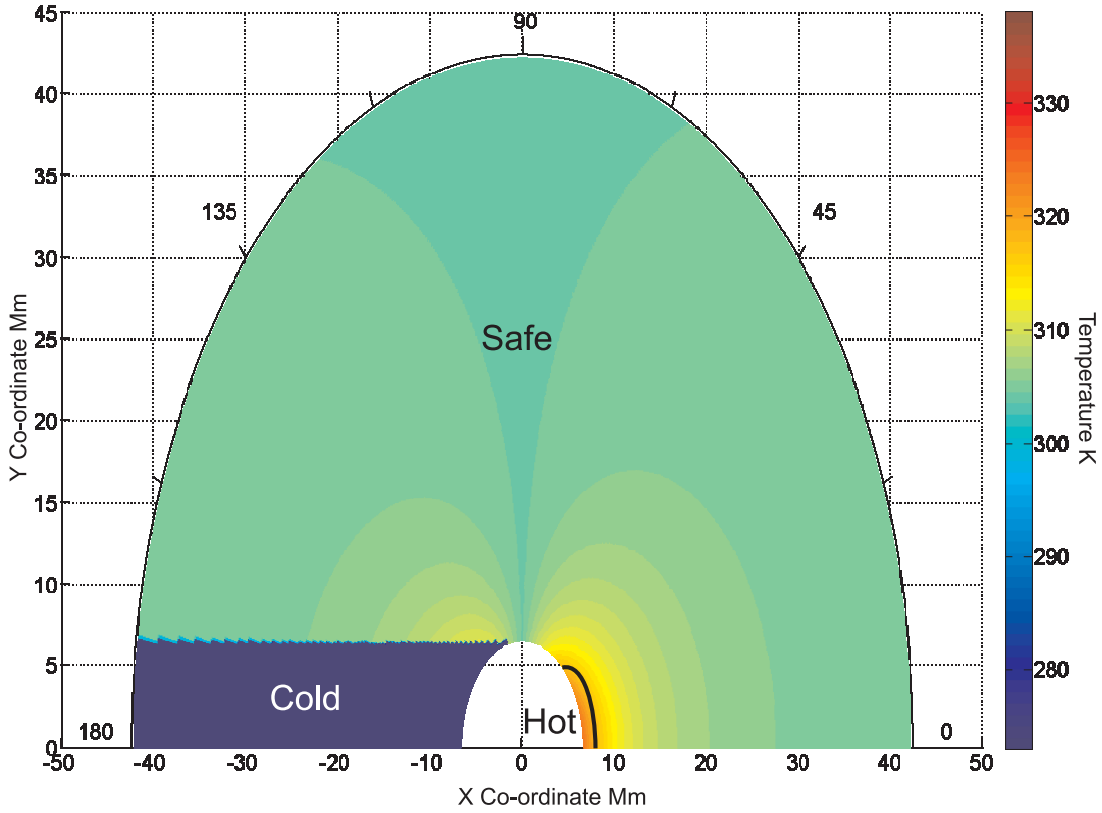

Figure 5.2: *Surface plot of the cold wing mounting equilibrium temperatures. The colour map is in kelvin, with a lower limit of 273 to preserve the detail of the sunlit temperatures.*

larger and warmer hot environment region is caused by the greater heat inputs. The equilibrium temperature of the panel at positions where the Earth's influence is negligible, is greater in the hot environment as the sole input (the Sun) is larger. This leads to a geosynchronous equilibrium temperature of 310 K compared to 305 K in the cold environment. Above the terminator (solar zenith angle = 90°) the panel surfaces are parallel to Earth inputs and is thus heated by only the Sun. As the solar zenith angle increases further, the equilibrium temperature increases as the angle of incidence for the Earth inputs decreases.

From these results, orbits can be defined that are safe. Such orbits are ones where the angle between the orbit plane and the Earth-Sun vector is sufficient that the panel does not enter either dangerous region. The environment cases are differentiated by the size and magnitude of the overheating region. As the cold environment represents the smallest the overheating region can be, it represents the most number of safe orbits where thermal control is not required due to the panel never experiencing an environment that would cause unsafe temperatures.

5.2.2 Transient Results

For both environments, a transient modelling of the wing mounting at 200 km and geosynchronous orbit was carried out. A circular LEO at 200 km will experience a short eclipse and pass through the overheating region at its greatest, testing if this short sharp heating/cooling regime will cause the battery to leave its temperature envelope. A geosynchronous orbit was modelled to test if the panel will overcool in eclipse and if the panel will reach its equilibrium temperature when sunlit away from Earth. In reality, these orbits would have properties typical of orbits at their altitudes; a Sun-synchronous LEO and a geosynchronous orbit above the Earth's equator respectively. In this work, the orbits are not defined beyond being circular and that the longitude of the ascending node causes the orbit to pass over the sub-solar point[5.2], the requirement being for the longest possible eclipse.

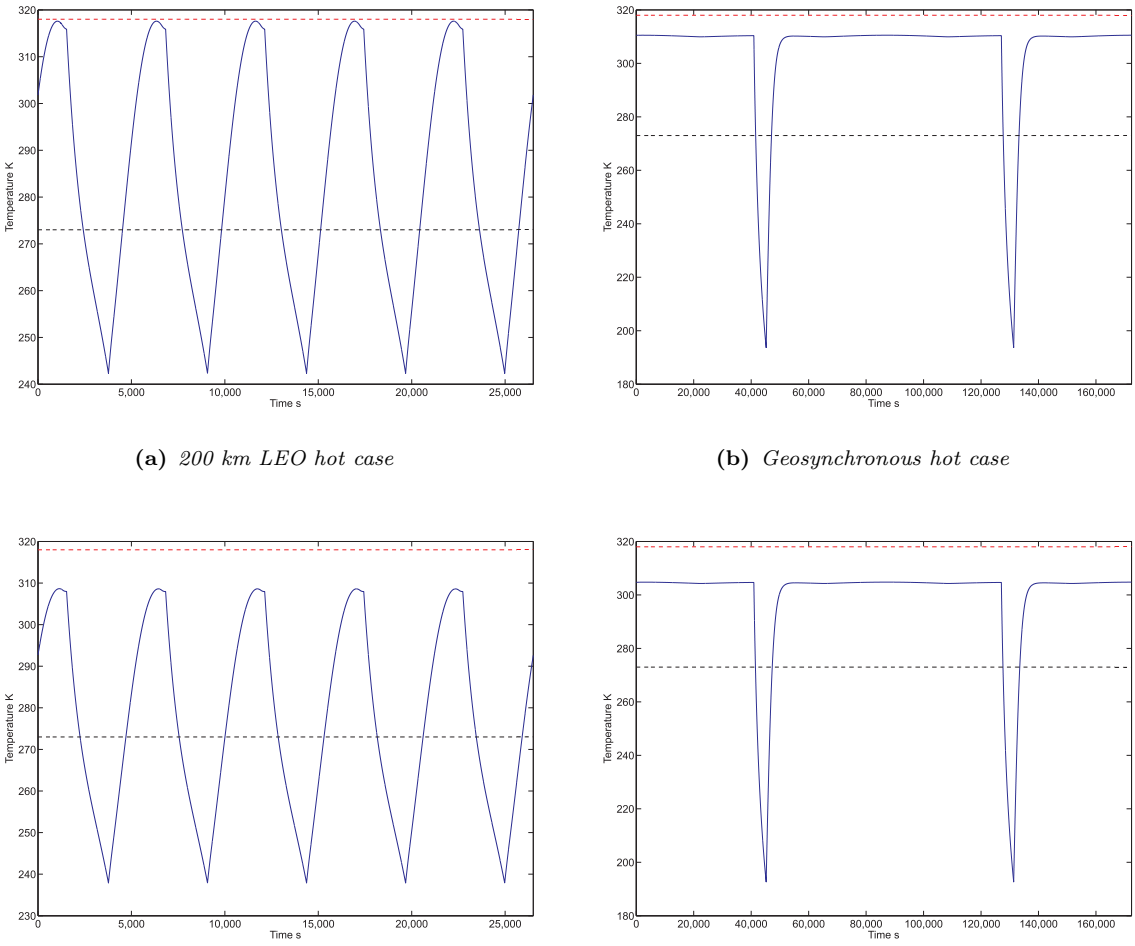

(a) *200 km LEO hot case*

(b) *Geosynchronous hot case*

(c) *200 km LEO cold case*

(d) *Geosynchronous cold case*

Figure 5.3: *The transient response of the wing mounting.*

[5.2] A right ascension of the ascending node of 0°.

The results are shown in fig. 5.3. The upper dashed line (in red) is the upper boundary and the lower dashed line (in black) is the lower boundary of the temperature envelope. The results for each altitude show the same patterns, which match well with the work by Li et al. [36]. The 200 km LEO varies rapidly with the changing environment, while the geosynchronous reaches a steady safe equilibrium temperature which it stays at and recovers to after a rapid cooling due to eclipse. The effect of the different environment cases is to move the pattern (the temperatures) up or down.
Overcooling occurs in all the results, though it is worse and longer in the cold cases where there is less heat from the Earth during eclipse and the eclipse entry temperature is lower. The geosynchronous eclipse is the worst as the panel receives little heat from the Earth at that altitude. The implication is that thermal control will be required for the panel to survive eclipse. However, the eclipse presented is the longest possible; orbits exist that have shorter eclipses. Thus, if the eclipse time is shorter than the time it takes the battery to become too cold, the orbit can be used without thermal control. Thus, orbits with eclipses shorter than the times to overcool shown in table 5.1 are safe to use without thermal control.

Table 5.1: *Overcooling of wing mounted panel.*

Case	Minimum Temperature	Time Overcold	Time to Overcool
200 km LEO Hot	242 K	2101 s	894 s
GEO Hot	194 K	5520 s	630 s
200 km LEO Cold	238 K	2454 s	722 s
GEO Cold	193 K	5850 s	560 s

Overheating does not occur, even in the 200 km LEO hot case where the model orbits through the hottest equilibrium region. The panel temperature does come very close to overheating, indicating that if the environment became warmer, the heat capacity were reduced or if the panel were to spend longer in the environment, overheating would occur. As the maximum temperature is very close to being too hot, it is thus useful to review the maximum temperature for all orbits that pass through the overheating region. For orbits of an altitude of 300 km to 3500 km, the maximum temperature of the panel becomes too high in the hot environment. This is a smaller range of orbits than predicted by the equilibrium model, reducing the overheating region. The maximum temperature is 319.1 K at an altitude of 1400 km. As this is only 1.1 K above the

boundary, it implies that orbits that spend less time in the hottest region will not suffer from overheating. The maximum temperature increase is caused by the increase in the sunlit time as the orbit period increases with increasing altitude but the eclipse time does not increase greatly over the altitudes considered in fig. 5.4.

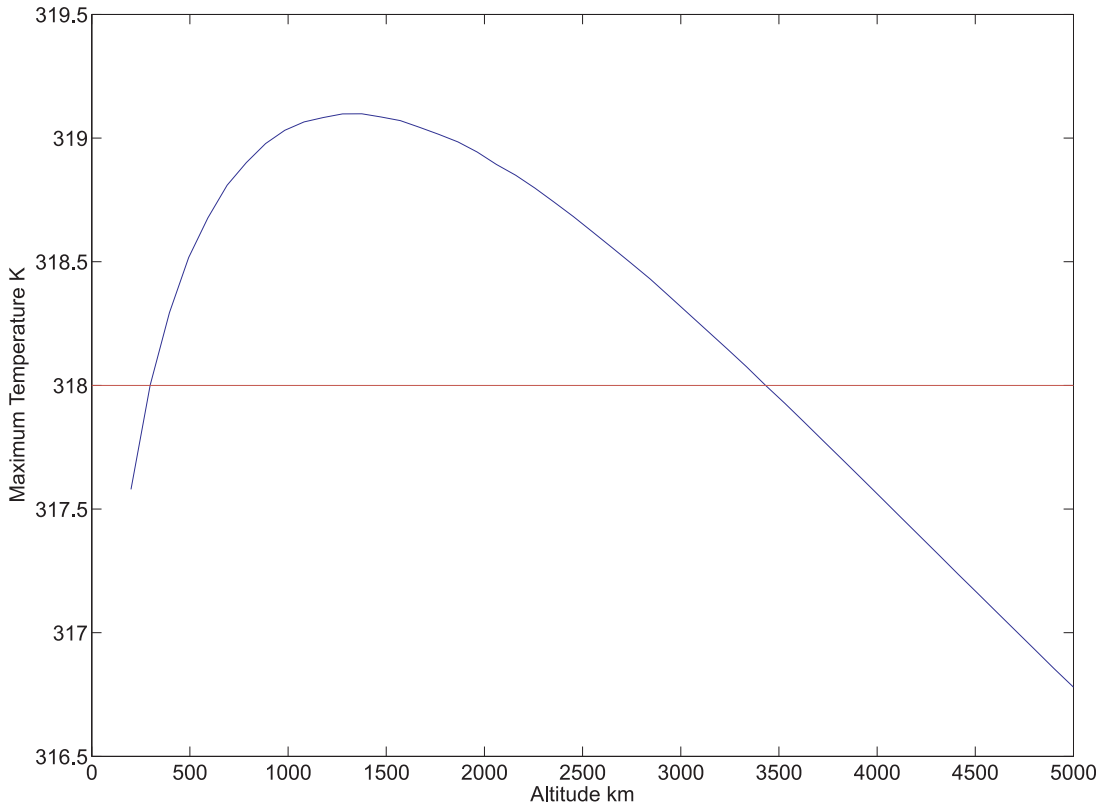

Figure 5.4: *Maximum temperature of the wing mounting with altitude. The red line is the upper temperature boundary.*

5.3 Body Mounted Results

The model for the body mounting represents a cuboid of 6 surfaces, treating the spacecraft as isothermal. The lack of heat flow has a greater effect due to the increased distances between radiating surfaces. While the surfaces associated with the node will radiate at the same temperature, large temperatures differences will be seen in the actual spacecraft, with the illuminated panels warmer than the spacecraft which would be warmer than the dark panels. Thus the equilibrium temperature will be an average temperature of the system, most likely that of the spacecraft. For the transient modelling, the much higher thermal inertia of the spacecraft implies that the results will match more the temperature of the spacecraft than the panels.

5.3.1 Equilibrium Results

The Earth pointing body mounting shows a slightly different temperature pattern to the wing mounting as the input from the Sun varies as the surface presented to it changes as the spacecraft rotates to maintain panel 3 pointing towards the Earth. As such the over heating region moves from the sub-solar point to where the angle between the panels and the Sun is 45 degrees and the maximum area is presented to the Sun. Where the spacecraft presents only one panel to the Sun, it is cooler than the wing array as it has a lower solar input and has a larger emitting surface area. At geosynchronous altitude the sunlit temperature varies, but is always safe. Eclipse temperatures are too cold, the region remaining unchanged from the wing mounting.

The hot environment shows a significantly larger hot region, fig. 5.5, which appears on both sides of the Earth and extends out to 16500 km with a maximum temperature of 349 K. In the cold environment, fig. 5.6, the region exists only on the Sun side of the Earth and extends only to 4000 km. The overheating region is caused by the increased input from the Sun adding to the more constant inputs from the Earth. The region on the shadow side of the Earth is smaller as there is no input from the albedo.

From figs. 5.5 and 5.6 orbits that do not require thermal control can be determined. Orbits at high altitude are always safe, provided they avoid eclipse. At lower altitudes, the larger overheating region in the hot environment means that only orbits around the dusk-dawn orbit can be considered always safe, though moving away from the hot environment opens up further orbits.

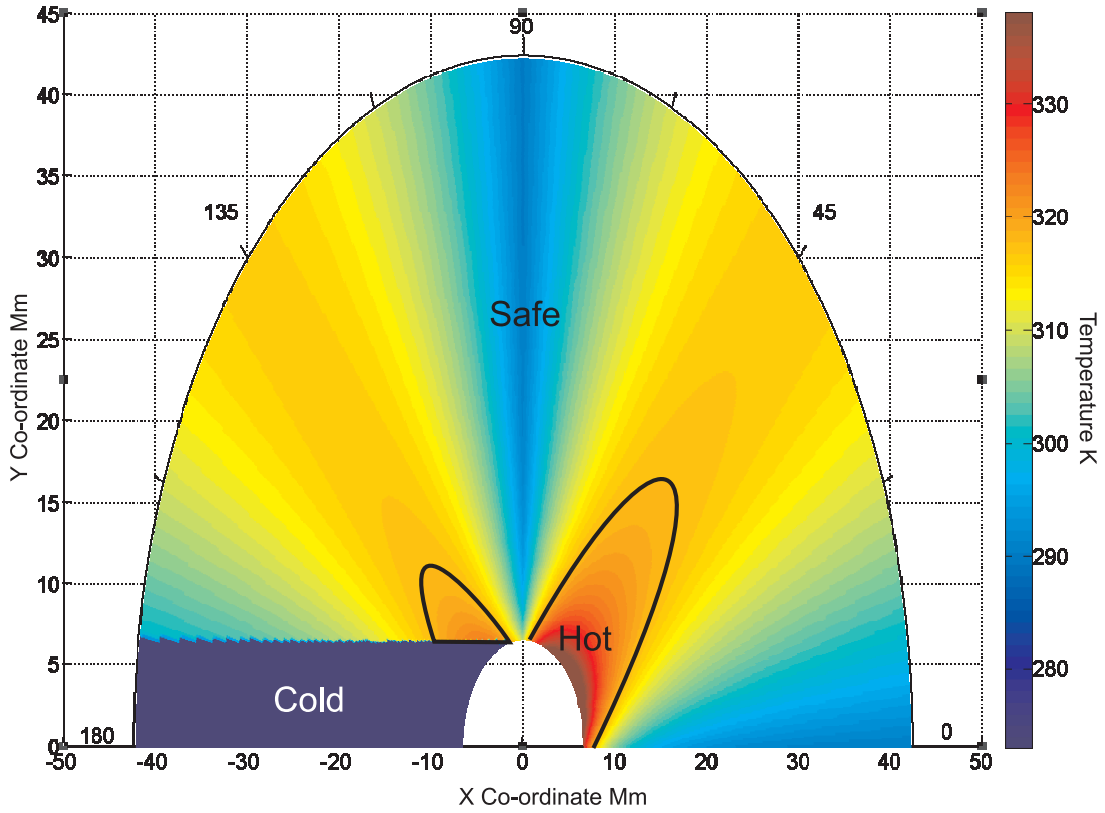

Figure 5.5: *Surface plot of the hot Earth pointing body mounting equilibrium temperatures. The colour map is in kelvin, with a lower limit of 273 to preserve the detail of the sunlit temperatures.*

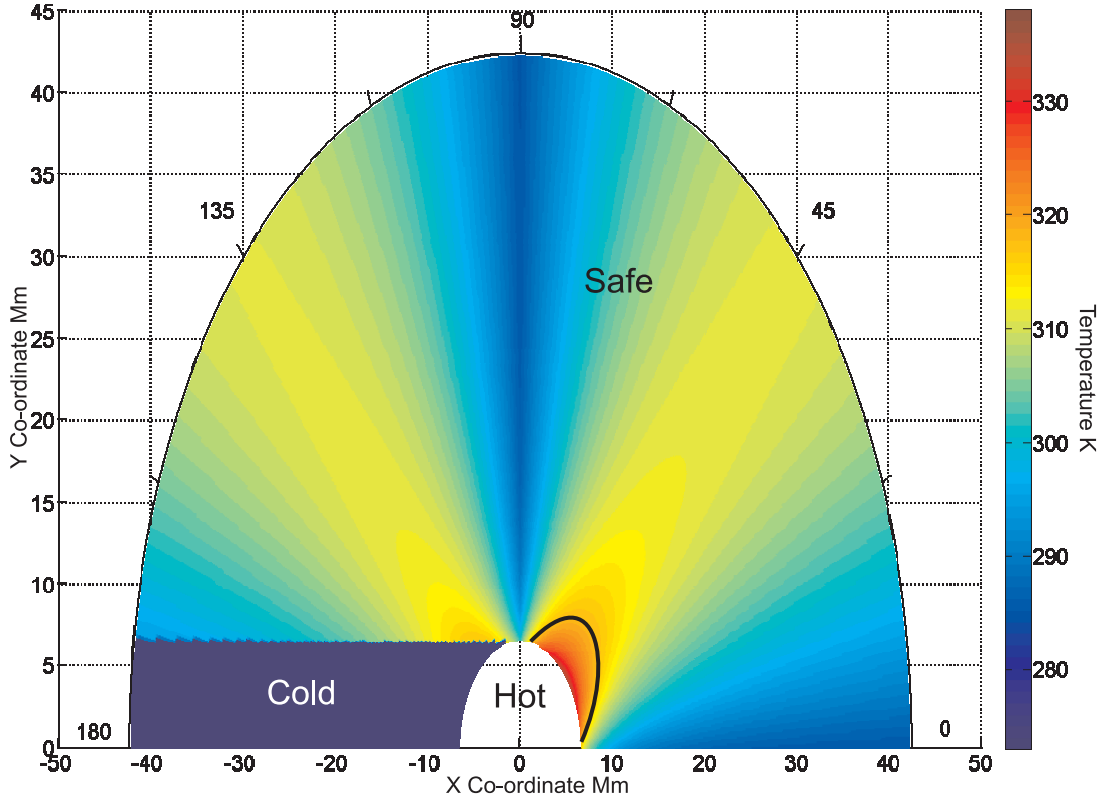

Figure 5.6: *Surface plot of the cold Earth pointing body mounting equilibrium temperatures. The colour map is in kelvin, with a lower limit of 273 to preserve the detail of the sunlit temperatures.*

5.3.2 Transient Results

The orbits used in the wing mounting are used for the Earth pointing body mounting. These orbits pass through the extremities of the environment, showing the boundaries of what will be encountered. The results are shown in fig. 5.7. The red dashed line is the upper boundary and the black dashed line is the lower boundary.

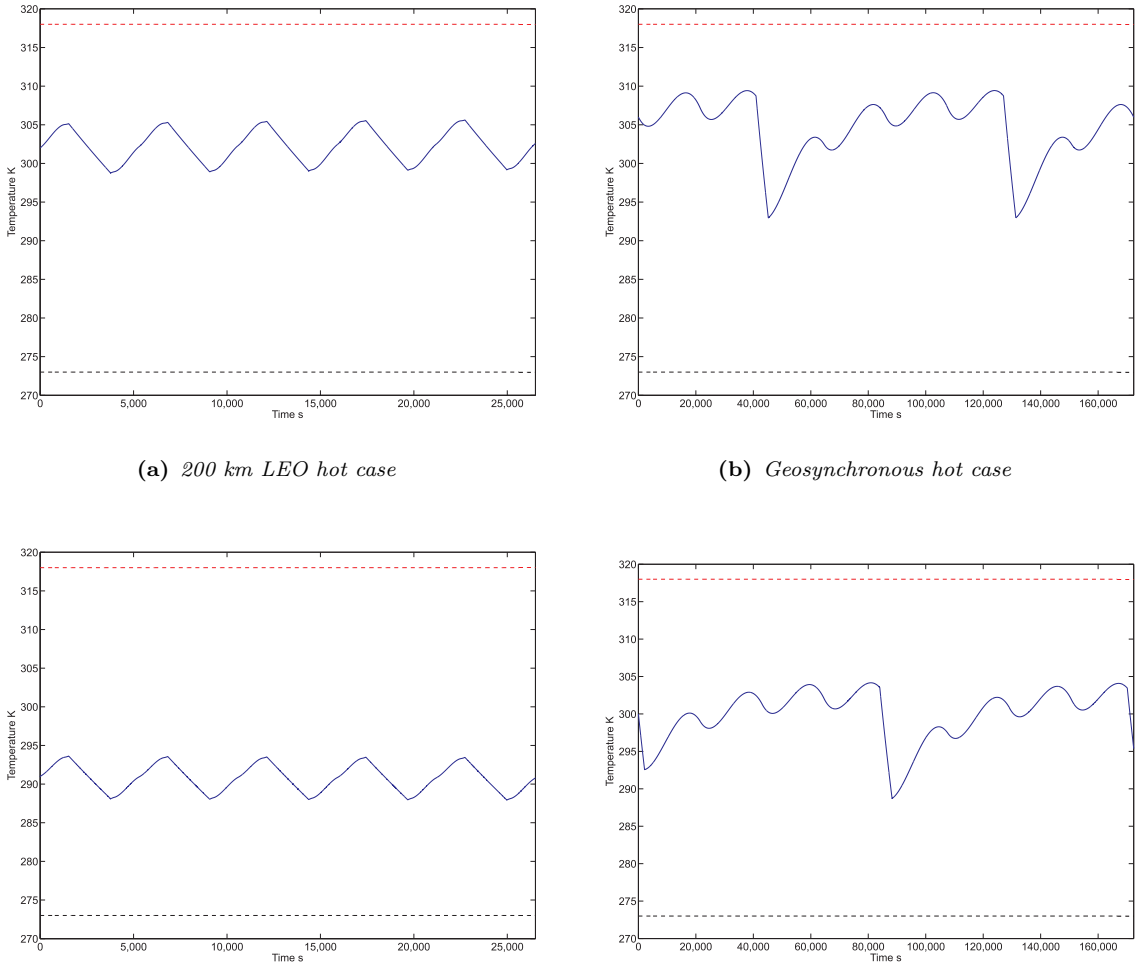

(a) *200 km LEO hot case*

(b) *Geosynchronous hot case*

(c) *200 km LEO cold case*

(d) *Geosynchronous cold case*

Figure 5.7: *Transient response of the Earth pointing body mounting.*

The effect of the different environments is small, resulting in changes of 10 K in LEO and 6 K in geosynchronous. The variation in the input from the Sun causes the difference in pattern from the wing mounting results. In geosynchronous orbit the spacecraft spends longer in the sunlight and rotates (to maintain Earth pointing) at a much slower rate. It has the time to be affected by the changes in the Sun's input, showing cooling when the input reduces. The LEO passes much more swiftly through the sunlit region and rotates more swiftly as well. It does show some response, but it is overridden by the rapid warming after eclipse. This orbit does not allow time for the

spacecraft to warm up enough to be largely effected by its rotation.
As noted above, the model represents the average temperature of the whole system. As the spacecraft has 10 times the thermal capacity of the panels combined, this average temperature will likely be the temperature of the spacecraft. As the spacecraft provides such a large amount of added capacity, the results in fig. 5.7 show a reduction in the reaction of the model to changes in the environment. As such, in all orbits considered the temperature of the model is never unsafe. More specifically, the temperature of the spacecraft is never unsafe. More detailed modelling is required to determine the temperature of the individual panels.

5.3.3 Variations of the Body Mounting

For brevity, the figures relating to the results of modelling the variations of the body mounting are located in appendix B.1. In the three panel variation removing the Earth facing panel has the effect of reducing the input from the Earth as the MLI reflects the incoming radiation. As such, while the results follow the same pattern as the four panelled Earth pointing, the temperatures are cooler with fewer orbits having issues with overheating. The Sun and space pointing variations have a different equilibrium temperature pattern to the Earth pointing variations as they maintain a constant incident area to the Sun's input. This makes their results similar to the wing results, with the overheating region centred over the sub-solar point. The Sun pointing case presents a smaller area to the Sun than the Earth pointing and is thus cooler, with fewer orbits having overheating. By contrast,the space pointing variation presents a larger surface area to the Sun and is thus hotter, with more orbits now suffering from overheating. Eclipse causes the equilibrium temperature to be too cold in all cases. Like the four panel Earth pointing variation, the high thermal inertia of the model prevents the battery temperature from becoming unsafe in the transient results of all the variations.

5.4 Recommendations from the Isothermal Model

The equilibrium results of the wing model predicted that eclipse would be too cold and there would be a region in LEO that is too hot. Orbits with high β angles[5.3] would not

[5.3]The β angle is the angle between the plane of the orbit and the Earth-Sun vector.

enter these regions and thus a range of orbits is defined where thermal control may not be required. The transient results of the wing mounting revealed that in both hot and cold environments, the hostile regions could be reduced. Orbits where the eclipses are shorter than the time it takes the panel to overcool may not need thermal control. Overheating in a cold environment was shown to not occur. The range of orbits where overheating occurs in the hot environment was reduced. Thermal control for the wing mounting should thus focus on maintaining the battery temperature during eclipse in the cold environment and avoiding overheating in the hot LEO case.

The steady state isothermal model of the body mounting predicted that regions of overcooling and overheating, in similar patterns to the wing model for all variations. The high thermal inertia of the spacecraft resulted in the model reacting slowly to the changes in environment and maintaining safe temperatures in all conditions except for the Sun pointing orientation in a cold environment, where it became too cold. As these results represent the temperature of the spacecraft and perhaps not the panels, thermal control for the body mounting could focus on keeping the temperature of the panels as close to the temperature of the spacecraft as possible, as the spacecraft temperature has been shown to be consistently safe.

For both mountings, the eclipse equilibrium temperature is further from the battery temperature envelope than the equilibrium sunlit temperature. Also, in the wing mounting transient results the minimum temperature is further from the safe envelope than the maximum temperature and the envelope itself exists at temperatures warmer than the average temperature of the wing results. The implication is that overcooling will be harder to prevent that overheating.

Chapter 6

Lumped Parameter Model

The isothermal model has provided data on the range of orbits that should not require thermal control. However, while it has identified which orbits do require thermal control of the battery temperature, the model is limited as a tool for modelling thermal control as it does not calculate nor model the internal heat flows and temperature distributions; required properties for accurate modelling of thermal control and its effects. The panels themselves are thin and will not experience a large temperature difference between surfaces, but the lack of detail is particularly important for the body mounted model where the presence of the spacecraft separates the panels and may lead to large temperature differences between panels and the spacecraft. Thus modelling of the MFPS applications in more detail is required and this chapter deals with the development and use of that model.

6.1 ThermXL

ThermXL is a spreadsheet based program that uses lumped parameters (LP) modelling, a software product of ALSTOM Power. The model is formed of nodes with heat flow paths defined between them. The nodes are used in four different ways. Boundary nodes are used to represent a surface, having the optical properties of that surface and interacting with the thermal environment. A fixed node is used to represent space. Mass nodes represent the mass and heat capacity of an amount of material. Interface nodes are used to allow the changing of conduction properties between materials.

6.1.1 Global Assumptions

- The panel is modelled as a set of layers, each layer is modelled by a conduction path with three nodes; a mass node to represent the mass of the layer and the heat capacity of the material that is conducting and an interface node at each end of the path. Interface nodes are shared between layers.
- Thus only heat flow through the panel is considered, not across it.
- The model does not consider how the cells are distributed throughout the core[6.1], only that they are of a consistent depth, as only the through properties of each layer are considered. As such, two 'paths' exist between the CFRP facesheets, one through honeycomb and one through the cells and the honeycomb between it and the facesheets.
- The solar cells are not modelled directly as they are too thin for the modelling software. The resulting conduction paths cause errors due to the large differences in orders of magnitude. The solar cells are thus treated as a smeared mass over the surface of the Sun side facesheet and their heat capacity and optical properties are added/applied to this facesheet.
- Radiation exchange inside the honeycomb is not modelled as it is 2 to 4 orders of magnitude smaller than the conduction heat flow. See appendix C.3 for further detail.
- Space is modelled as a node with a radiative connection to the boundary nodes. It has an emittance and view factor of 1 and is fixed at 4 K.
- Kirchoff's law [60] is used for radiation in the infrared range and it is assumed that the heat radiation given off by both the Earth and surfaces is in the infrared range. As such, when considering infrared radiation, the emittance is equivalent to the absorptance.
- No heat flow across the panels edges is considered, as aforementioned in section 4.2.
- No orbit perturbation is modelled as its effect is indirect (inputs are a function of position) and it would add unnecessary complexity
- Celestial bodies (ie the Earth and the Sun) are considered fixed to reduce complexity.

[6.1] Roberts et al. [33] has stated that distribution is required to reduce adverse effects on structural properties.

6.2 Wing Mounting Model

The wing model is composed of 13 nodes, 11 conduction paths and 2 radiation paths. A schematic diagram of the model is shown in fig. 6.1. The radiation paths link the boundary nodes 1 and 12 to the fixed space node 999. The Sun's radiation is incident on node 1. Albedo and Infra red radiation from the Earth is incident on the surface node that is facing the Earth; node 12 when the panel is between the Earth and the Sun and node 1 when the Earth is between the panel and the Sun. The cells are arranged 15 x 15 x 4 deep in the panel, shown in fig. 6.2, and are located at the centre of the honeycomb core; though it should be noted that this would be difficult to manufacture. All other properties as detailed in tables 4.1, 4.3 and 4.4.

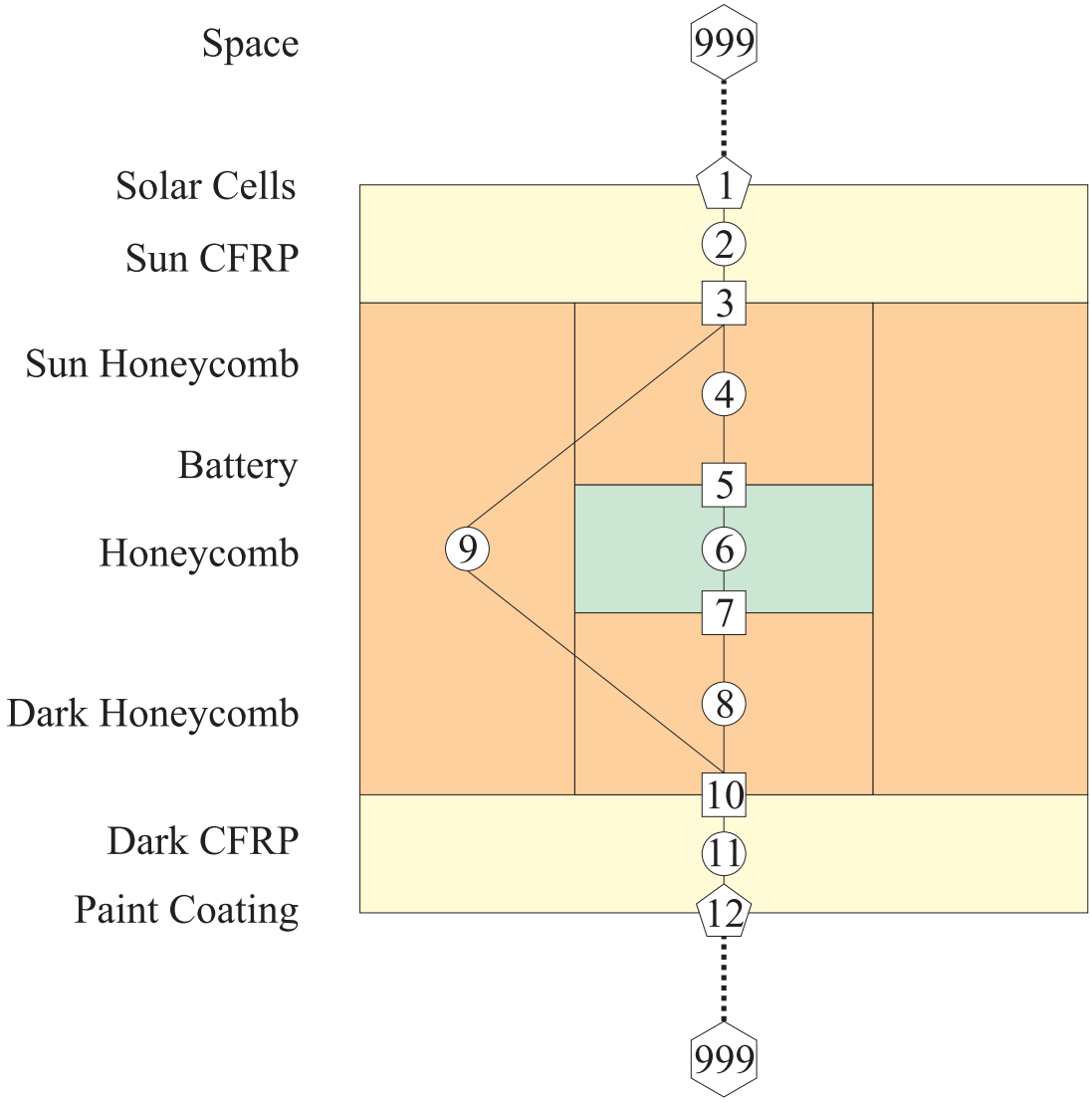

Figure 6.1: *Finite difference model of the wing mounted panel. Hexagons represent the fixed nodes, pentagons the boundary nodes, squares the interface nodes and circles the mass nodes. The battery represents all of the cells grouped together.*

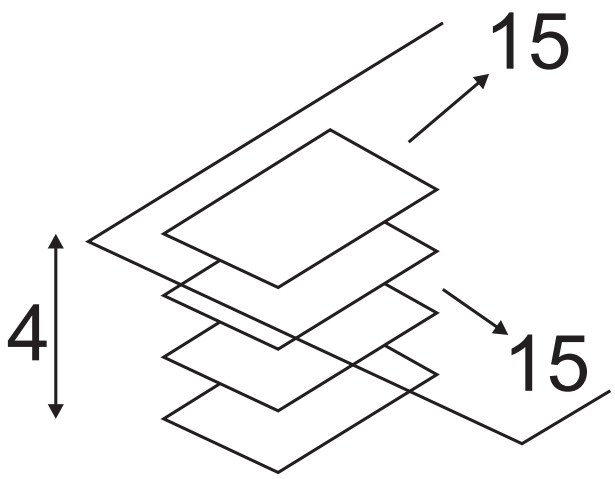

Figure 6.2: *Diagram of the arrangement of the cells in the panel.*

6.2.1 Steady State Results

The equilibrium temperature of the lumped parameter model is calculated at three positions in 200 km LEO and geosynchronous orbit for both hot and cold environments. The three positions are; 1) directly above the sub-solar point (SUN), 2) at a solar zenith angle of 90 degrees (BTW) and 3) in eclipse (ECL). These points represent the full range of heat inputs the panel will see. This is done to confirm the results against the isothermal model and to investigate the temperature difference across the panel at equilibrium.

These results show that when the wing panel is sunlit, a temperature difference of at most 3 K exists between the radiating surfaces. This is caused by the difference in the heating of the surfaces but the effect is reduced by the thinness of the panel allowing high heat flow between facesheets. The low temperature difference indicates that there is not currently a location in the panel where the battery could be placed to maintain its temperature within the envelope if the panel location was unsafe, as the temperature of the panel can be seen to be consistent. In eclipse the reduced difference in heat between surfaces reduces the temperature difference between the surfaces. The low temperature difference shows that there is no build up of heat in any layer or that any layer has been isolated from the heat flow, implying that the conduction of heat through the panel is high.

The predicted equilibrium temperatures of the battery when the panel is either sunlit or in eclipse and being warmed by the Earth show a good degree of agreement, table 6.2. The maximum difference is 0.3 K and the minimum 0.05 K. A greater difference between results in noted in GEO eclipse of several degrees, caused by the ThermXL

Table 6.1: *Equilibrium results of the finite difference model of the wing. Temperatures are in kelvin.*

Case / Node	Sun CFRP	Sun HC	Batt	Dark HC	HC	Dark CFRP
LEO HOT SUN	334.1	333.4	332.9	332.6	332.9	331.9
LEO HOT BTW	311.6	310.7	310.2	309.6	310.2	308.8
LEO HOT ECL	215.5	215.3	215.2	215.0	215.2	214.8
LEO COLD SUN	325.1	324.5	324.0	323.6	324.0	323.0
LEO COLD BTW	305.9	305.1	304.5	304.0	304.5	303.2
LEO COLD ECL	206.5	206.3	206.2	206.1	206.2	205.9
GEO HOT SUN	312.2	311.4	310.8	310.3	310.8	309.4
GEO HOT BTW	311.6	310.7	310.2	309.6	310.2	308.7
GEO HOT ECL	88.7	88.6	88.6	88.6	88.6	88.6
GEO COLD SUN	306.4	305.6	305.1	304.6	305.1	303.8
GEO COLD BTW	305.9	305.1	304.5	304.0	304.5	303.2
GEO COLD ECL	86.2	86.2	86.2	86.2	86.2	86.2

software. At very low temperature, the heat flow between the layers of the model and between the model and the environment leads to very small changes in the temperature of the nodes. Unlike the isothermal model which calculates the equilibrium temperature directly, ThermXL uses an iterative method, which has a convergence criteria that is easily triggered by the small changes at low temperature. However, as the temperatures predicted are over 150 K below the safe range, the difference has no real effect. Thus the isothermal model can be said to predict the temperature in the middle of the panel, which due to the geometry is the battery temperature. As such, the equilibrium results in section 5.2.1 can be considered true for the lumped parameter wing model. It can also be said that the correlation between the methods validates both methods.

6.2.2 Transient Results

The same orbits, 200 km LEO and Geosynchronous, used for the isothermal transient model are used to investigate the transient response of the lumped parameter model, section 5.2.2 details the reasoning. This is done to look at how the presence of temperature differences across the panel effects the battery temperature and to again correlate the results with the isothermal model.

The results, figs. 6.3 to 6.6, correlate well with the isothermal model and follow the

Table 6.2: *A comparison of the equilibrium temperatures predicted by the lumped parameter and isothermal models of the wing mounting. Temperatures are in kelvin.*

Case	LP Batt Temp	Iso Batt Temp	Temp Difference
LEO HOT SUN	333.0	332.8	0.2
LEO HOT BTW	310.2	310.0	0.2
LEO HOT ECL	215.1	215.1	0.0
LEO COLD SUN	324.0	323.8	0.2
LEO COLD BTW	304.5	304.3	0.2
LEO COLD ECL	206.2	206.1	0.1
GEO HOT SUN	310.8	310.5	0.3
GEO HOT BTW	310.2	309.9	0.3
GEO HOT ECL	88.6	85.0	3.7
GEO COLD SUN	305.1	304.8	0.3
GEO COLD BTW	304.5	304.3	0.2
GEO COLD ECL	86.2	81.5	4.7

pattern of the results presented by Li et al. [36]. The panel overcools when in eclipse, the temperature of the battery in the lumped parameter model matching that of temperature predicted by the isothermal model. Thus the wing lumped parameter model can be said to be a good representation of the reaction of the wing mounted panel to its environment.

The temperature difference across the panel seen in the equilibrium results when the panel is sunlit is present and to the same degree. Once deprived of sunlight, the temperature of the panel rapidly equalises, reinforcing the implication made earlier that the conduction of the panel is high, as heat from the centre is lost as rapidly as it is from the surfaces.

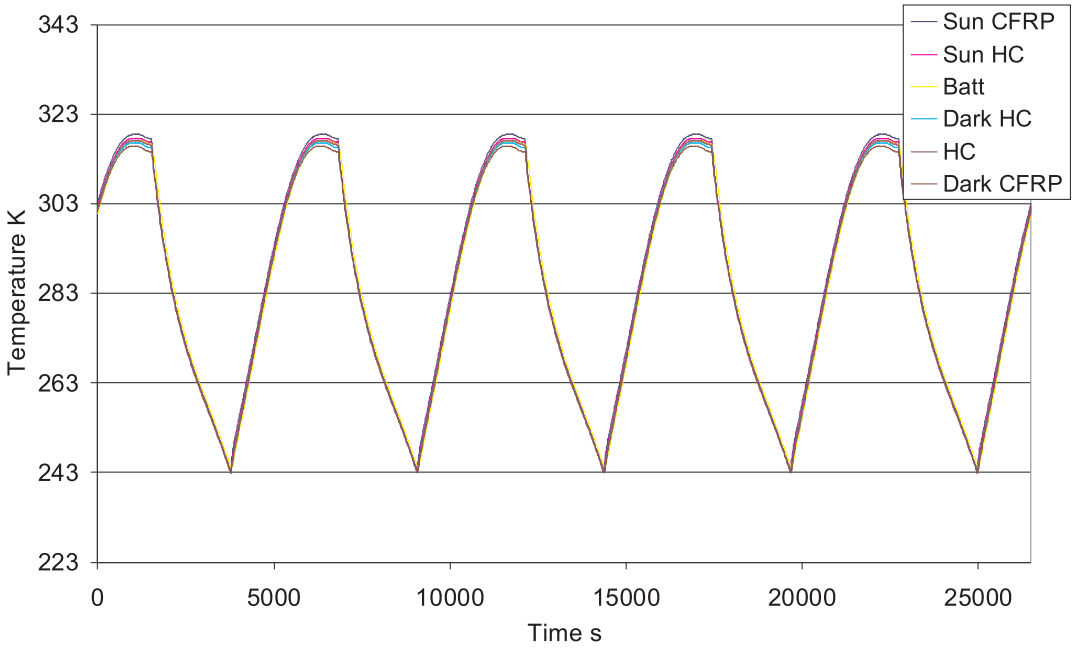

Figure 6.3: *Lumped parameter transient results of the wing panel in a hot LEO case.*

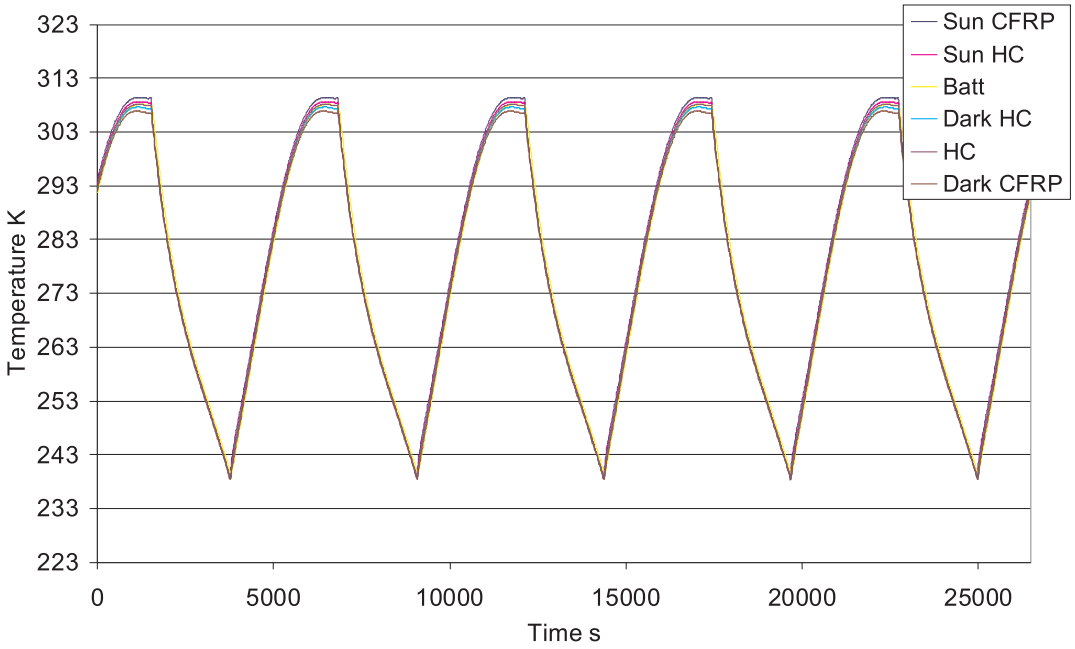

Figure 6.4: *Lumped parameter transient results of the wing panel in a cold LEO case.*

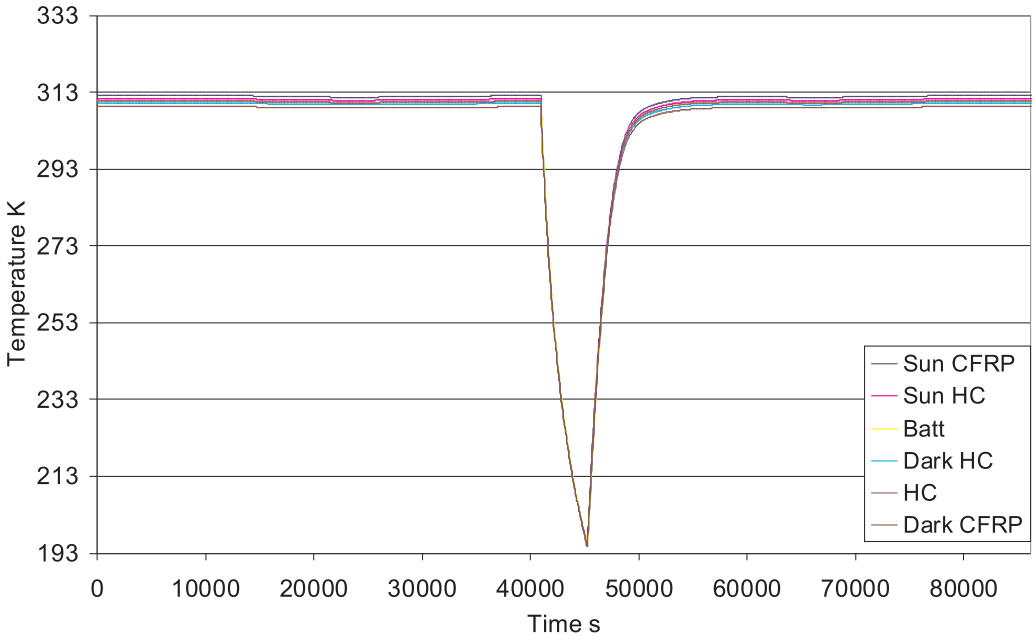

Figure 6.5: *Lumped parameter transient results of the wing panel in a hot GEO case.*

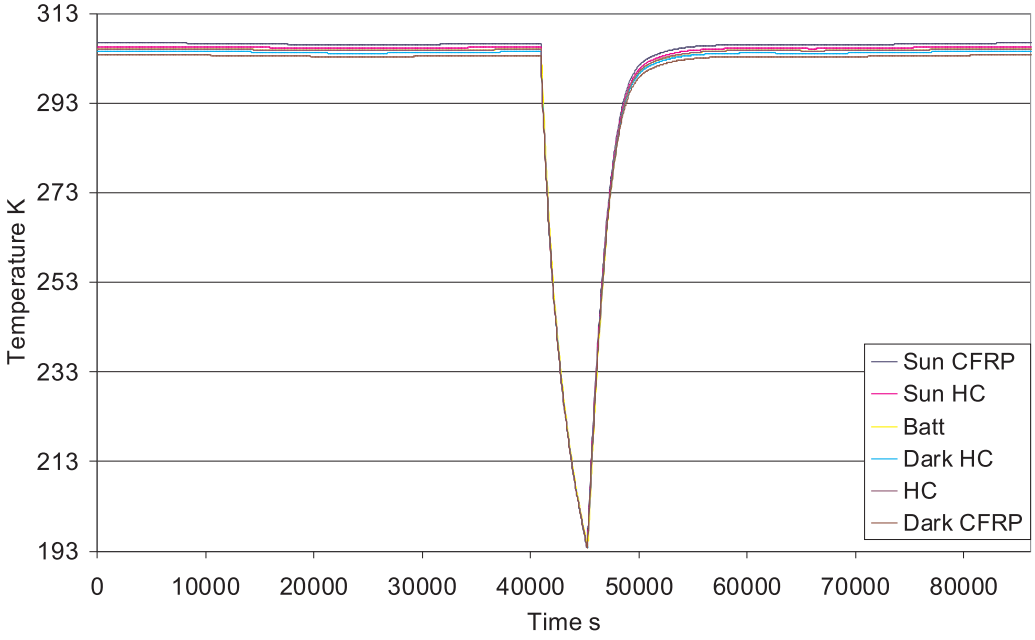

Figure 6.6: *Lumped parameter transient results of the wing panel in a cold GEO case.*

6.3 Body Mounting Model

The body mounting uses the same basic panel as the wing mounting model. Four of these panels are linked to a central node that represents the heat capacity of the spacecraft; fig. 6.7 shows the nodes used and the heat flow paths. The panels are linked to the spacecraft via a conductive path that represents the connectors and by a radiative link between the coated surface of the panel and the facing spacecraft surface. Each panel contains 5 x 5 x 4 cells. The MLI covered surfaces of the spacecraft are modelled as radiative links from the spacecraft node to the fixed space node. As the spacecraft is orientated so that only the solar panels receive inputs, section 4.1, the inputs from the Sun and the Earth are only on the nodes representing the solar cells. For the Earth pointing model, the Earth albedo and infrared are always on node 301 while the Sun's input moves between boundary nodes over the orbit. All other properties as detailed in tables 4.1, 4.3 and 4.5.

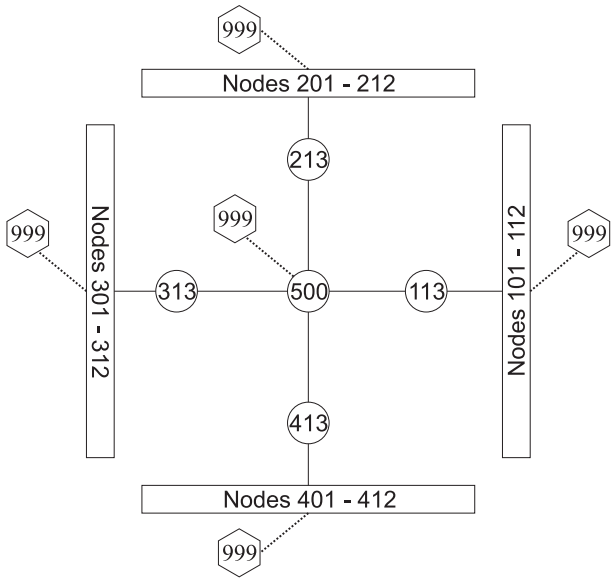

Figure 6.7: *Finite difference model of the body mounting. Hexagons represent the fixed nodes and circles the mass nodes. The panel nodes are not shown.*

The spacecraft is modelled as a single lumped mass to avoid constraining the results to a particular spacecraft design. This will affect how heat flows between the panels. On a real spacecraft, heat from a sunlit panel would warm the local area the connector was attached to. This heat would then distribute to the rest of the spacecraft mostly via the structure which in turn would warm the other panels. Thus in reality, a conduction path exists between the panel connectors and the heat would not be equally distributed in the spacecraft. In the model, the point spacecraft cannot have any conduction paths so

the heating of the spacecraft by the panel has an instant effect on the spacecraft temperature, speeding heat flow. Conversely, the model lumps the heat capacity of the spacecraft so that all the heat is distributed for warming all the spacecraft before a temperature rise occurs, whereas heat in the real spacecraft would perhaps reach the panels before it reached all of the spacecraft, particularly in a high conduction metallic structure.

6.3.1 Steady State Results

The equilibrium temperature of the lumped parameter model is calculated at four positions in 200 km LEO and geosynchronous orbit for both hot and cold environments. The four positions are; 1) directly above the sub-solar point (SUN), 2) at a solar zenith angle of 45 degrees (45Z), 3) at a solar zenith angle of 90 degrees (BTW) and 4) in eclipse (ECL). 3 sunlit positions are considered rather than two as due to the rotation of the spacecraft to maintain Earth pointing there are more possible illuminations due to the increased number of surfaces that are illuminated. The wing mounting results have shown that the temperature difference across the panel is small. Hence only the battery temperatures and the temperature of the spacecraft are considered.

The temperature of a panel, and thus the battery inside it, is dependent on its illumination and the temperature of the spacecraft. In all cases, when a panel is illuminated by the Sun, it becomes too hot. When not lit by the Sun, panels will overheat if the spacecraft temperature is too high or if they receive a large input from the Earth, panel 3 suffering most from this as it faces the Earth. In LEO orbit, this input is enough to prevent overcooling occurring outside of eclipse. In GEO the lack of Earth input allows the shadowed panels to overcool, with the spacecraft also cooler. The temperature of the spacecraft varies with the illumination of the system, being warmer when more heat is available.

The results in tables 6.3 and 6.4 show that there is a clear difference between the temperatures of the battery and the spacecraft. The temperature difference is such that there are no equilibrium locations where all the battery temperatures are inside of the envelope. The isothermal model also under predicts the temperature of the spacecraft, which was assumed to match the system temperature calculated by the isothermal model. The likely key cause of this is the variation in the temperature of the panels, which are 4 of the 6 radiating surfaces for the spacecraft. As the isothermal model does

Table 6.3: *Equilibrium results of the lumped parameter model of the Earth pointing body mounting in LEO with the temperature difference between battery and spacecraft in parenthesises. Temperatures are in kelvin.*

Node	Battery 1	Battery 2	Battery 3	Battery 4	Spacecraft
LEO HOT SUN	358.9 (12.6)	323.5 (-22.8)	337.3 (-9)	323.5 (-22.8)	346.3
LEO HOT 45Z	355.0 (-3.3)	331.9 (-26.4)	341.1 (-17.2)	361.6 (3.3)	358.3
LEO HOT BTW	288.3 (-25.4)	293.2 (-20.6)	300.9 (-12.9)	342.0 (28.2)	313.8
LEO HOT ECL	202.9 (-8.7)	210.5 (-1.2)	222.5 (10.8)	210.5 (-1.2)	211.7
LEO COLD SUN	342.1 (17.6)	303.3 (-21.2)	313.3 (-11.2)	303.3 (-21.2)	324.4
LEO COLD 45Z	342.7 (-0.6)	317.8 (-25.5)	325.3 (-18)	347.6 (4.3)	343.3
LEO COLD BTW	282.7 (-24.2)	287.0 (-19.9)	293.7 (-13.2)	334.1 (27.2)	306.9
LEO COLD ECL	195.5 (-7.6)	202.1 (-1)	212.6 (9.5)	202.1 (-1)	203.1

not represent these panels, it cannot accurately determine the heat loss from the spacecraft. This shows that the isothermal model is not accurate and its results cannot be used to determine thermal control requirements. The lack of safe equilibrium positions indicates that there are no safe equilibrium orbits and that transient modelling is required to identify if any orbits are safe without thermal control.

6.3.2 Transient Results

As with the wing mounting, 200 km LEO and geosynchronous orbits in both hot and cold environments are studied. The results are shown in figs. 6.8 to 6.11. The transient results will also reveal how the temperature of the spacecraft is affected by the changing illumination and temperature of the panels.

Table 6.4: *Equilibrium results of the lumped parameter model of the Earth pointing body mounting in GEO with the temperature difference between battery and spacecraft in parenthesises. Temperatures are in kelvin.*

Node	Battery 1	Battery 2	Battery 3	Battery 4	Spacecraft
HOT SUN	327.0 (30.9)	273.9 (-22.2)	274.6 (-21.4)	273.9 (-22.2)	296.1
HOT 45Z	332.2 (7.1)	297.5 (-27.6)	298.0 (-27.1)	332.2 (7.1)	325.1
HOT BTW	273.5 (-22.1)	273.5 (-22.1)	273.8 (-21.7)	326.7 (31.1)	295.6
HOT ECL	76.1 (-0.2)	76.1 (-0.2)	76.8 (0.5)	76.1 (-0.2)	76.2
COLD SUN	320.5 (29.7)	269.6 (-21.2)	270.1 (-20.7)	269.6 (-21.2)	290.8
COLD 45Z	326.3 (6.8)	293.0 (-26.5)	293.3 (-26.2)	326.3 (6.8)	319.5
COLD BTW	269.4 (-21.2)	269.4 (-21.2)	269.7 (-20.9)	320.4 (29.8)	290.6
COLD ECL	73.6 (-0.1)	73.6 (-0.1)	74.2 (0.4)	73.6 (-0.1)	73.7

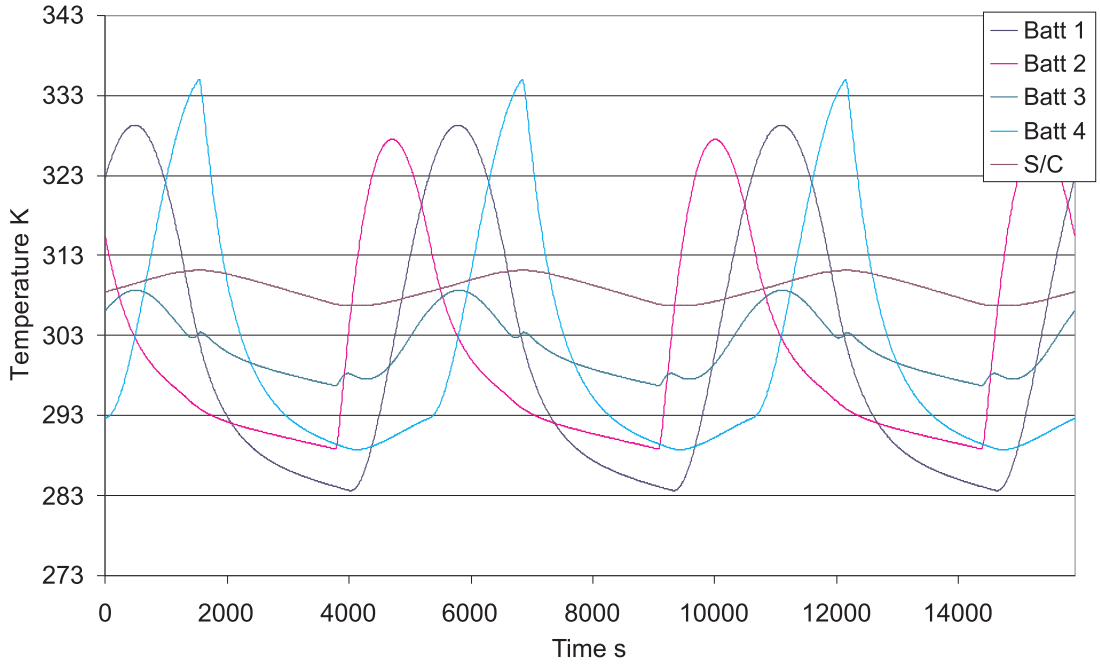

Figure 6.8: *Lumped parameter transient results of the Earth pointing body mounting in a hot LEO case.*

The transient results confirm the presence of large temperature differences across the system, as predicted by the equilibrium model. When in shadow, the panels assume a temperature that is about 20 K cooler than that of the spacecraft. When sunlit, they heat rapidly at a rate similar to the wing model as it exits eclipse. The spacecraft temperature varies little due to its high thermal inertia compared to the panels and its variations match with the variations in the net input of energy on the panels; increasing when two panels are being illuminated.

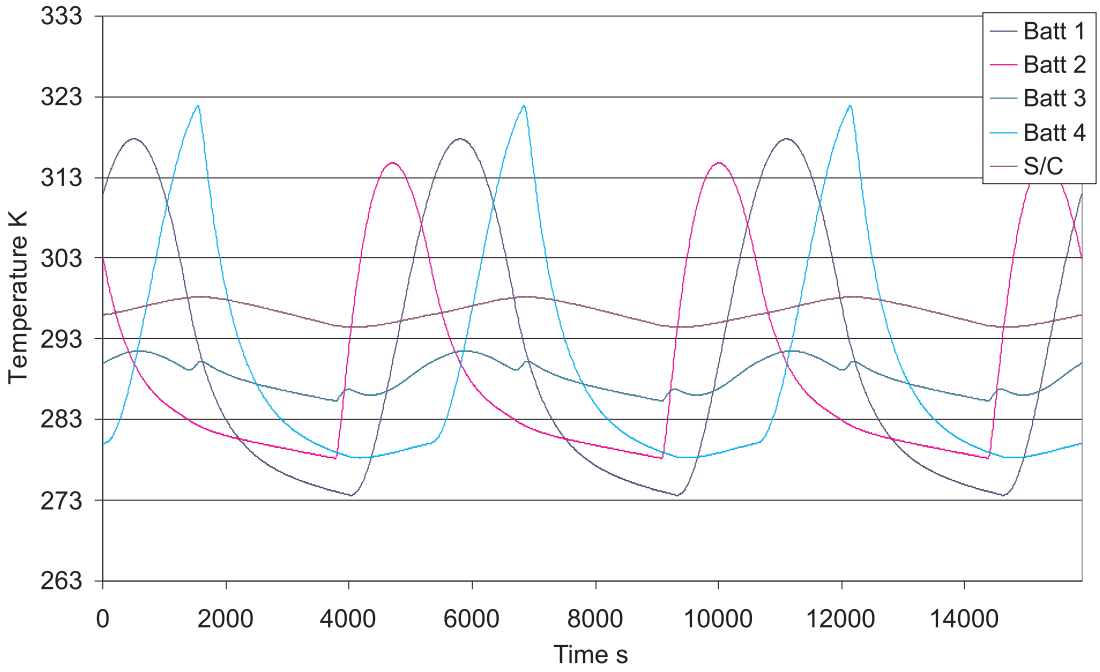

Figure 6.9: *Lumped parameter transient results of the Earth pointing body mounting in a cold LEO case.*

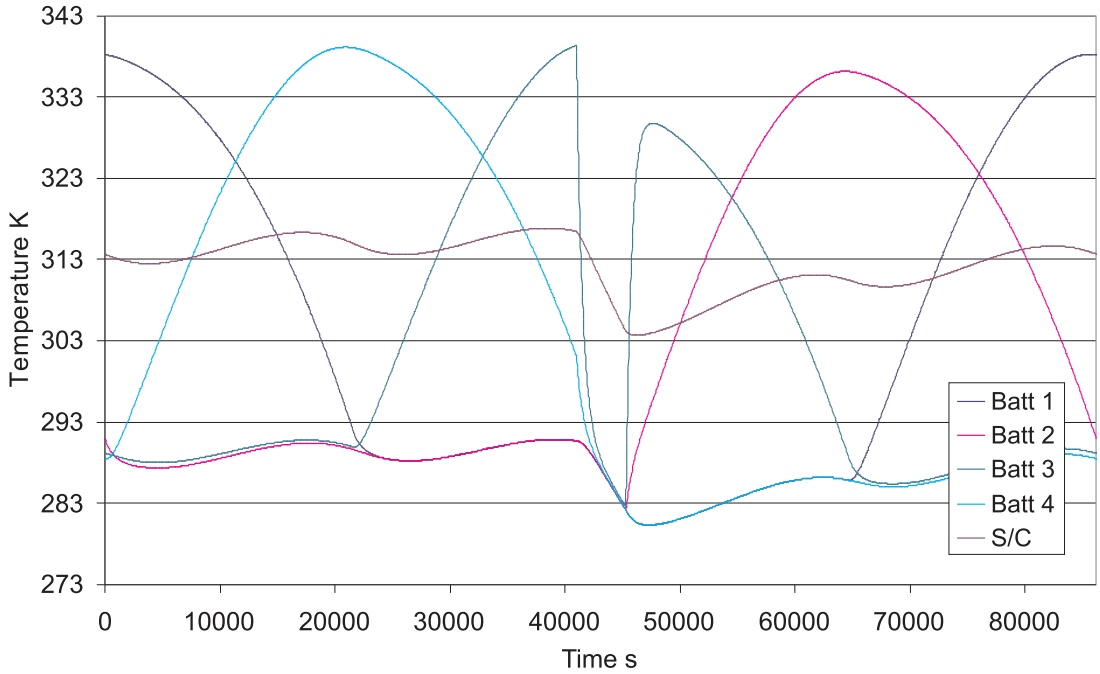

Figure 6.10: *Lumped parameter transient results of the Earth pointing body mounting in a hot GEO case.*

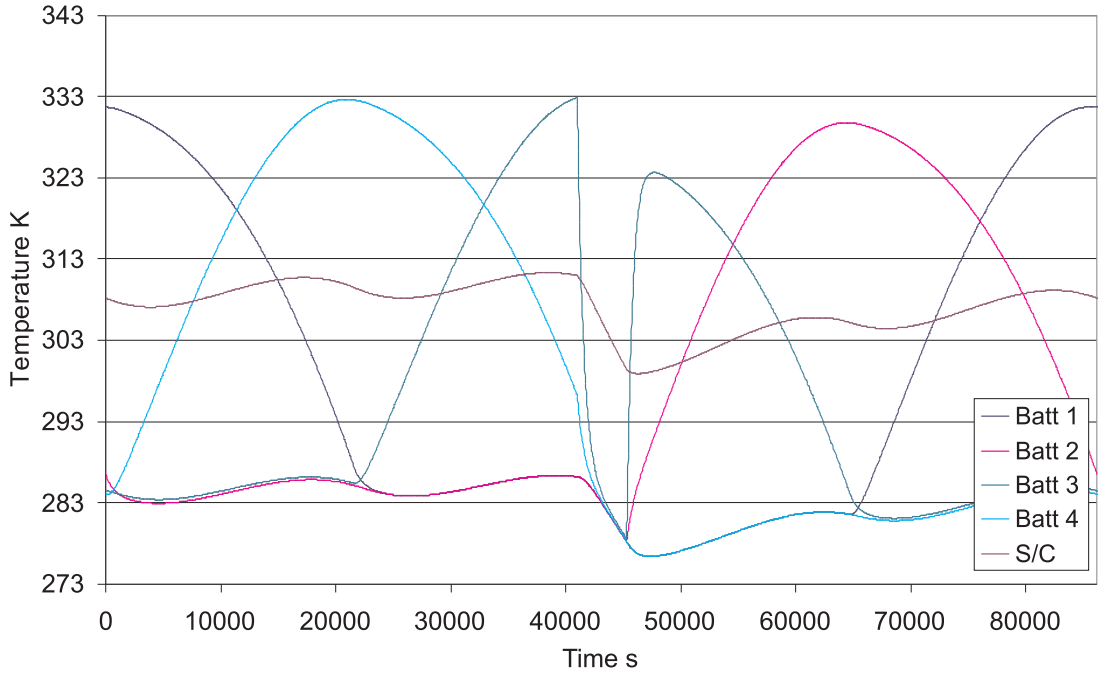

Figure 6.11: *Lumped parameter transient results of the Earth pointing body mounting in a cold GEO case.*

In LEO, the panels are hottest when they are sunlit, after which they cool to a temperature below that of the spacecraft when in shadow. Panel 4 is the warmest as the temperature of the spacecraft is highest and thus the panel loses less heat to the spacecraft. Panel 1 is the coldest as while it spends less time in shadow that panel 2, it gets no heat from the Earth. Panel 3 (the Earth facing panel) does not follow the pattern of the other panels. This is because the system enters eclipse before it can be warmed by the Sun. Close inspection of the LEO results shows that just before and after eclipse, the Earth facing panel experiences a small increase in temperature when sunlight does fall upon it. The Earth facing panel also does not become as cold as the other panels as it is warmed by the Earth's input. The consistent levels of heat from the Earth infra red are complimented by the presence of the Earth albedo on the sunlit side of the Earth, causing the variation in the Earth facing panel's temperature.
In geosynchronous orbit, the spacecraft is warmer as the system spends much more time sunlit compared to time in eclipse, allowing it to warm to greater temperatures. All of the panels overheat in the Sun in both cases and overcooling is not an issue, as the minimum temperature is 3 K above the lower boundary. Panel 4 is the warmest as the temperature of the spacecraft is highest and thus the panel loses less heat to the spacecraft. Panels 1 and 4 are the coldest as they do not experience any sunlight after eclipse and continue to cool in shadow. The temperature of the panels when shadowed

follows the variations of the spacecraft temperature. In this orbit, panel 3 follows the pattern of the other panels and eclipse only provides a brief interlude in its warming. It is important to note that as soon as the panel loses its sunlight, its temperature plummets to that of the other shadowed panels; another indication of the low thermal inertia of the panels. The spacecraft also experiences a large temperature drop during eclipse. This temperature drop and panel 3's pattern matching the other panels is because at this altitude there is no input from the Earth.

The thermal control requirement of the panels varies with altitude. In low orbits, the eclipse proportion is high and the sunlit time low. As such, the panels receive less heat and thus do not have enough heat stored to survive eclipse. With increasing altitude, the eclipse proportion decreases and the sunlit time increases. The increase in heating and the reduction in cooling raises the temperatures of the system. When at geosynchronous altitude, the heating is now such that the panels overheat. The implication thus exists that there will be altitudes where the battery temperature is always with its envelope. The temperature of the spacecraft is always safe, its high inertia prevents it from 'overreacting' to the changes the environment. It takes a large amount of energy to warm it and it has so much energy, it cools very slowly. Thus the target of thermal control is solely the panels.

6.3.3 Body Mounted Variations

Further details of the variations can be found in appendix B.2. The three panel variation results follow the same pattern as the four panel body mounting. The key difference is that the presence of the MLI on the Earth facing side reduces the inputs from the Earth and reduces heat loss from the spacecraft. With this warmer spacecraft overheating is increased. For the Sun pointing variation, where one panel is permanently sunlit, a consistent and stable temperature variation exists across the system. Having only one panel sunlit reduces the heat input in to the system, causing it to be cooler, reducing the overheating of the sunlit panel. The space pointing orientation has the incoming sunlight spread across two panel, so that the overheating of these panels is reduced. However, the system receives a greater heat input, leading to a higher spacecraft temperature which increases overheating.

6.4 Summary of Lumped Parameter Model

The lumped parameter model has revealed the temperature difference that exists across the wing mounted panel is small, which indicates that there is no heat build up in the panel. These results matched well with the isothermal model, reinforcing the conclusions of that model. The thermal control requirements of the wing mounted panel remain unchanged at preventing overcooling in eclipse and overheating above the subsolar point.

Table 6.5: *Maximum and minimum temperatures encountered in the transient lumped parameter model.*

Case	Maximum	Minimum
Wing LEO Cold	308.1 K	239.5 K
Wing LEO Hot	317.1 K	244.1 K
Wing GEO Cold	305.1 K	194.1 K
Wing GEO Hot	310.9 K	195.2 K
Earth Pointing Body LEO Cold	325.4 K	280.1 K
Earth Pointing Body LEO Hot	339.3 K	290.5 K
Earth Pointing Body GEO Cold	332.9 K	276.4 K
Earth Pointing Body GEO Hot	339.3 K	280.3 K

The lumped parameter model of the body mounted panels shows the isothermal model was too simplistic as it did not predict the large temperatures differences that exist between panels and spacecraft. The lumped parameter model revealed that the panels can become too hot when sunlit and that shadowed panels may become too cold. As the temperature of the spacecraft was found to be safe in most cases, thermal control should work towards bringing the panel temperatures closer to that of the spacecraft or to protect the battery from the temperatures changes the panels experience. The temperature differences across the system showed that there were no equilibrium conditions where all of the battery temperatures were safe and that thermal control would be required in all orbits. The panel temperature was found to be dependent on Sun illumination but unlike the wing mounting, loss of illumination from the Sun was not caused by eclipse alone, but also by the rotation of the spacecraft. To summarise, table 6.5 shows the maximum and minimum temperatures encountered by the wing and the Earth pointing model in the transient LP model.

Chapter 7

Review of Thermal Control

The previous chapters have shown that the thermal properties of the baseline design of the MFPS applications (for example; the heat exchange with the environment, the thermal inertia and the internal heat flow) are not sufficient to maintain a safe battery temperature in all orbits. Thus, a local thermal control method must be added to the design. To state explicitly, the objective of the local thermal control is to prevent the battery exiting its temperature envelope. There are many methods of thermal control which are assessed in this chapter as to how they solve the problem and the potential viability of that solution.

7.1 Thermal Control Requirements

The viability of a solution is determined by how well the thermal control solution meets its requirements beyond maintaining battery temperature. MFPS provide a mass saving to the spacecraft design and through this the potential for a cost saving to the mission. The requirements of the thermal control are based on avoiding the overriding of these benefits. A thermal control system that meets these requirements will be a viable one.

Feasibility The thermal control system is required to maintain the battery temperature within a given envelope. It is preferred that one solution should prevent both overheating and overcooling and it is further preferred it should do so without alteration of its properties each orbits as the focus shifts from overcooling in eclipse to overheating in sunlight.

Mass The most direct requirement is that of mass which must be kept to a minimum. As the benefits of MFPS are realised through the mass saving, the mass of the

thermal control system should be as low as possible. Extra mass, particularly when added to the wing array mounting, lowers the structural resonant frequency, which may require additional structure to stiffen. A heavier solar array will perhaps require a stronger deployment mechanism and support structure. Mass is the key requirement and the viability of the TCS will be determined by how much of the MFPS mass saving it uses before the other requirements are considered. TCS and variations with lower masses are thus preferred.

Size The size of the thermal control solution is limited so that it will fit into the panel and leave room for battery and structure.

Complexity Complexity (moving parts, large numbers of parts, computer control) causes two problems. Firstly the more complex a system is, the greater the reliability issue. As such, complex systems are less reliable or require extra complexity or redundancies to maintain a given reliability. Secondly greater complexity results in a longer and more difficult design process, the cost of which may outweigh the MFPS benefits.

Power The need of the TCS for electrical power. This is an increase in complexity and will most likely require additional power generation and power storage, both mass increases.

Cost The direct financial cost of the system; the cost of design, manufacture and assembly should be low.

Support Support defines whether the system requires components in the main body of the spacecraft or an active control. The support requirement is a component of the complexity.

Effects The negative effects of the thermal control method on the functionality of the MFPS should be kept to a minimum. This mostly refers to the effect of including the TCS in the sandwich panel at the expense of the core, which may reduce the stiffness of the panel. It is unlikely that the TCS will have much effect on the power storage function.

7.2 Thermal Control Technologies

This section presents a short review of current thermal control technologies to introduce each method and provide a brief qualitative appraisal of their capabilities and performance that is specific to this application.

7.2.1 Optical Properties

This refers to altering the optical properties of the surfaces so that the amount of energy that is reflected, absorbed and emitted is changed. The two characteristics in question are the absorptance (α) and the emittance (ϵ). The absorptance determines the amount of radiation that is absorbed by a surface. The emittance determines the amount of radiation that is emitted by a surface. The absorptance and the emittance vary with the wavelength of the radiation and are equal for a given wavelength, according to Kirchhoff's law.

7.2.1.1 Coatings

In the realm of spacecraft design, absorptance is quoted for the range of highest output of the solar spectrum[7.1]. As spacecraft operate at temperatures around room temperature they emit in the infra-red spectrum and the emittance is quoted for these wavelengths. As these two spectral ranges do not overlap, the radiative input and output of a surface can be selected, with absorptance determining heat input and emittance heat output. Badari Narayana and Venkata Reddy [61] present an example of a satellite where the optical properties were key in the design of its passive TCS.
For the wing mounting, the placement of solar cells on one side of the panel limits the use of coatings to alter the optical properties to only the shadowed side of the panel. Though in shadow, the absorptance is of use as it determines the input from the Earth albedo. To prevent overheating the emittance is increased and absorptance decreased to improve energy loss and reduce albedo input. To prevent overcooling, emittance is reduced to lower heat loss and absorptance increased for greater albedo for a higher eclipse entry temperature. As noted in section 5.1.3, the emittance of a surface will also affect the input from the Earth IR.
However, the usefulness to the body mounting is more limited as the four surfaces that

[7.1] 0.4 to 0.6 μm [50]

interact with the thermal environment are solar cells and thus not available for alteration. The remaining two surfaces on the spacecraft could be used to alter the spacecraft temperature but not the panel temperature directly. Increasing the emittance of spacecraft surfaces may prevent overheating occurring at high altitudes. The emittance cannot be decreased further to prevent overcooling at low altitudes. The optical properties of the facing surfaces of the panel and spacecraft could be altered to affect the radiative heat exchange between them.
Adding a coating, either a surface treatment or a paint, is nearly an ideal solution as its mass is very low. Indeed, as a coating is always required to protect the CFRP facesheet, the added mass would be near zero. The size of this solution is negligible as it is external, there is no complexity, no support requirement and altering the coating has no effect on the structure or power storage. The hostile nature of the space environment, typically damage caused by ultra-violet light, atomic oxygen and particulates, causes the optical properties of most surfaces to vary over the lifetime of a spacecraft, with the effect dependent upon the material. Consideration of this factor is important as it could lead to the temperature of the battery becoming unsafe

7.2.1.2 Louvres

Louvres are a system where by the optical properties of a surface can be altered in flight. Louvres are used in situations where the optimum properties to avoid overheating and overcooling are conflicting. Some louvres also increase the radiating surface area. The altering of the optical properties is done through various mechanisms; passive thermal deformation, Hwangbo and Kelly [62], mechanical shutters, Domingo and Ramirez [63] and Micro-Electro-Mechanical System (MEMS) applications, Osiander et al. [64]. All of these solutions require adding mass to the system, with the mechanical system the heaviest and requiring the most additional support and control. Size is not an issue as the system is mounted to the outside of the panel. As louvres operate via movement to reveal a different optical coating, the complexity is potentially high and the reliability of the system comes into question.

7.2.1.3 Multi-Layer Insulation

Multi-Layer Insulation (MLI) consists of layers of Mylar or Kapton coated with silver or aluminium. These layers are opaque to radiation emitted by the room temperature

spacecraft and are insulated from each other by a polyester scrim. Thus radiation from the spacecraft surface is reflected back to it, with each layer emitting less heat for the next layer out to reflect back. MLI is used to greatly reduce the heat loss from a surface with effective emittances[7.2] of 0.02 achievable. MLI is also reflective to Albedo and Solar radiation (typically with an effective absorptance of 0.25), so it insulates the surface from the environment. Having more mass than a paint coating, MLI would only be used in cases where the emittance required to prevent overcooling is lower than that possible with a coating.

7.2.2 Conduction Modifiers

Conduction is governed by Eq. 7.1;

$$Q = \frac{kA_x}{x_k}\Delta T \tag{7.1}$$

where Q is heat flow (W), k is conduction (W/m^2), A_x is cross sectional area of the conductor (m^2), x_k is the length of the conductor (m) and ΔT is the temperature difference between the conductor ends (K). A_x, k and x_k can be represented by Eq. 7.2;

$$G_l = \frac{kA_x}{x_k} \tag{7.2}$$

where G_l is the linear conductance of the conductor, a property that represents all the physical properties of the conductor. A high linear conductance allows for a high heat flow.

Specific linear conductance is the linear conductance of a conductor per unit mass, Eq. 7.3

$$\frac{G_l}{Mass} = \frac{kA_x}{x_k}\frac{1}{A_x x_k \rho_k} = \frac{k}{x_k^2 \rho_k} \tag{7.3}$$

where ρ_k is the density of the conductor. As the conductor length is determined by the spacecraft and panel geometry, the best conductors have a high conductivity and low density and the parameter can be used to evaluate competing conductors.

7.2.2.1 Thermal Links

A thermal link is a connection of high conductivity between two components. A thermal link can comprise of either a dedicated component (a thermal strap) or the conduction

[7.2]The true optical properties of the MLI would be the properties of the outermost layer of the MLI. Naturally, using this value would not represent the insulating properties of the MLI. The effective optical properties thus represent the insulating effect of the MLI as if it were a coating.

properties of an existing structure can be altered to become a thermal link. Such a system would be used to alleviate heat build up or to improve heat flow to a cold component. As the temperature difference across the wing panel is very small and the panel is thin, improving the conductivity to the coated surface to increase heat flow to the surface for radiation will not have a significant effect against overheating. Improving heat distribution about the panel would similarly have no useful effect.
In the body mounted orientation where the panels have large temperature differences between each other and the spacecraft, improving heat flow from the lit panels would prevent overheating and improving heat flow to the shadowed panels would prevent overcooling. This could consist of adding thermal straps between the panels and the spacecraft or adjusting the conductive properties of the connectors. This is a low complexity, passive solution where low mass can be achieved through the use of highly conducting materials. The solution does not affect the panel nor require additional resources from the spacecraft.

7.2.2.2 Insulation

Insulation is effectively an opposite of a thermal link; a material of low conductivity is used to reduce heat flow. The most obvious application would be to wrap the cells in insulation, perhaps replacing the entire honeycomb core with a more insulating material. This reduction in the heat flow could prevent the battery from leaving its temperature envelope in both body and wing mountings. The determining factor is how much mass of insulating material is required and how much heavier than the honeycomb core the material is. The size of the insulation is a factor and will have effects on the structure if it is weak and replaces a large amount of core. Insulation is a simple solution and requires no additional support.

7.2.2.3 Thermal Switches

A thermal switch, like a louvre, is a compromise solution to conflicting requirements, where improved conduction is needed to prevent overheating yet unwanted during cooling. A thermal switch is a conductive connection between objects that can be deactivated, usually by movement to separate a pair of conducting surfaces. Above a given temperature an extra conduction path exists to prevent overheating and is removed below the given temperature to prevent overcooling. An example would include

a mechanical system, Wing and Cunningham [65], or a shape memory alloy (SMA) that contracts below a certain temperature, Krishnan et al. [66].
Considering just the panel, a thermal switch could be used in conjunction with insulation to add a path for rejecting heat during sunlight or to replace a thermal link that is not wanted during eclipse; connecting the battery to a radiator during sunlight and disconnecting during eclipse, such as used by Novak et al. [67]. For the body mounting as a whole a thermal switch could replace a thermal strap if temporary isolation of the panel is required.
If a simple passive switch is used (an SMA) the mass and size will be reduced compared to a complex mechanical system that would require support and take up much space. With good design and material properties no extra mass would be used compared to the thermal link or insulation replaced.

7.2.2.4 Heat Pipes

A heat pipe is an advanced form of thermal link. The internal structure of the heat pipe is shaped to allow the wicking of a fluid, the convective movement of which transports heat along the heat pipe, effectively improving the conduction. Heat pipes are used in spacecraft to aid dissipation of heat from high heat generating components to radiators, Bernardin [68]. They have also been adapted for use in a MFTS, Wirtz et al. [41].
Like thermal links, heat pipes have little use in the wing mounting. In the body mounting, they would be used to replace a thermal strap if the specific linear conductance was better or the strap did not provide enough conduction. The mounting of the heat pipe would have to be adapted to cope with the thermal stresses of the structure. The use of a simple passive heat pipe in this manner would have little effect on the panel and only mass and function need to be considered.

7.2.3 Phase Change Materials

Phase Change Materials (PCM) offer a more mass efficient way to increase the thermal inertia of a system than adding masses of material with a high specific heat capacity. When a material changes state (or phase) a large amount of energy transfer is required; for the transition between liquid and solid this is referred to as the latent heat of fusion[7.3]. For a solid to melt, the heat of fusion must be added to it and vice versa for

[7.3]Henceforth referred to as the heat of fusion.

freezing. While the material is changing state, its temperature remains fairly constant. This energy requirement can be exploited to reduce the temperature change experienced by placing a PCM in contact with a component as it provides a large boost to the heat capacity. Sharma et al. [69] provide an overview of current PCM technology.

PCMs have been used on spacecraft to damp the temperature change of intermittent use high heat output electronics, Kandasamy et al. [70]. Terrestrial applications include uses in houses such as heat tiles, Barbour and Hittle [71], where they are used to store thermal energy to reduce heating costs. In both the wing and body mountings, the battery could be surrounded by PCM and the heat of fusion used to damp the temperature change of the battery, preventing overheating and overcooling. PCMs have been used as thermal control for cells in terrestrial applications, Khateeb et al. [72], Mills and Al-Hallaj [73].

As PCMs are a simple passive system the two key requirements are mass and size. A high heat of fusion and a high density are required to minimise the mass and volume of the PCM. PCMs suffer a mass penalty as the liquid phase requires containment to stop it escaping. If the PCM is contained in a sealed section of the honeycomb core, the section may have to be reinforced against the expansion of the PCM. If an enclosure is used, it must be capable of carrying the loads of the core it replaces. Both of these options require space be left for the expansion of the PCM when it is liquid, an inefficiency. Polymer PCMs may be blended with another polymer to ensure it remains solid, examples by Krupa et al. [74], Kaygusuz and Sari [75], but the heat of fusion of the resulting composite is reduced as a fraction of it is no longer 'active' as a PCM. Another option to contain the PCM is by using microencapsulation, Liu et al. [76], where the PCM in encapsulated inside micro-scale balls of another material with a higher transition temperature. This method has produced better fractions of 'active' material but some of the material is still packaging.

7.2.4 Active Systems

Active thermal control technologies are one in which an electrical power supply is required. As this increases demand on the electrical power system (more battery capacity or solar cells required) they are unfavoured but are discussed for completeness.

7.2.4.1 Heaters

Heaters have been used on spacecraft for some time to maintain temperatures during eclipse and thus require extra battery capacity to operate. They would be mounted amongst the cells in the panel and used to add heat during eclipse, a feasible strategy for both mountings. They would have no effect on reducing overheating. While the mass and size of modern heaters is small as the heaters are in the form of patches, Schmidt [77], they are complex requiring control and investment in reliability. The mass of the extra cells is likely to be greater than the mass of the heaters.

7.2.4.2 Thermoelectric Heat Pump

A thermoelectric heat pump exploits the Peltier Effect to create a heat flow against the prevailing temperature gradient, Harpster et al. [78]. This requires the application of an electrical current to a solid state component. This would be used to pump heat to or from the battery as required. While the wiring and the device itself would not be heavy or large, the system is complex and would require control for optimisation and support from the spacecraft in terms of electrical power. The extra power would be a source of extra mass.

7.2.4.3 Pumped Fluid Loops

Essentially a plumbing system where the cells would be surrounded by a network of fluid containing pipes. This fluid is pumped around the network, being cooled or heated as required to maintain battery temperature. While perhaps the most effective, it is the most massive, most complex and requires significant support from the spacecraft, Bhandari et al. [79].

7.3 Thermal Control Technologies Summary

From this assessment, several thermal control technologies can be put forward for consideration. Heat pipes have been rejected as an individual solution and instead considered a subset of thermal links and may be considered if other technologies cannot supply the required conduction. The active systems Thermoelectric Heat Pump and Pumped Fluid Loops are also rejected as their complexity and added mass are deemed

to be too great, despite their potential effectiveness. Table 7.1 shows which thermal control solutions will be tested with which application.

Table 7.1: *Summary of potential thermal control applications.*

Thermal Control Technology	Deployed Wing	Body Mounted
Coatings	Y	Y
Louvres	Y	Y
Thermal Link	N	Y
Insulation	Y	Y
Thermal Switch	Y	Y
PCM	Y	Y
Heaters	Y	Y
Thermoelectric Heat Pump	N	N
Pumped Fluid Loops	N	N

Chapter 8

Thermal Control of the Wing Mounted Array

Several thermal control solutions have been identified as having application to the wing mounting. This chapter details the numerical modelling of these using the lumped parameter model. The solutions are here assessed for first their feasibility (a safe battery temperature maintained) and then for their viability. The viability is assessed primarily on how much mass is required for the thermal control system as this is the primary benefit of MFPS.

8.1 Optical Properties

8.1.1 Coatings

8.1.1.1 Emittance

The emittance of the coating on the shadowed side of the wing panel can be altered. Lower values will reduce the heat loss during eclipse and will reduce the Earth heat input when on the Sun side of the Earth. This will have the effect of decreasing the rate of temperature decrease in eclipse, extending the time between eclipse entry and overcooling occurring. The reduction in Earth heat input will reduce the maximum temperature of the panel. The reduction in maximum temperature will reduce the eclipse entry temperature, reducing the time to overcool.

Altering the emittance suffers from a conflict of design requirements. To improve the eclipse performance, a low emittance is required to reduce heat loss to avoid overcooling.

However this requirement is opposed by the need to prevent overheating which requires that the emittance (i.e. heat loss) be as high as possible. Lowering the emittance also reduces the IR input from the Earth which may cause cooling. To determine if a range of emittances exist which fulfills both of these requirements, the emittance of the panel was varied for a 200 km LEO and a geosynchronous orbit in both hot and cold environments, Figures 8.1 and 8.2, using the peak and nadir temperature once the results had settled into a consistent temperature pattern.

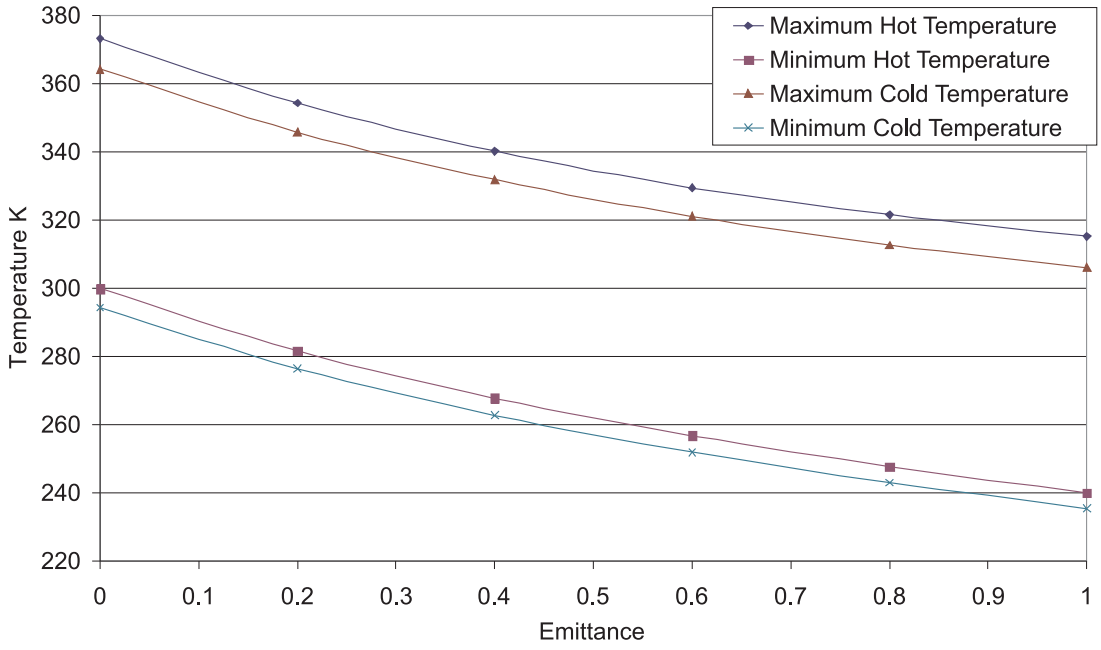

Figure 8.1: *The minimum and maximum temperatures of the battery against coating emittance in 200 km LEO for both environments.*

The results show the decrease in the battery temperature with increasing emittance, an indication that the reduction in heat input from the Earth is smaller than the decrease in heat loss. Table 8.1 shows the values of emittance that are required to avoid overheating and overcooling. In LEO, values of the emittance exist to avoid overheating and overcooling. Unfortunately, these limits do not overlap and as such there is not a range of emittance values which can be used to maintain a safe battery temperature. In geosynchronous orbit, the problem is worse as there are no emittance values that give a safe eclipse, though emittance values that ensure no overheating occurs are available.

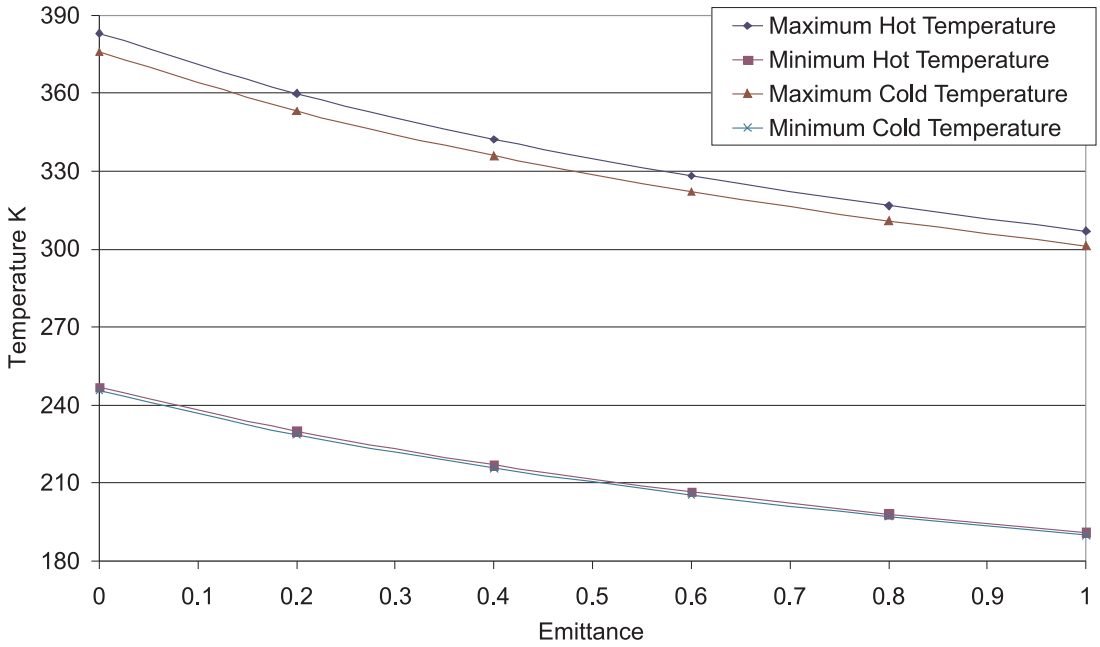

Figure 8.2: *The minimum and maximum temperatures of the battery against coating emittance in geosynchronous for both environments.*

Table 8.1: *The minimum and maximum values of emittance to prevent overheating and overcooling.*

Case	Minimum for overheating	Maximum for overcooling
LEO Hot	0.90	0.32
LEO Cold	0.66	0.25
GEO Hot	0.77	No Value
GEO Cold	0.66	No Value

Table 8.2: *Times to overcool for a panel with the minimum emittance to prevent overheating. Times in seconds.*

	Hot Environment	Cold Environment
LEO	917	1150
GEO	840	950

While no value of emittance exists to maintain a safe battery temperature in all orbits, selecting a minimum emittance to avoid overheating does allow some orbits to become viable. The maximum eclipse time is determined by the time it takes the battery to overcool with an emittance set to preventing overheating. This is defined as the time to overcool: table 8.2. The minimum emittance is directly affected by the environment, being lower in the cold cases and at higher altitude where there is less heat input.

8.1.1.2 Absorptance

The absorptance of the paint coating can be increased from the default to increase the amount of Earth albedo the panel absorbs. This will increase the maximum temperature of the panel and thus increase the eclipse entry temperature, though the effect will only be noticeable in low Earth orbits where the albedo flux is high. Figure 8.3 shows the variation of maximum and minimum temperature with absorptance. Unfortunately, there is no value of absorptance which prevents overcooling in eclipse. Indeed, the absorptance has very little effect on minimum temperature, indicating that there is little gain in the time taken to overcool.

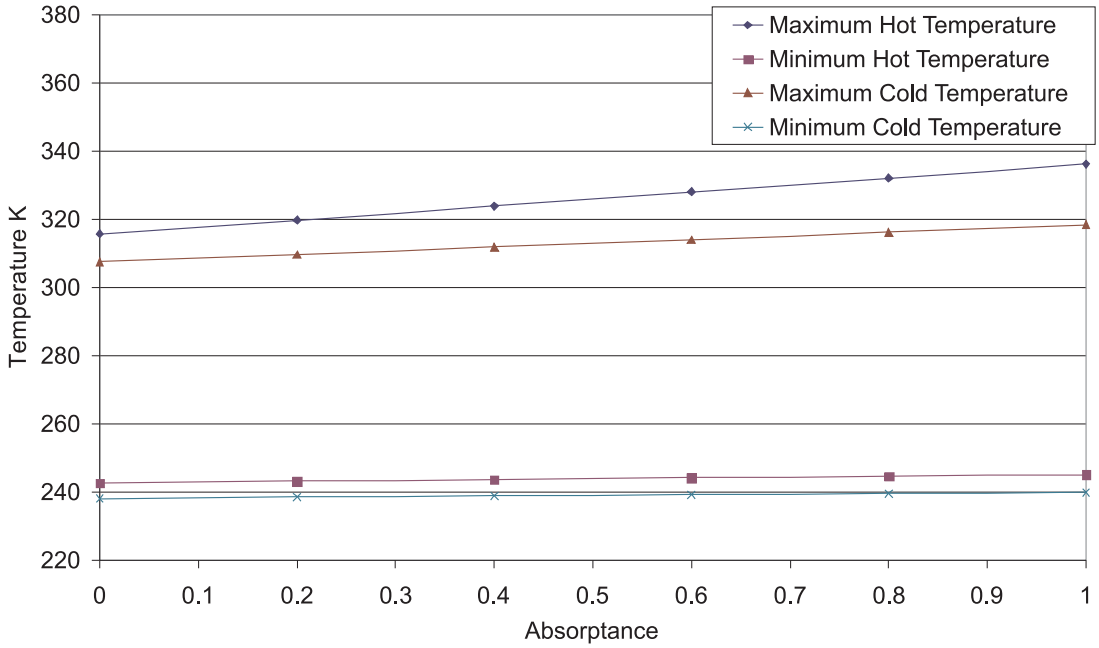

Figure 8.3: *The minimum and maximum temperatures of the battery against coating absorptance in 200 km LEO for both environments.*

8.1.1.3 Coating Viability

Selecting a coating for the shadowed surface of the wing panel does not provide a solution for all orbits. The emittance can be successfully used to increase the time to overcool, but this increase is limited by the need to avoid overheating the panel in sunlight due to decreased heat emission. The emittance reduction works mostly by reducing heat loss as the increase in entry temperature caused by an increased albedo absorption was shown to have a small effect on minimum temperatures. For those orbits where an emittance value exists that results in neither overcooling nor overheating, the use of coatings is a very viable thermal control because, as discussed in section 7.2.1.1,

altering the coating is a near no added mass solution and as such very little of the MFPS benefit is used. The only technical issue is that of cost as the expense of coatings varies.

8.1.2 Louvres

Louvres allow the use of multiple optical properties. The above discussion of optical properties revealed that there is a conflict in the emittance requirements to avoid overheating and overcooling. Ideally, the emittance would be set to 0 for eclipse and 1 during sunlight. To assess if altering the emittance would be a feasible solution, a thermally activated louvre that switches between an emittance of 0 below a given temperature and an emittance of 1 above this temperature was modelled. This was modelled as a variation of the emittance of the dark surface. Figures 8.4 and 8.5 show the results of this for a range of switching temperatures for 200 km LEO orbits in both hot and cold environments. Geosynchronous is not considered as the above results have shown that no safe value of emittance to prevent overcooling exists.

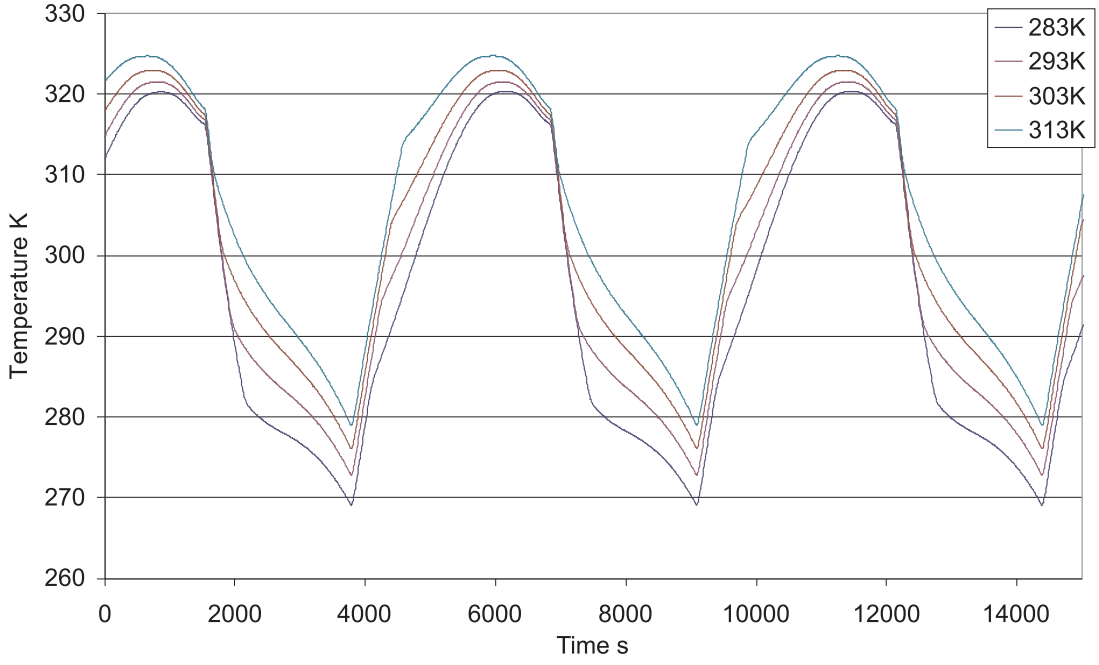

Figure 8.4: *The effect of switching temperature on louvre performance in a hot LEO.*

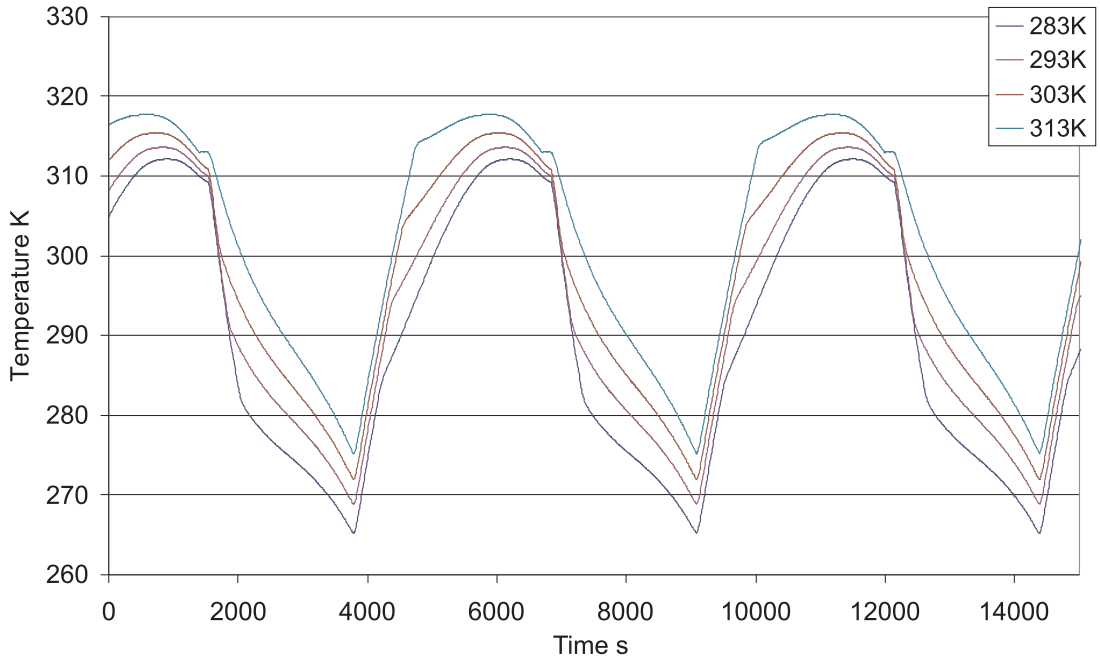

Figure 8.5: *The effect of switching temperature on louvre performance in a cold LEO.*

Decreasing the switch temperature reduces the temperatures of the battery as the panel spends increasing time with a higher emittance. In the hot environment, this does not result in a safe switching temperature as the panel becomes too cold before it stops overheating. Results from section 8.1.1.1 indicated that an emittance of 0.9 would prevent overheating in the hot environment. The louvre results imply that this works through a combination of high heat loss *and* a low sunlight entry temperature rather than just high heat loss.

In the cold environment, the reduced heat input means that overheating is not an issue for the range of switch temperatures considered. To prevent overcooling, a switch to the lower emittance is required above 306 K. There thus exists in the cold LEO case a theoretical thermal control solution using an idealised louvre. The envelope of this solution is bounded by the heat input to the module. Warmer environments reduce the temperature above which the switch needs to occur to prevent overcooling, but also reduce at a faster rate the temperature below which the switch must occur to prevent overheating. The envelope is illustrated in fig. 8.6, where the envelope is formed by two lines; the blue line showing how the minimum switch temperature changes with increased heat input and the red line showing how the maximum switch temperature changes with input. Below the blue line overcooling occurs and above the red line overheating occurs, as highlighted by the shaded regions. The gap betweens these lines closes, such that the envelope extends to just above the medium heat input.

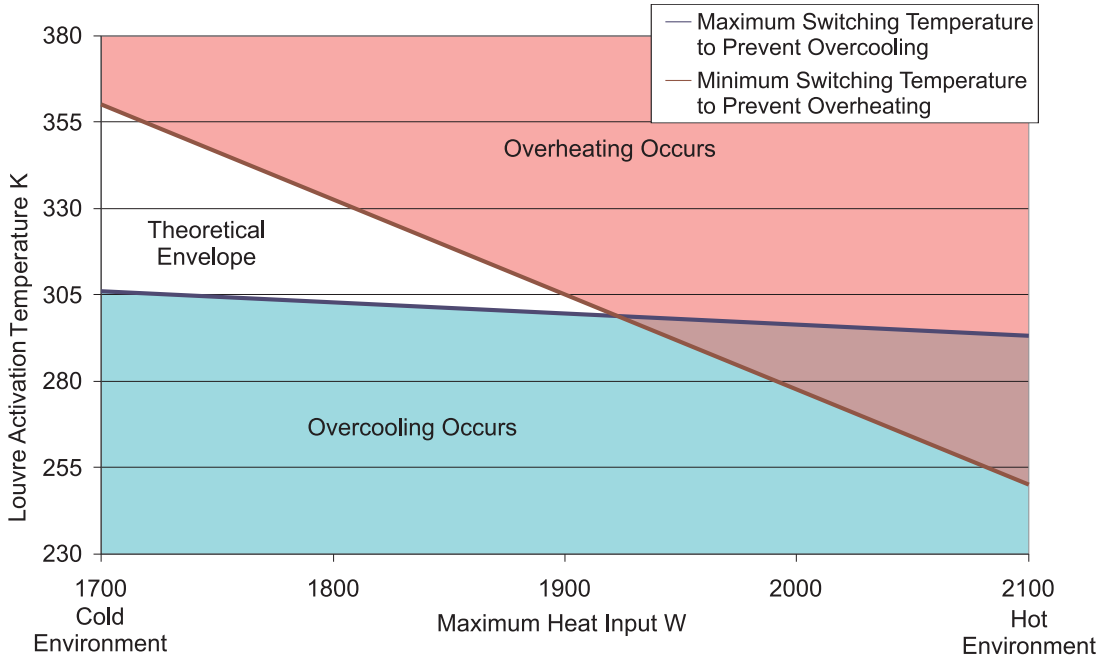

Figure 8.6: *Envelope of the theoretical louvre, showing how limits on the temperature at which louvre must activate vary with the environment.*

In order to determine if feasible solutions exist within the theoretical envelope, realistic values for the emittances were used. Figure 8.7 shows a range of switching temperatures for the minimum and maximum emittances identified in Table 8.1; 0.25 and 0.66. The results show that these limits are not sufficient with battery temperatures becoming unsafe for each switch temperature. The best possible emittances [50] are 0.04 for a buffed metal (aluminium or copper) and 0.94 for a black paint. Figure 8.8 shows a range of switching temperatures for these emittances. For these new emittances a feasible solution occurs if the switch temperature is kept above 303 K.

Feasibility has been shown for the LEO cold environment that experiences the longest eclipses. For orbits with a greater β angle, the eclipse shortens and the input from the albedo decreases, reducing the limitations on preventing overcooling and overheating. Louvre feasibility has been shown to be dependent on orbit and environment and louvre viability is dependent upon the mass of the louvre system. While they do enable some orbits it is only worth pursuing if the mechanism is of low mass, complexity and power requirement. Classical mechanical systems fail to meet these requirements due to their size and complexity. Current louvre research is looking at the use of MEMS [64], which may meet these goals. Louvres can only be recommended as a viable solution if these new technologies meet their objectives.

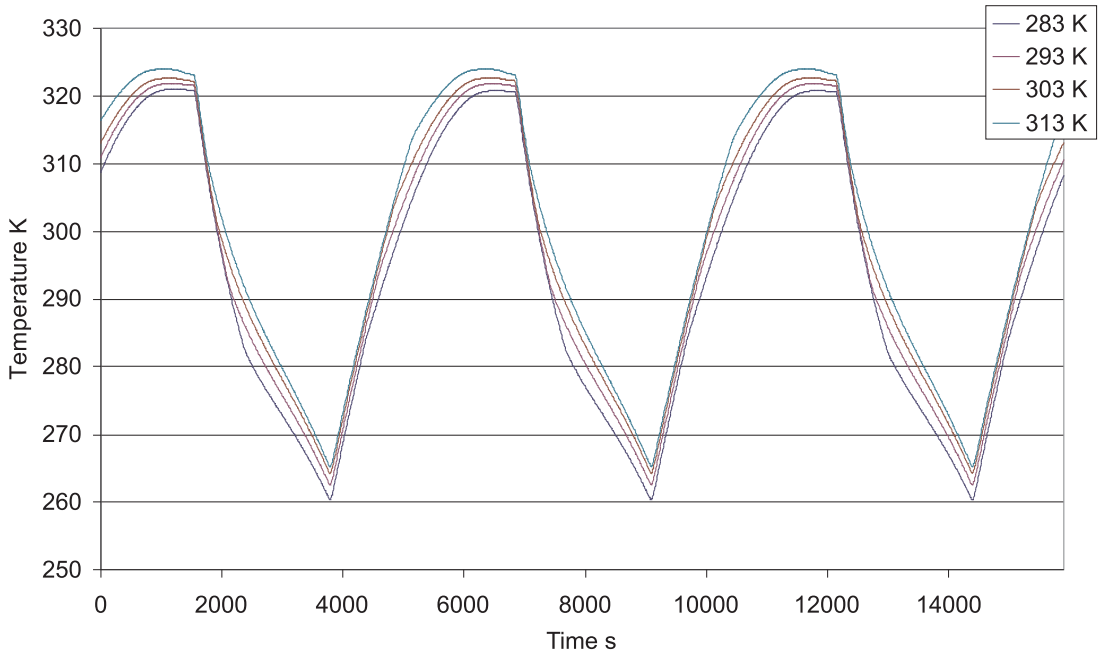

Figure 8.7: *Effect of switch temperature on louvre performance for a switch between 0.25 and 0.66.*

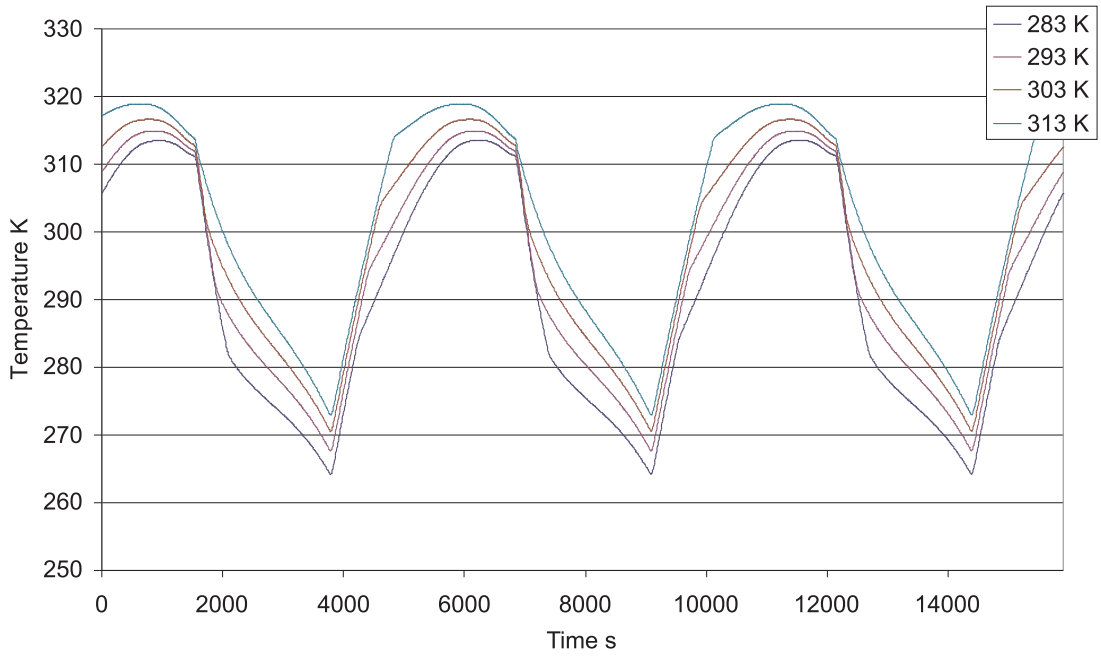

Figure 8.8: *Effect of switch temperature on louvre performance for a switch between 0.04 and 0.94.*

8.2 Insulation

Surrounding the battery in insulation will reduce the heat flow to and from the battery. To assess if this sufficiently slows the rate of change of temperature of the battery to maintain its temperature within bounds, the honeycomb is replaced by a carbon aerogel, Wiener et al. [80]. This is an extreme case, used to assess feasibility. Aerogels are the least thermally conductive materials at room temperature currently available. The aerogel used has a density of 312 kg/m^3, a specific heat capacity of 500 J/kgK and a thermal conductivity of 0.005 W/mK. Figures 8.9 to 8.12 show the transient temperature response for 200 km and geosynchronous altitudes in both hot and cold environments.

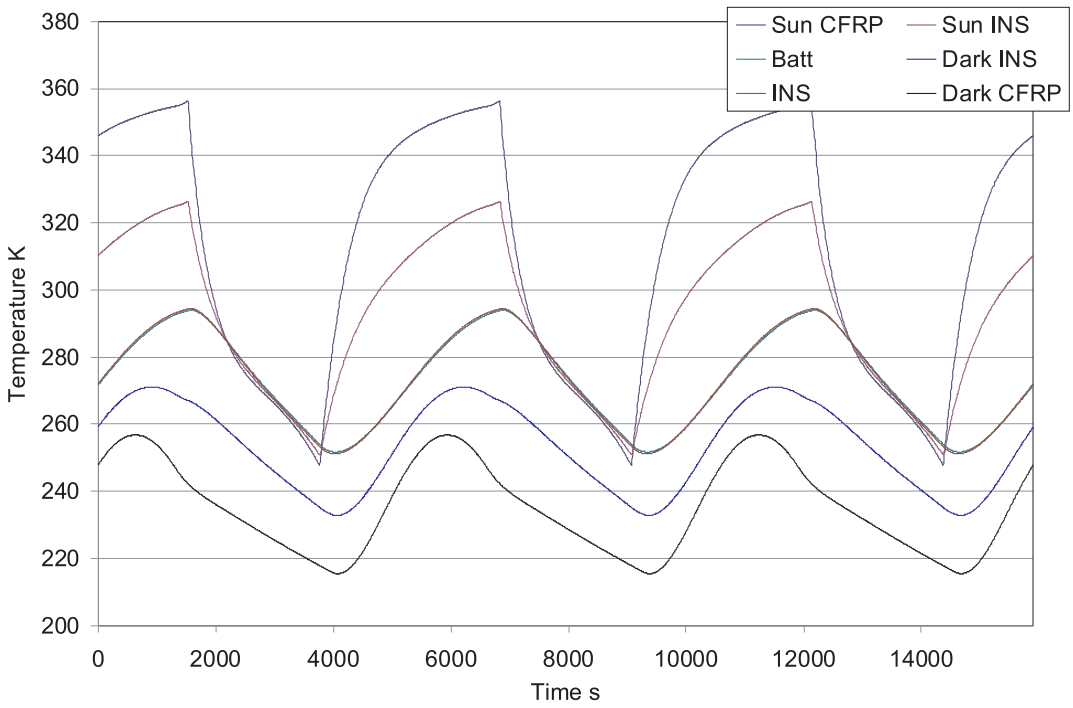

Figure 8.9: *Effect of insulating the wing on the transient temperature response in a cold 200 km LEO.*

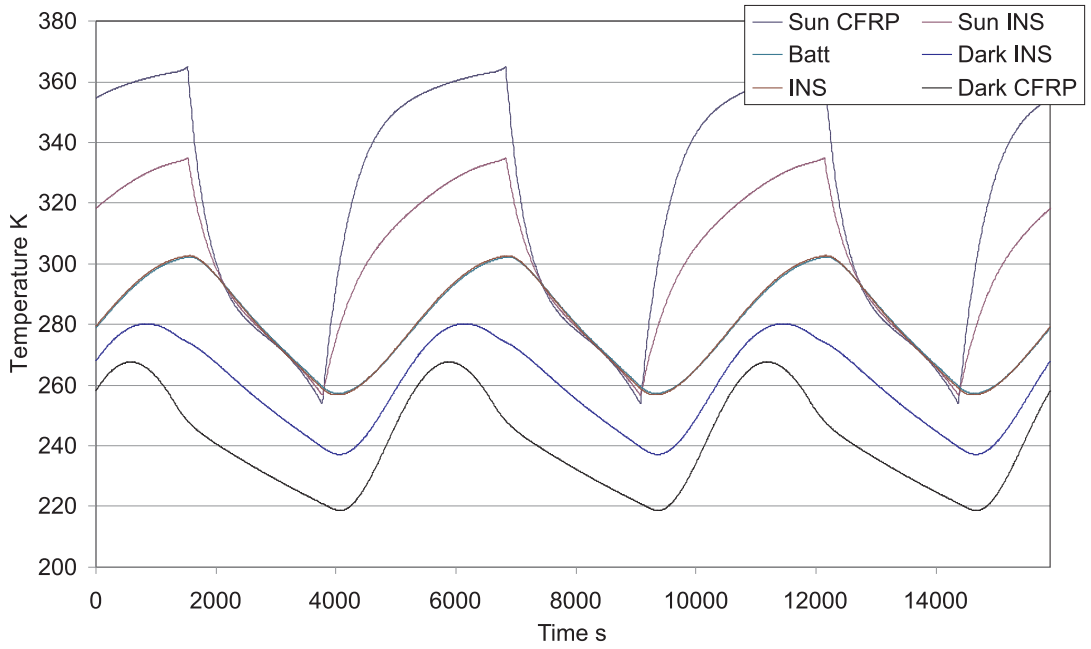

Figure 8.10: *Effect of insulating the wing on the transient temperature response in a hot 200 km LEO.*

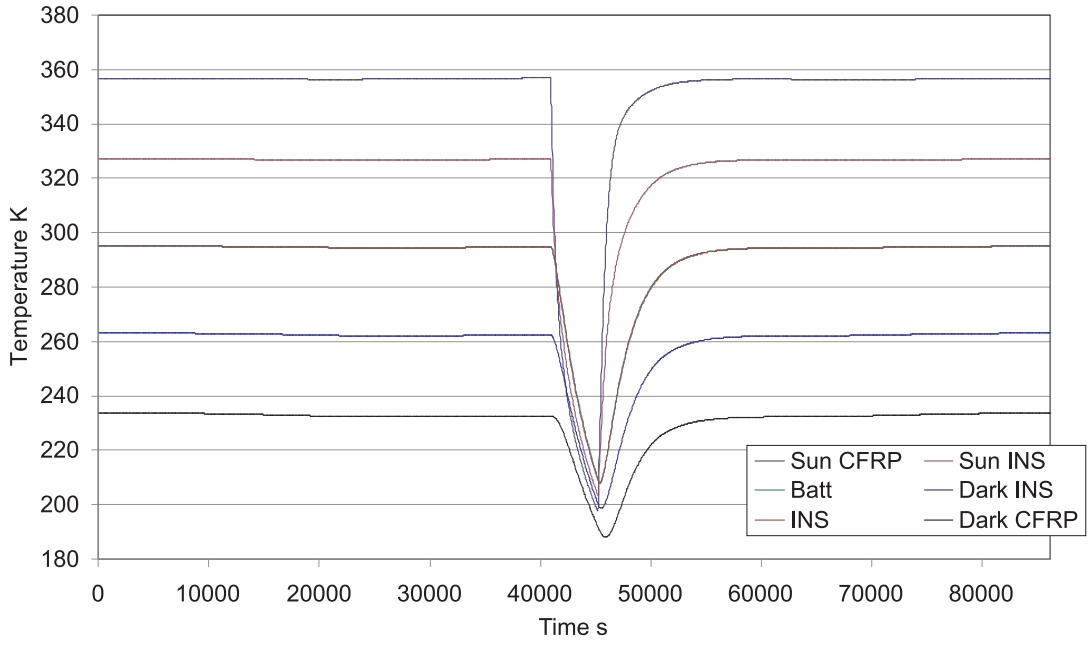

Figure 8.11: *Effect of insulating the wing on the transient temperature response in a cold geosynchronous.*

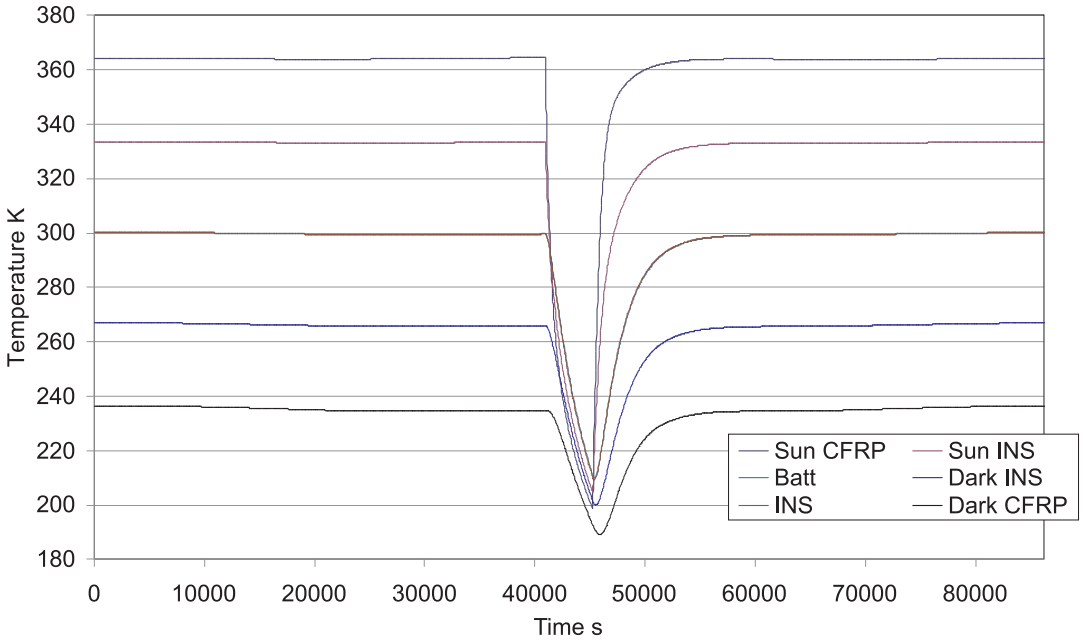

Figure 8.12: *Effect of insulating the wing on the transient temperature response in a hot geosynchronous.*

As seen in figs. 8.9 to 8.12, the aerogel insulation has the effect of thermally separating the facesheets, creating a 100 K temperature difference between them in sunlight. The sunlit facesheet sees only the input of the Sun and has reduced heat loss, causing it to become hotter. The shadowed facesheet now has at best only heat input from the Earth and thus cools. The battery temperature is the average of the facesheet temperatures. This insulation is effective at preventing overheating in both LEO and GEO, but does not succeed in preventing overcooling in any altitude or environment.

The presence of insulation reduces the temperature variation of the battery, bringing the extremity temperatures closer to the mean, though there is a reduction in the mean temperature. This implies an amount of insulation may exist for which the minimum temperature is safe. Tables tables 8.3 and 8.4 show the effect on the minimum, maximum and mean temperatures of the battery of increasing insulation.

Table 8.3: *Variation of battery temperature with core conductivity for a cold 200 km LEO.*

Core Conductivity	Minimum Battery Temperature	Maximum Battery Temperature	Mean Battery Temperature
W/mK	K	K	K
5.796	239.5	308.1	277.3
2	239.9	308.1	277.3
1	240.1	308.2	277.4
0.5	240.3	308.3	277.6
0.005	251.7	294.0	273.2
0.001	257.0	269.9	263.4

Table 8.4: *Variation of battery temperature with core conductivity for a cold GEO orbit.*

Core Conductivity	Minimum Battery Temperature	Maximum Battery Temperature	Mean Battery Temperature
W/mK	K	K	K
5.796	194.1	305.1	299.1
2	194.8	305.1	299.2
1	195.0	305.3	299.4
0.5	195.1	305.5	299.6
0.005	208.3	295.1	289.4
0.001	230.1	274.0	268.0

The LEO results show that increasing insulation does reduce the both the mean temperature and the range of the variation. However, the mean temperature of the battery drops below the lower limit before the range becomes small enough for the minimum temperature to be safe. The geosynchronous results show that improving the insulation by 500 % is still not enough to prevent the battery from overcooling. The mean temperature is reduced to 268 K, implying that the greater insulation has caused the temperature of the dark face to become so cold that the average temperature between the facesheets is below the battery safe limit.

Tables 8.3 and 8.4 show that no matter the properties of the insulation, the battery becomes too cold in the longest eclipses. Even if it had provided a solution, it is likely that a high thickness of insulation would be required. This is a mass and volume increase that would require a further increase in mass and volume in strengthening the structure to support the larger and heavier panel. In addition to this, the insulating material would have to have sufficient structural properties to adequately replace the core, which aerogels currently do not.

The addition of insulation does not provide a solution to the longest eclipses. However, with aerogel insulation instead of honeycomb core, the times between eclipse entry and overcooling are shown in table 8.5. The aerogel adds 1.56 kg (52 % of the MFPS saving) to the panel for these increases. When the structural issues already mentioned are considered, this is a poor return given that the insulation already accounts for half of the MFPS mass benefit.

Table 8.5: *Times to overcool for aerogel core. Times in seconds.*

Case	Insulated Time to Overcool	Baseline Time to Overcool	Difference
200 km LEO Hot	1527	894	633
200 km LEO Cold	1209	722	487
GEO Hot	1121	630	491
GEO Cold	992	560	432

8.3 Thermal Switches

Section 8.2 above has shown that the issue with using insulation is not one of overheating in sunlight while the temperature remains safe during eclipse. As such, the use of a thermal switch to connect the battery to the colder dark surface to emit excess heat is not required.

8.4 Heaters

To prevent overcooling in eclipse, a patch heater is embedded amongst the cells, modelled as a heat input to the battery node. Two models are considered: one where

the heater is active throughout eclipse and one where the heater only becomes active if the temperature drops below a threshold, 278 K. Table 8.6 shows the minimum power required and energy expended by the patch heater. In all cases the power requirement is high, about 35 % of the Sun's input in LEO and about 54 % in geosynchronous. Using a temperature switch requires less additional battery capacity. This is despite the temperature switch power being higher in order to effectively stop the cooling and hold the battery temperature. This higher heater power is used for a much shorter time than the eclipse switch. The effect of the eclipse switch is to reduce the rate of cooling for all of eclipse and thus the energy used is greater.

Table 8.6: *Heater power required to maintain battery temperature during eclipse for the wing mounting.*

Scenario	Eclipse Switch		Temperature Switch	
	Power W	Energy Whr	Power W	Energy Whr
LEO Cold	309	192	343	160
LEO Hot	273	169	321	134
GEO Cold	464	556	476	513
GEO Hot	461	533	475	500

In LEO, the presence of the heater maintaining a safe battery temperature means that the eclipse exit temperature is warmer. This presents an issue in the hot LEO case, as maximum temperature is very close to the upper limit. The result would be that more orbits will suffer from overheating as the time to overheating is reduced by the warmer eclipse exit.

To survive the longest eclipses requires a significant investment in extra battery capacity, a requirement that is increased when inefficiency of the heaters is accounted for. In geosynchronous orbit this is up to an extra 57 % of extra capacity giving a mass increase of 3 kg and 19 % giving 1 kg in LEO. This is a potentially unviable solution to the longest eclipse as it requires a majority of the MFPS mass benefit to be used, however, shorter eclipses will require less extra capacity. For example, using 25 % of the MFPS mass saving as extra cells gives a capacity of 125 Whr. In a cold geosynchronous altitude this gives 945 seconds of heat at 476 watts and this allows the battery to withstand eclipses that are shorter than this. The range of orbits where a heater can be viably used is dependent on the amount of mass benefit that can be sacrificed and the efficiency of

the heaters. However, this does not include extra mass incurred from the EPS having to meet the increased power demand during sunlight to recharge the extra cells.
Table 8.7 shows how the power and energy requirements change with the switch temperature in a cold LEO. The results follow the same pattern as seen in the comparison between the eclipse switch and the temperature switch in table 8.6: With a lower switch temperature, more power is required to prevent overcooling but the heater is active for a shorter time. Thus the required extra capacity is less at lower switch temperatures, increasing the length of eclipse that can be made safe for a given TCS mass.

Table 8.7: *Effect of increasing the temperature below which the heater activates.*

Switch Temperature K	Power W	Energy Whr
275	366	152.3
278	343	160.0
281	334	163.7
284	327	177.4

8.5 Phase Change Materials

The increase in heat capacity offered by exploiting the heat of fusion of a phase change material can be used to prevent both overcooling and overheating. Increasing the heat capacity for the same rate of heat exchange will slow the rate of temperature change. The results in section 6.2 indicate that for this panel overcooling in eclipse is the concern. However using the PCM to prevent overcooling in eclipse will increase the eclipse exit temperature which could cause the panel to overheat. Fortunately, the PCM will melt in sunlight giving the same boost to the heat capacity as its freezing did. Thus, the freezing of a PCM slows the rate of cooling to prevent overcooling and the melting of the same PCM slows the rate of heating to prevent overheating.
As modelling the complexities of a PCM is beyond the scope of this work, a simpler approach is used to determine if the increase in heat capacity is effective. The model does not represent the PCM as a component in the panel but only as an increase in the heat capacity of the battery. This removes the need to model the phase transition of the

PCM and how its properties vary with the phase transition. The increase in the heat capacity of the panel due to the presence of added material (the PCM) is also not modelled so that only the effect of the heat of fusion is seen. A Gaussian distribution over a range of 5 K with a 3σ is used to model the phase transition, see appendix C.2. The gaussian distribution is given by

$$H_{pcm} = e^{-1.2T^2} \tag{8.1}$$

where H_{pcm} is the heat capacity in J/K and T is the temperature in K.

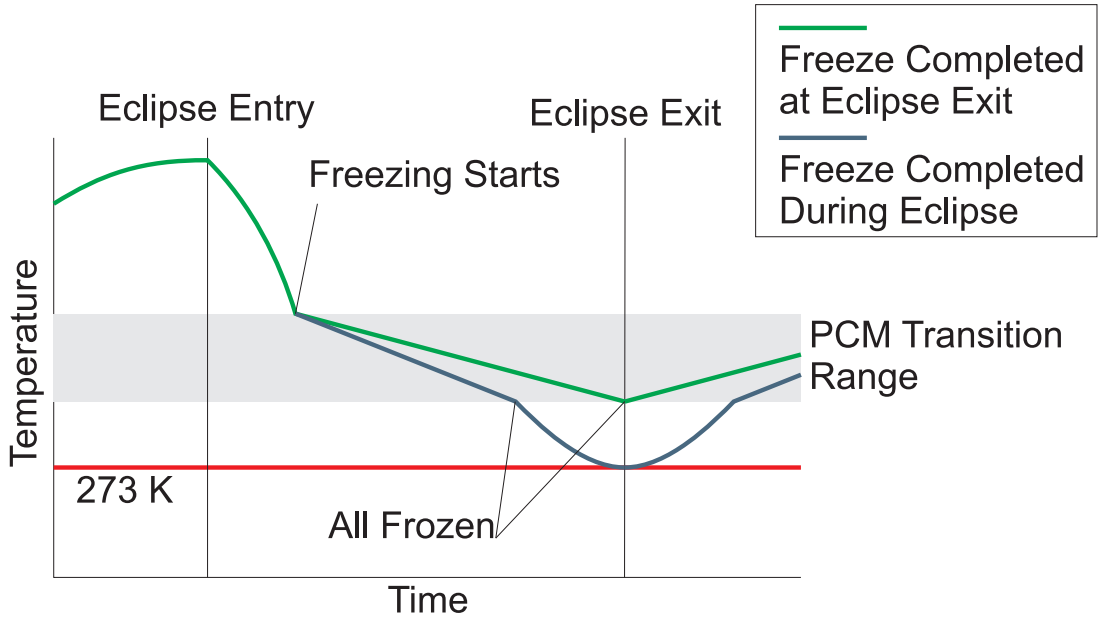

Figure 8.13: *Illustration of the different options for determining the required PCM amount.*

Once the PCM has completed its phase transition, the heat capacity returns to its normal value and the temperature change resumes its rapid rate. The amount of PCM required is determined as the amount of PCM that completes its transition at the point where the panel exits the hostile environment. For example, in eclipse the amount of PCM used is such that the PCM completes freezing when the panel exits eclipse. The amount of PCM could be reduced by allowing it to freeze before eclipse exit. The minimum amount of PCM is thus such that enough of a delay has been provided so that when the panel resumes a rapid temperature reduction, it exits eclipse before it becomes too cold. Figure 8.13 illustrates this. The more conservative approach of PCM freezing at eclipse exit is used.

The amount of PCM required is represented by the amount of extra energy required to pause the battery temperature in the PCM transition range. This is referred to as the

pause energy and has the unit J/K. This can be converted into the mass of a PCM using the PCM's heat of fusion (J/kgK). Figures 8.14 and 8.15 show how the pause energy varies with the transition temperature. At both altitudes, the cold environment requires more pause energy as the eclipse entry temperature is lower. This is more pronounced in LEO as the difference in input is greater due to the proximity of the Earth. The pause energy in geosynchronous is much higher, around three times as much. This is because the geosynchronous eclipses are longer and the rate of cooling greater due to the lack on input from the Earth.

Figures 8.14 and 8.15 reveal that the lower the transition temperature the lower the required pause energy and thus the less PCM required. At lower temperatures, the heat loss from the surfaces is reduced and thus the rate of change of temperature decreases as the panel reaches its equilibrium temperature. In eclipse this equilibrium temperature is far below the lower limit of the battery but the net power flow out of the panel is still lower at lower temperatures. Thus by combining the boost in heat capacity offered by the PCM with a reduced net heat loss, an amount of PCM can provide for a longer pause in the cooling rate. In addition to this, a higher transition temperature is reached sooner by the panel as it cools. As such, the time between the PCM beginning to freeze and eclipse exit is increased, requiring more PCM to bridge the gap.

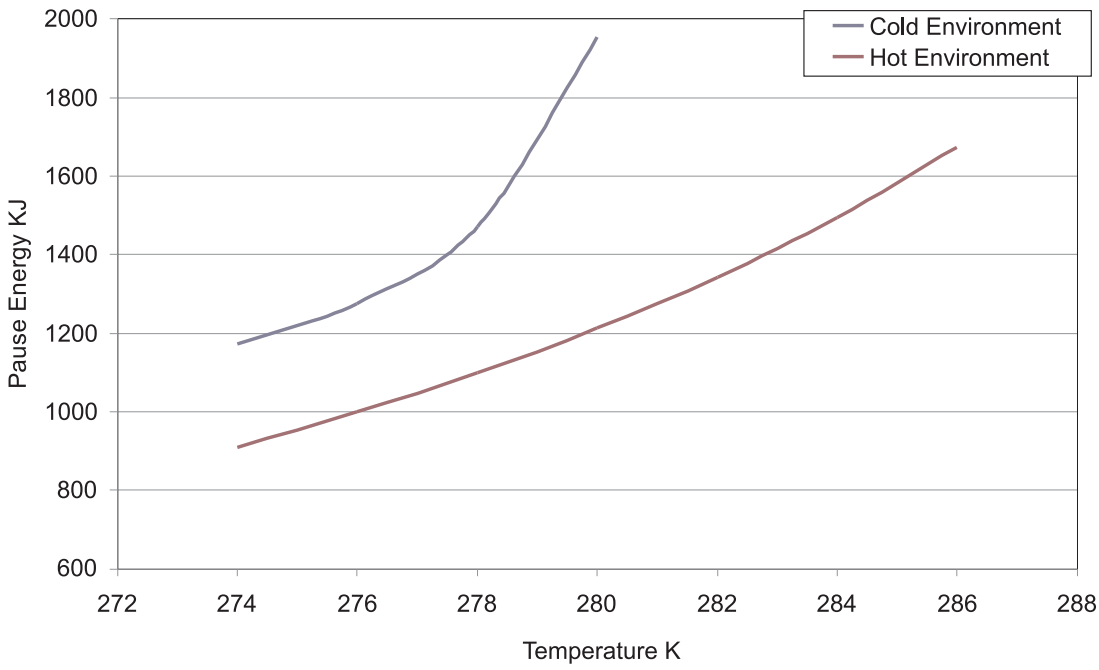

Figure 8.14: *The variation of required pause energy to prevent overcooling with transition temperature in 200 km LEO.*

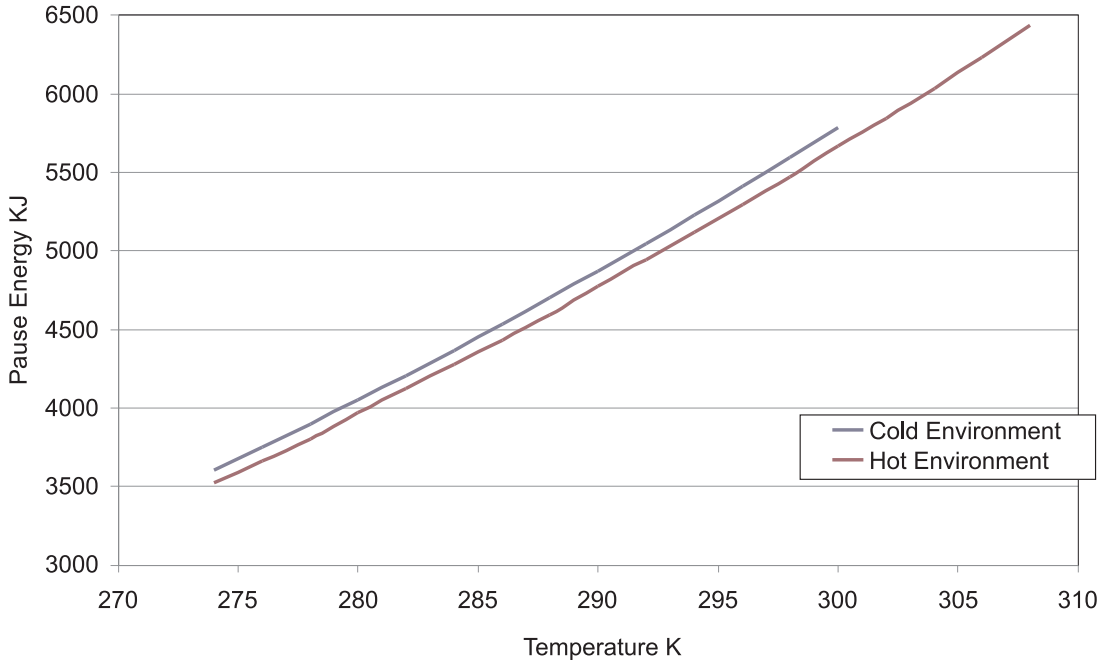

Figure 8.15: *The variation of required pause energy to prevent overcooling with transition temperature in geosynchronous orbit.*

In figs. 8.14 and 8.15 the full range of possible transition temperatures between 273 K and 318 K are not explored. At both orbit altitudes there is an upper limit to the transition temperature. In LEO, the transition temperature is limited by the requirement to melt the PCM fully before the next eclipse. Melting the PCM causes there to be an equivalent pause in the rate of temperature change, similar to that used to prevent overcooling. While this pause is useful for preventing overheating, if melting the PCM continues for too long, the eclipse entry temperature is lowered and thus the time between eclipse entry and PCM freezing beginning is reduced which in turn increases the time between freezing beginning and eclipse exit, making the existing amount of pause energy insufficient. When the PCM then freezes fully and the panel resumes rapid cooling the eclipse exit temperature and all temperatures after it are colder causing the following eclipse entry temperature after the sunlit period to be colder, making the problem worse. If the pause energy is increased, to meet the extended requirement, eventually a point is reached at which there is not enough energy during sunlight to melt the PCM.

Unfortunately, it is not possible to trap the panel within the transition range of the PCM as the maximum net power gain during sunlight at 288 K[8.1] on a hot LEO is 478 W, whereas the minimum net power at 288 K in eclipse is -473 W. As such, at this

[8.1] 288 K is the transition temperature at which this effect begins to occur.

temperature the tendency is for a slow loss of energy, causing the PCM to slowly freeze entirely after which the panel continues to cool and the battery temperature becomes too low.

In geosynchronous orbit the transition temperature is limited by the equilibrium temperature of the system which the transition temperature must be below in order for it to be effective during eclipse. The transition temperature is also limited at this altitude by the need to melt the PCM before the next eclipse. Interpreting between the altitudes looked at, with increasing altitude the sunlit time increases allowing the melting of greater amounts of PCM, allowing the use of higher transition temperatures, though at higher altitudes away from Earth the equilibrium temperature drops so that one limit is exchanged for another, higher one.

It is worth noting that if the prevention of overheating is required, the amount of pause energy required will be greatly reduced as the equilibrium temperature in sunlight is much closer to the temperature range of the panel. However, for the prevention of overheating at high altitudes where the sunlit time can be many hours long, the amount of PCM required would be extreme.

8.5.1 Viability of Phase Change Material Use

Having shown that it is possible for a PCM to maintain the temperature of the battery within its envelope, the viability of using a PCM is assessed. From chapter 7 viability is primarily defined by the mass of the thermal control system. Tables 8.8 and 8.9 show the required mass of a selection of PCMs that have transition temperatures within the battery temperature envelope [8.2]. The selection is limited to those PCMs that have a transition temperature in the range considered in figs. 8.14 and 8.15. The mass of each PCM is determined by interpolating the results in figs. 8.14 and 8.15 to find the pause energy which is then divided by the heat of fusion of the PCM. The mass of PCM is thus dependent on the transition temperature which determines the pause energy required and the heat of fusion which determines the amount of mass required to provide that amount of heat capacity.

The results show that with the exception of Hydrazine and water used in a hot LEO, the mass of PCM required is greater than the MFPS saving. In the exceptional case, the PCM accounts for nearly 80% of the saving. It is thus clear that while the use of a PCM

[8.2] PCM data sources: A - [59], B - [69], C - [81], D - [50].

is feasible it is not a viable solution to the longest orbits in the worst case scenarios. A PCM could be used to prevent overcooling in orbits with shorter eclipses. Figure 8.16 shows the time taken to freeze (i.e. the delay in cooling to cover the gap between overcooling and eclipse exit) for Hydrazine, Formic Acid, Trimethylolethane + Urea (62.5 % + 37.5 %) and Vanadium Fluoride VF5. These PCMs are selected as they have the highest heat of fusion for their type. Though only Hydrazine is considered feasible for the longest eclipse in all four cases, orbits with shorter eclipses will have longer sunlit periods in which to melt a larger amount of PCM, reducing the melting issue. The results are for the coldest eclipse which is at geosynchronous altitude. As the model only considered the time it takes for the PCM to freeze, the eclipse entry temperature is not required and thus a specified environment is not needed. For LEO the heat from the Earth would reduce the amount of PCM required by reducing the cooling during eclipse.

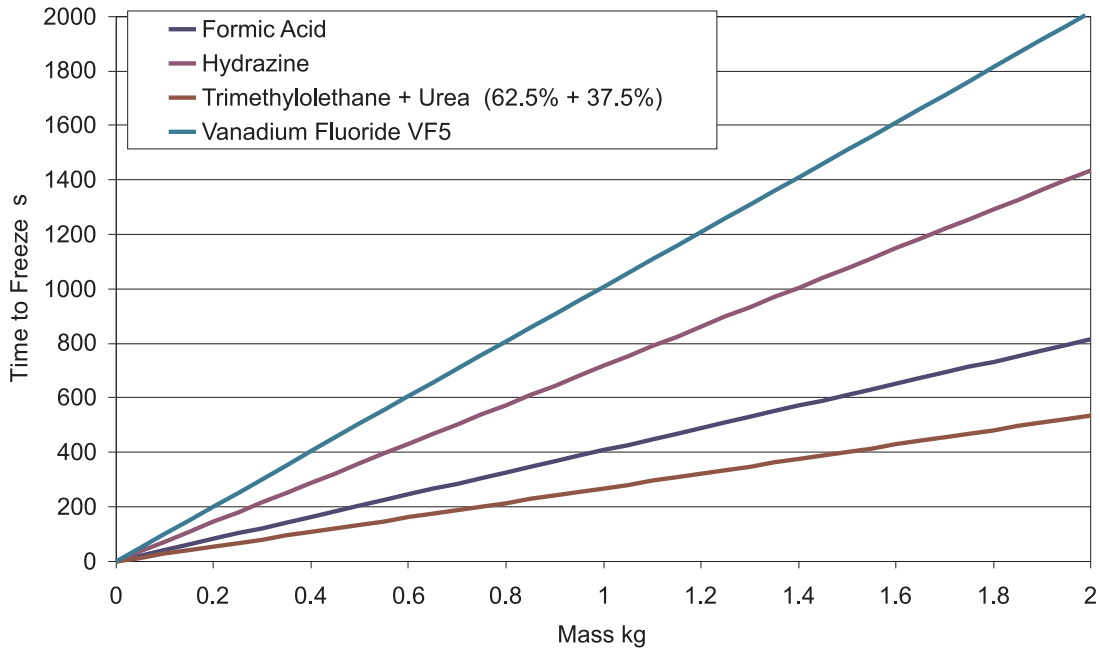

Figure 8.16: *The time taken to freeze a selection of PCMs in geosynchronous eclipse.*

Figure 8.16 shows that sacrificing a third (1 kg) of the MFPS saving allows for a delay of 1000 seconds if using Vanadium Fluoride VF5 and for a 700 second delay if Hydrazine is used. The eutectic PCM (Trimethylolethane + Urea (62.5 % + 37.5 %)) is the worst performing as it has the lowest heat of fusion. Figure 8.16 reinforces that the best performing PCMs are those with high heats of fusion. Essentially, fig. 8.16 shows the amount of MFPS saving that must be used up as PCM for a wanted time delay. However, this potential feasibility is limited as it corresponds to a model in which the PCM is only a heat capacity addition to the battery. The implementation of a PCM

thermal control system would require the battery to be surrounded by the PCM. There are several factors that effect the viability.

When a PCM is used as a thermal buffer for an electronic device, a high conductivity is required so that the PCM melts quickly and heat flows quickly through it to the radiator. In this vein, research has been carried out to improve the conductivity of PCMs, for example Elgafy and Lafdi [84], Zhang et al. [85]. In the use considered here, faster melting of the PCM is not wanted. Indeed, as the assessment of the use of insulation above section 8.2 has shown, surrounding the battery with an insulating material slows its reaction to eclipse. Low heat flow would also slow the freezing of the PCM, potentially reducing the amount of PCM required. Surrounding the battery with PCM would thus be beneficial.

The addition of the PCM into the wing mounted panel will increase the heat capacity of the panel as the material in solid or liquid state will have a heat capacity that will add to the panels and thus slow the rates of cooling and heating. The reduction in cooling rate will reduce the gap between overcooling and eclipse exit that the PCM must bridge. The reduction in heating rate however, will reduce the eclipse entry/maximum sunlit temperature which will impact on the amount of PCM that can be melted.

The distribution of the PCM around a distribution of the cells in the panel may require extra PCM to be used. If the cells are distributed, then each grouping of cells will require an amount of PCM around them. While the PCM will affect the temperature of the panel as a whole, there maybe localised areas that require more phase change material around them.

The most important factor that will increase the mass of the PCM TCS is that of containing the PCM. The honeycomb core is perforated and is thus unsuitable for containing the liquid phase of the PCM. The containment of the PCM is further complicated by the density change the material undergoes during transition, requiring any container to have empty space in it. The possible methods to contain a PCM have already been discussed in section 7.2.3 and all of them require the mass of the TCS to increase. The net effect of this is to decrease the delay in the cooling possible for a given amount of MFPS saving used by a PCM. The panel mass is also likely to increase due to modifications to support the PCM and its containment inside the structure.

The viability of a PCM TCS is limited to that of preventing overcooling in short eclipses. The TCS is feasible for longer eclipses, but it has been shown that a PCM does

not currently exist with sufficient heat of fusion for the loss of MFPS saving to be viable.

Table 8.8: *The mass of phase change material required for the worst case orbits, part 1.*

Source	Type	PCM	Transition Temperature	Heat of Fusion	LEO Cold Mass	LEO Hot Mass	GEO Cold Mass	GEO Hot Mass
			K	kJ/kg	kg	kg	kg	kg
D	Salt Hydrate	Water	273	333	3.4	2.6	10.6	10.4
A	Organic	Hydrazine	274.4	393	3.0	2.4	9.3	9.0
D	Organic	n-Tetradecane	279	228	7.2	5.1	17.4	17.1
C	Organic	Rubitherm GmbH RT5	279	156	10.5	7.4	25.5	24.9
C	Salt Hydrate	$LiClO_3 \cdot 3\,H_2O$	281.1	253		5.1	16.3	16.0
[82]	Fatty Acid	Formic Acid	281.4	247		5.3	16.8	16.5
B	Eutectic	$CaCl_2 \cdot 6\,H_2O + CaBr_2 \cdot 6\,H_2O$ (45 % + 55 %)	287.7	140		13.7	33.4	32.7
D	Organic	p-Xylene	289	164			29.2	28.6
B	Organic	Caprilic Acid	289.3	149			32.3	31.6
D	Fatty Acid	Acetic Acid	290	187			26.1	25.5
D	Organic	n-Hexadecane	290	237			20.6	20.1
D	Fatty Acid	Glycerol	291	199			24.9	24.4
C	Salt Hydrate	$KF \cdot 4\,H_2O$	291.5	231			21.7	21.2
[83]	Fatty Acid	Propyl Palmitate	292	186			27.2	26.6
C	Fatty Acid	Butyl Stearate	292	140			36.1	35.3
A	Metallic	Vanadium Fluoride VF5	292.5	714			7.1	7.0
D	Organic	n-Heptadecane	295	213			25.0	24.4

Table 8.9: *The mass of phase change material required for the worst case orbits, part 2.*

Source	Type	PCM	Transition Temperature	Heat of Fusion	LEO Cold Mass	LEO Hot Mass	GEO Cold Mass	GEO Hot Mass
			K	KJ/kg	kg	kg	kg	kg
D	Salt Hydrate	Sodium Chromate	296	164			33.0	32.3
B	Eutectic	$C_{14}H_{28}O_2$ + $C_{10}H_{20}O_2$ (34 % + 66 %)	297	147.7			37.3	36.5
D	Fatty Acid	Polyethylene Glycol	298	146			38.3	37.5
B	Salt Hydrate	$Mn(NO_3)_2 \cdot 6\,H_2O$	298.5	148			38.1	37.3
B	Organic	Latic Acid	299	184			30.9	30.3
B	Eutectic	CH_3CONH_2 + NH_2CONH_2 (50 % + 50 %)	300	163			35.4	34.7
D	Organic	n-Octadecane	301	244				23.6
D	Salt Hydrate	Phosphomium Chloride	301	752				7.7
B	Organic	Methyl Palmitate	302	205				28.5
C	Salt Hydrate	$CaCl \cdot 6\,H_2O$	302	190				30.8
B	Eutectic	Trimethylolethane + Urea (62.5 % + 37.5 %)	302.8	218				27.2
B	Eutectic	$Ca(NO_3) \cdot 4\,H_2O$ + $Mg(NO_3)_3 \cdot 6\,H_2O$ (47 % + 53 %)	303	136				43.7
B	Eutectic	$CH_3COONa \cdot 3\,H_2O$ + NH_2CONH_2 (40 % + 60 %)	303	200.5				29.7
D	Salt Hydrate	Sodium Sulfate	304	215				28.1
D	Organic	n-Nonadecane	305	187				32.8
B	Salt Hydrate	$Na_2CO_3 \cdot 10\,H_2O$	305	267				23.0
B	Salt Hydrate	$Na_2SO_4 \cdot 10\,H_2O$	305.4	241				25.6

8.6 Summary of Viability for Wing Mounted Panel

This chapter has shown that there is not a viable thermal control system that will enable the use of MFPS in all orbits. However, the TCS considered do enable a limited range of orbits. Table 8.10 compares the performance of these considered TCS. The table shows how efficient each system is in terms of the increase in the time to overcool[8.3] per percentage of the MFPS saving used by the TCS. As coatings add no mass to the panel, their efficiency is effectively infinite and they are considered the best performing TCS. Table 8.11 shows the maximum eclipse time for which the TCS is effective. The maximum eclipse time for the insulation is defined by the time to overcool when the entire core is replaced by an aerogel; this being the maximum amount of insulation possible without altering the structure. For heaters and PCM in geosynchronous, the maximum eclipse is defined as time to overcool if the entire MFPS saving is used. For LEO PCMs, the upper limit is defined by the amount of PCM that can be melted, as discussed from the results shown in fig. 8.14.

This chapter has shown that there is not a viable thermal control system that will enable the use of MFPS in all orbits. All of the TCS considered do enable some orbits. Table 8.10 compares the performance of the considered TCS. The table shows how efficient each system is in terms of the increase in the time to overcool[8.4] per percentage of the MFPS saving used by the TCS. As coatings add no mass to the panel, their efficiency is effectively infinite and they are considered the best performing TCS. Table 8.11 shows the maximum eclipse time for which the TCS is effective. The maximum eclipse time for the insulation is the time to overcool for when the entire core is replaced by an aerogel. For heaters and PCM in geosynchronous, the maximum eclipse is defined as time to overcool if the entire MFPS saving is used. For LEO PCMs, the upper limit is defined by the amount of PCM that can be melted, as discussed from the results shown in fig. 8.14.

Of PCM, insulation and heaters, the use of heaters is preferred as not only is it the more mass efficient, the extra battery capacity could potentially be put to other use during shorter eclipses and the addition of patch heaters has little effect on the structure of the panel, unlike the PCM and its containment or the replacement of the honeycomb core with aerogel. MEMS louvres potentially provide a solution that can maintain battery

[8.3] Compared to table 5.1.

[8.4] Compared to table 5.1.

Table 8.10: *The efficiency of each thermal control system in terms of the delay increase per percentage of the MFPS saving used. Values in s per %.*

TCS	LEO Cold	LEO Hot	GEO Cold	GEO Hot
Coating	∞	∞	∞	∞
Insulation	9	12	8	9
Heaters	46	49	36	34
PCM (VF5)	29	21	29.5	29.5

Table 8.11: *The maximum eclipse time in seconds each TCS can make safe.*

TCS	LEO Cold	LEO Hot	GEO Cold	GEO Hot
Coating	1150	917	950	840
Insulation	1209	1527	992	1121
Heaters	5347	5787	4125	4000
PCM (VF5)	1634	2184	3510	3580

temperature during the longest cold eclipses in LEO, however the technology is still at the prototype state and potential mass of the louvre, while better than a traditional mechanical system, is not yet known, making comparative assessment difficult.
The mass of TCS could be reduced by combining the TCS considered. In particular, using both a heater and a louvre. By switching from a high emittance to a low emittance for eclipse, the louvre reduces the heat loss during eclipse and thus less output from the heater is required. Adjusting the emittance would also work well with a PCM. Again, the use of a low emittance during eclipse reduces the heat loss of the panel; increasing the time between eclipse entry and overcooling and increasing the delay from the PCM freezing. This low emittance would also aid in melting the PCM, reducing this factor. However, a low emittance after the PCM has melted will cause the battery to overheat. A louvre that switches to a higher emittance to limit the maximum temperature to within the envelope once the PCM has melted would solve this issue.

Chapter 9

Thermal Control of the Body Mounted Panels

In the same manner as carried out in chapter 8, the feasibility and viability of a selection of thermal control solutions is assessed for the body mounted panel.

9.1 Coatings

The spacecraft temperature can be reduced by increasing the emittance of the coating but the increase is limited as too cold a spacecraft will not warm the shadowed panels sufficiently to prevent overcooling. Table 9.1 shows the minimum and maximum emittances required.

Table 9.1: *The minimum and maximum emittances of the spacecraft.*

Case	Overcooling Emittance	Overheating Emittance
200 km LEO Cold	0.05	0.18
200 km LEO Hot	0.4	0.87
Geosynchronous Cold	0.1	0.53
Geosynchronous Hot	0.2	0.85

The results show that there are no feasible values for emittance that prevent both unsafe temperature conditions. This is because the range of temperatures is greater than 45 K. Thus as the temperatures of the system reduce, overcooling occurs before overheating stops. While not feasible, the use of emittances can be used to minimise the extent of

temperature extremes in the other cases considered. Either through a compromise value between overcooling and overheating or through elimination of one of these.

9.2 Louvres

Louvres were used in section 8.1.2 when the wing mounting encountered conflicting emittance requirements and they are again considered here. The goal would be to switch between an emittance to prevent overheating and an emittance to prevent overcooling. In addition to the technology discussed in section 7.2.1.2 the implementation options include a variety of switches. The louvre could activate when the system enters eclipse or activate when either the spacecraft or a panel becomes too cold or too hot. An eclipse switch that changes the emittance to a lower value to reduce heat loss would not be feasible as the high emittance during sunlight will cause the spacecraft to be too cold at eclipse entry. The louvre switching regime must ensure sufficient heat capacity in the spacecraft for eclipse. Figures 9.1 and 9.2 show the effect of switching between emittances of 0.02 and 0.94[9.1] in a hot LEO and in a hot GEO case. 0.85 is not used as the overheating emittance as this is the minimum emittance to prevent overheating when the spacecraft has been allowed to be cold when it exits eclipse. This louvre switching regime only activates when a panel temperature reaches 315K (3 K short of the limit to give time for the system to respond) and thus a greater heat loss rate is required as the starting condition is warmer.

Switching to a higher emittance has lowered the average temperature of the spacecraft such that both overcooling and overheating now occurs. The results indicate that a louvre is not a feasible TCS. This is because switching to a higher emittance reduced the spacecraft stored thermal energy, leaving it unable to supply the shadowed panels with enough heat to prevent overcooling after eclipse. Indeed, in GEO the spacecraft is now so cold that panels are always too cold in shadow. If this had stopped overheating from occurring, then switching to lower emittances could have been investigated to find the range of emittances that prevent both. However, overcooling occurring before overheating has been solved indicates an unresolvable requirement on spacecraft temperature.

[9.1] The highest realistic emittance [50].

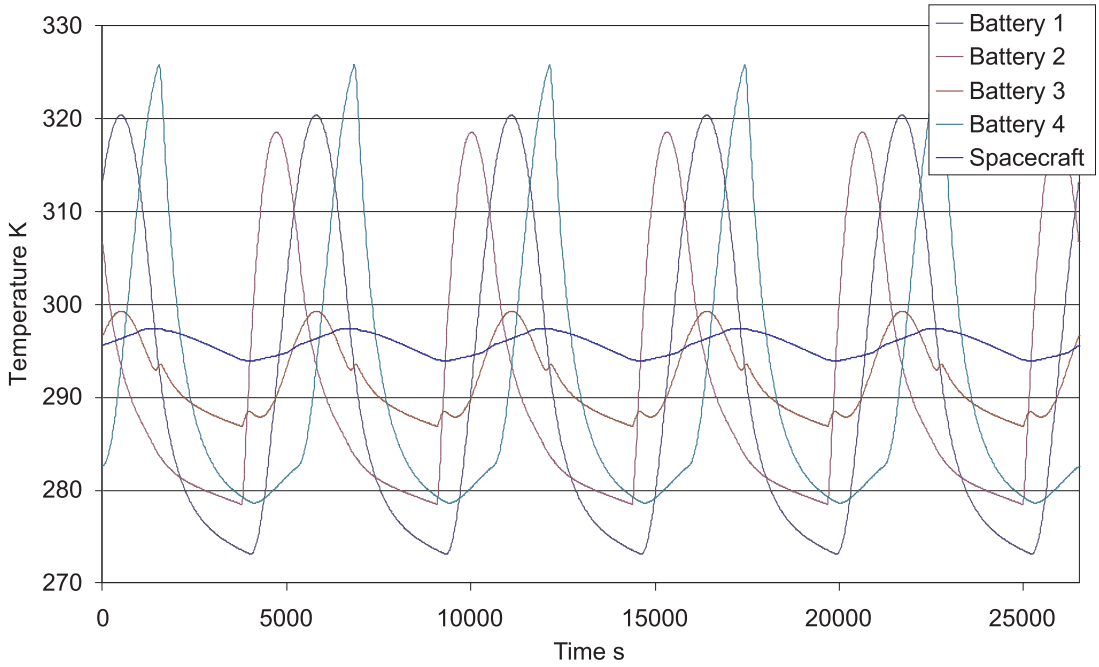

Figure 9.1: *The effect of a louvre on the body mounting Earth pointing system in a hot LEO case.*

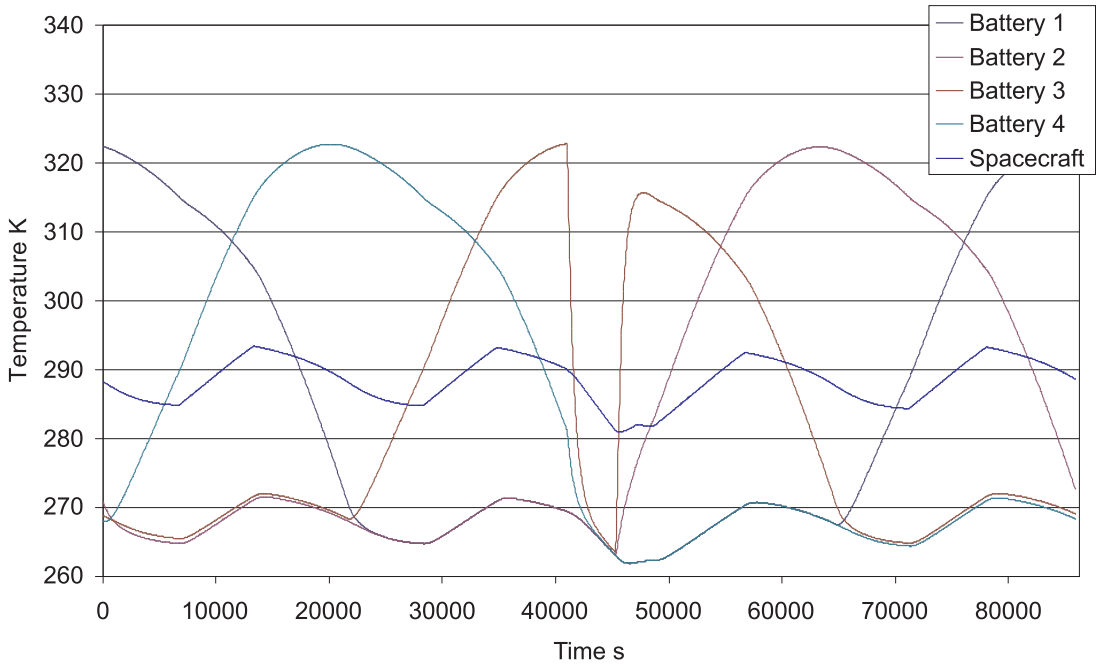

Figure 9.2: *The effect of a louvre on the body mounting Earth pointing system in a hot GEO case.*

9.3 Insulation

The honeycomb core in each of the four panels is replaced by a carbon aerogel; as with the wing panel this is an extreme case to establish feasibility. Figures 9.3 to 9.6 shows the transient temperature response of the battery for 200 km LEO and geosynchronous altitude orbits for both environments. In all four figures, the insulation has slowed the flow of heat such that after more than 40 orbits, the temperatures have yet to stabilise.

The combination of insulation in the panels and MLI on the smaller surfaces of the spacecraft traps the heat emitted by the electronics inside the spacecraft. The spacecraft is thus very hot and has a temperature that averages about 410 K in GEO and is rising above 380 K in LEO. As such, the panel temperatures are very high as they cannot lose heat to the spacecraft. The lowest panel temperature is 320 K in GEO and 295 K in LEO. The temperatures are lower in LEO as the system has a smaller sunlit period and thus gains less energy.

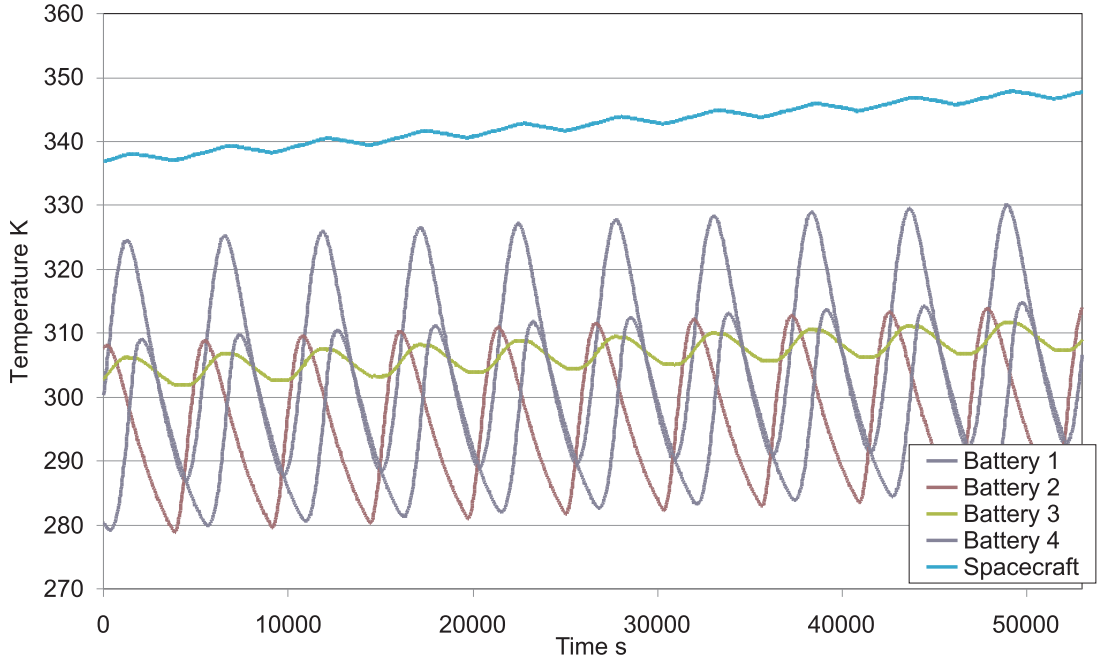

Figure 9.3: *Effect of insulating the Earth pointing system in a 200 km cold LEO.*

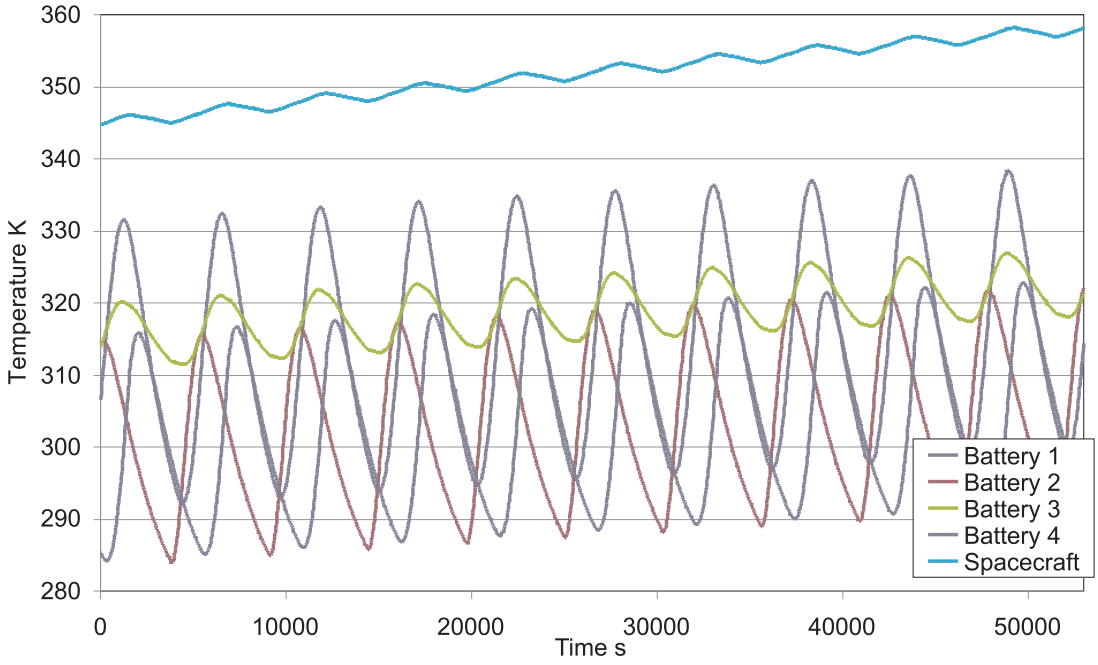

Figure 9.4: *Effect of insulating the Earth pointing system in a 200 km hot LEO.*

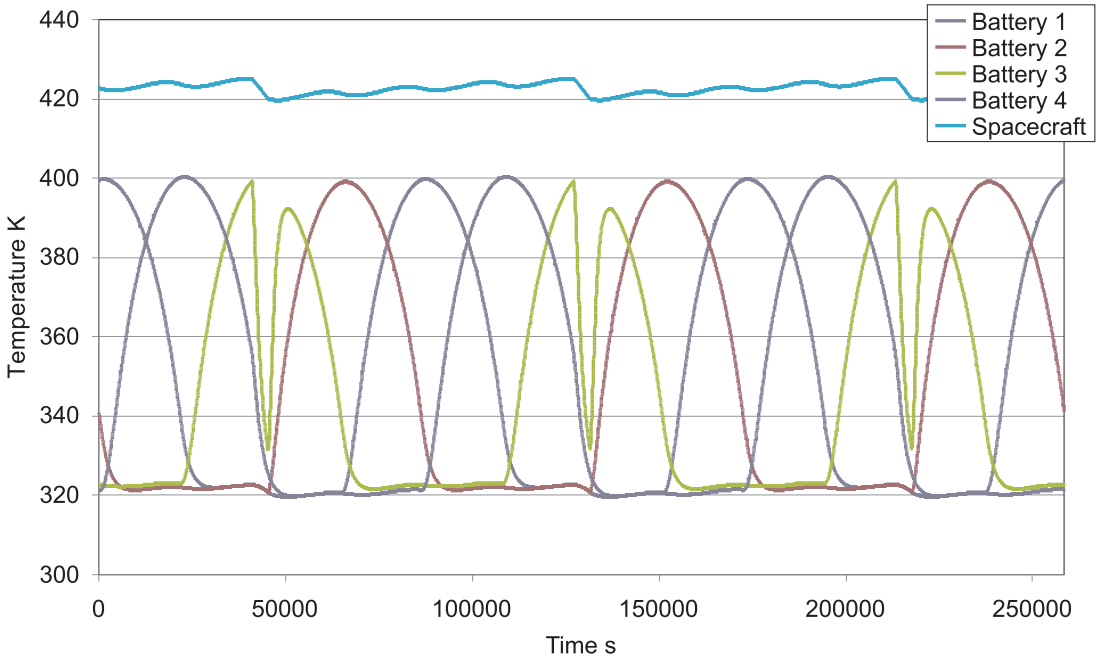

Figure 9.5: *Effect of insulating the Earth pointing system in a cold GEO.*

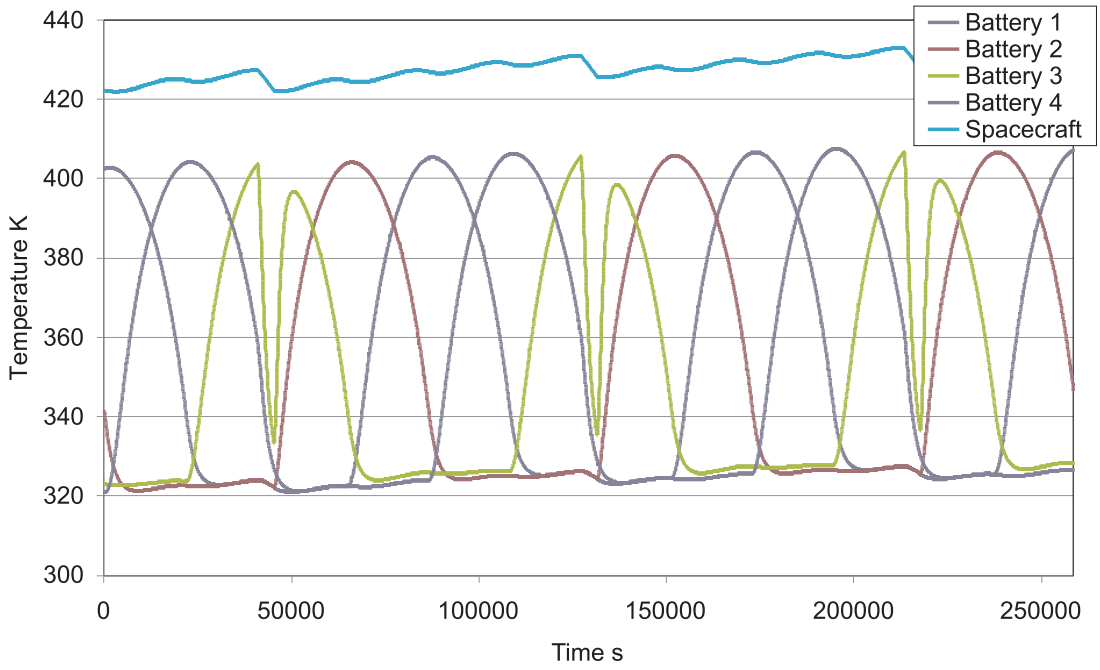

Figure 9.6: *Effect of insulating the Earth pointing system in a hot GEO.*

Replacing the MLI with a higher emittance coating will lower the spacecraft temperature and thus lower the average temperature of the battery. To examine this possibility fig. 9.7 shows how the minimum and maximum temperatures change with increasing emittance for the hot LEO. The emittance is required to be above 0.39 to prevent overheating and below 0.69 to prevent overcooling, thus there is a feasible range of emittance values. This is possible as the insulation has the effect of reducing the temperature range to below 45 K. However, as discussed in section 8.2, the effect on the structural properties of the panel by using an aerogel core mean that extra structural mass will be required in addition to the 6.7 kg of aerogel used to replace the core. At 5 times the MFPS saving this is clearly not a viable solution.

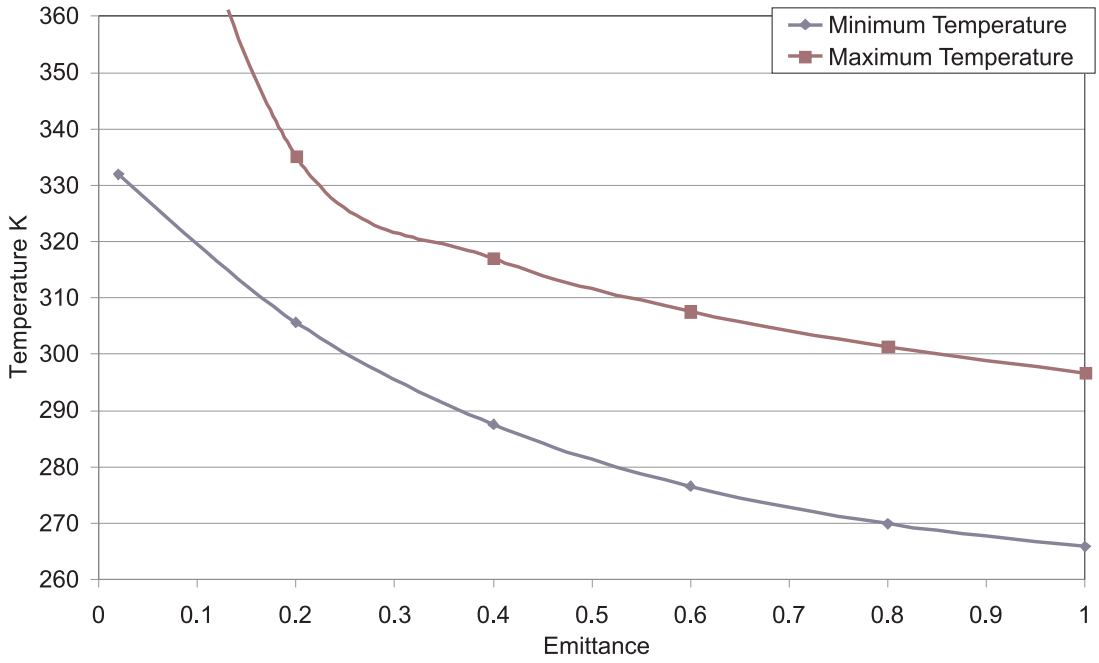

Figure 9.7: *Effect of increasing emittance on the insulated Earth pointing system in a 200 km hot LEO.*

9.4 Thermal Switches

Potentially, a thermal switch could be used with the insulation in section 9.3, which would activate to increase conduction of heat from the spacecraft through the panels to prevent the spacecraft and panels from overheating. However, this would be an addition of yet more mass to an already heavy TCS.

9.5 Thermal Links

A thermal link increasing heat flow between the body of the spacecraft and the panels could either be a thermal strap or an adjustment of the existing connectors. The linear conductance between a panel and spacecraft is the sum of the conductance of the connectors. The exchange of heat between panels and spacecraft could also be improved by increasing the emittance of the coatings of the facing surfaces, however, this radiation exchange is an order of magnitude smaller than that of a conductive heat flow and thus will have little effect.

9.5.1 Defining Linear Conductance Requirement

Three separate conditions could occur where a battery temperature is unsafe. Firstly when illuminated by the Sun, the shadowed panels do not receive enough heat and

become too cold. Improving the conduction from sunlit panels to spacecraft to shadowed panels will ensure that enough heat reaches the shadowed panels. However, increasing the heat flow to these panels will also increase heat loss so the spacecraft and the sunlit panel will cool. There is thus a maximum amount of conduction that can be allowed, the surpassing of which will cause parts of the system to become too cold.

The second condition is that of eclipse. To survive eclipse, the spacecraft acts as a thermal energy store which slowly releases heat to the panels to prevent them from becoming too cold in eclipse. In this condition a minimum conduction is required to maintain panel temperature but a maximum conduction exists, above which too much heat is lost and the spacecraft becomes too cold. The minimum conduction required can be reduced if the spacecraft is warmer when it enters eclipse. Here again a conflict exists where increased conduction from the sunlit panels to add warmth to the spacecraft must be balanced by the increase in conduction to the shadowed panels which increases heat loss. The problem is further compounded in this Earth pointing orientation as over the course of an orbit the spacecraft's rotation causes all the panels to experience both being sunlit and shadowed.

The third condition is where the sunlit panel overheats. Improving the conduction between panels and spacecraft will allow more heat to pass from the spacecraft to the shadowed panels, cooling the spacecraft. This increased heat loss allows the sunlit panel to cool. As with the first condition, there is a maximum conduction, above which too much heat is lost and the shadowed panels will become too old. Conditions one and two may combine to create colder temperatures. As such, these two conditions are revised to the single condition of linear conductance to prevent overcooling.

Fig. 9.8 shows the effect on panel temperatures of varying the total linear conductance between the panels and the spacecraft. The change in the linear conductance was modelled by varying the linear conductance of the conduction path that represents the connectors. The existing linear conductance provided by the aluminium connectors is 3.5 W/K and forms the middle linear conductance shown. These results are a good example of how increasing the flow of heat between panels and spacecraft brings the panel temperature closer to the spacecraft. Over the course of the orbits considered, there is a slow change in the temperature of the system, caused by the slow response of the spacecraft to the environment. The system has thus not achieved a consistent temperature pattern. The consistent temperature pattern maximum and minimum

temperatures can be predicted by fitting exponential curves with offsets to the data, the offset being the temperature that the system is tending towards.

The consistent temperature patterns vary with linear conductance and thus the minimum linear conductances to keep the battery temperature safe can be deduced by fitting curves to the data. It was found that quadratic curves fitted to this data in low orbits predicted that there would indeed be a maximum linear conductance, above which overcooling would occur. However, investigation of this prediction found it to be false as a model run at this high linear conductance did not have any panels that overcooled. The results showed that with increasing linear conductance the temperatures tended towards a consistent temperature pattern. An exponential curve with an offset was thus fitted to the data and the concept of a maximum linear conductance was rejected. Curve fitting was used to predict the temperatures to reduce the required simulation time. To ensure confidence in the predictions, a sample of the simulations were run for longer to check that the consistent temperature pattern matched the predictions

Taking the results in fig. 9.8 as an example, the minimum temperature and maximum panel temperature over the ten orbits for a linear conductance of 3.5 W/K are shown in fig. 9.9. The end values are not used as they are incomplete orbits. For each linear conductance, exponential curves with offsets are fitted to these results, indicating the temperatures tended towards. Thus, in fig. 9.10, the variation of minimum and maximum temperatures with linear conductance can be plotted and a curve fitted to the data. From this curve the minimum linear conductances needed can be determined, as illustrated on fig. 9.10.

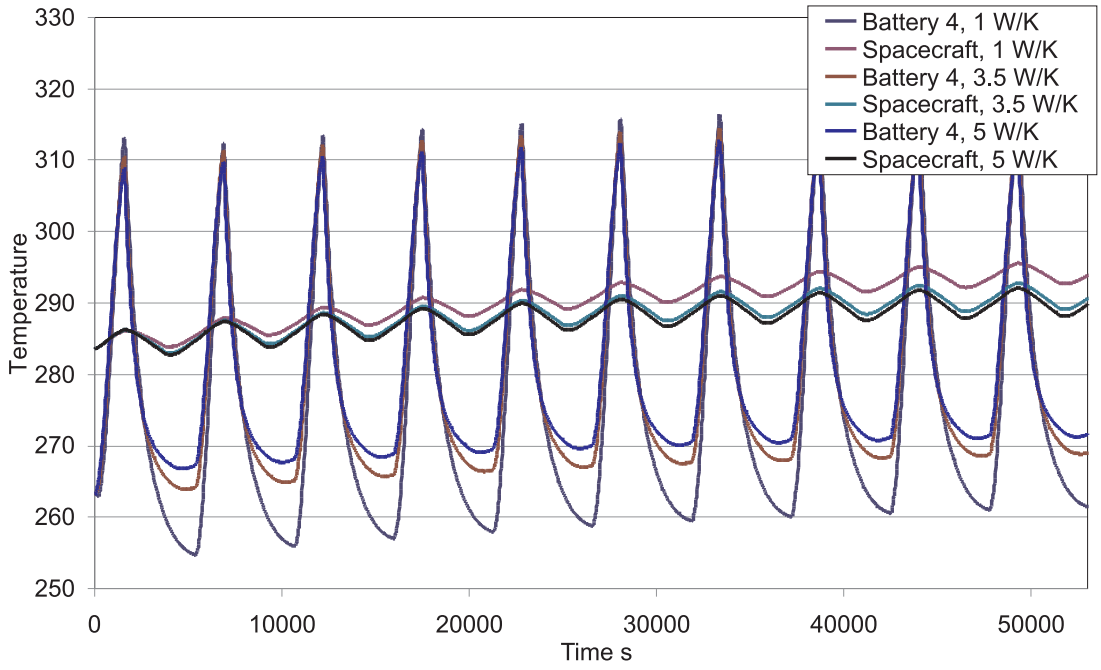

Figure 9.8: *A sample of the effect of varying linear conductance on the body mounted in a hot 200 km LEO.*

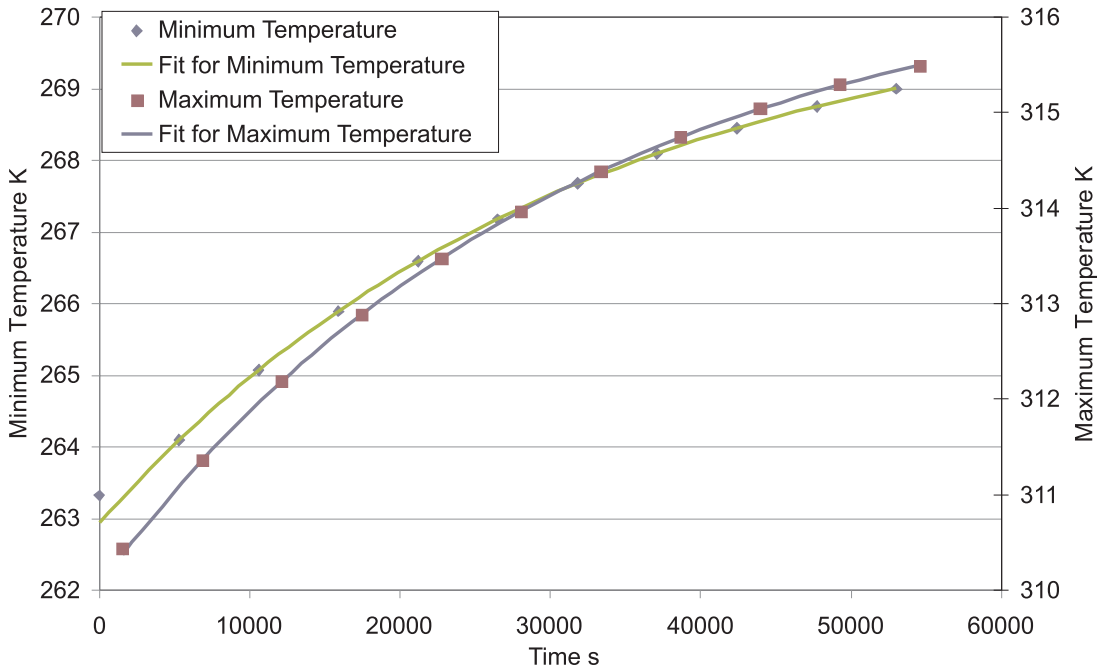

Figure 9.9: *Minimum and maximum temperatures for ten orbits in hot 200 km LEO for a linear conductance of 3.5 W/K.*

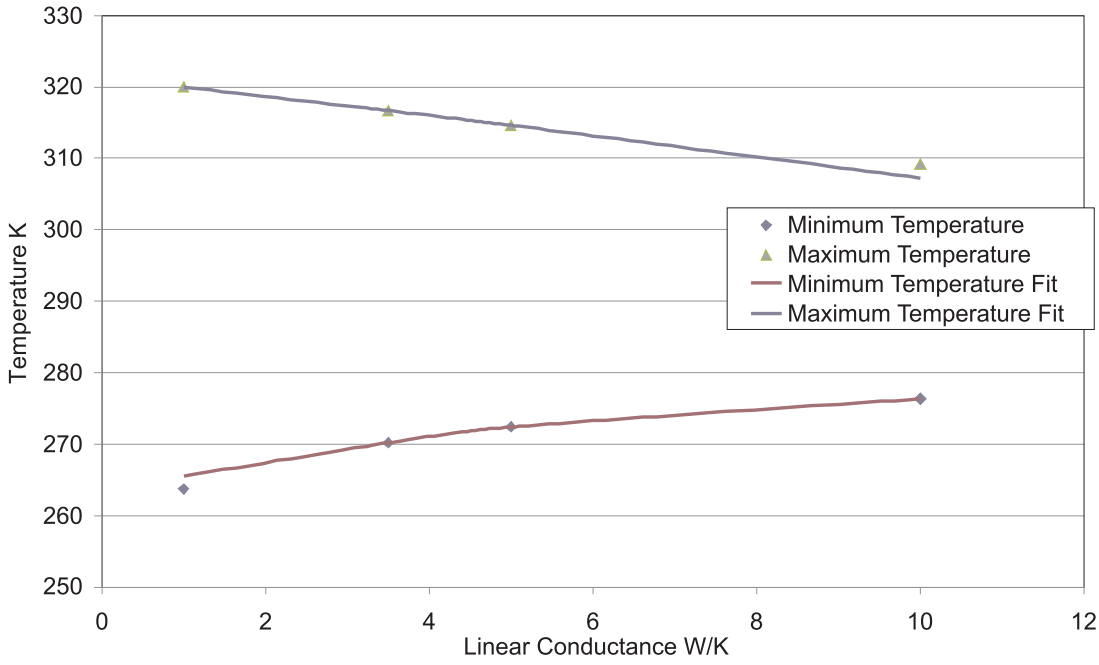

Figure 9.10: *Illustration of the minimum linear conductance determination for a hot 200 km LEO.*

9.5.2 Linear Conductance Requirement

The change of requirement with altitude from preventing overcooling to preventing overheating indicates that the minimum linear conductance will vary with altitude. Figures 9.11 and 9.12 show the variation of minimum linear conductance[9.2] with altitude. The line at 3.5 W/K indicates the existing linear conductance provided by the aluminium connectors.

The requirement to prevent overcooling is consistently below the existing linear conductance, as could be predicted by the lack of overcooling in the baseline results. In the cold environment, the requirement initially decreases with altitude as the spacecraft spends longer in sunlight, experiences a small rise as the input from the Earth decreases, falls again as the spacecraft temperature rises further and then experiences a slow small increase at high altitude due to the lengthening time spent in shadow. In the hot environment, the increased input is so much that at very low altitudes, the radiation heat flow between the panel and spacecraft is enough, as the required linear conductance is 0 W/K. From this, the requirement then follows the same pattern as the cold environment, though at a third of the value.

[9.2] Uniform across all panels.

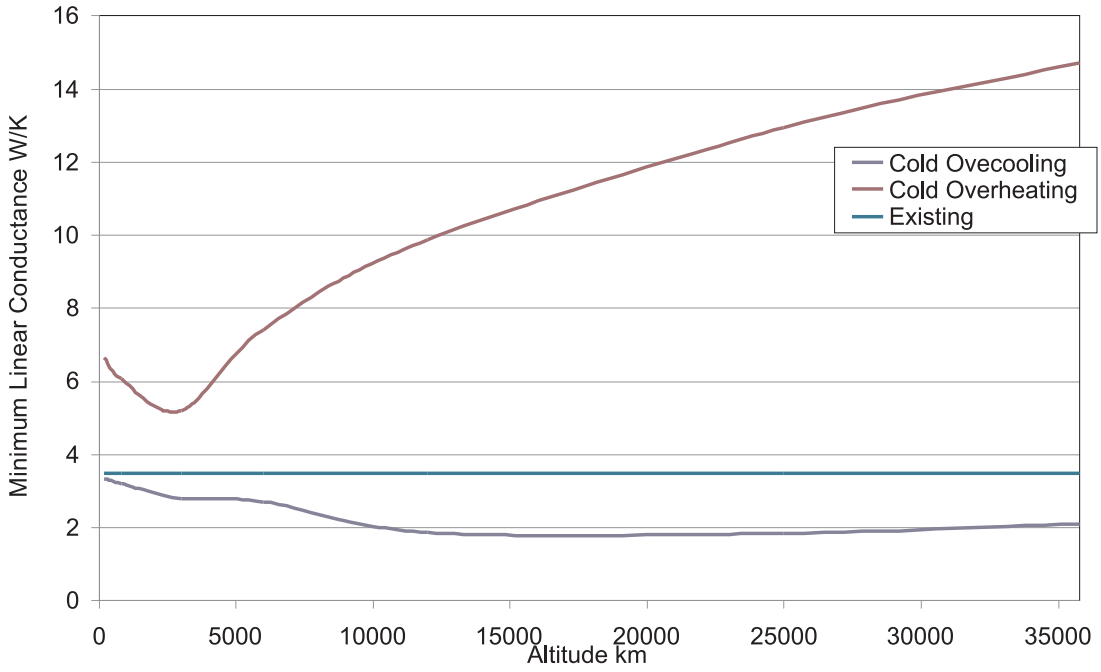

Figure 9.11: *Variation of required linear conductance to prevent overcooling with altitude in the cold environment.*

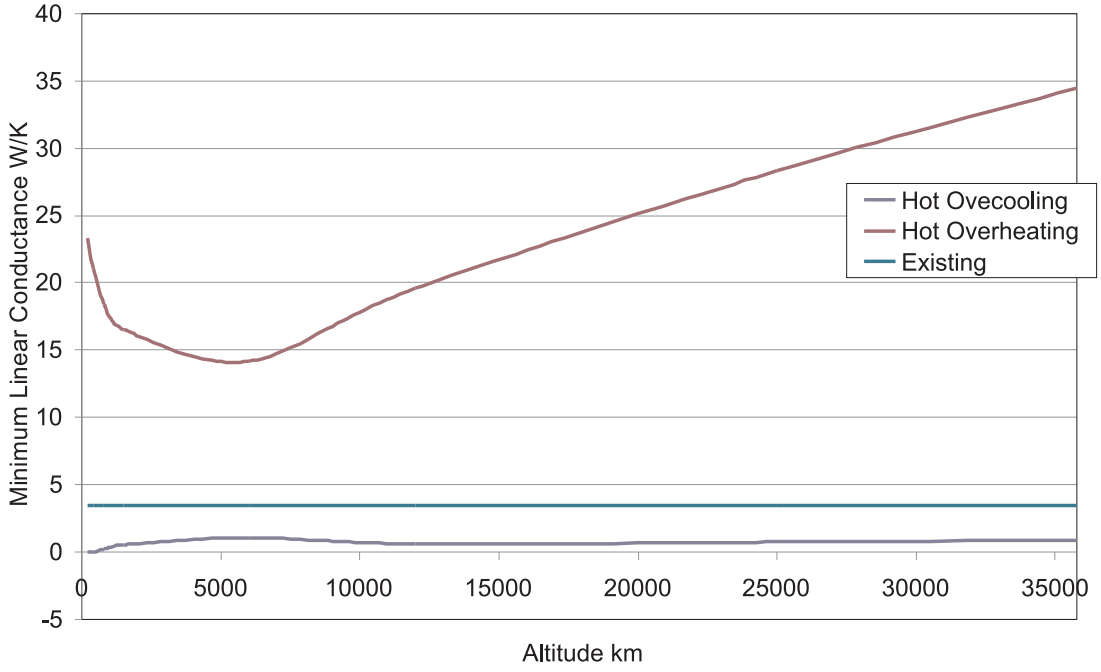

Figure 9.12: *Variation of required linear conductance to prevent overcooling with altitude in the hot environment.*

In both environments, the overheating requirement decreases as the input from the Earth reduces and then increases as the spacecraft temperature increases. The requirement is always above the existing linear conductance. As such, while there is no orbit altitude where the battery temperatures are safe with the current linear

conductance, figs. 9.11 and 9.12 show that altering the linear conductance is feasible.

9.5.3 Viability of Thermal Links

Figure 9.13 shows a typical commercial thermal strap used to transmit heat loads. This particular strap uses k1100 carbon fibres, giving it a thermal conductivity of 980 W/mK at 273 K [86]. Assuming that the strap mountings are highly conductive, that the strap is straight across the gap between panel and spacecraft (a length of 20 mm) and that the cross sectional area is 22 mm[29.3]; the linear conductance is 1.1 W/K for a mass of 1 g, not including the mountings. This results in a specific linear conductance of 1114 W/kgK. To meet the highest requirement of 35 W/K a mass of 31 g is needed per panel, not including mountings. Another potential thermal strap is available from k Technology [87]. Also based on carbon, they have a linear conductance of 0.82 W/K for a mass of 77 grams including mountings; a specific linear conductance of 10 W/kgK. This provides a more realistic figure than the previous mountingless strap considered. The mass of four of these straps is 24 % of the MFPS saving. This small increase is not enough to enable any orbits in either environment.

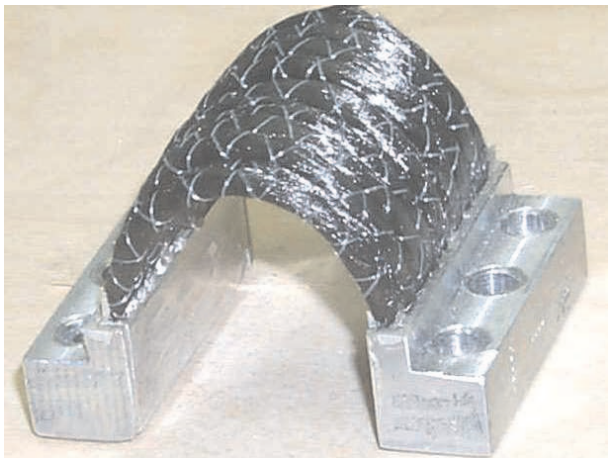

Figure 9.13: *An example of a thermal strap, ©Technology Applications, Inc.*

Tables 9.2 and 9.3 consider how the existing connectors could be altered to provide the required linear conductance. From section 7.2.2 three methods are available. Firstly, a material with a higher thermal conductivity can be used. Table 9.2 presents a selection of materials that have better conductivity and presents the mass of the connectors if they were made of this material. As can be seen, materials exist for which the linear conductance of the connectors can be greatly improved and the mass of the connectors

[9.3]Estimating from the figure.

reduced. Table 9.3 shows the increase in mass required if the cross sectional area of the connectors was increased. Sacrificing half of the 1.3 kg MFPS saving increases the linear conductance to 20.8 W/K, which meets the requirement of all cold altitudes and all hot altitudes between 600 km and 12000 km.

The mass of the connectors can be reduced at no cost to the MFPS benefit by reducing the distance between the panel and spacecraft. Halving the distance to 10 mm, gives a 0.06 kg mass saving and doubles the linear conductance to 7 W/K. Referring to figs. 9.11 and 9.12 this meets the requirements for cold altitudes below 5500 km but no hot altitudes. Combining an increase in area with a 50 % reduction in thickness would double the effectiveness of the results in table 9.3. Unfortunately, while altering the connectors has been shown to be viable, these connectors have structural requirements of holding the panels in place and 'absorbing' thermal expansion differences. As such, the extent of how the connectors can be altered is limited.

Table 9.2: *Effect of altering the body to panel connector material on linear conductance and mass.*

Material	Thermal Conductivity	Density	Linear Conductance of Four Connectors	Total Connector Mass	% Mass Change
	W/mK	kg/m^3	W/K	kg	%
Aluminium Alloy	138	2700	3.5	0.11	
Copper Alloy	385	7760	9.8	0.32	2.9
Tungsten	163	1930	4.2	0.08	0.7
Diamond	2000	3520	51.0	0.14	1.3
Carbon Fibre	640	2130	16.3	0.09	0.8
Silver Alloy	295	10300	7.5	0.42	3.8
Molybdenum Alloy	155	3330	4.0	0.14	1.2

Table 9.3: *Effect of altering the body to panel connector geometry on linear conductance and mass.*

Area	Total Mass	Linear Conductance of Four Connectors
cm^2	kg	W/K
2.5	0.1	1.7
5	0.1	3.5
10	0.2	6.9
20	0.4	13.8
40	0.9	27.6
80	1.7	55.2

Optimisation of the design of the connectors between panel and spacecraft has been shown to have the potential for not only making all orbits feasible, but to also provide extra savings through the alteration of geometry and material. Thus improving the flow of heat between panels and spacecraft is a very viable option. However, if the connectors are not available for structural reasons, then the use of additional thermal straps is not viable for any orbit, as the mountings of the straps add too much mass for the conductivity added.

9.6 Phase Change Materials

In the same manner as described in section 8.5, a phase change material is added to the panels. The PCM is added to all panels that experience overheating: all panels in GEO, panels 1, 2 and 4 is the hot LEO and only panel 4 in the cold LEO. Section 8.5 has shown that a PCM is more effective the closer the transition temperature is to the equilibrium temperature it is trying to prevent. As such, a PCM with a transition temperature close to 318 K is required. Tables 8.8 and 8.9 do not contain any PCMs that have a transition temperature above 308 K, so Disodium Phosphate Dodecahydrate [9.4] is used. Table 9.4 shows the mass required for each case. The pause energy presented is the minimum pause energy for each panel.

[9.4] Chemical Symbol $Na_2HPO_4 \cdot 12\,H_2O$, transition temperature 313 K, heat of fusion 279 KJ/kg, salt hydrate, Sharma et al. [69].

Table 9.4: *Mass of PCM required to maintain battery temperature in the Earth pointing body mounting.*

Case	Panel 1 Pause Energy KJ	Panel 2 Pause Energy KJ	Panel 3 Pause Energy KJ	Panel 4 Pause Energy KJ	Total Mass kg
LEO Cold	-	-	-	0.6	0.002
LEO Hot	16	14	-	35	0.24
GEO Cold	2860	1990	1280	2970	32.6
GEO Hot	4190	2530	2320	3680	45.6

In LEO, the masses of PCM required are low. Even if the extra mass issues, as discussed in section 8.5, led to a doubling of requirement, this would only be a 37 % loss of the MFPS saving in the hot LEO case. The LEO cases move from feasible to viable because of the short times the panels spend too hot. In the cold LEO case, this time is especially short and involves only one panel, leading to the very loss mass requirement seen. The GEO cases however are not viable due to the extremely large masses required. This is because the panels in GEO are too hot for long periods of time.

9.7 Heaters

The use of heaters is not considered in this application as the Earth pointing body mounted system does not experience overcooling.

9.8 Summary of Viability for Body Mounted Panel

The thermal control solutions considered for the Earth pointing body mounted orientation have shown a range of viability and feasibility. Altering the heat flow between the panels and the spacecraft is dependent on if a thermal requirement can be added to the design of the connectors. It has been shown that it is possible to enable all orbits with such a redesign, with the added bonus of further mass savings from the connector themselves, ensuring that there is no loss of MFPS savings. However, if the connectors cannot be redesigned, then the use of thermal straps alone has been shown to be not viable as while the conducting materials themselves are lightweight, the mass of

the mountings uses up too much of the MFPS benefit.
PCMs have been demonstrated to provide a feasible solution for overheating in the LEO, despite the mass of containment. From this it can be inferred that a limited number of orbits can be enabled where very limited overheating occurs, though for overcooling a heater is a more efficient solution. The replacement of the honeycomb core with aerogel was shown to be a feasible solution if the spacecraft's emittance was increased to allow for the radiation of heat from the electronics inside the spacecraft. However, the mass of the aerogel was too high and the TCS is not viable for any orbit. Lastly the alteration of heat loss from the spacecraft, either through different coatings or through louvres was found to an unfeasible solution by itself for all orbits. Changing the optical properties of the spacecraft has been shown in the insulation case to aid the viability of other TCS.

9.9 Effect of Configuration Variations

Details of the viability assessment of TCS for the variations can be found in appendix B.3. The three variations to the body mounting orientations each have different effects on the viability of the TCS considered. The three panel Earth pointing orientation is warmer due to its reduced heat loss. This makes efforts to prevent overcooling more viable. However, this warming increases overheating issues, reducing viability for TCS that prevent overheating.
The Sun pointing spacecraft is cooler and there are panels that are permanently shaded. This makes prevention of overcooling less viable. The concentration of heat for a long period of time on one panel dampens the improvement in overheating TCS viability.
The space pointing orientation has the most beneficial effects as the spacecraft is warmer than in the Sun pointing orientation, making it easier to prevent the shadowed panels from overcooling and the heat from the Sun is distributed over two panels, making it easier to prevent overheating.

Chapter 10

Discussion

The thermal analysis must be accurate enough that conclusions can be drawn from it. As any numerical simulation will be greatly affected by the design of the MFPS and the numerical assumptions made, assessments of these effects are required. As such, this chapter is formed of two themes; firstly a discussion of how the input values to the models affect the potential viability of thermal control and secondly the effects of the assumptions and methods used to build the model are assessed.

10.1 Effect of Battery Cell Thermal Envelope

The work so far has concentrated on a battery cell that has the thermal envelope of 273 K to 318 K. As another cell chemistry with more restrictive thermal limits could be used in the COTS MFPS, it is thus important to determine what effect this would have on the required thermal control authority. Thus a cell that has a thermal envelope 10 K stricter is considered (283 K to 308 K).

Figures 5.1 and 5.2 show the equilibrium temperatures in both hot and cold environments. When the stricter envelope is applied to these results, the regions in which a battery temperature is unsafe are larger. In the cold environment, the overheating region extends to a higher altitude, with fewer orbits now with safe equilibrium temperatures. In the hot environment, the geosynchronous equilibrium temperature is 310 K. This has a disastrous effect as there are now no safe equilibrium temperatures in this environment at any altitude. Applying the stricter limits to the transient results in fig. 5.3 shows that overheating is now an issue in the cold LEO and hot GEO cases. As all of the body mounting orbits have been shown to require thermal

control, a stricter thermal envelope has a less dramatic effect, but does increase the gap between the extremity temperatures and the envelope. The key changes implied by figs. 6.8 to 6.11 is that overheating now occurs in the cold LEO cases and overcooling occurs at geosynchronous altitude. Both overcooling and overheating of panels now occurs in all orbits, indicating that thermal control has become more difficult.
Table 10.1 shows the effect on the requirements on the use of coatings for the wing application. The emittances required to prevent overheating and overcooling have moved further apart, with increased emittance now required to prevent overheating and reduced emittance required to prevent overcooling. The increase in emittance is such that in the hot LEO case, there is no emittance value that will prevent overheating. The emittances being further apart means that the use of the emittance to prevent overheating will give a reduced time to overcool when the panel enters eclipse compared to the MFPS with the wider limit and vice versa, reducing the number of orbits that are enabled by using coatings. Similarly, this larger gap between the overheating and overcooling requirements makes the use of louvres less feasible. Indeed, fig. 8.8 shows that what was once a feasible louvre in the cold LEO case is now not feasible as the minimum and maximum temperatures for even the best possible emittances are outside the tighter envelope.

Table 10.1: *Effect of the stricter battery thermal envelope on coating emittance requirement.*

Case	Strict Envelope		Baseline Envelope	
	Minimum for overheating	Maximum for overcooling	Minimum for overheating	Maximum for overcooling
LEO Hot	X	0.19	0.9	0.32
LEO Cold	0.94	0.12	0.66	0.25
GEO Hot	0.98	X	0.77	X
GEO Cold	0.85	X	0.66	X

Table 10.2 shows how the time to overcool when using insulation is reduced when the lower battery temperature has been increased. The effect is to reduce the viability of using insulation to prevent overcooling in eclipse. A heater with an activation temperature of 284 K[10.1] is required to output 450 W of power to prevent overcooling during eclipse. This requires 210 Whr of extra battery capacity which is 46 % of the

[10.1] A 1 K safety margin.

MFPS as 1.27 kg. This is an increase from the 19 % for the 273 K limit in a cold LEO. $CaCl_2 \cdot 6\,H_2O$ + $CaBr_2 \cdot 6\,H_2O$ (45 % + 55 %) [10.2] is a PCM that could used to prevent overcooling during eclipse. In a cold LEO orbit, fig. 8.14 has shown that there is no feasible amount of PCM that can prevent overcooling below 273 K, implying strongly that it is also not feasible for the stricter condition of 283 K. To prevent overcooling in the hot LEO case, 12.3 kg of $CaCl_2 \cdot 6\,H_2O$ + $CaBr_2 \cdot 6\,H_2O$ (45 % + 55 %) is required, a clearly unviable amount. Using 25 %, 50% and 75 % of the MFPS saving gave 759 s, 878 s and 998 s of delay before overcooling occurs, a clear reduction of the performance seen in fig. 8.16.

Table 10.2: *Effect of stricter battery thermal envelope on the time to overcool offered by insulation.*

Case	Strict Envelope Time	Baseline Envelope Time	Difference
200 km LEO Hot	1045 s	1527 s	-482 s
200 km LEO Cold	743 s	1209 s	-466 s
GEO Hot	777 s	1121 s	-344 s
GEO Cold	647 s	992 s	-345 s

Table 10.3 shows how the linear conductance requirement of the Earth pointing body mounting is altered by the stricter battery limits. In all cases there is a substantial increase, one that greatly reduces the viability of using of improved conductance as a thermal control solution. The stricter limits also produce cases where there is no solution. In LEO, overcooling cannot be prevented as the increase in heat flow to the shadowed panels also increases the heat loss of the system. In geosynchronous orbits, overheating cannot be prevented as while there is improved conduction away from the sunlit panels, the rate at which the system loses heat from the solar cells is unchanged, limiting how cold the system can get.

To summarise, as would be expected, stricter limits on the temperature of the battery reduces the viability of the available thermal control solutions and thus the range of orbits that the battery can be used in is reduced. In the reverse case, a battery with a wider operating temperature range would be viable to use in a greater range of orbits.

[10.2] Transition temperature 287.7 K, heat of fusion 140 kJ/kg, eutectic, Sharma et al. [69].

Table 10.3: *Effect of stricter battery thermal envelope on the required linear conductance. Baseline values are in parentheses.*

Case	Overheating W/K	Overcooling W/K
200 km LEO Hot	11.4 (0.53)	X (5.5)
200 km LEO Cold	3.8 (2.5)	X (31.1)
GEO Hot	X (34.5)	5.7 (0.9)
GEO Cold	X (14.7)	11.7 (2.1)

10.2 Effect of the Application Design

The design of the MFPS applications is, as would be expected, a key factor in determining the viability of TCS. The design of the MFPS is represented by the values that form the inputs to the numerical models.

10.2.1 Estimated Values

The following properties are considered separately as they have been estimated; see appendix D for calculation and table 10.4 for details of these properties. They are thus a potential source of error in the model, in addition to their effects on TCS viability.

The density and specific heat capacity are not stated in favour of the heat capacity of the component in situ as this is the thermal property that is effected. Table 10.4 shows how the minimum and maximum predicted temperatures alter with variation in these properties, for a hot LEO case of the wing mounting. The table shows the initial value, its value ± 50 % and the resulting minimum and maximum temperatures, with the change from the original in parenthesis. The results show that a 50 % change in the conductivity does not cause changes in the predicted temperatures greater than 1 K, showing that the model is not sensitive to changes in the conductivity. Greater conductivity improves heat flow and causes the extremity temperatures to become worse. The heat capacity has up to a 4 % effect on the battery temperature. This potentially significant variation is caused by the importance of the heat capacity in determining the response of the panel to its environment. Changes or errors in the heat capacity will therefore have an effect on the accuracy of the specific examples.

Table 10.4: *The effect of errors in the estimated properties. Temperatures are in kelvin and the values in parenthesises are the changes from the baseline results. The orbit is a 200 km hot LEO.*

Property	Value	-50 %	+50 %	Resulting Minimum Temperature (Change)		Resulting Maximum Temperature (Change)	
				-50 %	+50 %	-50 %	+50 %
Cell Conductivity	0.72 W/K	0.36	1.08	243.8 (0.9)	317.2 (-0.3)	242.5 (-0.3)	317.7 (0.1)
Facesheet Conductivity	1.28 W/K	0.64	1.92	243.3 (0.4)	317.4 (-0.1)	242.8 (-0.1)	317.5 (0)
Cell Heat Capacity	0.89 J/K	0.45	1.34	235.3 (-7.6)	321.2 (3.6)	248.8 (5.9)	314.5 (-3.1)
Facesheet Heat Capacity	2964 J/K	1482	4447	233.4 (-9.5)	322.0 (4.5)	250.2 (7.3)	313.7 (-3.9)

10.2.2 Design Values

The following properties are design values, values that have been chosen as they are representative of current spacecraft design. Tables 10.5 and 10.6 show how variation in these values affects the predicted temperature for the wing and body mounted panels in a hot 200km LEO. Some of these variables are not direct input values themselves. Instead, they are variables that are a function of direct input values. Rather than vary these input values that have the same effect, only the variable they effect is altered.

- Battery size - the effect of the dimensions of each battery cell.
- Solar cell heat capacity - a function of thickness, density and specific heat capacity.
- Honeycomb effective area - the geometry of the honeycomb.

The results in tables 10.5 and 10.6 show that when altering the design values, the change in temperatures are caused by three broad effects. The greatest effect is caused by alteration of the solar cell optical properties, which effects how the MFPS interacts with its environment. Reduction in the absorptance greatly reduces the heat input shifting the thermal issues towards overcooling. Solar cells with low emittances have the opposite effect, causing a large warming to the MFPS. Indeed, in the 50 % changes considered above, with low absorptance, all temperatures are too cold and with low emittance all temperatures are too hot, with a correspondingly large effect on viability.

Table 10.5: *Effect of altering the MFPS design on the wing mounted panel in a hot 200 km LEO. Temperatures are in kelvin and the values in parenthesises are the changes from the baseline results. The orbit is a 200 km hot LEO.*

Property	Value	-50 %	+50 %	Resulting Minimum Temperature (Change)		Resulting Maximum Temperature (Change)	
				-50 %	+50 %	-50 %	+50 %
Cell Size	14.76 cm^2	7.4	22.1	236.9 (-5.9)	320.7 (3.1)	248.9 (6.1)	314.2 (-3.3)
Battery Depth	4	2	6	242.4 (-0.5)	317.8 (0.2)	246.5 (3.6)	316.2 (-1.4)
Solar Cell Heat Capacity	514.3 J/K	257.15	771.45	242.1 (-0.7)	317.9 (0.4)	243.6 (0.7)	317.2 (-0.4)
Honeycomb Material Conductivity	138 W/mK	69	207	243.1 (0.2)	317.6 (0.1)	243.2 (0.4)	317.5 (-0.1)
Honeycomb Specific Heat Capacity	880 J/kgK	440	1320	241.6 (-1.3)	318.2 (0.6)	244.1 (1.2)	316.9 (-0.6)
Honeycomb Effective Area	0.042	0.021	0.063	241.8 (-1.1)	318.3 (0.7)	243.9 (1.1)	316.9 (-0.7)
Panel Area	1 m^2	0.5	1.5	252.5 (9.6)	312.0 (-5.5)	238.9 (-4)	319.7 (2.1)
Battery Capacity	1000 Whr	500	1500	236.9 (-5.9)	320.7 (3.1)	248.3 (5.5)	314.6 (-2.9)
Sun CFRP Thickness	0.0018 m	0.0009	0.0027	238.3 (-4.6)	319.9 (2.3)	246.7 (3.9)	315.4 (-2.1)
Honeycomb Thickness	0.012 m	-	0.018	-	-	244.8 (2)	316.8 (-0.8)
Dark CFRP Thickness	0.0018 m	0.0009	0.0027	238.6 (-4.3)	319.5 (1.9)	247.0 (4.2)	315.6 (-2)
Solar Cell Absorptance	0.91	0.46	-	216.2 (-26.6)	236.7 (-80.8)	-	-
Solar Cell Emittance	0.8	0.4	-	253.7 (10.9)	339.1 (21.5)	-	-

Table 10.6: *Effect of altering the MFPS design on the body mounted panel in a hot 200 km LEO. Temperatures are in kelvin and the values in parenthesises are the changes from the baseline results. The orbit is a 200 km hot LEO.*

Property	Value	-50 %	+50 %	Resulting Minimum Temperature (Change)		Resulting Maximum Temperature (Change)	
				-50 %	+50 %	-50 %	+50 %
Cell Size	14.76 cm^2	7.4	22.1	270.6 (0.2)	318.4 (0.5)	271.0 (0.6)	317.6 (-0.4)
Battery Depth	4	2	6	270.6 (0.2)	318.1 (0.2)	270.6 (0.2)	317.6 (-0.4)
Solar Cell Heat Capacity	246.90 J/K	123.45	370.35	270.5 (0.2)	318.4 (0.5)	270.8 (0.4)	317.9 (-0.1)
Honeycomb Material Conductivity	138 W/mK	69	207	270.6 (0.2)	318.1 (0.1)	270.7 (0.3)	318.3 (0.3)
Honeycomb Specific Heat Capacity	880 J/kgK	440	1320	270.7 (0.3)	318.6 (0.6)	270.8 (0.4)	317.6 (-0.3)
Honeycomb Effective Area	0.042	0.021	0.063	270.5 (0.1)	318.8 (0.8)	270.9 (0.5)	317.5 (-0.4)
Panel Area	0.48 m^2	0.24	0.72	275.6 (5.2)	310.3 (-7.7)	267.9 (-2.5)	321.8 (3.9)
Battery Capacity	111 Whr	55.5	166.5	270.6 (0.3)	318.7 (0.8)	270.8 (0.4)	317.6 (-0.3)
Sun CFRP Thickness	0.0018 m	0.0009	0.0027	270.4 (0)	319.8 (1.8)	271.1 (0.8)	316.5 (-1.4)
Honeycomb Thickness	0.012 m	0.006	0.018	-	-	270.7 (0.4)	317.3 (-0.7)
Dark CFRP Thickness	0.0018 m	0.0009	0.0027	270.4 (0)	319.5 (1.5)	271.0 (0.6)	316.5 (-1.4)
Solar Cell Absorptance	0.91	0.455	-	243.3 (-27.1)	255.9 (-62.1)	-	-
Solar Cell Emittance	0.8	0.4	-	326.4 (56)	371.4 (53.5)	-	-
Spacecraft Heat Capacity	177488 J/K	88744	266232	269.3 (-1.1)	317.9 (-0.1)	271.1 (0.8)	314.2 (-3.7)
Emittance of Facing Surfaces	0.94	0.47	-	267.0 (-3.4)	323.4 (5.5)	-	-

It is worth noting that alteration of these properties can be seen as a good model for altering the packing factor of the solar cells, as the key effect of this is to alter the optical properties of the Sun facing surface, with the effects as described.

The next most significant factor on the extremity temperatures are those design values that alter the heat capacity of the MFPS. As would be expected, with higher heat capacity, the minimum and maximum temperatures tend towards the battery temperature envelope. The design values affecting this most are the area of the panel, the battery capacity and the thickness of the facesheets. As such, for an MFPS that is larger, has greater battery capacity or has thicker facesheets, the thermal control requirements will be easier.

The results in tables 10.5 and 10.6 and table 10.4 show that small variations in the conductivity of the panels have little effect on the MFPS temperatures. This is mostly caused by the facesheets and honeycomb core having low conductivities, so that a 50 % change will not have a great effect. Section 8.2 has shown the effects of a very low conduction and thus it is reasonable to assume that with higher conductivity, heat flow will be greater and thus the rate of change of temperature of the battery will increase, resulting in more extreme temperatures. This will reduce TCS viability as the range of battery temperatures to be suppressed is increased.

The following design properties have already been assessed as part of a thermal control option:

- The conductivity of the core material has been assessed in the discussion on the use of insulation, sections 8.2 and 9.3.
- The optical properties of the coating on the shadowed side of the wing mounting has been considered in section 8.1.1.
- The optical properties of the coating given to the spacecraft sides that do not have a panel mounted to them is discussed in section 9.1.
- The properties of the connectors between panel and spacecraft in the body mounting form a key part of section 9.5.

10.3 Assessment of Model Assumptions and Methods

10.3.1 Assumptions and Simplifications

Each of the following assumptions made in the modelling is assessed here for its affect on the predicted battery temperatures.

- Modelling each layer as a single lumped node with a heat capacity with conduction paths to two interfaces nodes forces the temperature profile across the layer to two linear variations; between interface node and heat capacity node and between heat capacity node and the other interface node. This is a simplification of the reality in which a more complex distribution would be observed. As the individual layers are very thin, the largest being 12 mm, it is unlikely that any complex thermal gradients could develop or that they would produce a significant effect on the layer temperature.
- The reduction of an entire layer to a single node removes from consideration the flow of heat across the layer and temperature variation across a layer. This is not considered to alter the results as there is no heat loss from the panel edges, as detailed in section 4.2. If heat were lost from the panel's edges, then the distribution of temperature across each layer would not be uniform and would vary from being hottest at the centre to coldest at the panel edges. Modelling the layer as only one node suppresses this effect.
- The cells are collected together in a single group rather than distributed about the honeycomb and the grouping has a consistent depth. The cells and the honeycomb core around them are modelled thus by a single lumped mass node each, representing parallel paths through the panel, with no heat flow between them. Lumping the cells together has the effect of increasing the rate of heat flow as the battery thermal conduction, though very low, is still better than that of the honeycomb core once the small contact area with the cells and the effect of the core shape is taken into account, see appendix D.3. Thus a battery at the centre of the grouping would lose heat faster through the surrounding cells; faster than it would through a honeycomb surrounding. Given the low contact area and conductivity of the honeycomb/cell interface, the insulation of the cells caused by

the lack of heat flow between them in the numerical models is near negligible.

- The solar cells were converted to a smeared mass while their optical properties were applied to the Sun side facesheet. This was done as their thinness and high thermal conduction caused their linear conductance to be so many orders of magnitude greater than that of the honeycomb and battery so as to prevent convergence. This is a reduction in detail of the model. While the heat capacity of the solar cells is retained the effect of the extra layer of conducting material is lost. The effect on the model accuracy should be minimal as the high linear conductance of the layer meant that the layer provided no insulation and would not have slowed the dispersion of heat through the model. As such its absence will produce only a minimal increase in heat flow.
- The removal of heat exchange by radiation inside the honeycomb from the models effectively increases the insulating properties of the honeycomb. However, as stated, the radiation exchange is 2 to 4 orders of magnitude smaller than the conductive flow of heat through the metal of the core, appendix C.3. As such this simplification will have no real effect on the temperature distribution in the panel.
- The model does not account for the variation of optical properties of the surfaces with frequency/wavelength in the infrared spectrum. Kirchoff's law is applied to all surfaces and it is assumed that emittance quoted for a surface is correct and constant for all heat input and radiation emission. Potential error is difficult to quantify as the emittance could vary both up and down. The emittances in Gilmore [50, Appendix A] are quoted for room temperatures. As such, when the model diverges away from room temperatures, the accuracy of the emittances and thus the model reduces. Fortunately, the battery temperature envelope of 273 K to 318 K is a room temperature range. As such the more effective a thermal control solution is at keeping the system temperature close to and within the battery envelope the more reliable the emittance value is. I.e, the model is more accurate for thermal control solutions that meet the requirements.
- Orbit perturbation is not considered to simplify the model. This was done as the focus of the model is thermal modelling, not modelling of the spacecraft orbit about the Earth. The effect of modelling orbit perturbation or allowing the orbit to proceed would be for the thermal conditions to drift away from the worst case scenario. Thus this assumption is conservative as it forces the panel to experience

only the worst case thermal environments.

- Beyond the Earth and the Sun, the environment consists only of background space which is given a temperature of 4 K. Variation of this temperature will be small and produce only a negligible effect on radiation of heat from the spacecraft, which is determined by the difference in temperature between the surface and space. The removal of all other objects is considered to have no effect as all other celestial bodies are too far away from the panel to have any thermal effect on the panel.
- The eclipse simulation used in the model treats the Earth's shadow as a cylinder, when in fact it is tapered due to the difference in size between the Earth and the Sun. The spacecraft is simulated as having the full power of the Sun on it until it enters the shadow. In reality, the spacecraft would experience a period of increasing shadowing as the Earth gradually blocked out the Sun, known as penumbra. A cylindrical eclipse acts at the centre of the penumbra so that the extra solar energy before eclipse is balanced by the reduction in solar energy caused by the removal of the second half of the penumbra. The observable effect for a simulation modelling penumbra would be that of cooling starting earlier but at a slower rate. In a 200 km LEO the time spent in penumbra is approximately 30 seconds (0.6 % of orbit time) and approximately 250 seconds in geosynchronous (0.3 % of orbit time), estimating from the case studies by Ortizlongo and Rickman [88]. These very small percentages of the orbit time indicate that the effect of this modelling is slight to negligible.
- The modelling of the spacecraft in the body mounted application has already been discussed in section 6.3.

10.3.2 Numerical Methods

In this work, two models have been used; an isothermal model and a lumped parameter model. The limitations of the isothermal model have already been discussed in chapters 5 and 6. The isothermal model calculates the equilibrium temperature of the isothermal node (which represents the MFPS) directly by solving Eq. 5.5 and is thus not subject to errors in a numerical method. To calculate the transient response an explicit fourth order Runge-Kutta approximation is used. The method uses a fixed time step which is the key source of potential errors. The constant time step does not react well to the changing nature of the inputs, which at the eclipse boundaries have abrupt changes.

This error will affect the predicted eclipse exit and entry temperatures by slightly rounding off the instantaneous change in heat input.

The lumped parameter model solves the equilibrium condition using an iterative method based upon solving Eq. 10.1[10.3]. For low temperature equilibriums, (less than 100 K) the method has been seen to have difficulty as at these low temperatures the difference between heat loss and heat input is very small; so small that the model suffers from converging before it reaches the correct solution. This error can be reduced by using a harsher convergence criteria but this increases run times.

$$\sum Q = 0 \tag{10.1}$$

$$\sum Q = MC\frac{dT}{dt} \tag{10.2}$$

For the transient method, ThermXL uses a finite difference approach which includes iteration at each time step and an adaptive time step, based on Eq. 10.2[10.4]. Iterating the results at each time step improves the accuracy of each individual time step while adaptive time stepping ensures that the simulation reacts to sharp changes in the environment. The errors associated with each time step are kept to a minimum by the software as each time step is typically less than 1 second and the convergence criteria for each time step is 1×10^{-4}, though this is at the cost of run time.

To conclude this discussion, the results of appendix C have shown that these two models match well to the results produced by finite element software, raising confidence further that the numerical methods used are producing only small errors that do not reduce the usefulness of the conclusions drawn from the results.

[10.3] Where Q is the heat input.

[10.4] Where Q is the heat inputs, M is mass, C is specific heat capacity, T is temperature and t is time.

Chapter 11

Conclusion

Multifunctional Power Structures (MFPS) offer system level mass benefits to spacecraft. The principle of combining the functions of power storage and structural integrity allows for the reduction and potential elimination of the parasitic masses associated with a discrete battery pack and a reduction in spacecraft bus volume as space inside the bus is longer required for a discrete battery pack. The potential for the technology to provide benefits has been shown by the literature, specifically the work by Roberts and Aglietti [7] which focuses on MFPS manufactured from Commercial off the Shelf components (COTS).

A thermal issue exists as the cells have strict temperature envelopes which they must stay inside to maintain the specified performance. This has been one of the main issues preventing the practical implementation of this technology. If MFPS are to be used on spacecraft, an assessment of which orbits they can and cannot be used in is required and this forms the objective of this thesis.

In order to do this, numerical models of example applications of COTS MFPS technology were created. These models consisted of a MFPS panel that would form part of a deployed wing solar array and a MFPS panel that would be mounted to the body of a spacecraft. These applications were chosen as they represent applications where the MFPS panel is a distinct component of the spacecraft system and is separate enough from the spacecraft that its temperature could not be controlled by a global Thermal Control System (TCS).

The assessment of orbit viability was carried out by first assessing which orbits would require thermal control by looking at both the equilibrium temperatures and the transient response of the models. With these done, a review of thermal control

technologies was carried out in which each TCS was assessed for feasibility (capability to maintain battery temperature) and then viability (the 'cost' of the TCS compared to the MFPS savings). From these results, it can be concluded that orbit viability is affected by two groups of parameters; the properties of the orbit and the properties of the MFPS. These parameters represent ranges of values that form the design space that the MFPS application exists within.

11.1 Contribution to Viability by the Orbit

The orbit defines the environment that the MFPS encounters. The effect of the orbit can be distilled into five key factors:

Eclipse Length The length of the eclipse determines the time the MFPS will spend without its main source of heat, the Sun. This will invariably lead to cooling, the length of which will determine the minimum temperature the MFPS will experience. Figures 6.3 and 6.4 show that without the Sun, the MFPS will cool to very cold temperatures. As demonstrated by fig. 5.1 eclipse equilibrium temperatures are so cold that cooling is continuous throughout eclipse. These figures reinforce that the length of eclipse is a key factor in overcooling, as the geosynchronous orbit minimum temperature is much colder than the 200 km LEO. Correspondingly, with decreasing eclipse length overcooling becomes less of an issue.

Sunlit Time The counterpoint to the eclipse length, the amount of time the MFPS spends in sunlight determines the maximum temperature. Figures 6.3 and 6.5 show the effect of extended sunlit times; the panel approaches and eventually achieves the sunlit equilibrium temperature. If this equilibrium temperature is safe, then there is no overheating. However, if the temperature is too hot, then as discussed in sections 8.5 and 9.6, the overheating is a significant problem as temperature rate changing TCS are not effective.

Entry Temperatures Related to the sunlit and eclipse times are the eclipse exit and entry temperatures. The eclipse exit temperature determines how much warming can occur before overheating. A higher eclipse entry temperature gives the MFPS a greater stored heat to survive eclipse. In effect the sunlit and eclipse times are

complimentary in that longer sunlit times mean the MFPS can survive a longer eclipse and a longer eclipse means a longer time in the Sun before overheating. Thus the orbit proportion that is eclipse strongly effects the orbit viability. Also, as the entry temperatures are limited by the temperature limits of the cells used, it can be recommended that thermal control is best served by the battery entry temperature being at the limit for the environment. For example, being as low as possible when entering sunlight

Earth Input The heat from the Earth has a 'measurable' effect when the spacecraft is within 10000 km of the Earth's surface. Proximity to the Earth's surface increases equilibrium temperatures in both sunlight and eclipse, often making the sunlit equilibrium too hot. A spacecraft that spends eclipse close to the surface of the Earth will find its cooling rate reduced by heat from the Earth, indicated by the much warmer eclipse equilibrium temperature in LEO in table 6.2. Conversely, a spacecraft that spends its sunlit time close to the Earth will have its heating rates increased by both Earth heat output and the albedo, increasing overheating.

Environment Throughout the study, two extreme environments have been considered, a hot environment and a cold environment. Both of these environments present benefits and hindrances. The hot environment promotes overheating but the resulting warmer eclipse entry temperatures is beneficial against overcooling. The cold environment reduces the risk of overheating but hinders efforts to prevent overcooling. The difference between the two environments is shown in figs. 3.6 and 3.7

11.2 Contribution to Viability by the MFPS Design

The design of the MFPS dictates how it reacts to the orbit it is placed in.

Optical Properties of Surfaces The optical properties of the surfaces of the MFPS are key in determining orbit viability. The rate at which heat is lost and gained by the MFPS determines rate of temperature change and, crucially, the equilibrium temperature. As shown in fig. 5.1, surfaces with high emittance ensure that equilibrium temperatures remain in the safe region. For orbits without safe equilibrium temperatures, the conflicting requirements of eclipse and sunlight

prevent a constant emittance from being used. The use of a coating with a low absorptance reduces overheating by reducing the input from Earth albedo.

Heat Capacity The heat capacity of the module determines the rate at which the MFPS responds to the environment, as shown by the assessment of the design values given in section 10.2. The thermal engineer has little to no freedom to determine the heat capacity of the MFPS panel, which is determined by the structure of the panel and the amount of battery capacity it contains. With higher heat capacity (heavier structure or greater battery capacity), the time taken for the MFPS to leave the safe region in either eclipse or sunlight increases greatly. The MFPS thus survives for longer in hostile environments which allows more orbits to be considered.

Orientation and Location For a deployed wing array MFPS, there is little variation in orientation as the spacecraft it is attached to will always be orientating so that these panels are perpendicular to the Sun. This orientation reduces the input from the Earth as the angle of incidence reduces near the terminator, leading to a cooler orbit. The lack of a substantial connection to the spacecraft effectively reduces the heat capacity of the system, increasing temperature change rates and therefore reducing the number of viable orbits and increasing the requirements on any potential TCS.

The body mounted MFPS has this extra heat capacity available but it is presented by the problem of panels shaded by the spacecraft and sunlit panels that have one of their radiating surfaces facing the warm spacecraft. These can lead to overheating and overcooling, as shown by figs. 6.8 and 6.10. The body mounting also shows how the pointing requirement of the spacecraft affects the temperature distribution. If the pointing requirement results in the spacecraft rotating with respect to the Sun, fig. 4.1, then the panels will potentially experience both overcooling and overheating over the course of an orbit as they are sunlit and shadowed in turn. These varying inputs lead to the temperature fluctuations that may be solved through the use of TCS that affects temperature change rates. When the pointing requirement results in the inputs being fixed, as in the Sun and space pointing orientations, then the panels tend towards overheating or overcooling, depending on their illumination. This creates a harsher situation as

TCS that alter rate of temperature change are not feasible here, as shown discussed in appendix B.3.2.4 and appendix B.3.3.4.

Number of Panels Reducing the number of body mounted panels means that more of the spacecraft surface is available to have its optical properties optimised to maintain the safe temperature of the remaining panels. As has been shown by appendix B.3.1.1 the presence of an extra surface improves the viability of the remaining surfaces. In the cases where the number of panels is reduced further, it is likely that the orientation of the spacecraft will have a Sun pointing aspect so that the remaining panels are illuminated. As such, the number of shadowed panels will decrease before the number of sunlit panels is decreased. This removal of shadowed panels reduces or removes overcooling and eases the limitations as TCS that might cause overcooling of the shadowed panels can now be considered to prevent overheating.

Properties of Spacecraft The properties of the spacecraft that the MFPS is attached to are influential on the thermal constraint. The greater the connection to the spacecraft (shown in section 9.5) and the greater the heat capacity of the spacecraft table 10.6, the more it contributes to keeping the MFPS within the safe limits of the battery. This extends to the temperature of the spacecraft, which as shown in chapter 9, strongly affects temperate of the MFPS attached to it.

Target Temperature Envelope A narrower temperature envelope reduces the orbit viability, as demonstrated by section 10.1.

11.3 Orbit Viability

Finally, taking into consideration how the orbit and MFPS design affect the thermal control requirements, as detailed above, the following can be concluded as the core of this thesis' contribution to the state of the art.

For a panel forming part of a deployed wing array:

- In both hot and cold environments, orbits that have no eclipse and pass above the sub solar point by at least 6000 km in the hot environment and 2000 km in the cold environment will always have an equilibrium temperature that is between 273 K and 318 K. These orbits do not require any thermal control and thus the MFPS

can be safely implemented without a TCS.

- A maximum length of eclipse exists, which is dependent upon altitude and environment and is defined by the time it takes the battery to become too cold. At low altitudes, orbits which have eclipses shorter than 890 s (hot)/ 720 s (cold) will not overcool and in addition will have a β angle such that they will not spend enough time above the sub-solar point to overheat. At geosynchronous altitudes, orbits that have eclipses shorter than 630 s (hot) / 560 s (cold) will not experience overcooling. Such orbits do not require a thermal control system. As these altitudes are the boundary cases of the eclipse environment, it can be said with confidence that the longest eclipse times for altitudes between 200 km and GEO will fall between the above values.
- For low Earth orbits that have eclipses shorter than 910 s (hot) / 1150 s (cold) and geosynchronous eclipses shorter than 840 s (hot) / 950 s (cold), applying a coating with the minimum emittance to prevent overheating is the best solution. As the panel will always have a coating on its dark side this simple method of thermal control can be implemented without mass penalty.
- For orbits with longer eclipses, the addition of a PCM is the most mass efficient solution for preventing both overcooling and overheating. The use of heaters may be twice as efficient, but cannot prevent overheating and indeed can cause overheating in low Earth orbit. Replacing the core with an insulating material prevents overheating and overcooling, but is less mass efficient and is only effective in orbits with eclipses shorter than 1520 s (hot) / 1200 (s cold) in low Earth orbit and 1120 s (hot) / 990 s (cold) in geosynchronous orbit. Louvres are potentially a mass efficient solution, but have been shown to be feasible only in a cold low Earth orbit.
- The upper limit on the length of eclipse that can be made a safe is determined by the amount of the MFPS saving that is willing to be sacrificed. In this respect, a heater is the preferred option at high altitudes[11.1], where overheating is not an issue. To clarify, using the entire MFPS saving as added phase change material can enable orbits with eclipses up to 3500 seconds whereas this mass used as extra battery capacity for a heater would enable orbits with eclipses up to 4000 seconds.

For a set of MFPS panels mounted to the body of a spacecraft:

[11.1] Estimating from fig. 5.4, this is above 6000 km in altitude.

- Due to the temperature range that exists across the spacecraft there are no orbits where the equilibrium temperatures of all of the cells are safe. This also holds true when the transient temperature variation is considered. There are thus no orbits for the body mounted system where a thermal control solution is *not* required.
- Adjusting the design and material of the connectors between the panel and the spacecraft was found to be a very effective thermal control solution in all orbits and environments. So effective that a further reduction in mass may be possible.
- If the connectors cannot be optimised, the range of orbits that can be controlled is very limited. Heaters can be used to prevent overcooling in low Earth orbit and perform better than the addition of a PCM, which is only viable in a hot low Earth orbit. There are no solutions to overheating in geosynchronous orbits, though body mounted panels are less likely to be used at this altitude.

11.4 Case Studies

To further illustrate the conclusions of this thesis the following case studies are presented. Table 11.1 shows the orbital elements of the orbits used on the case studies. In each case, the MFPS model of a single wing panel was placed in these orbits to assess viability of using MFPS in these orbits. For each orbit two cases are considered, one where there is no eclipse and one where the eclipse is at its longest; given by the two right ascension of the ascending node (RAAN) values. The transient results are presented.

Table 11.1: *The orbital elements of orbits used in the case study. The multiple RAANs indicate differing eclipse times.*

Element	Molniya	ISS	Galileo GPS	Dawn-Dusk
Semi-Major Axis (km)	26560	6738	29593	7051
Eccentricity	0.722	0.002	0	0
Inclination (degrees)	63.4	51.66	56	98
RAAN (degrees)	0 / 90	0 / 90	0 / 90	59.28 / 90
Argument of Periapsis (degrees)	270	0	0	270
Initial True Anomaly (degrees)	0	0	0	0

A Molniya orbit is a good example of a highly elliptical Earth orbit. Figure 11.1 shows

how the temperature of the battery varies in both environments and eclipse lengths. For the sunlit case, the Molniya orbit has the properties that enable the use of MFPS as it does not enter eclipse and it spends its sunlit time away from the influence of the Earth. As such, the battery temperature is safe at all times. However, the orbit will process and will reach the state where by the worse case eclipse occurs. While the battery will not overheat, overcooling does occur in eclipse. Thus, when given a Molniya orbit, thermal control is required before a MFPS can be used in this orbit.

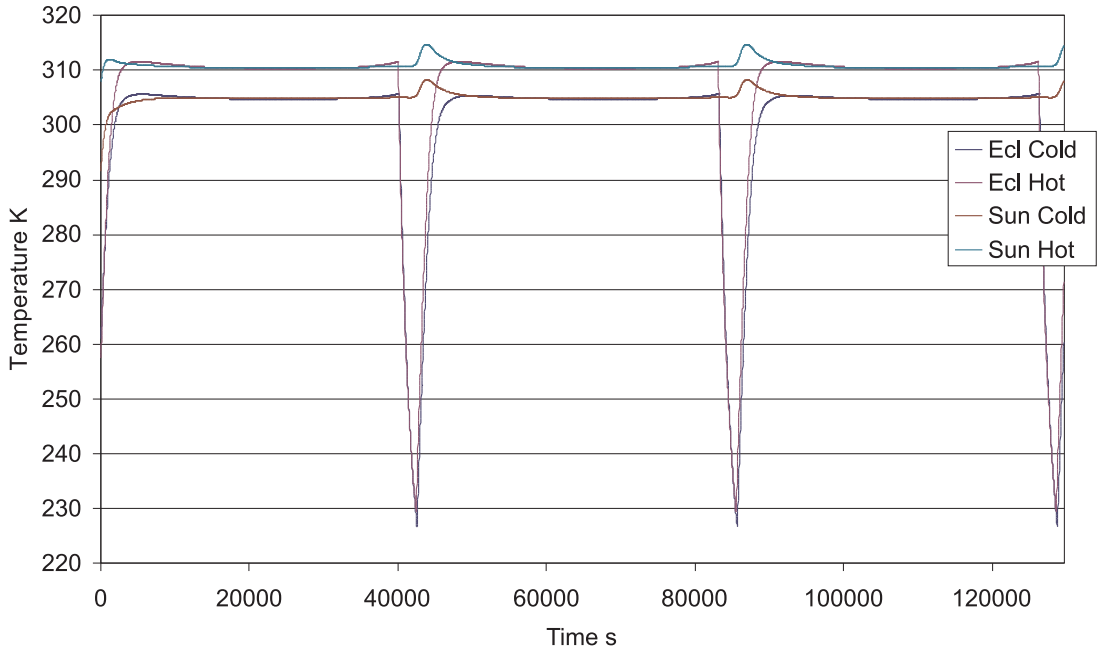

Figure 11.1: *Battery temperature of the MFPS panel in a Molniya orbit.*

The first step is to determine if an emittance value for the reverse side of the panel can be found that enables MFPS use in this orbit. In the hot environment the minimum emittance to avoid overheating is 0.793 and the maximum to avoid overcooling 0.166. In the cold environment the minimum emittance is 0.683 and the maximum 0.129. With these values not overlapping, a thermal control method that adds mass to the system must be used. For this thermal control, the emittance could be set to prevent overcooling and thus the TCS would work to prevent overheating. As the spacecraft spends a large proportion of its time sunlit, this would lead to large masses. As such, the emittance is set to prevent overheating and the TCS will work to prevent overcooling. Using a heater, this requires 370 Watts of heater power and 169 Whr of extra battery capacity in the hot case and 349 Watts of heater power and 156 Whr of extra battery capacity to prevent overcooling. That is 1.02 kg and 0.94 kg extra mass in the hot and cold environments respectively. Using a phase change material, 3.18 kg and 2.9 kg of

Hydrazine would be required in the hot and cold environments respectively. Thus for a sacrifice of at least 1 kg, a mission using a Molniya orbit could viably use a MFPS panel as part of a deployed wing solar array.

The orbit of the International Space Station (ISS) is a good example of a low Earth orbit; the temperature profiles are shown in fig. 11.2. When the spacecraft does not enter eclipse nor pass over the sub-solar point, the temperature of the battery remains safe. However, when the orbit proceeds to where the eclipse is longest, overcooling occurs. For MFPS to be used, thermal control is required. Unfortunately, the optical properties (minimum 0.924/0.74 and maximum 0.372/0.3 for hot/cold environments) do not provide a solution. Optimising to tackle overcooling leads to the following: 340/309 Watts of heater power requiring 118/97 Whr extra battery capacity giving 0.71/0.58 kg of extra battery mass in each environment. For a PCM this is 2.93 kg in the hot environment and 1.96 kg in the cold environment. The shorter eclipse time than the Molniya orbit lowers the mass that must be sacrificed if a MFPS was to be used in this orbit.

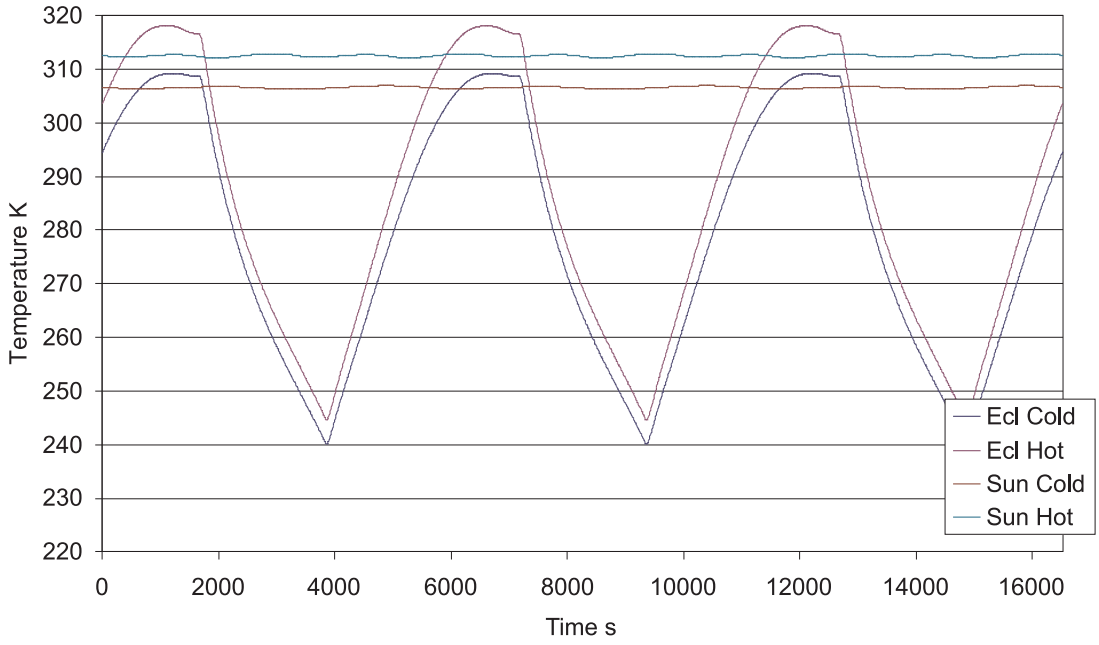

Figure 11.2: *Battery temperature of the MFPS panel in an ISS orbit.*

The next orbit considered is that of the Galileo Global Positioning System. This is a high Earth orbit, which is reflected in the temperature of the battery, fig. 11.3. The high altitude means that there is little influence from the Earth, shown by the lack of temperature variation when the panel is sunlit. As experienced by the previous two orbits, in constant sunlight the battery remains safe but becomes unsafe when the

longest eclipses occur. In this case, the choice of optical properties is very limited as there is no value of emittance that will prevent overcooling in either environment. Emittance values of 0.791 and 0.68 will prevent overheating and these are used when other TCS are considered.

In eclipse, 436/407 Watts of heater power requiring 329/305 Whr of extra battery capacity giving 1.98/1.83 kg of extra battery mass in each environment is needed to prevent overcooling. For a PCM this is 6.18 kg in the hot environment and 5.64 kg in the cold environment. In this orbit, large amount of the MFPS saving are used to support the TCS, greatly reducing the viability of using a MFPS in this orbit.

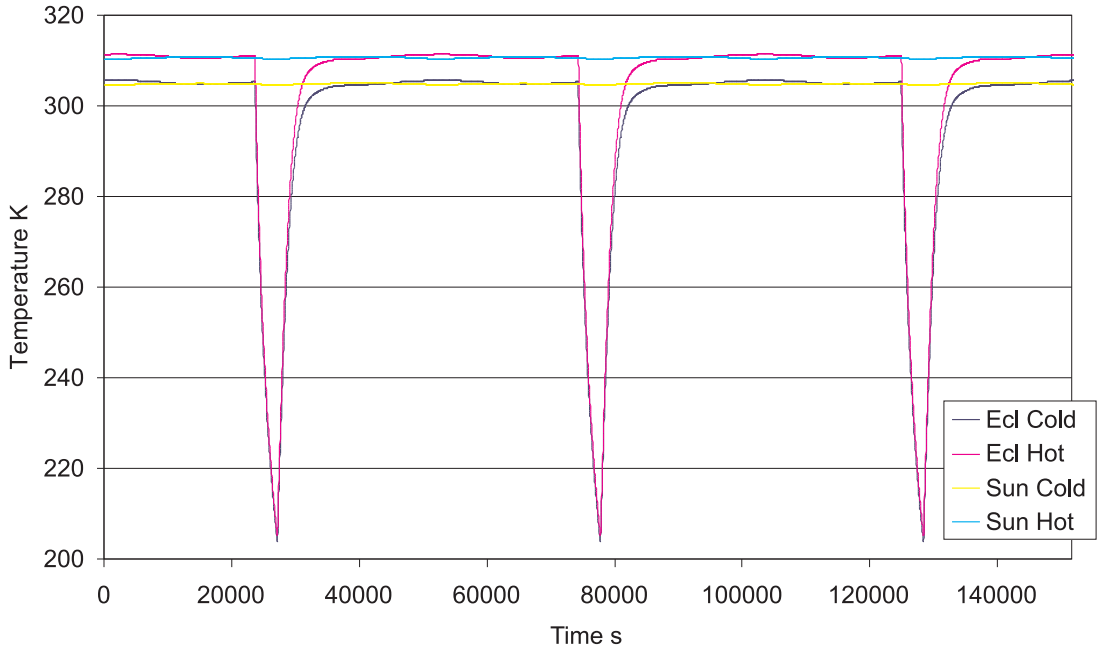

Figure 11.3: *Battery temperature of the MFPS panel in a Galileo GPS orbit.*

The final orbit considered is a dawn-dusk orbit, specifically that of the HINODE spacecraft [89], selected as it is the minimum albedo input case. Continuing the pattern set by the other orbits, the longest eclipse causes the battery to overcool, fig. 11.4. The emittance values are as follows: 0.848/0.712 minimum and 0.681.0.607 maximum. These values are much closer to each other as the minimum temperature is much warmer in this orbit, when compared to the other case studies. Using heaters with the minimum emittance, 287/230 Watts of heater power requiring 132/92 Whr extra battery capacity giving 0.79/0.55 kg of extra battery mass in each environment. For a PCM this is 0.49 kg in the hot environment and 0.32 kg in the cold environment. In this case, the use of a PCM is potentially a better choice, depending on containment required.

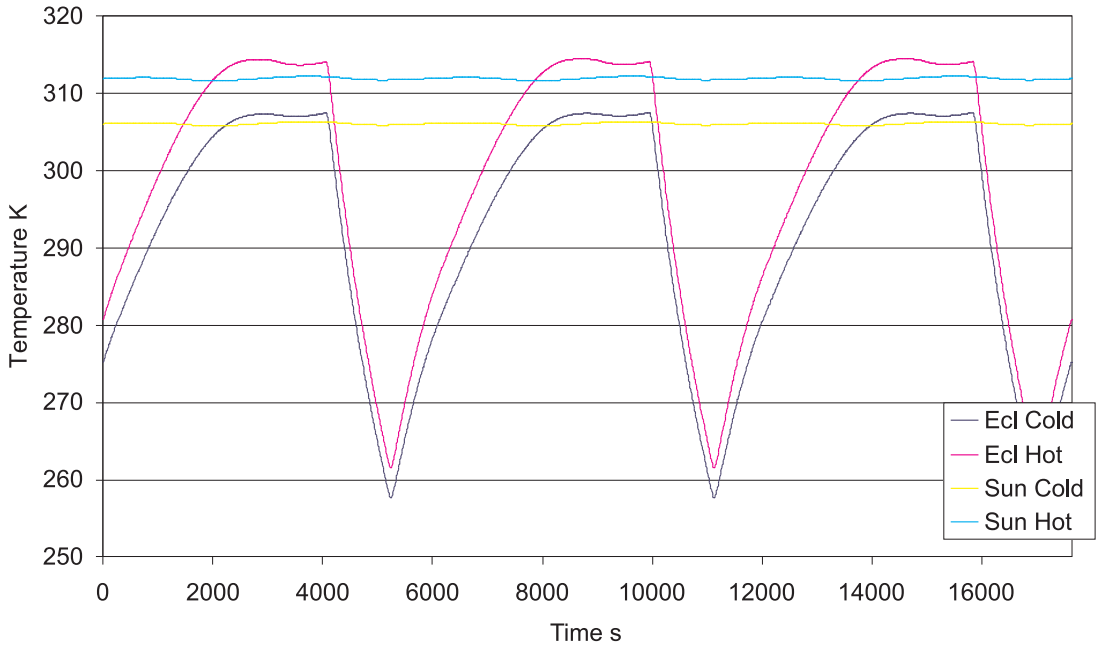

Figure 11.4: *Battery temperature of the MFPS panel in a Dawn-Dusk orbit.*

These case studies show that is most practical orbits, for a COTS MFPS to be used a sacrifice of the mass saving is required. These orbits do not meet the criteria for no mass penalty, as set out above. The equilibrium temperature is not safe along all points of the orbits, defined by these orbits going into eclipse. Analysis of the transient results shows that the panel has insufficient heat capacity to survive eclipse. The use of coatings is then shown to not provide a sufficient slow down in heat loss and thus a TCS that requires a mass sacrifice must be introduced.

11.5 Summary

The objective of this work was to address a technical issue in the implementation of multifunctional power structures. The issue is that of thermal control of the cells that are embedded into the core of the MFPS structure. The issue has not been covered by the published literature, where a gap exists between research into multifunctional structures and research into thermal control.

This thesis has worked towards filling that gap by assessing the range of orbits in which a MFPS using lithium ion polymer technology can be viably used. In this context, viability was defined as an orbit where the battery temperature could be kept within its envelope and the mass of the TCS required to do this did not negate the mass saving from the use of a MFPS. The key contribution of this thesis is to show that there are

many viable orbits. Orbits exists where no thermal control is needed as the equilibrium temperatures of the battery are safe and orbits exists where the transient response of the MFPS panel is sufficient to prevent overcooling or overheating. This thesis also establishes the limits of how current thermal control technologies can extend the range of viable orbits and assesses the performance of these thermal control solutions.

11.6 Further Work

This thesis has focused on the use of multifunctional power structures in Earth orbit, which is only one potential area of application. The mass saving offered by the use of MFPS to spacecraft with interplanetary missions has benefits beyond launch due to the added engines burns such a spacecraft must make to reach its destination. The environment beyond Earth orbit is determined by proximity to the Sun. Missions venturing closer to the Sun will find the equilibrium temperatures rising. Once the equilibrium temperature becomes too high, a MFPS TCS would have to focus on reducing this equilibrium temperature. In orbit of objects within the Earth's orbit, eclipse would thus be a blessing and used to help cool the spacecraft. Further out, the issue when the spacecraft is between planets would be the reduction in solar input and the colder equilibrium temperatures this would cause. This cooling of the Sun input makes eclipse when orbiting more distant planets more of a challenge for preventing overcooling.

This thesis has focused on applications of an MFPS built from commercial off the shelf components. As shown in the literature, many other possible MFPS exist, section 2.1. A natural extension to this work would be to examine the thermal constraints of these multifunctional structures, with the same goal as this work: to remove the thermal obstacle from their use. In addition to the power storage structures considered in the literature review, other possible multifunctional structures that could be looked at including electronics Rayman et al. [42], communications Kim et al. [90] or mechanisms Elzey et al. [91], all of which may contain components with strict temperature envelopes.

Appendix A

Publications

A.1 Conferences

- Thermal Management Issues for Multifunctional Solar Arrays, J A Foster, G S Aglietti, First CEAS European Air and Space Conference, 10-13 Sept 2007 Berlin Germany
- Multifunctional Power Structures and Related Thermal Issues, S C Roberts, J A Foster, G S Aglietti, SMASIS2008, 28-30 October 2008 Ellicott City MD USA
- Purpose Built and Off The Shelf Multifunctional Spacecraft Power Structures, G S Aglietti, J A Foster, S C Roberts, C W Schwingshackl, ECSSMMT 11, 15-17 Sept 2009 Toulouse, France
- Thermal Control of Multifunctional Power Structures Using Phase Change Materials, J A Foster, G S Aglietti, 60th IAC, 12-16 October 2009, Daejeon, Republic of Korea

A.2 Journals

- The Thermal Environment Encountered in Space by a Multifunctional Solar Array; J A Foster, G S Aglietti; Aerospace Science and Technology. Vol 14, No 3, 213-219, 2010. Received 5 June 2009; Accepted 18 December 2009; Available online 22 February 2010.
- Strategies for Thermal Control of a Multifunctional Power Structure Solar Array; J A Foster, G S Aglietti; Journal of Aerospace Engineering, American Society of Civil Engineers. Under Review, Submitted 7th Jun 2010.

Appendix B

Variations of the Body Mounting

This appendix contains the detailed discussion of the effect the variations of the body mounting have on the range of viable orbits a body mounted MFPS can be used in.

B.1 Isothermal Model of the Variations

B.1.1 Three Panel Variation

In fig. B.1, the equilibrium temperature of the three panel variation up to an altitude of 3200 km is shown. The key difference is the reduction in the overheating region, which though it extends beyond 3200 km, is smaller and the peak temperature reduced. The overheating region beyond the terminator is also gone. In the cold environment, the overheating region is reduced to extending out to just 1500 km. Overheating has been reduced by the use of MLI, which is reflective to radiation from the Earth, on the Earth pointing surface. The reduction in heat input means that even at peak sunlight, the spacecraft temperature is lower. As already seen, eclipse is too cold, but the lack of a significant overheating region enables most orbits that do not enter eclipse.

200 km and 3200 km low Earth orbits are considered in the transient modelling, shown in fig. B.2. The results are similar to the results of the 4 panel spacecraft, though reduced in temperature as the environment is cooler. Eclipse and the overheating region seen in the hot environment cause temperature changes, but the spacecraft temperature remains safe.

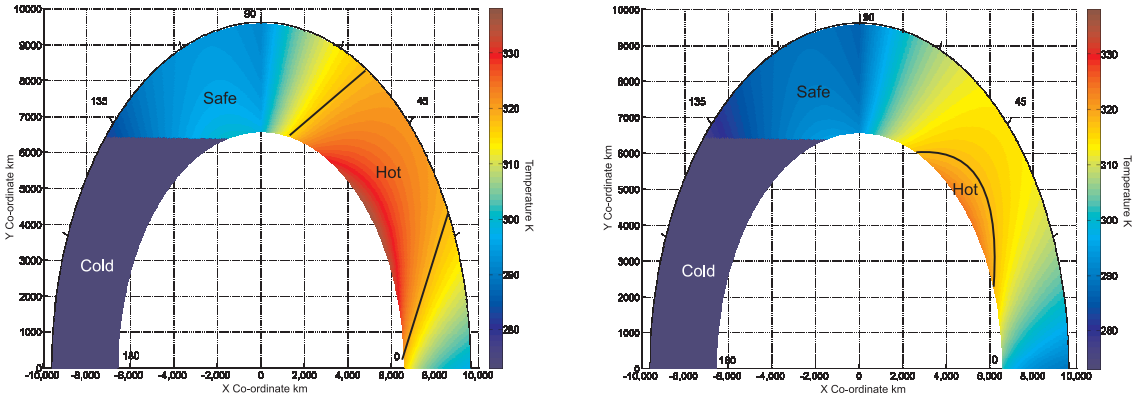

(a) *Hot environment temperatures*

(b) *Cold environment temperatures*

Figure B.1: *Equilibrium temperatures of the three panel variation.*

B.1.2 Sun Pointing Variation

Figure B.3 and fig. B.4 show the equilibrium and transient results of the body mounting when it maintains a Sun pointing condition. The temperatures are much cooler as the Sun input is lower. Eclipse is too cold and the overheating region is very small in both environments. The transient results show the hot 200 km LEO case through this region does not overheat. The high thermal inertia of the spacecraft prevents the model from overcooling in both environments, indicating a large number of safe orbits.

B.1.3 Space Pointing Variation

Figure B.5 and fig. B.6 show the equilibrium and transient results of the body mounting when it maintains a space pointing condition. Temperatures are warmer and overheating regions exist in both cases, causes by the increase in Sun input. The region is particularly large in the hot environment. The region is a slightly irregular shape, an effect of the variation of the inputs from the Earth with a peak temperature of 356 K. The transient results indicate that despite this hot overheating region, the thermal inertia of the panel is sufficient to prevent the model from overheating.

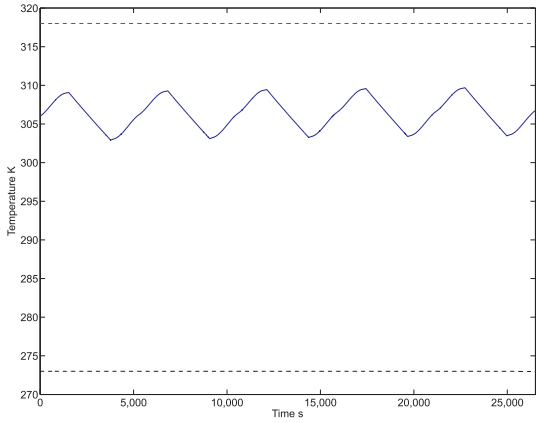

(a) *200 km LEO hot case*

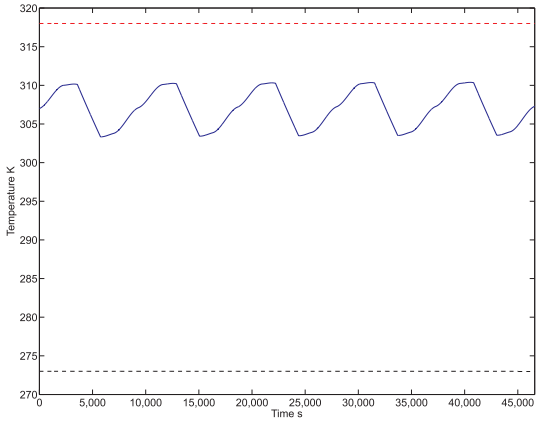

(b) *3200 km LEO hot case*

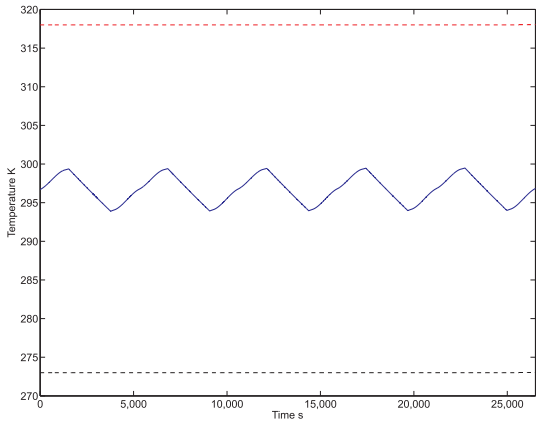

(c) *200 km LEO cold case*

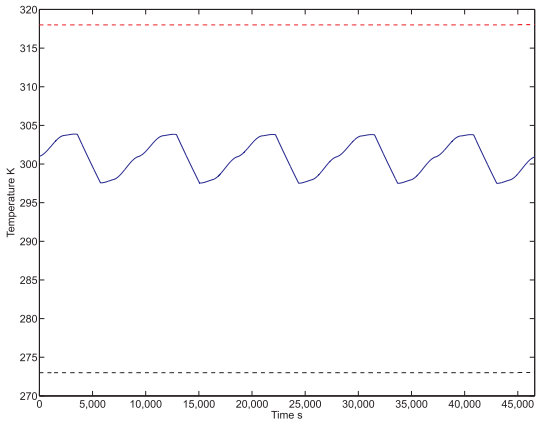

(d) *3200 km LEO cold case*

Figure B.2: *Transient temperatures of the three panel variation.*

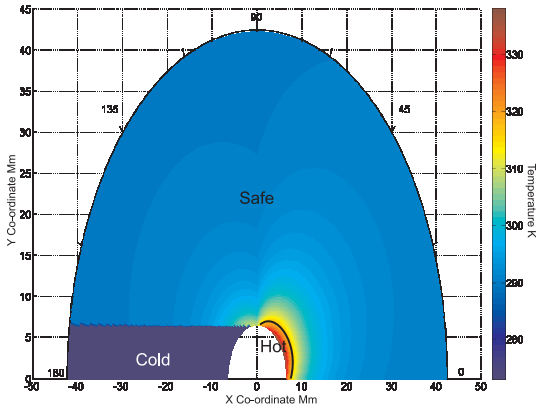

(a) *Hot environment temperatures*

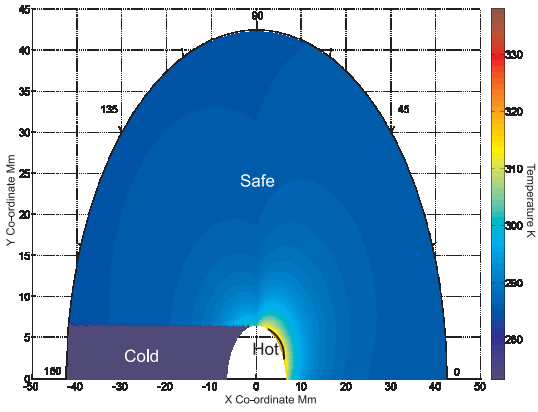

(b) *Cold environment temperatures*

Figure B.3: *Equilibrium temperatures of the Sun pointing variation.*

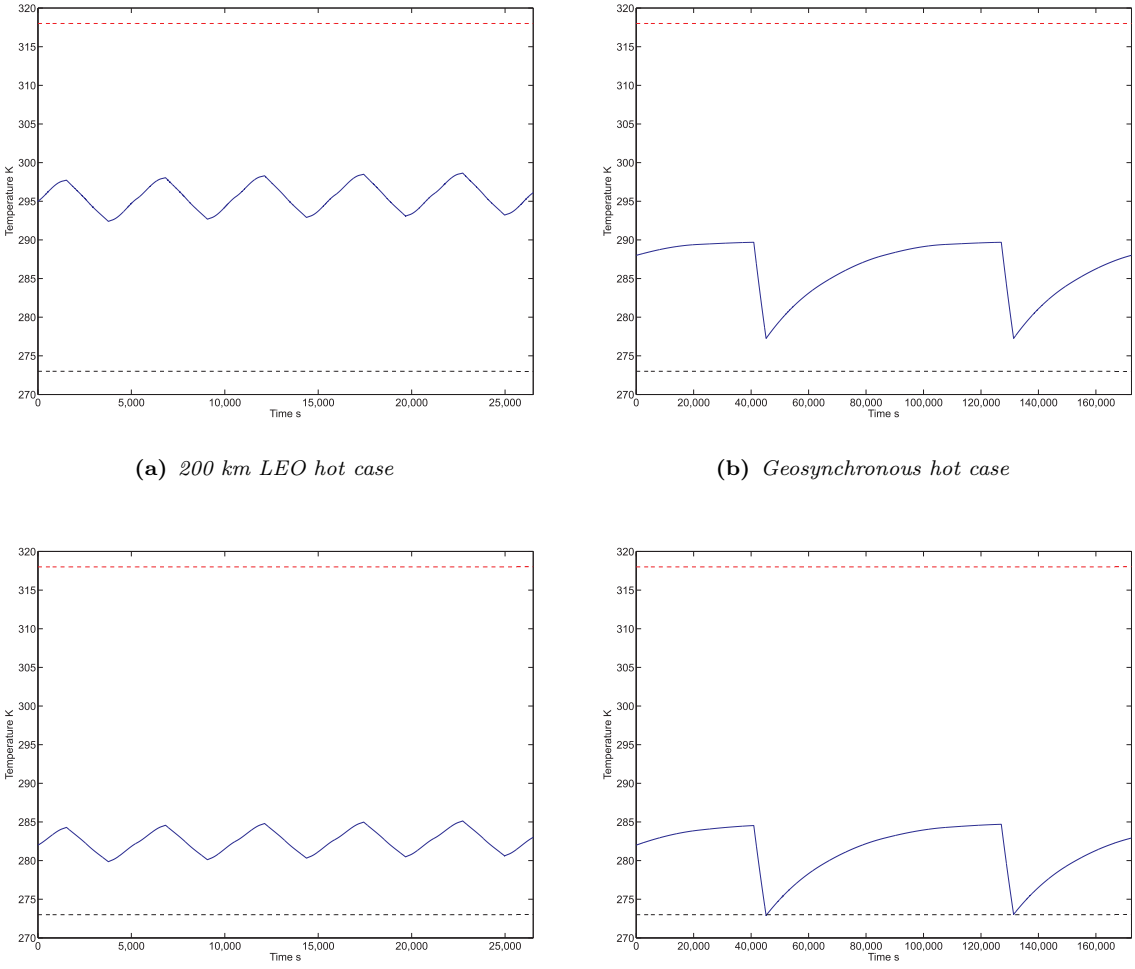

(a) *200 km LEO hot case*

(b) *Geosynchronous hot case*

(c) *200 km LEO cold case*

(d) *Geosynchronous cold case*

Figure B.4: *Transient temperatures of the Sun pointing variation.*

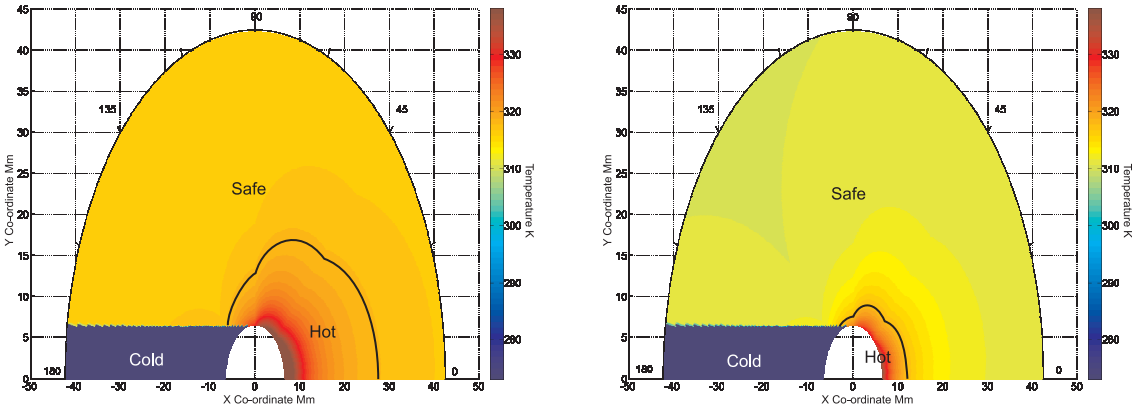

(a) *Hot environment temperatures*

(b) *Cold environment temperatures*

Figure B.5: *Equilibrium temperatures of the space pointing variation.*

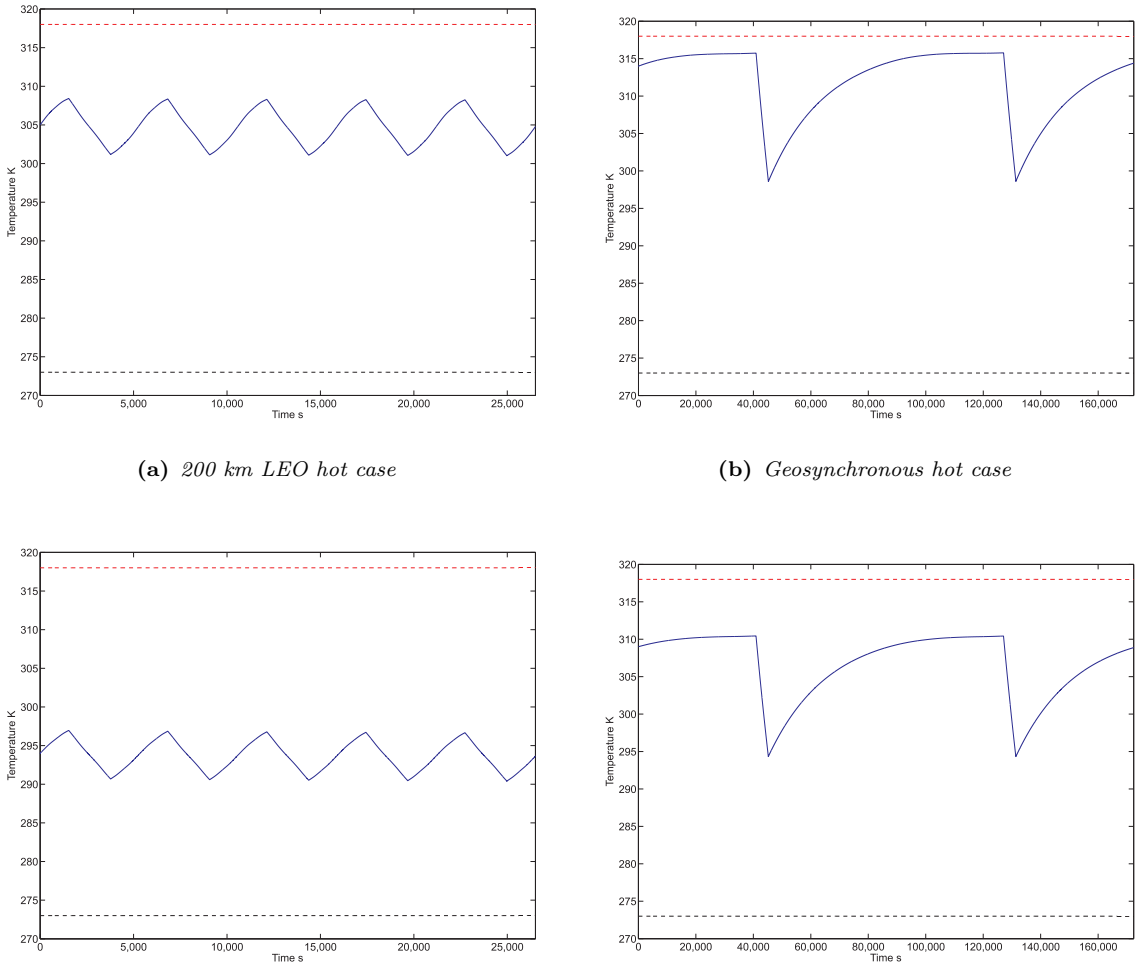

(a) *200 km LEO hot case*

(b) *Geosynchronous hot case*

(c) *200 km LEO cold case*

(d) *Geosynchronous cold case*

Figure B.6: *Transient temperatures of the space pointing variation.*

B.2 Lumped Parameter Modelling of the Variations

In order to be concise, only the transient results will be considered as the lumped parameter equilibrium results of the body mounting have shown that the equilibrium results do not help determine thermal control requirements.

B.2.1 Earth Pointing with Three Panels

Figures B.7, B.8, B.9 and B.10 show that the temperature pattern of the three panel variation is strongly similar to the baseline pattern. As the MLI has a low absorptance and a very low emittance, the spacecraft loses much less heat compared to the heat loss from the panel, causing the spacecraft to be warmer. As such the panels no longer become too cold when in shadow. However, the change now causes the panels to become too hot in sunlight. At an altitude of 3200 km, the increase in the sunlit time of each panel causes the panels to reach higher temperatures. The reduction in eclipse proportion causes the spacecraft temperature to be warmer. Thus the 3200 km results are much warmer then the results at 200 km. Though the panels have greater heat capacity due to the increased number of cells in them, this increase is not enough to counteract the warmer spacecraft temperature.

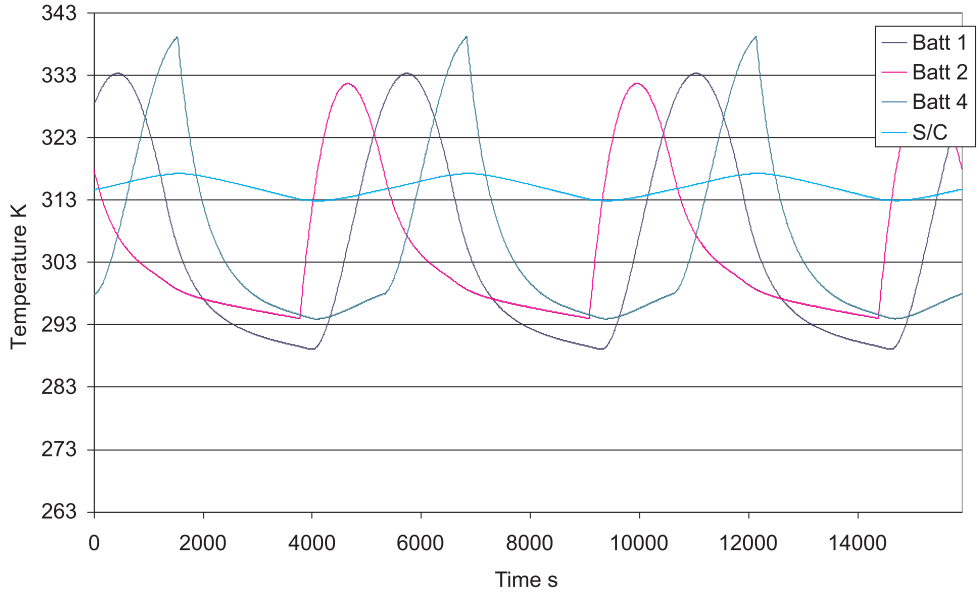

Figure B.7: *Lumped parameter transient results of the three panel body mounting in a hot 200 km LEO case.*

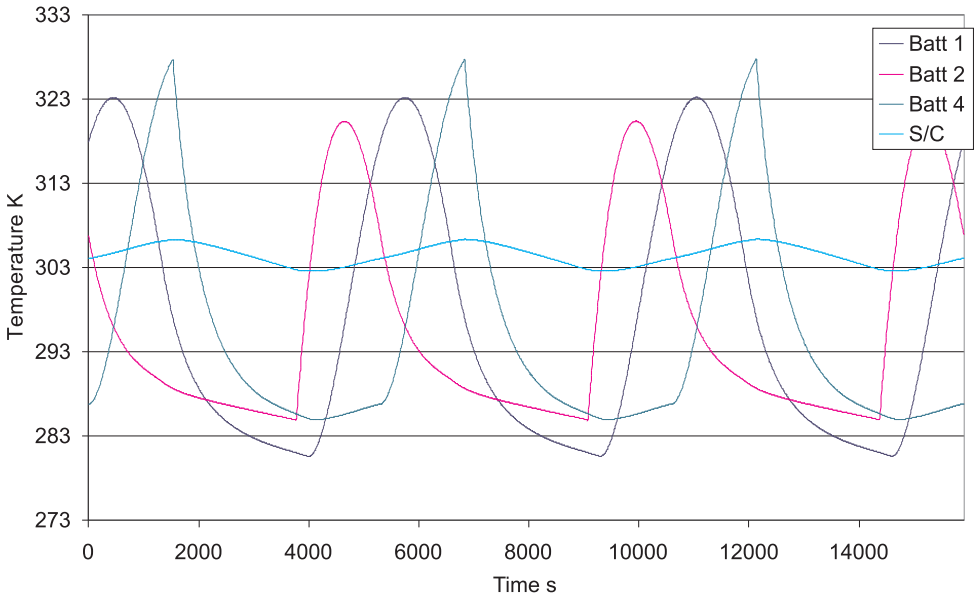

Figure B.8: *Lumped parameter transient results of the three panel body mounting in a cold 200 km LEO case.*

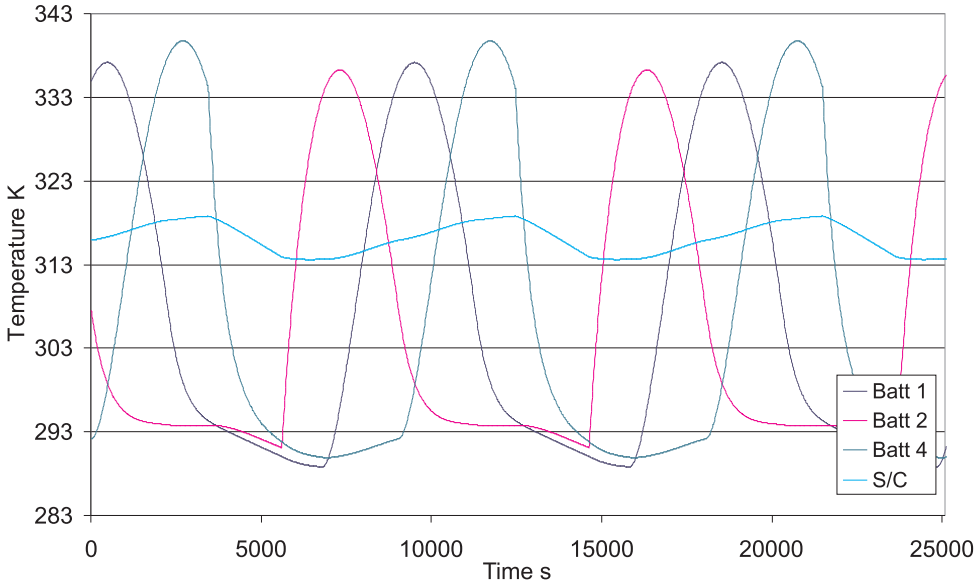

Figure B.9: *Lumped parameter transient results of the three panel body mounting in a hot 3200 km LEO case.*

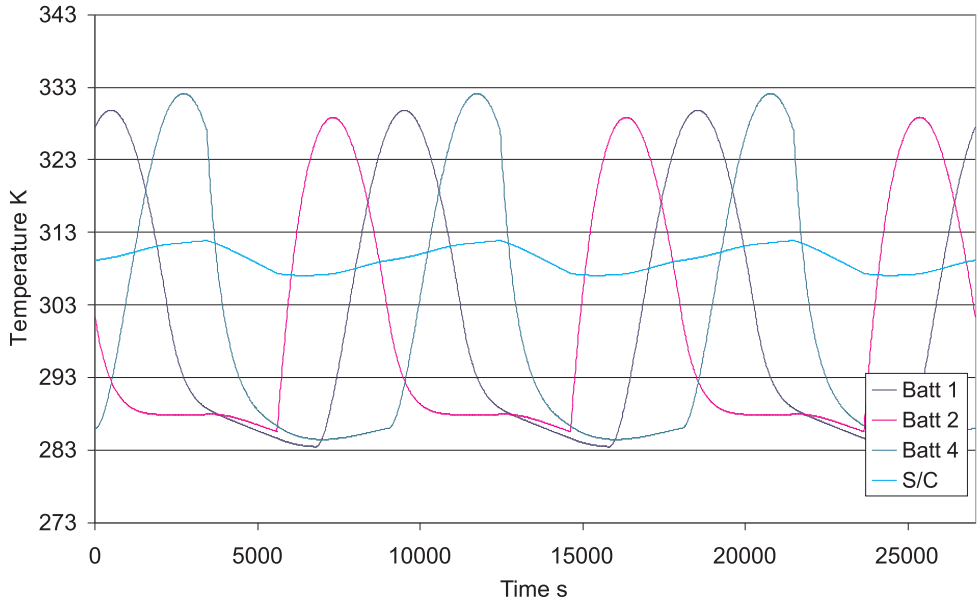

Figure B.10: *Lumped parameter transient results of the three panel body mounting in a cold 3200 km LEO case.*

B.2.2 Sun Pointing

Figures B.11, B.12, B.13 and B.14 show there is a new pattern when the system is orientated so that one panel (panel 1) is permanently facing the Sun. The spacecraft temperature varies with the inputs as it has done with the previous body mounting orientations and remains safe in all orbits and cases. Panel 1 is heated by the Sun and suffers overcooling during eclipse. The panels that are left in the shadow suffer from overcooling in all orbits and cases.

In 200 km LEO, the shadowed panels are lit by the Earth, with panel 3 the warmest as it is also illuminated by the Earth albedo. The Earth infrared warms panel 1 during eclipse, preventing it from becoming as cold as the shadowed panels. The shortness of the eclipse also helps to prevent panel 1's temperature becoming colder. In both environments panel 1 becomes too hot while the other panels' temperatures are always safe.

Out at geosynchronous orbit the panels see no influence other than the Sun and thus they follow the temperature variation of the spacecraft. The shadowed panels are 20 K cooler than the spacecraft while panel 1 is 33 K warmer. With a longer eclipse and no Earth warming, the spacecraft experiences a 10 K temperature drop in eclipse, with the temperature of panel 1 sharply dropping to match the temperature of the shadowed panels. When sunlit, panel 1 overheats in both environments and the shadowed panels

are too cold in both. The effect of the hotter environment is to shift the spacecraft temperature (and thus the other temperatures) up by 4 K.

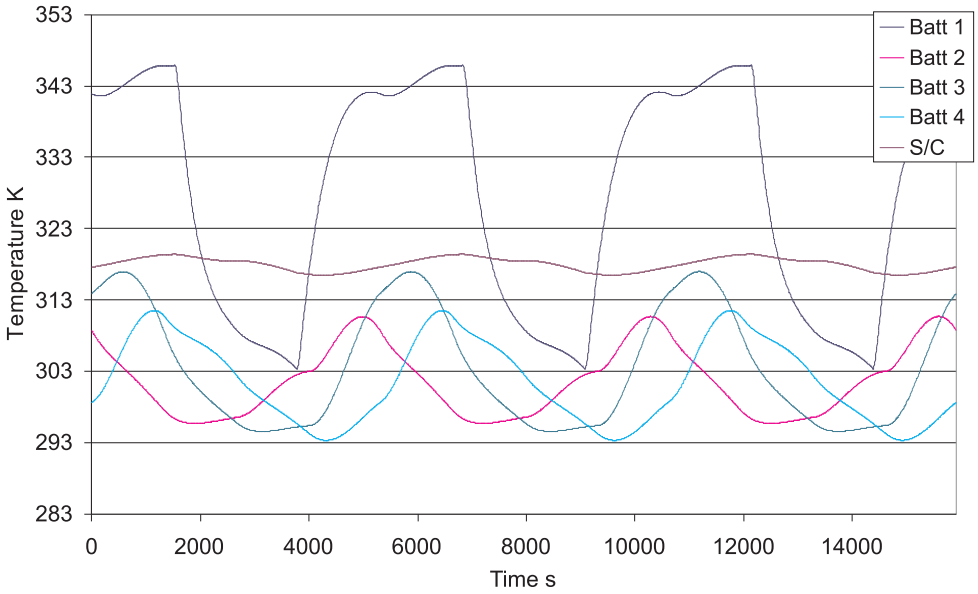

Figure B.11: *Lumped parameter transient results of the Sun pointing body mounting in a hot 200 km LEO case.*

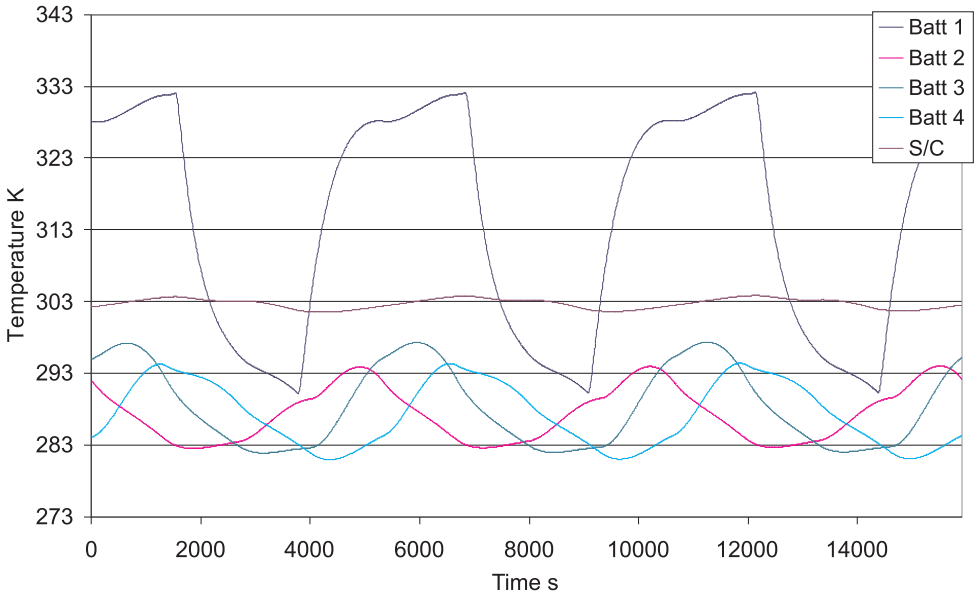

Figure B.12: *Lumped parameter transient results of the Sun pointing body mounting in a cold 200 km LEO case.*

When one panel is permanently sunlit, a consistent and stable temperature variation exists across the system. Having only one panel surface sunlit reduces the heat input into the system, causing it to be cooler, leading to overcooling of the panels without sunlight to occur in all orbits, not just LEO.

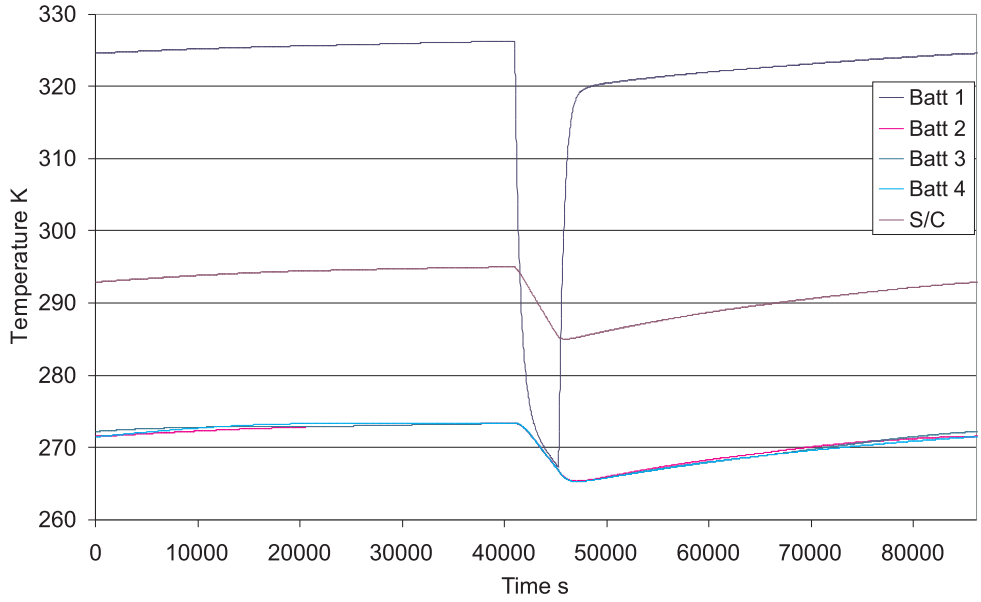

Figure B.13: *Lumped parameter transient results of the Sun pointing body mounting in a hot GEO case.*

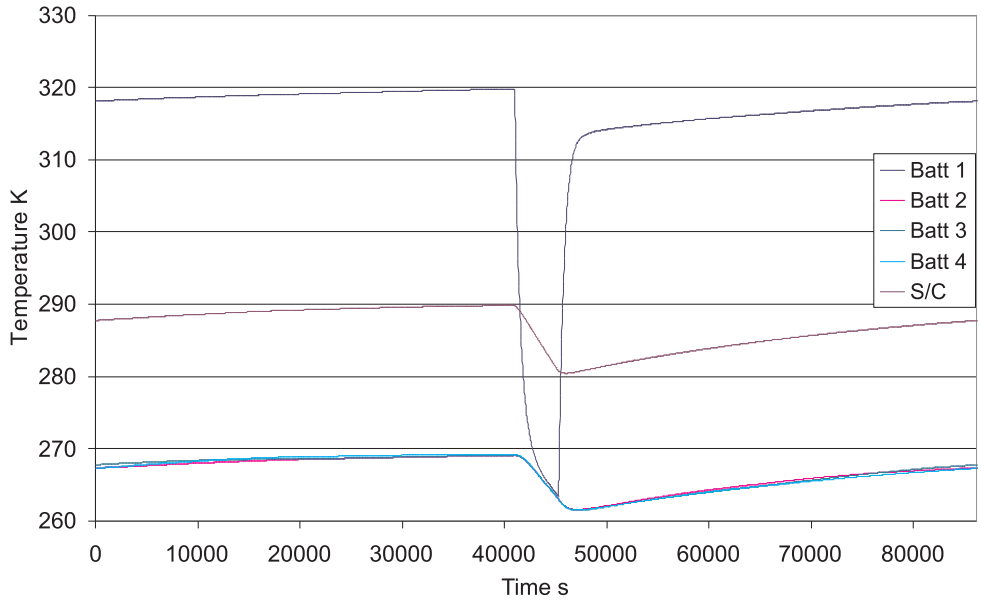

Figure B.14: *Lumped parameter transient results of the Sun pointing body mounting in a cold GEO case.*

B.2.3 Space Pointing

In 200 km LEO a new pattern emerges, fig. B.15 and fig. B.16. Panels 1 and 2 are the warmer panels and their temperature is dependent on the Sun. The panels are cooler than the panel 1 in the Sun pointing orientation as each panel has an angle of incidence of 45 degrees to the Sun, reducing the input. The net input is higher and thus the spacecraft temperature is warmer. The difference in the temperature plots of panels 1 and 2 is caused by the inputs from the Earth.

In both environments, panels 1 and 2 suffer from significant overheating, with panel 1 warmer as its inputs from the Earth come at the end of its sunlit time, when the spacecraft is warmest. Panels 3 and 4 are always safe in the cold environment, but suffer from overheating in the hot case due the high temperature of the spacecraft. Panel 1 cools to a lower temperature than panel 2 as it is during the end of eclipse that it receives its maximum input form the Earth infrared.

In geosynchronous orbit, the pattern in fig. B.17 and fig. B.18 is similar to that found in the Sun pointing results. Here, panels 1 and 2 become too hot in the hot environment and panels 3 and 4 become too cold in the cold environment. The space pointing orientation is a more hospitable environment for the panels. The warmer spacecraft supplies more heat to the shadowed panels and while both shadowed panels receive albedo input, warming them before eclipse. The reduced Sun input on the sunlit panels does not warm them enough to cause overheating. The input from the Earth IR occurs at 45°compared to the other orientations but is otherwise unaffected.

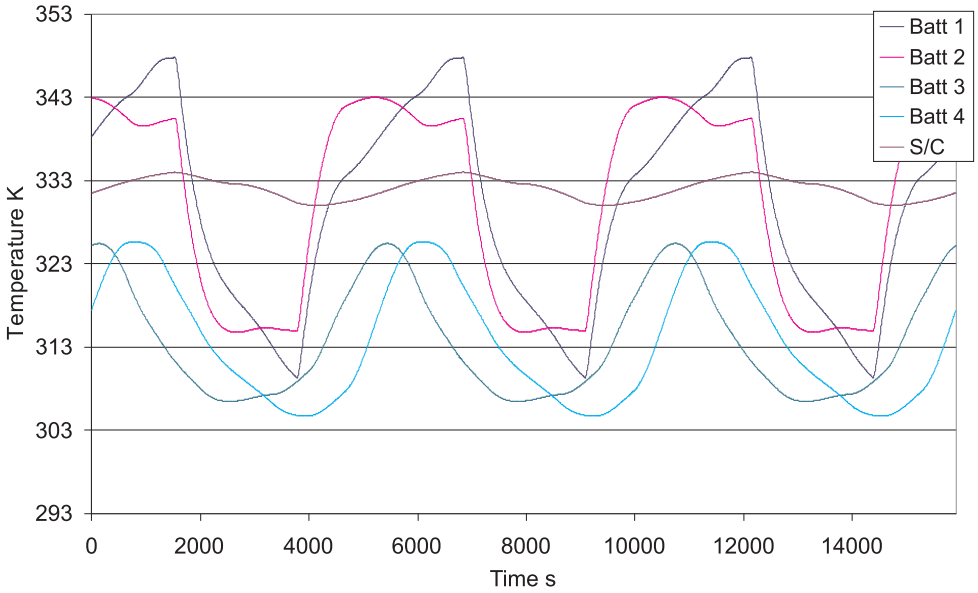

Figure B.15: *Lumped parameter transient results of the space pointing body mounting in a hot 200 km LEO case.*

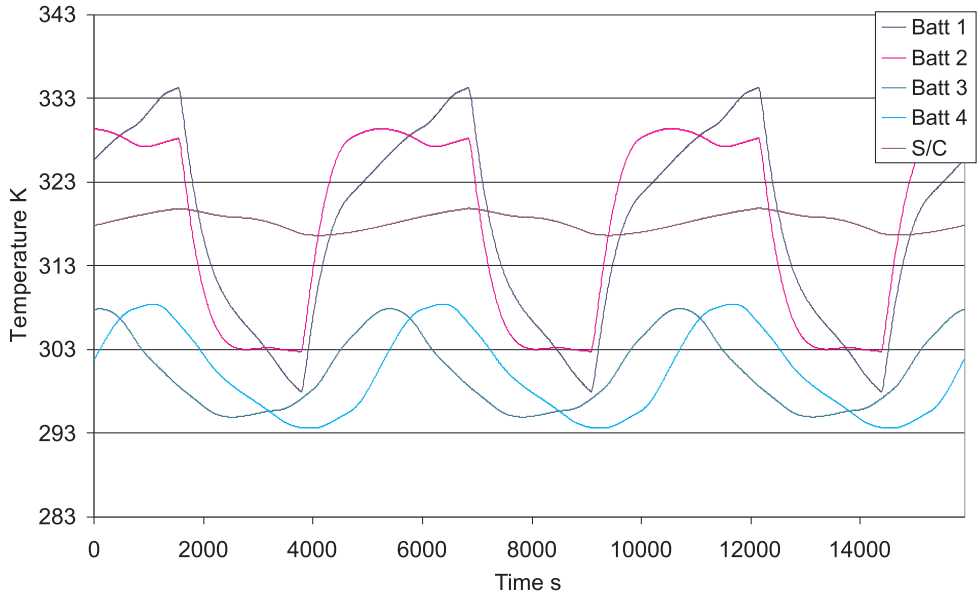

Figure B.16: *Lumped parameter transient results of the space pointing body mounting in a cold 200 km LEO case.*

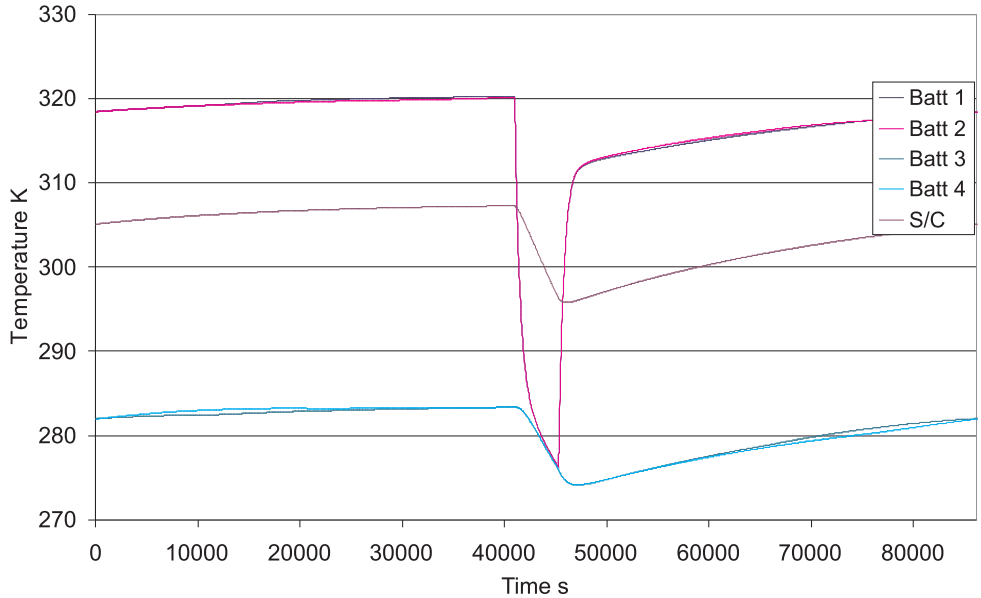

Figure B.17: *Lumped parameter transient results of the space pointing body mounting in a hot GEO case.*

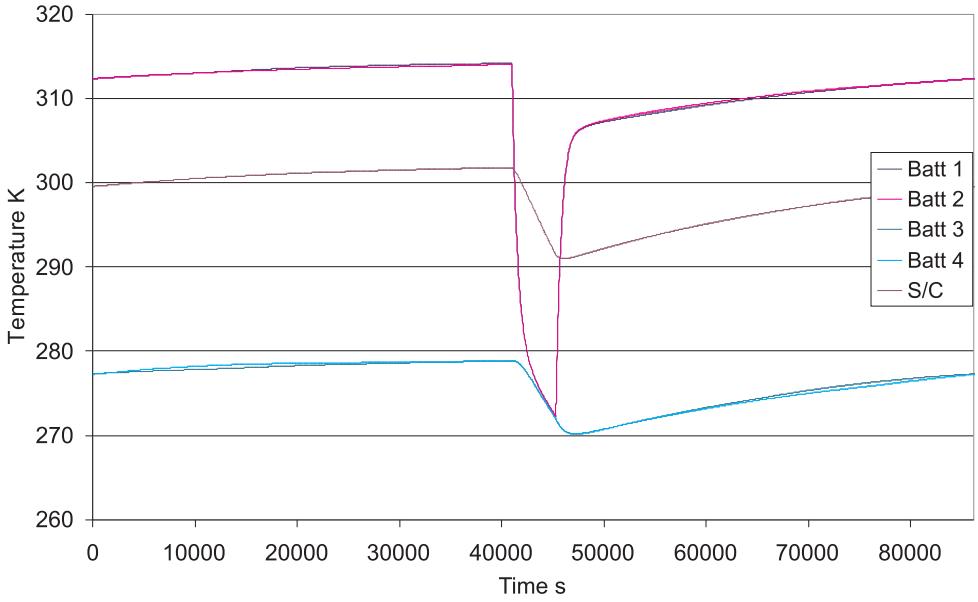

Figure B.18: *Lumped parameter transient results of the space pointing body mounting in a cold GEO case.*

B.3 Thermal Control of the Variations

The remainder of this chapter is dedicated to a brief review of how each of the variations in configuration affect the viability of thermal control.

B.3.1 Three Panel Earth Pointing

The three panel Earth pointing variation is much warmer and only overcools in a cold environment in LEO. This has the following effect on the viability of the thermal control solutions.

B.3.1.1 Optics

Table B.1 shows the minimum emittance of the exposed surfaces of the spacecraft required to prevent overheating, which is the issue in question and the maximum emittance required to prevent overcooling which limits attempts to prevent overheating. In all cases a conflict of requirement occurs and there is no solution. The effect of the orientation is to increase emittances due to the warmer spacecraft.

Table B.1: *Emittance values for the three panel body mounting.*

Case	Overheating	Overcooling
Cold 200 km LEO	0.19	0.12
Hot 200 km LEO	0.51	0.51
Cold 3200 km LEO	0.19	0.12
Hot 3200 km LEO	0.33	0.18

B.3.1.2 Insulation

Figure B.19 shows the effect of using an aerogel core. The results show the same pattern as the four panel orientation though due to the presence of three MLI covered surfaces, the temperatures are warmer, with the spacecraft maximum temperature tending towards 404 K. Though section 9.3 has shown that the emittance of the spacecraft can be altered to provide a set of safe temperatures, the 5.1 kg mass of insulation used is still an unviable amount.

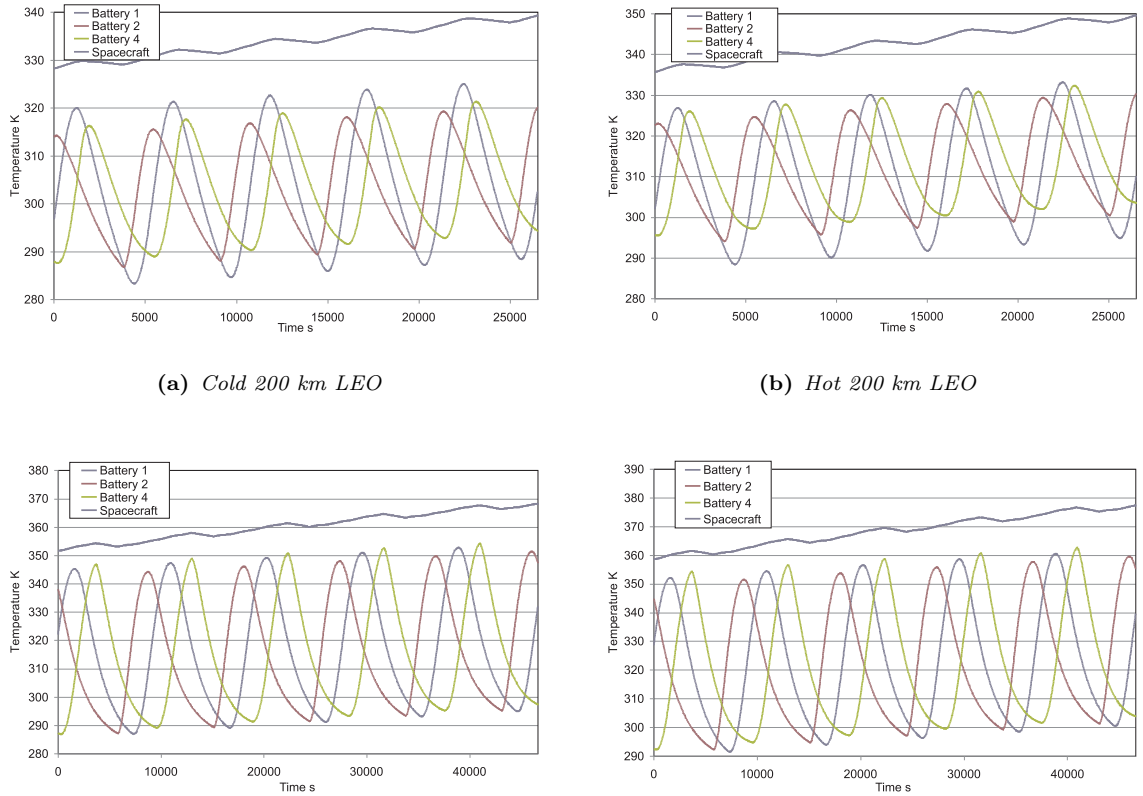

(a) *Cold 200 km LEO*

(b) *Hot 200 km LEO*

(c) *Cold 3200 km LEO*

(d) *Hot 3200 km LEO*

Figure B.19: *The effect of using an aerogel core on the three panel Earth pointing body mounting.*

B.3.1.3 Thermal Links

Table B.2 shows the minimum required linear conductance between the panels and the spacecraft. The change in the requirements fits the change in results pattern between the four and three panelled Earth pointing orientations. The warmer spacecraft reduces the overcooling requirement in the cold cases (3.34 W/K to 0.7 W/K at 200 km and 2.8 W/K to 0.3 W/K at 3200 km. This warming increases the altitude below which the radiative flow of is sufficient to prevent overheating. The minimum linear conductance is always above 3.5 W/K so improved conduction is required. There is little effect on feasibility as the viability of added conduction is dependent upon redesign of the connectors, not the required linear conductance.

Table B.2: *Minimum linear conductance for the three panelled Earth pointing orientation.*

Case	Overcooling W/K	Overheating W/K
Cold 200 km LEO	0.7	6.4
Hot 200 km LEO	-	26.7
Cold 3200 km	0.3	10.9
Hot 3200 km	-	24.7

B.3.1.4 Phase Change Material

Section 9.6 has shown that the optimum mass of phase change material required can be many times the MFPS saving. As such, table B.3 shows the effect of distributing the MFPS saving (1.3 kg) over the affected panels, as a faster method to determine viability. The table shows the difference in the temperature of concern caused by adding the PCM. The panels experience small periods of overheating in sunlight and thus Disodium Phosphate Dodecahydrate is used.

Using 1.3 kg of PCM (without containment) is not effective in preventing overheating at higher altitudes. Nor is it effective in preventing overheating in the hot LEO case, with the warmer system the cause of this difference. In the cold 200 km LEO case, just as for the Earth pointing orientation, the use of a PCM has been shown to be feasible, effectively reducing the maximum temperatures by up 13 K, though this is clear increase in mass from the 2 g required previously. Thus this hotter orientation reduces the

viability of using PCM.

Table B.3: *Mass of PCM required to maintain battery temperature in the three panel Earth pointing body mounting.*

	Extremity Temperature (Effect) K		
Case	Panel 1	Panel 2	Panel 4
LEO Cold	313.6 (-9.6)	312.7 (-7.7)	313.9 (-13.8)
LEO Hot	326.6 (-6.9)	328.9 (-2.7)	333.3 (-5.9)
3200 km Cold	330.1 (-0.27)	327.8 (-1.1)	331.6 (-0.6)
3200 km Hot	338.6 (-1.4)	336 (-0.3)	340.2 (-0.4)

B.3.1.5 Heaters

The use of heaters is not considered in this application as the three panelled Earth pointing body mounted system does not experience overcooling.

B.3.2 Sun Pointing

B.3.2.1 Optics

At geosynchronous altitudes, the shadowed panels are too cold for long periods of time. As the emittance of the spacecraft is 0.02 the temperature of the spacecraft (and thus the heat flow to the panels) cannot be improved by reducing the emittance further, even if that were possible. To further render the use of coatings difficult overheating also occurs. This overheating could be prevented by increasing the spacecraft emittance, cooling it down to allow more heat flow from the sunlit panels, but as stated, overcooling already occurs and increases the emittance would make this problem worse. As such, the emittance of the spacecraft is not considered geosynchronous.
In LEO, the cold environment requires that the emittance be both greater than 0.75 to prevent overheating and below 0.31 to prevent overcooling. In the hot environment, even with the maximum possible emittance, not enough heat is lost to prevent overheating, while an emittance less than 0.8 is needed to prevent overcooling. It is thus clear that this is not a feasible thermal control solution.

B.3.2.2 Insulation

Figure B.20 shows the effect of using an aerogel core. The effect of the insulation on the spacecraft is the same as for the Earth pointing orientation. The key difference here is that the insulation increases the differences between the panels caused by the uneven and unchanging heating by isolating the panels from the spacecraft. Insulation is thus not a feasible solution.

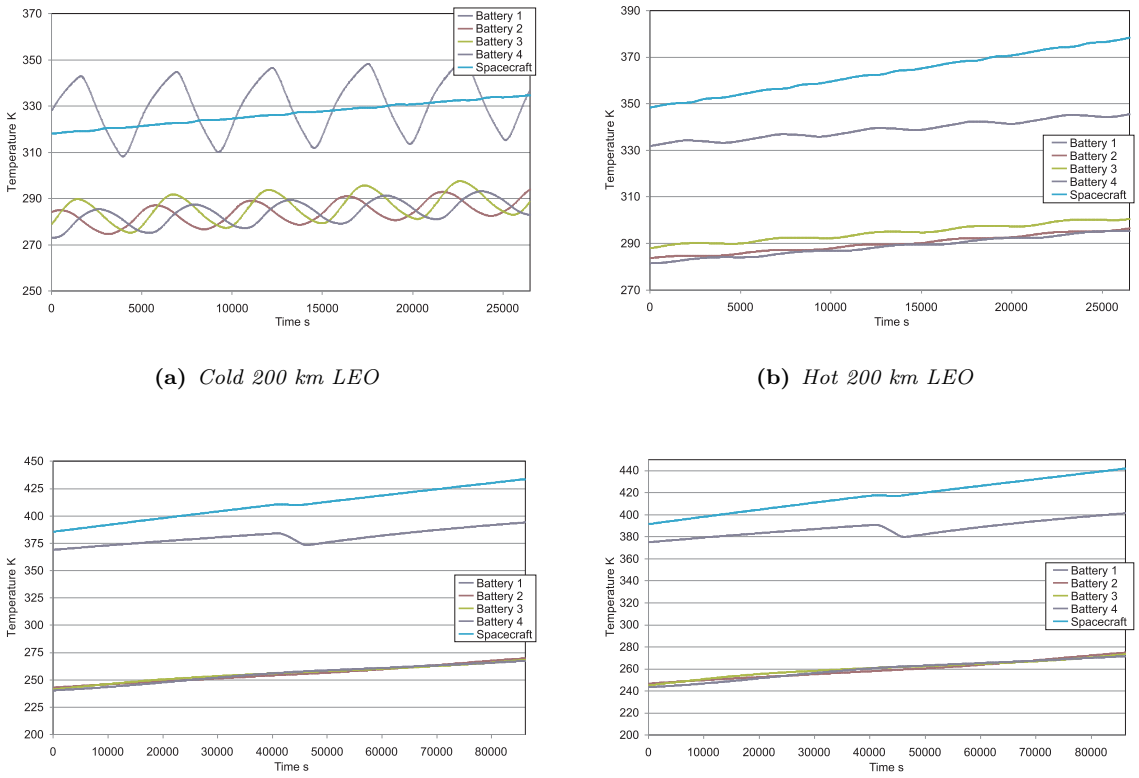

(a) *Cold 200 km LEO*

(b) *Hot 200 km LEO*

(c) *Cold GEO*

(d) *Hot GEO*

Figure B.20: *The effect of using an aerogel core on the Sun pointing body mounting.*

B.3.2.3 Thermal Links

This orientation creates a fixed heating pattern, with panel 1 suffering from overheating and the shadowed panels overcooling in GEO. The minimum conduction to move heat from the sunlit panel to the shadowed panels is presented in table B.4. Two requirements are given, one the minimum to prevent overheating and one the minimum to prevent overcooling. In the cold case there is not a solution to prevent overcooling. This is because with increasing linear conductance, rather than the spacecraft warming the shadowed panels, the shadowed panels cool the spacecraft, causing the loss of the thermal inertia required to prevent overcooling. This is because the shadowed panels do

not experience any warming and thus their continual low temperature causes too great a heat loss from the spacecraft. By contrast in LEO, the flow of heat by radiation is enough to prevent overcooling.

Table B.4: *Minimum linear conductance for the Sun pointing orientation.*

Case	Overcooling W/K	Overheating W/K
Cold 200 km LEO	-	10.8
Hot 200 km LEO	-	74.6
Cold GEO	X	4
Hot GEO	15	6.3

The viability to prevent overheating suffers in LEO, as the high inputs from the Earth negate any potential cooling from reduced solar input. At GEO, the overheating viability is improved as the spacecraft is cooler. The viability in GEO suffers as preventing the shadowed panels from overcooling becomes unfeasible.

B.3.2.4 Phase Change Material

In GEO, the Sun pointing orientation causes the shadowed panel to spend long periods of time too cold. In the hot case a PCM to prevent overcooling would be suitable to prevent overcooling of panel 1 (the sunlit panel) during eclipse. However, as shown by chapter 8, it is likely that more than 1.3 kg of PCM will be required to prevent such a long overcooling period.

In LEO, no overcooling occurs, but panel 1 experiences overcooling. Figure B.21 shows the effect of adding 1.3 kg of Disodium Phosphate Dodecahydrate as a PCM to prevent overcooling. The results show that while the PCM does initially prevent overheating, the panel does not spend enough time in eclipse to resolidify the PCM fully, meaning less PCM is available to oppose the next heating period. This eventually leads to the panel overheating as the PCM starts to act in opposition to the intention by preventing the panel from cooling. In both environments, the maximum allowable PCM mass is shown to be unfeasible.

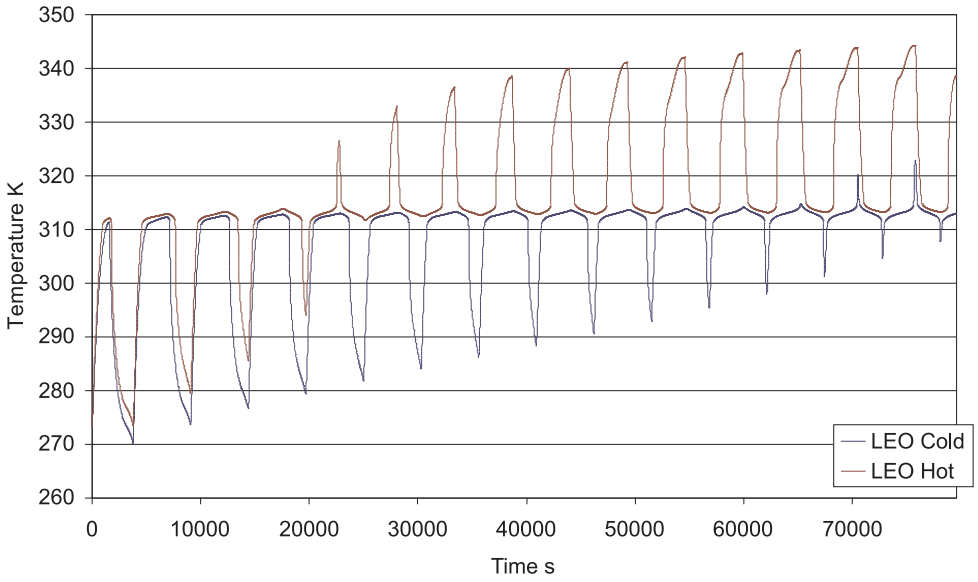

Figure B.21: *The effect of PCM use on the Sun pointing body mounting in LEO.*

B.3.2.5 Heaters

The use of heaters is not considered in this application as the Sun pointing body mounting does not experience overcooling.

B.3.3 Space Pointing

B.3.3.1 Optics

The requirements on the coating of the spacecraft changes with environment and altitude. In LEO, overcooling does not occur, allowing for an increase in the emittance to try to prevent overheating. In the cold LEO case, a viable emittance range exists, between 0.58 (to prevent overheating) and 0.62 (to prevent overcooling), though it is a narrow range. For the hot LEO, even with the highest possible emittance for the spacecraft, overcooling never occurs and overheating cannot be solved, making it unfeasible. Given the narrow range of the viable emittances in the LEO case, it is likely that the viable envelope closes rapidly with hotter environments.
In the cold geosynchronous cases panels 3 and 4 are too cold for the majority of an orbit while overheating in the sunlit period does not occur. Here raising the spacecraft temperature by further lowering of the emittance is not possible. The hot geosynchronous case provides an opportunity for altering the coating as the minimum temperature is above 273 K and thus a small increase in the spacecraft emittance to reduce the small overheating may be possible. Figure B.22 shows the effect of increasing

emittance on the maximum and minimum temperatures of the hot geosynchronous case. The figure reveals that there are no feasible emittances and that though the spacecraft is warmer, the permanent shadowing greatly limits the maximum emittance.

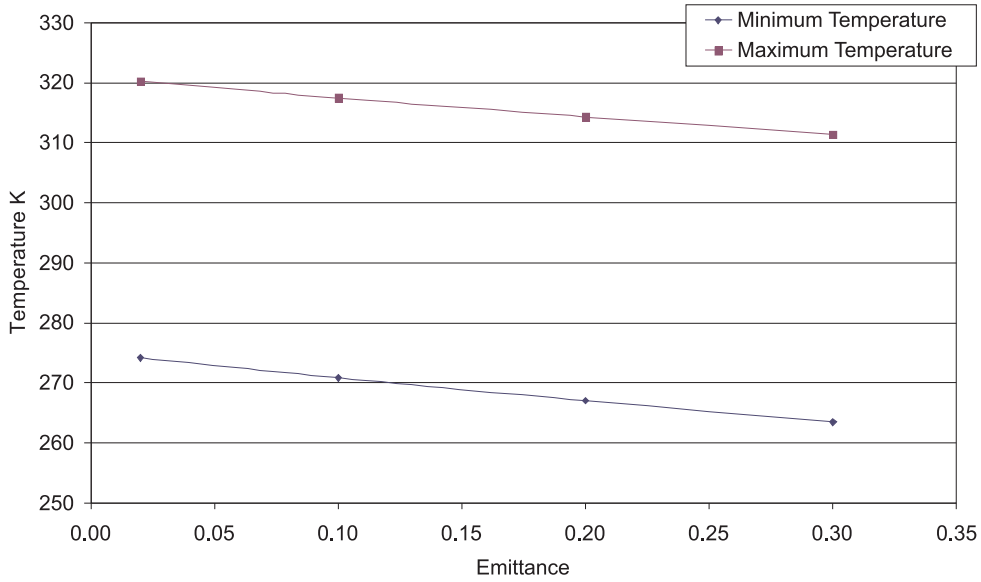

Figure B.22: *The variation of temperatures with emittance in the space pointing orientation.*

B.3.3.2 Insulation

The same effect as in the Sun pointing orientation can be seen in fig. B.23 indicating that insulation is not a feasible solution.

B.3.3.3 Thermal Links

Similar to the Sun pointing system, the panels that are sunlit or shadowed are unchanging, though the sunlight is distributed over two panels. In GEO, the increase in solar input warms the system, reducing the overcooling requirement and increasing the overheating requirement. Table B.5 shows the increase in net heat input does reduce the requirement to prevent overcooling and that the reduction in heat input per individual panel has reduced the requirement to prevent overheating, thus improving the viability. In LEO however, this extra input only serves to further the overheating issues. While the system is now warm enough that radiative heat flow between the shadowed panels and the spacecraft is not enough to prevent overcooling, the overheating requirement has increased greatly, so far in the hot environment such that no matter the linear conductance, the panels do not lose enough heat. In such a case, increased emittance to promote heat loss of the spacecraft would be a suitable addition

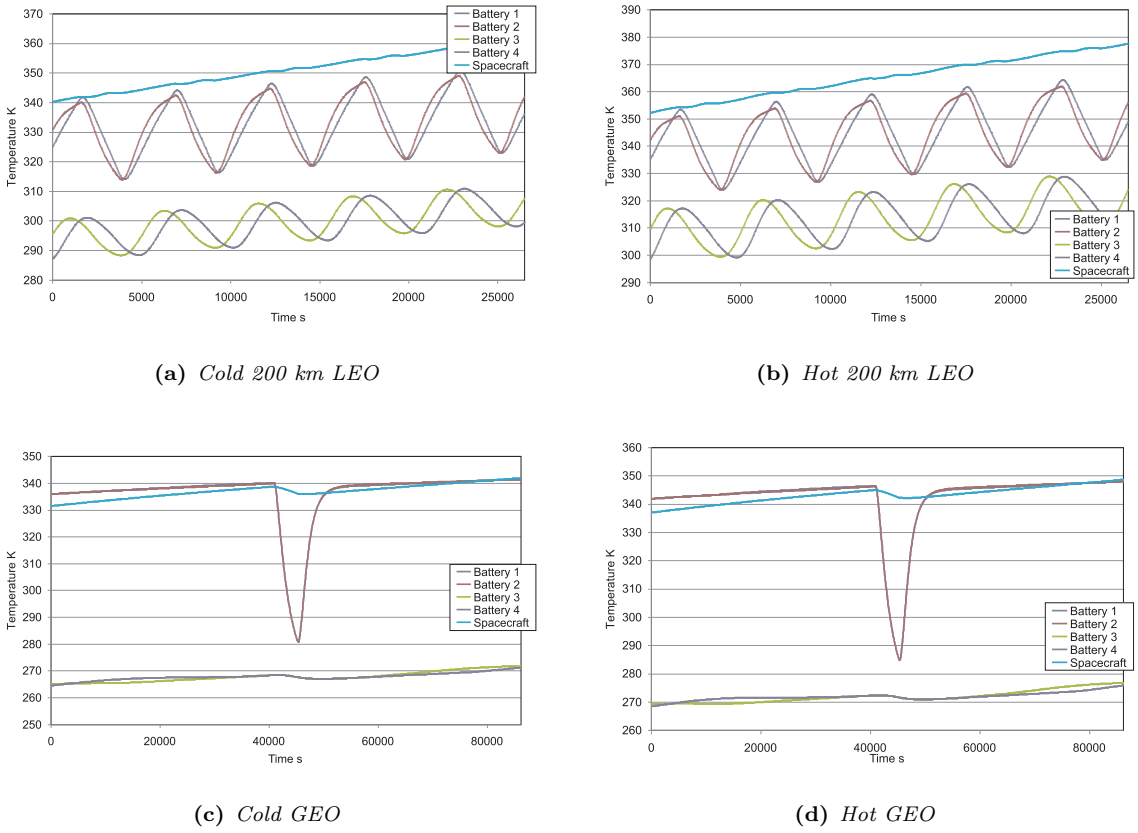

(a) *Cold 200 km LEO*

(b) *Hot 200 km LEO*

(c) *Cold GEO*

(d) *Hot GEO*

Figure B.23: *The effect of using an aerogel core on the space pointing body mounting.*

Table B.5: *Minimum linear conductance for the space pointing orientation.*

Case	Overcooling W/K	Overheating W/K
Cold 200 km LEO	-	39
Hot 200 km LEO	-	X
Cold GEO	5.2	1.8
Hot GEO	3	4.9

B.3.3.4 Phase Change Material

To assess if using the entire MFPS saving as PCM will maintain safe battery temperatures, 1.3 kg is distributed amongst the affected panels. The use of Disodium Phosphate Dodecahydrate to prevent of overheating of the sunlit panels in LEO and the hot GEO case is not considered as the time spent too hot is thousands of seconds, which 0.65 kg of PCM per sunlit panel is not going to be able to overcome. In the cold LEO case panels 3 and 4 are safe but in the hot LEO case they experience some overheating. Using 0.65 kg of Disodium Phosphate Dodecahydrate in each panel reduces the peak

temperatures to less than 314 K. Overcooling occurs in the cold geosynchronous case for all panels. The cold time for the shadowed panels is clearly too long for 1.3 kg of Hydrazine, so it is distributed over the sunlit panels to prevent their overcooling. Panels 1 and 2 now have minimum temperatures of 275 K and 275 K.
The greater net heat input in this orientation raises the temperatures of all of the components. This reduces the requirements on preventing overcooling. The results indicated that for the hot LEO and cold geosynchronous cases the use of 1.3 kg of PCM is successful in preventing overcooling. The use of PCMs to prevent overcooling may be therefore be feasible, but it is unlikely to be so for the longest eclipses due to extra mass required to contain the PCM, reducing the useful proportion of the MFPS saving used.

B.3.3.5 Heaters

The use of heaters is not considered in this application as the Space pointing body mounting does not experience overcooling.

Appendix C

Validation of Modelling

C.1 Confidence in Accuracy of Software

In order to have confidence in the results generated by the various models, a validation procedure is followed where by the modelling tools are compared to basic theory. Validation of the ThermXL lumped parameter model is done by comparing the results of a simple modelling using theory and with the results of a finite element analysis (FEA). The validation model is an aluminium section of 0.1 m by 0.1 m cross section and 1 m in length. The aluminium has a thermal conductivity of 210 $Wm^{-1}K^{-1}$, a density of 270 kgm^{-3} and a specific heat capacity of 900 $Jkg^{-1}K^{-1}$. The absorptance is 0.9 and the emittance is 0.5. The model radiates from the ends of the beam only and an input of 5000 Wm^{-2} is applied to one face. The starting temperature is 250K. This model is physically simple and thus easier to model.

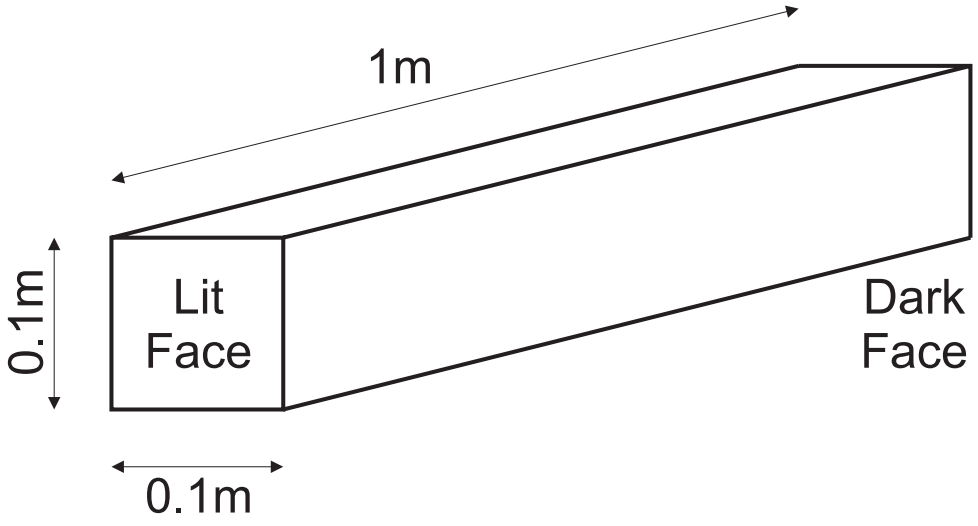

Figure C.1: *The validation model.*

C.1.1 Modelling Techniques

C.1.1.1 Isothermal Model

An isothermal model is coded in Matlab from theory. The aluminium bar is modelled as a single node with two radiating surfaces. The equilibrium temperature is found by equating the inputs with the outputs and solving for temperature. In the case of the validation model, this is when the heat input is equalled by the radiation of the end surfaces.

The following equations, Swinerd [92], determine the transient thermal response. The time constant is given by;

$$\tau = \frac{H}{4\,(2\epsilon_1)\,\sigma A_s T_{eq}^3} \tag{C.1}$$

where τ is time constant, H is the heat capacity in joules per kelvin, ϵ is the emittance of the surface, σ is the Stefan-Boltzmann constant, A_s is the emitting surface area and T_{eq} is the equilibrium temperature of the model. The time, t, taken for an object to reach to a temperature, T_{target}, is given by;

$$t = \tau\left(\ln\left(\frac{z+1}{z-1}\right) + 2\arctan(z) - C\right) \tag{C.2}$$

$$t = \tau\left(\ln\left(\frac{1+z}{1-z}\right) + 2\arctan(z) - C\right) \tag{C.3}$$

$$z = \frac{T_{target}}{T_{eq}} \tag{C.4}$$

Equation C.2 is used when the equilibrium temperature is below the initial temperature ($z > 1$) and Eq. C.3 is used when the equilibrium temperature is above the initial temperature ($z < 1$). The constant C is given by the starting conditions, where $T_{target} = T_{start}$ at t=0.

$$C = \ln\left(\frac{z_i+1}{z_i-1}\right) + 2\arctan(z_i) \tag{C.5}$$

$$C = \ln\left(\frac{1+z_i}{1-z_i}\right) + 2\arctan(z_i) \tag{C.6}$$

$$z_i = \frac{T_{start}}{T_{eq}} \tag{C.7}$$

Equation C.5 is used when the equilibrium temperature is below the initial temperature ($z_i > 1$) and Eq. C.6 is used when the equilibrium temperature is above the initial temperature ($z_i < 1$).

C.1.1.2 Lumped Parameter Model

A twelve node model is created in ThermXL using the method outlined in chapter 6; dividing the bar into five layers, giving five mass nodes, two edge nodes, four interface nodes and one boundary node to represent cold space.

C.1.1.3 Finite Element Model - Patran/Nastran

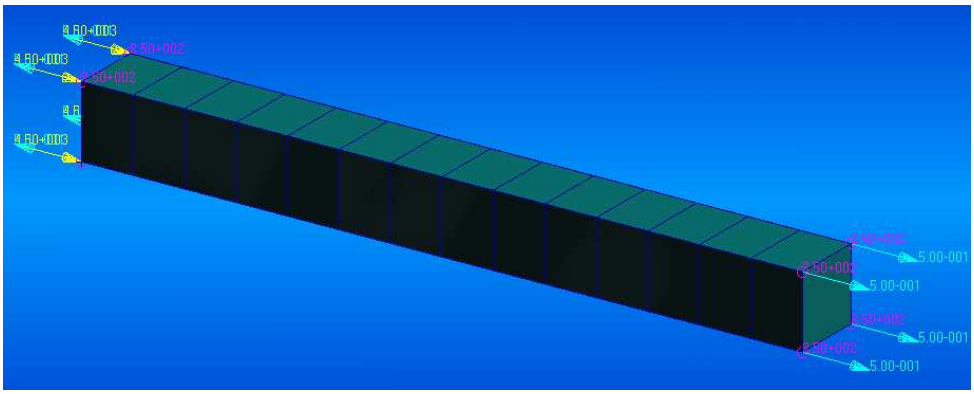

Figure C.2: *Patran finite element model.*

Patran and Nastran are used to build and solve a sixty node, fourteen element model of the validation model, as shown in fig. C.2.

C.1.2 Results

The isothermal model predicts the equilibrium temperature to be 530.8 K and the transient results are shown in fig. C.3. The lumped parameter model predicts the equilibrium temperatures of the nodes range to be between 535.8 K and 525.5 K. The transient results are shown in fig. C.4. The finite element model predicts the equilibrium temperatures of the nodes range to be between 535.9 K and 525.6 K. The transient results are shown in fig. C.5.

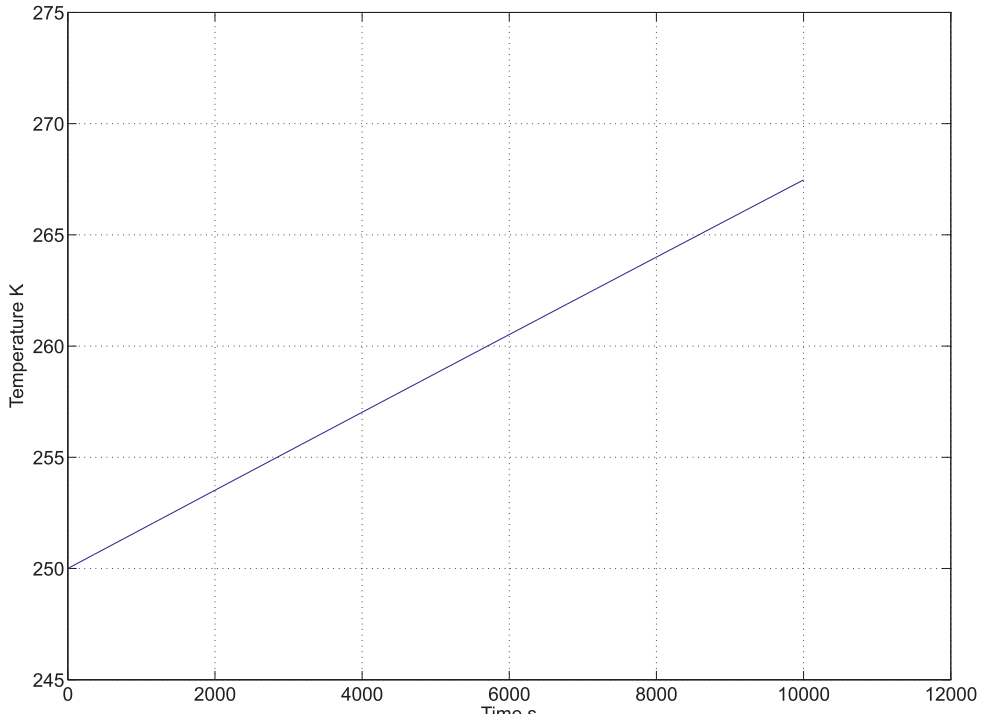

Figure C.3: *Transient results of isothermal model validation.*

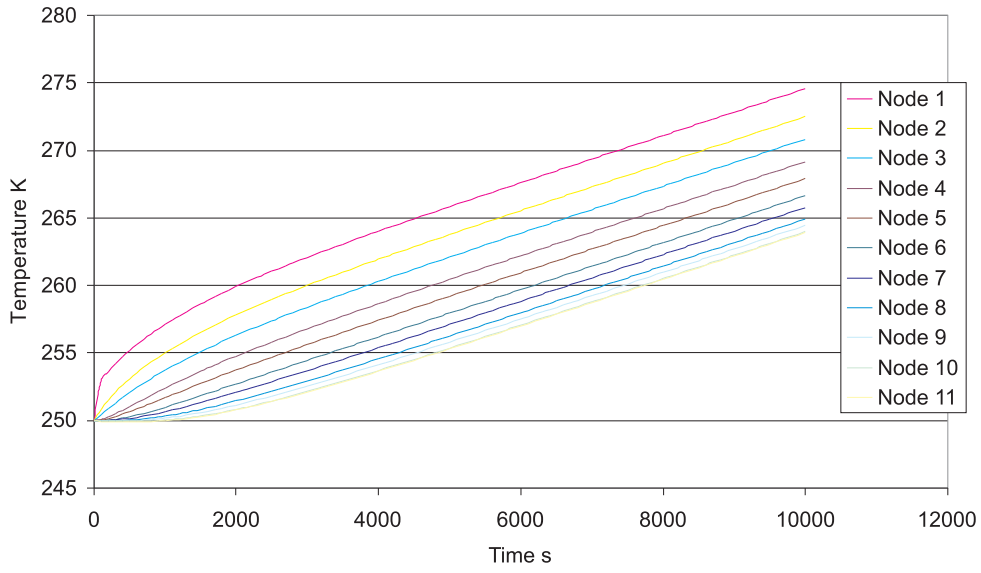

Figure C.4: *Transient results of lumped parameter model validation.*

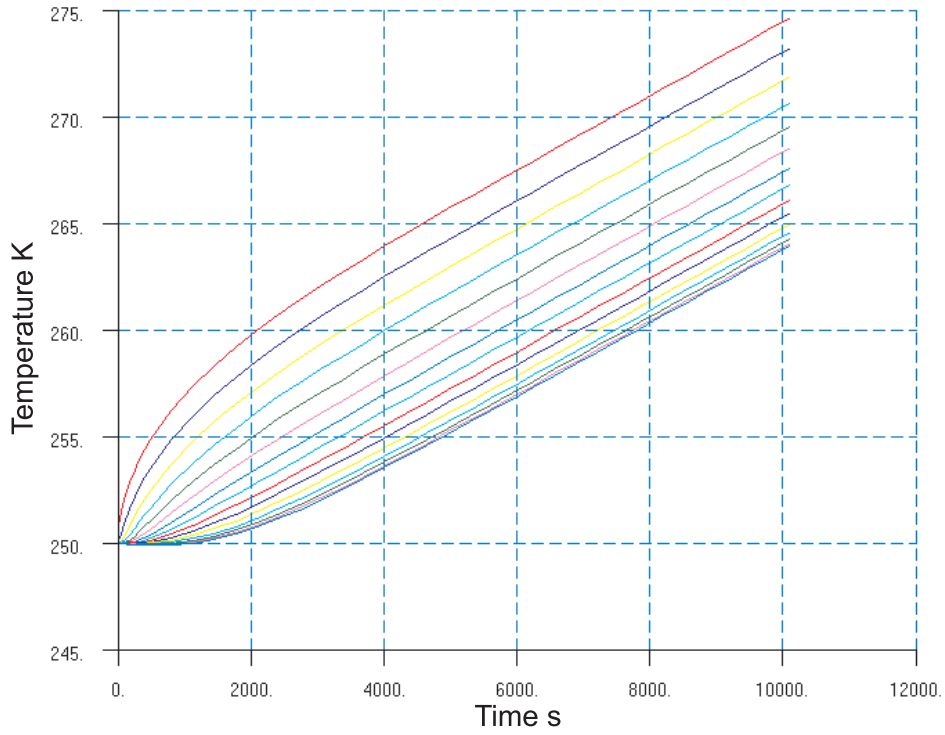

Figure C.5: *Transient results of finite element model validation.*

C.1.3 Conclusion

The isothermal model predicts the temperature of the middle of the bar in both equilibrium and transient simulations. The lumped parameter and finite element models agree on the range of equilibrium temperatures. The models also agree on the how the bar temperature increases, on how the temperature distribution establishes and on the final temperatures reached after one thousand seconds. Thus the lumped parameter modelling technique used has been validated against a simple theoretical model and against commercial finite element software.

C.2 Transition Range of Phase Change Material

The transition of a phase change material between matter states occurs over a temperature range. Figure C.6 from Kuznik et al. [93] gives an example of how the heat of fusion is distributed. Modelling this complicated distribution is beyond the scope of this work, so a simplification is required. The simplification considered is to distribute the heat of fusion evenly over a finite temperature range. Figure C.7 shows the simplified distributions; a linear distribution over 1, 2, 5 and 10 K and a gaussian distribution over

10K with a 3σ cutoff for a phase change material with a transition temperature of 278 K. The gaussian distribution represents a changing rate of phase transition, a simple model of the temperature and conductivity variations that occur in the PCM during transition. Figure C.8 shows the effect of these distributions for one geosynchronous eclipse.

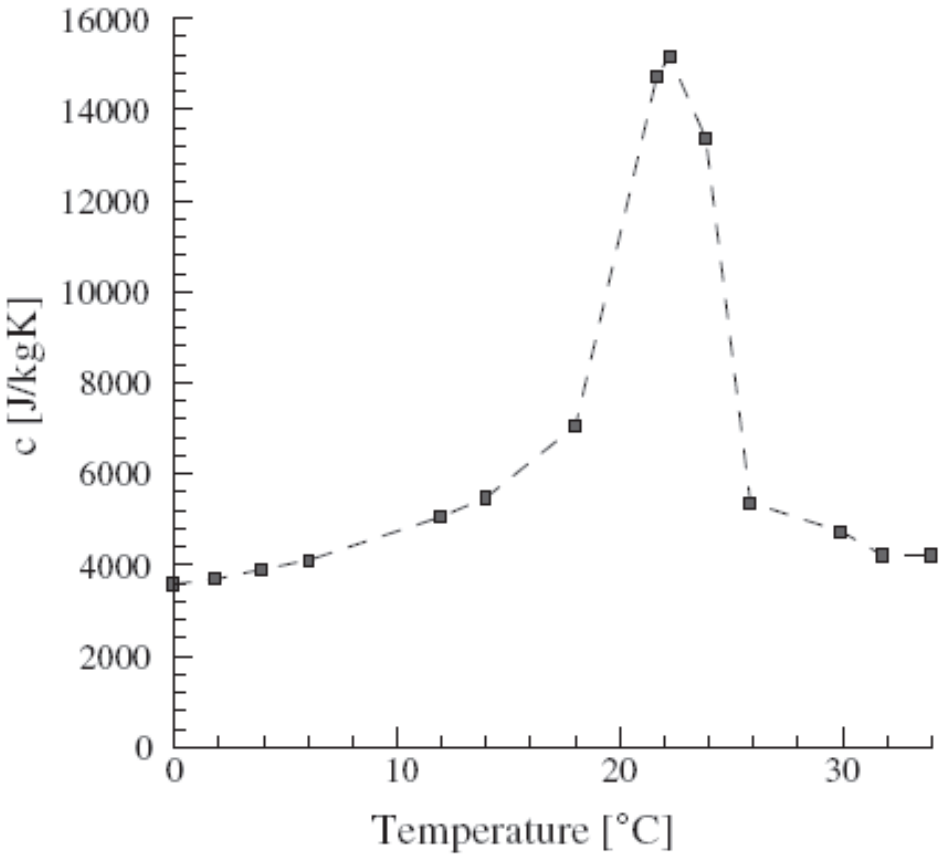

Figure C.6: *An example of varying heat capacity during PCM transition [93].*

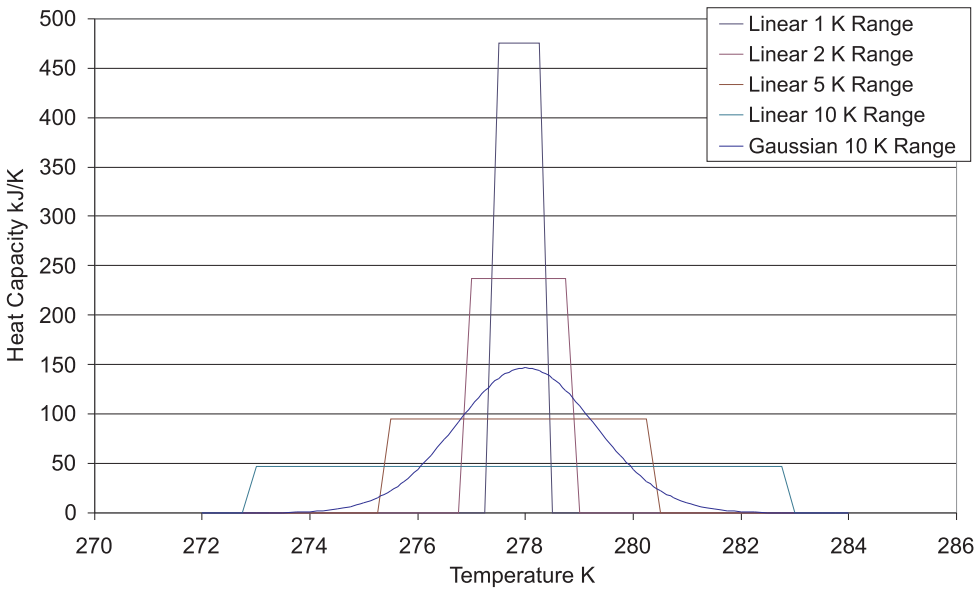

Figure C.7: *Possible models of heat capacity distribution of a PCM.*

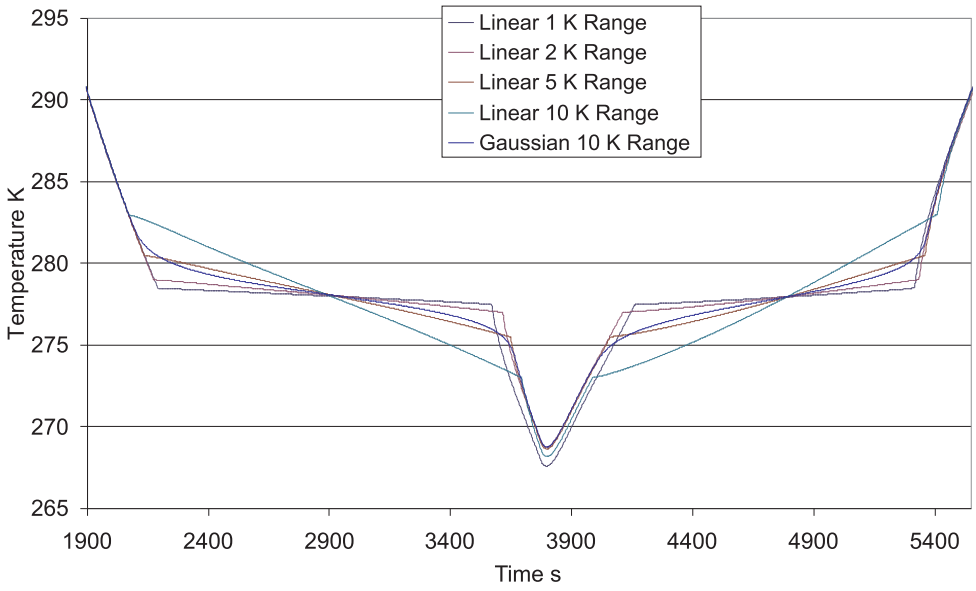

Figure C.8: *Temperature profiles in eclipse caused by the heat capacity distribution models.*

Increasing the temperature range of the linear distribution causes cooler temperature when the model exits from being in the phase change transition range, as would be expected. The increase in range also produces an increase in the delay time as the decrease in net power at lower temperatures experienced by the wider ranged distributions reduces the energy temperature loss further. The gaussian distribution matches well with the 5 K linear distribution, expected as their profiles in fig. C.7 are the most similar.

The goal of the modelling is to determine if increasing the heat capacity of the panel can prevent overcooling. As established in section 8.5 the amount of PCM required is calculated so that freezing is complete. These results indicate that the narrower the transition temperature range the more PCM will be needed. Indeed, a difference of 250 seconds exists between the 1 K and 10 K linear distributions. This indicates that the worse case scenario is to use a 1 K Linear distribution but such a narrow range is unrealistic compared to reality, fig. C.6. The best fit with reality is the gaussian distribution and it is this that is used. Ultimately, the amount of extra energy absorbed is the same for each distribution and the work focuses on the viability of this extra energy not the technical issues of modelling the freezing of the PCM.

C.3 Comparison of Conduction and Radiation

To assess if the flow of heat by radiation inside the honeycomb core is worth modelling, the following comparison was carried out. The heat flow by conduction and radiation was calculated for the honeycomb core used in the MFPS panel. Heat flow by radiation is calculated using:

$$Q_r = \sigma \epsilon_1 \epsilon_2 A_s F (T_1^4 - T_2^4) \tag{C.8}$$

Where Q_r is the heat flow, σ is the Stefan-Boltzmann constant, ϵ the emittance of the surface, A_s is area of the radiating surface, F is the view factor and T is the temperature of the surface. The heat flow from conduction is calculated as outlined in section 7.2.2. The following properties were used:

- Area of core - 1 m^2
- Effective core fraction - 0.042
- ϵ_1 - 0.8
- ϵ_2 - 0.8
- Radiating area - 0.958 m^2
- View factor - 1
- T_1 - 310 K
- T_2 - 305 K
- Thermal conductivity - 138 W/mK
- Core thickness - 12 mm
- Conducting area - 0.042 m^2

For a large 5 K temperature difference, the largest difference between the surfaces of the panel seen, the heat flow by radiation is 20 Watts and the heat flow by conduction is 2415 Watts. With two orders of magnitudes in difference between the values the simplification to remove the radiative heat flow does not have a noticeable effect on the results.

C.4 Cell Heat Output

As noted in section section 3.5.1, information about the heat output of the cells during charging and discharge is not available for 'normal' charging regimes, only for overloading cases that investigate failure mechanisms of the battery cell. As such, the

heat output of the battery cell was estimated from experimental data so that the its effect on the thermal control viability could be assessed. The chemistry of lithium ion cell is exothermic when discharging and during thermal runaway and is endothermic during charging. In all cases, electrical resistance causes some heat generation.
The cell is charged and discharged, while the temperature of the cell is recorded. The cell is charged/dischagred using a Schulze Chamäleon isl 6-330 d battery charger that is connected to a 12v car battery. The temperature of the cell is measured using two T type thermocouples, one on each side of the cell. Air temperature is measured with a third K type thermal couple. The signals from the thermocouples are processed by a Comark Tempscan which is connected to a PC by serial cable for data recording. The cell is suspended from a retort stand using nylon thread which is attached the cell using epoxy resin. This ensures that the conduction path from the cell to the environment is as insulative as possible.
Lithium Ion Polymer cells produce the most heat when being charged at fast rates. As such, the cell is charged and discharged at the safest possible rate. The cell is thus charged at a peak current 300 mA and discharged at a current of 500 mA. To avoid over charging the cell it was charged by only 100 mAh. To avoided over discharging the cell only the added energy was discharged. These results are used with Eq. C.9;

$$Q_B = A_B h(T_B - T_{air}) \tag{C.9}$$

where Q_B is the heat output of the battery cell, A_B is the surface area of the cell (29.52 cm^2), h_{air} is the convection co-efficient (10 W/mK) and T_B and T_{air} are the temperature of the cell and air respectively.

Table C.1: *Equilibrium temperatures tended to by the cell during charge and discharge.*

Case	Cell Sensor 1	Cell Sensor 2	Cell Average	Air Temperature
Charge 1	299.6 K	295.2 K	297.4 K	300.8 K
Charge 2	301.8 K	301.2 K	301.5 K	301.3 K
Charge 3	301.9 K	301.6 K	301.8 K	300.8 K
Discharge 1	312.1 K	311.6 K	311.9 K	300.8 K
Discharge 2	310.7 K	311.6 K	311.2 K	301.5 K
Discharge 3	312.4 K	309.9 K	311.1 K	299.0 K

During the first charging, there was an increase in the air temperature that was matched

by an increase of the cell. This change has affected the predicted equilibrium temperatures for the first charging. Considering chargings 2 and 3, where the air temperature was more stable, the temperature difference between the cell and the air is less than one kelvin. Using these results, the heat output at the maximum charge rate is 0.02 Watts per cell. For the defined MFPS panels, this is 14 Watts distributed over the wing array panel and 1.6 Watts over each body mounted panel. During discharge, the cell is predicted to reach a temperature that is roughly 10 K higher than air temperature in all three discharges. From this, the heat output per cell at maximum discharge rate is calculated to be 0.31 Watts. This is 274 Watts for each wing array panel and 31 Watts for each body mounted panel.

The very small amount of heat produced by the cell during charge would not be enough to produce noticeable effects when the spacecraft is sunlit. In high Earth orbits, even in the hottest environment, an extra 14 Watts would not be enough to cause overheating. At lower altitudes, the additional 14 Watts would cause a very small increase in the number of orbits that experience overheating. The larger heat output when the cell is discharging, when the spacecraft is in eclipse, would have a positive effect on the results, warming the panel and thus increasing the range of viable orbits. The absence of this heat output in the numerical model is thus conservative, with the model representing the worst case scenario where the panel has the least heat input.

Appendix D

Material Properties

D.1 CFRP Facesheet

The conductivity of the carbon fibre is calculated using the following equations from Karam [94].

$$k_l = V_f k_f + (1 - V_f) k_m \tag{D.1}$$

$$k_t = \frac{k_m(1 + \xi\eta V_f)}{1 - \eta V_f} \tag{D.2}$$

$$\eta = \frac{\left(\frac{k_f}{k_m}\right) - 1}{\left(\frac{k_f}{k_m}\right) + \xi} \tag{D.3}$$

$$\xi = \left(\frac{a}{b}\right)^{\frac{1}{3}} \tag{D.4}$$

where k_l is the longitudinal conductivity of the ply, k_t is the transverse conductivity of the ply, V_f is the volume fraction of fibres, k_f and k_m are the conductivity of the fibre and the matrix and a and b are the major axis and minor axis of the cross section of the fibre where a is defined as being perpendicular to the direction of heat flow. It is assumed that the fibres are circular in cross section and thus ξ is 1. The conductivity through the laminated plies is the same as the transverse conductivity and is 1.28 W/mK. The conductivity across the laminate is a 50/50 combination of longitudinal and traverse as a bi-weave is used and is thus 93.5 W/mK.

A rule of mixtures using the volume fraction is used to calculate the density, 1570 kg/m^3, and a rule of mixtures using the mass fraction is used to calculate the specific heat capacity, 1049 J/kgK.

D.2 Battery Cell

The Varta PoLiFlex cell [31] is made up of a lithium cobalt dioxide cathode, lithium hexafluorophosphate in solution in organic carbonate immortalised with polyvinylidene fluoride as the electrolyte and a graphite anode, Ilic et al. [58]. It also includes aluminium and copper current collectors and the aluminium casing. The mass fractions and properties of these materials are given in table D.1. To model the cell each of these materials is assumed to form a layer of the cell. From this, the thermal properties can be calculated.

Density The mass of the cell is 6 grams and it has a volume of 3624 mm^3 [31], This gives a density of 1655 kg/m^3.

Specific Heat Capacity The specific heat capacity is calculate by using a rule of fractions. The specific heat capacity of the cell is 804 J/kgK.

Thermal Conductivity The orthotropic thermal conductivity of the cell is calculated using the method outlined by Chen and Evans [95]. The conductivity through the cell is 0.72 W/mK and across it 62.7 W/mK.

Table D.1: *The properties of the components of a lithium polymer cell.*

Material	Conductivity	Density	Specific Heat Capacity	Mass Fraction	Thickness
	W/mK	kg/m^3	J/kgK		mm
Aluminium Connectors [59]	210	2700	880	0.07	0.1
LiCoO2	2 [96]	2200 [97]	731 [98]	0.27	0.7
PVdF [59]	0.186	1780	1280	0.17	0.6
Graphite [59]	24	2250	708	0.26	0.7
Copper [59]	398	8920	386	0.12	0.1
Aluminium Housing [59]	210	2700	880	0.11	0.4

D.3 Honeycomb Core

The thermal properties of the honeycomb core in the direction through the panel are calculated by noting that only 4.2 % of the facesheet surface is covered by honeycomb. The linear conductance through the core, the mass and the heat capacity of the honeycomb are thus adjusted to account for this. An alternative method, which allows calculation of the thermal conductivity in all directions, is given by Gilmore [50, App B] which concurs with the 4.2 % value. This method also calculates the linear conductance of the honeycomb in the other two directions; along the honeycomb ribbons it is 0.05 W/K and across the ribbons it is 0.02 W/K, indicating that heat flow across the honeycomb layer is very low.

References

[1] Space transportation costs: Trends in price per pound to orbit 1990-2000. Technical report, Futron Corporation, Bethesda, MD, USA, 2002.

[2] A. Das and M.W. Obal. Revolutionary satellite structural systems technology: A vision for the future. In *Proceedings of the 1998 IEEE Aerospace Conference. Part 1 (of 5)*, volume 2, pages 57 – 67, Snowmass at Aspen, CO, USA, 1998.

[3] J.C. Sercel, B. Hanks, N.W. Boynto, and C. Cassapakis. Modular and multifunctional systems in the New Millennium Program. In *34th AIAA Aerospace Sciences Meeting and Exhibit*, AIAA Aerospace Sciences Meeting and Exhibit, pages 15–18. AIAA, 1996.

[4] C.L. Moore. Gossamer spacecraft technology for space solar power systems. In *IEEE Aerospace Conference Proceedings*, volume 7, pages 73585 – 73589, Big Sky, MT, United states, 2001.

[5] P. Rossoni and P.V. Panetta. Developments in nano-satellite structural subsystem design at NASA-GSFC. In *Proceedings of the 13th AIAA/USU Conference on Small Satellites*. NASA, 1999.

[6] P.W. Fortescue, J.P.W. Stark, and G.G. Swinerd. *Spacecraft Systems Engineering*. Wiley, 3rd edition edition, 2003.

[7] S.C. Roberts and G.S. Aglietti. Satellite multifunctional power structure: Feasibility and mass savings. *Journal of Aerospace Engineering*, 222(G1):41–51, 2008.

[8] B. Jackson and K. Epstein. A reconfigurable multifunctional architecture approach for next-generation nanosatellite design. In *IEEE Aerospace Conference Proceedings*, volume 7, pages 185 – 193, Big Sky, MT, United states, 2000.

[9] M. Bandecchi, B. Melton, and F. Ongaro. Concurrent engineering applied to space mission assessment and design. *European Space Agency Bulletin*, 99:34 – 40, September 1999.

[10] X. Wang, M. Kato, H. Naito, C. Yamada, G. Segami, and K. Kibe. A feasibility study of commercial laminated lithium-ion polymer cells for space applications. *Journal of the Electrochemical Society*, 153(1):A89 – A95, 2006. ISSN 00134651.

[11] Y. Choquette and D. Lessard-Deziel. Proton and electron radiation effects on dry lithium metal polymer batteries. In *Radiation Effects Data Workshop, 2002 IEEE*, pages 120–126, 2002. doi: 10.1109/REDW.2002.1045541.

[12] G.S. Aglietti, C.W. Schwingshackl, and S.C. Roberts. Multifunctional structure technologies for satellite applications. *Shock and Vibration Digest*, 39(5):381 – 391, 2007. ISSN 05831024.

[13] J.P. Thomas and M.A. Qidwai. The design and application of multifunctional structure-battery materials systems. *JOM*, 57(3):18 – 24, 2005. ISSN 10474838.

[14] J.P. Thomas, M.T. Keennon, A. DuPasquier, M.A. Qidwai, and P. Matic. Multifunctional structure-battery materials for enhanced performance in small unmanned air vehicles. In *Proceedings of the ASME Materials Division - 2003*, volume 98, pages 289 – 292, Washington, DC., United states, 2003.

[15] J. P. Thomas, M. A. Quidwai, R. K. Everrett, Antoni S. Gozdz, D. Culver, M. T. Keennon, and J. M. Grassmeyer. Composite materials with multifunctional structure-power capabilities. In *American Society for Composites 16th Technical Conference Proceedings*, Virginia Tech, Blacksburg, VA, 2001.

[16] M.A. Qidwai, J.P. Thomas, and P. Matic. Design and performance of composite multifunctional structure-battery materials. In *Proceedings of the American Society forComposites 17th Technical Conference*. CRC Press, 2002.

[17] P. Liu, E. Sherman, and A. Jacobsen. Design and fabrication of multifunctional structural batteries. *Journal of Power Sources*, 189(1):646 – 650, 2009. ISSN 03787753.

[18] J.F. Snyder, R.H. Carter, and E.D. Wetzel. Electrochemical and mechanical behavior in mechanically robust solid polymer electrolytes for use in

multifunctional structural batteries. *Chemistry of Materials*, 19(15):3793 – 3801, 2007. ISSN 08974756.

[19] E.L. Wong, D.M. Baechle, K. Xu, R.H. Carter, J.F. Snyder, and E.D. Wetzel. Design and processing of structural composite batteries. In *International SAMPE Symposium and Exhibition (Proceedings)*, volume 52, pages SAMPE Baltimore/Washington Chapter –, Baltimore, MD, United states, 2007.

[20] D Marcelli, J Summers, and B Neudecker. LiBaCore II - power storage in primary structure. In *43rd AIAA/ASME/ASCE/AHS/ASC Structures, Structural Dynamics, and Materials Conference*, 2002. AIAA-2002-1242.

[21] E. Fosness, J. Guerrero, K. Qassim, and S.J. Denoyer. Recent advances in multi-functional structures. In *IEEE Aerospace Conference Proceedings*, volume 4, pages 23 – 28, Big Sky, MT, United states, 2000.

[22] P.C. Lyman and T.L. Feaver. Powercore: Combining structure and batteries for increased energy to weight ratio. *IEEE Aerospace and Electronic Systems Magazine*, 13(9):39–42, September 1998. ISSN 0885-8985.

[23] J.B. Olson, T.L. Feaver, and P.C. Lyman. Structural lithium-ion batteries using dual-functional carbon fabric composite anodes. In *Proceedings of the 14th International Conference on Composite Materials*, San Diego, CA, USA, 2003.

[24] W. Metzger, R. Westfall, A. Hermann, and P. Lyman. Nickel foam substrate for nickel metal hydride electrodes and lightweight honeycomb structures. *International Journal of Hydrogen Energy*, 23(11):1025 – 1029, 1998. ISSN 03603199.

[25] T. Pereira, Z. Guo, S. Nieh, J. Arias, and H.T. Hahn. Embedding thin-film lithium energy cells in structural composites. *Composites Science and Technology*, 68(7-8): 1935 – 1941, 2008. ISSN 02663538.

[26] B.J. Neudecker, M.H. Benson, and B.K. Emerson. Power fibers: Thin-film batteries on fiber substrates. In *Proceedings of 14th International Conference on Composite Materials (ICCM 14)*, Proceedings of 14th International Conference on Composite Materials (ICCM 14), pages 739–745. DARPA, 2004.

[27] C. Clark, J. Summers, and J. Armstrong. Innovative flexible lightweight thin-film power generation and storage for space applications. In *Proceedings of the*

Intersociety Energy Conversion Engineering Conference, volume 1, pages 692 – 698, Las Vegas, NV, USA, 2000.

[28] C.W. Schwingshackl, G.S. Aglietti, and P.R. Cunningham. Parameter optimization of the dynamic behavior of inhomogeneous multifunctional power structures. *AIAA Journal*, 44(10):2286 – 2294, 2006. ISSN 00011452.

[29] C.W. Schwingshackl, G.S. Aglietti, and P.R. Cunningham. Experimental determination of the dynamic behavior of a multifunctional power structure. *AIAA Journal*, 45(2):491 – 496, 2007. ISSN 00011452.

[30] S.C. Roberts and G.S. Aglietti. Battery performance degradation under vibration loading. In *7th International Conference on Dynamics & Control of Systems and Structures in Space*, 2006.

[31] Varta. PoLiFlex PLF263441 D datasheet. Web Based Portable Document Format, Accessed May 2008. URL `http://www.varta-microbattery.com`.

[32] S.C. Roberts and G.S. Aglietti. Multifunctional power structures for spacecraft application. In *The Proceedings of the 57th International Astronautical Congress*, 2007.

[33] S C Roberts, J A Foster, and G S Aglietti. Multifunctional power structures and related thermal issues. In *Proceeding of SMASIS2008*, Ellicott City MD USA, October 2008.

[34] W. Xing and H. Sugiyama. Improvement in the low temperature performance of gelled polymer lithium-ion cells. *Journal of Power Sources*, 117(1-2):153 – 159, 2003. ISSN 03787753.

[35] M. Mohamedi, H. Ishikawa, and I. Uchida. In situ analysis of high temperature characteristics of prismatic polymer lithium - ion batteries. *Journal of Applied Electrochemistry*, 34(11):1103 – 1112, 2004. ISSN 0021891X.

[36] P. Li, H. Cheng, and W. Qin. Numerical simulation of temperature field in solar arrays of spacecraft in low earth orbit. *Numerical Heat Transfer; Part A: Applications*, 49(8):803 – 820, 2006. ISSN 10407782.

[37] J. Marcos, M. Segura, J.C. Antolin, A. Landaberea, F. Lamela, and G. Atxaga. Multifunctional equipment design by using high thermal conductivity fibres. In *Proceedings of the European Conference on Spacecraft Structures, Materials and Mechanical Testing 2005*, volume 1, pages 1049–1056. ESA, 2005.

[38] R. John, G. Atxaga, H.J. Frerker, and A. Newerla. Advancement of multifunctional support structure technologies (AMFSST). In *Collection of Papers Presented at The 13th International Workshop on THERMal INvestigation of ICs and Systems, THERMINIC*, pages 98 – 103, Budapest, Hungary, 2007.

[39] D.T. Queheillalt, G. Carbajal, G.P. Peterson, and H.N.G. Wadley. A multifunctional heat pipe sandwich panel structure. *International Journal of Heat and Mass Transfer*, 51(1-2):312 – 326, 2008. ISSN 00179310.

[40] D.T. Queheillalt, Y. Katsumui, and H.N.G. Wadley. Electron beam - directed vapor deposition of multifunctional structures. In *Materials Research Society Symposium - Proceedings*, volume 672, pages O5.6.1 – O5.6.6, San Francisco, CA, United states, 2001.

[41] R. Wirtz, T. Zhao, and Y. Jiang. Thermal and mechanical characteristics of a multi-functional thermal energy storage structure. In *Thermomechanical Phenomena in Electronic Systems -Proceedings of the Intersociety Conference*, volume 1, pages 549 – 556, Las Vegas, NV, United states, 2004.

[42] M.D. Rayman, P. Varghese, D.H. Lehman, and L.L. Livesay. Results from the Deep Space 1 technology validation mission. *Acta Astronautica*, 47(2-9):475 – 487, 2000. ISSN 0094-5765. doi: DOI: 10.1016/S0094-5765(00)00087-4.

[43] D.M. Barnett and S.P. Rawal. Multifunctional structures technology demonstration on New Millennium Program (NMP) Deep Space 1 (DS1). Technical report, JPL, 2000.

[44] D.M. Barnett, S. Rawal, and K. Rummel. Multifunctional structures for advanced spacecraft. *Journal of Spacecraft and Rockets*, 38(2):226 – 230, 2001. ISSN 00224650.

[45] S.P. Rawal. Thermal management for multifunctional structures. *IEEE Transactions on Advanced Packaging*, 22(3):379 – 383, 1999. ISSN 15213323.

[46] A. Megahed and A. El-Dib. Thermal design and analysis for battery module for a remote sensing satellite. *Journal of Spacecraft and Rockets*, 44(4):920 – 926, 2007. ISSN 00224650.

[47] W.H. Yang, H.E. Cheng, and A. Cai. Thermal analysis for folded solar array of spacecraft in orbit. *Applied Thermal Engineering*, 24(4):595 – 607, 2004. ISSN 13594311.

[48] S. Sanz Fernandez de Cordoba. The 100km boundary for astronautics. website, Published 21/06/2004 Accessed 28/09/07. URL `http://www.fai.org/astronautics/100km.asp`.

[49] D.D.V. Bhanderi and T. Bak. Modeling earth albedo for satellites in earth orbit. In *Collection of Technical Papers - AIAA Guidance, Navigation, and Control Conference*, volume 8, pages 6220 – 6231, San Francisco, CA, United states, 2005.

[50] D.G. Gilmore, editor. *Spacecraft Thermal Control Handbook*. AIAA, 2002.

[51] B.J. Anderson, C.G. Justus, and W. Batts. Guidelines for the selection of near earth thermal environment parameters for spacecraft design. NASA Technical Memorandum TM-2001-211221, NASA, August 2001.

[52] C.G. Justus, G. W. Batts, B. J. Anderson, and B. F. James. Simple Thermal Environment Model (STEM) user's guide. Technical Report TM-2001-211222, NASA MSFC, October 2001.

[53] C.R. Pals and J. Newman. Thermal modeling of the lithium/polymer battery. I. discharge behavior of a single cell. *Journal of the Electrochemical Society*, 142(10): 3274 – 3281, 1995. ISSN 00134651.

[54] C.R. Pals and J. Newman. Thermal modeling of the lithium/polymer battery. II. temperature profiles in a cell stack. *Journal of the Electrochemical Society*, 142(10): 3282 – 3288, 1995. ISSN 00134651.

[55] Y. Chen and J.W. Evans. Three-dimensional thermal modeling of lithium-polymer batteries under galvanostatic discharge and dynamic power profile. *Journal of the Electrochemical Society*, 141(11):2947 – 2955, 1994. ISSN 00134651.

[56] R. Siegel and J.R. Howell. *Thermal Radiation Heat Transfer*. Taylor and Francis, 3rd edition edition, 1992.

[57] H. Yoon, J.E. Granata, P. Hebert, R.R. King, C.M. Fetzer, P.C. Colter, K.M. Edmondson, D. Law, G.S. Kinsey, D.D. Krut, J.H. Ermer, M.S. Gillanders, and N.H. Karam. Recent advances in high-efficiency III-V multi-junction solar cells for space applications: Ultra triple junction qualification. *Progress in Photovoltaics: Research and Applications*, 13(2):133 – 139, 2005. ISSN 10627995.

[58] D. Ilic, P. Birke, K. Holl, T. Wohrle, P. Haug, and F. Birke-Salam. PoLiFlex, the innovative lithium-polymer battery. *Journal of Power Sources*, 129(1 SPEC. ISS.): 34 – 37, 2004. ISSN 03787753.

[59] Automation Creations Inc. Matweb. Website, Accessed 24/06/07. URL `www.matweb.com`.

[60] F. Reif. *Fundamentals of statistical and thermal physics*. McGraw-Hill Kogakusha, Tokyo, International Student ed. edition, 1965.

[61] K. Badari Narayana and V. Venkata Reddy. Thermal design and performance of HAMSAT. *Acta Astronautica*, 60(1):7 – 16, 2007. ISSN 00945765.

[62] H. Hwangbo and W.H. Kelly. Transient response of thermal louvers with bimetallic actuators. *AIAA Paper*, 1980. ISSN 01463705.

[63] M. Domingo and J.J. Ramirez. Mechanical design and test of Rosetta platform louvres. *European Space Agency, (Special Publication) ESA SP*, (524):289 – 292, 2003. ISSN 03796566.

[64] R. Osiander, S.L. Firebaugh, J.L. Champion, D. Farrar, and M.A.G. Darrin. Microelectromechanical devices for satellite thermal control. *IEEE Sensors Journal*, 4(4):525 – 531, 2004. ISSN 1530437X.

[65] L.D. Wing and J.W. Cunningham. Automatic thermal switch, August 1981.

[66] V. B. Krishnan, J. D. Singh, T. R. Woodruff, W. U. Notardonato, and R. Vaidyanathan. A shape memory alloy based cryogenic thermal conduction switch. In U. B. Balachandran, editor, *American Institute of Physics Conference*

Series, volume 711 of *American Institute of Physics Conference Series*, pages 26–33, June 2004.

[67] K.S. Novak, C.J. Phillips, G.C. Birur, E.T. Sunada, and M.T. Pauken. Development of a thermal control architecture for the mars exploration rovers. In *SPACE TECHNOLOGY AND APPLICATIONS INT.FORUM-STAIF 2003: Conf.on Thermophysics in Microgravity; Commercial/Civil Next Generation Space Transportation; Human Space Exploration; Symps.on Space Nuclear Power and Propulsion (20th); Space Colonization (1st)*, volume 654, pages 194–205. AIP, 2003. doi: 10.1063/1.1541295.

[68] J.D. Bernardin. The performance of methanol and water heat pipes for electronics cooling applications in spacecraft instrumentation. In *Proceedings of the ASME Summer Heat Transfer Conference*, volume 4, pages 669 – 679, San Francisco, CA, United states, 2005.

[69] A. Sharma, V.V. Tyagi, C.R. Chen, and D. Buddhi. Review on thermal energy storage with phase change materials and applications. *Renewable and Sustainable Energy Reviews*, 13(2):318 – 345, 2009. ISSN 13640321.

[70] R. Kandasamy, X. Wang, and A.S. Mujumdar. Transient cooling of electronics using phase change material (PCM)-based heat sinks. *Applied Thermal Engineering*, 28(8-9):1047 – 1057, 2008. ISSN 13594311.

[71] J.P. Barbour and D.C. Hittle. Modeling phase change materials with conduction transfer functions for passive solar applications. *Journal of Solar Energy Engineering, Transactions of the ASME*, 128(1):58 – 68, 2006. ISSN 01996231.

[72] S.A. Khateeb, S. Amiruddin, M. Farid, J.R. Selman, and S. Al-Hallaj. Thermal management of Li-ion battery with phase change material for electric scooters: Experimental validation. *Journal of Power Sources*, 142(1-2):345 – 353, 2005. ISSN 03787753.

[73] A. Mills and S. Al-Hallaj. Simulation of passive thermal management system for lithium-ion battery packs. *Journal of Power Sources*, 141(2):307 – 315, 2005. ISSN 03787753.

[74] I. Krupa, G. Mikova, and A.S. Luyt. Phase change materials based on low-density polyethylene/paraffin wax blends. *European Polymer Journal*, 43(11):4695 – 4705, 2007. ISSN 00143057.

[75] K. Kaygusuz and A. Sari. High density polyethylene/paraffin composites as form-stable phase change material for thermal energy storage. *Energy Sources, Part A: Recovery, Utilization and Environmental Effects*, 29(3):261 – 270, 2007. ISSN 15567036.

[76] X. Liu, H. Liu, S. Wang, L. Zhang, and H. Cheng. Preparation and thermal properties of form stable paraffin phase change material encapsulation. *Energy Conversion and Management*, 47(15-16):2515 – 2522, 2006. ISSN 01968904.

[77] R.A. Schmidt. Effects of a void beneath a kapton heater patch in a vacuum. In *American Society of Mechanical Engineers, Heat Transfer Division, (Publication) HTD*, volume 375, pages 25 – 28, Anaheim, CA, United states, 2004.

[78] J.W.C. Harpster, P.R. Swinehart, and F. Braun. Solid state thermal control for spacecraft. *Solid-State Electronics*, 18(6):551 – 555, 1975. ISSN 00381101.

[79] P. Bhandari, G.C. Birur, and M.B. Gram. Mechanical pumped cooling loop for spacecraft thermal control. In *26th International Conference on Environmental Systems*, Monterey, CA, USA, July 1996.

[80] M. Wiener, G. Reichenauer, F. Hemberger, and H.-P. Ebert. Thermal conductivity of carbon aerogels as a function of pyrolysis temperature. *International Journal of Thermophysics*, 27(6):1826 – 1843, 2006. ISSN 0195928X.

[81] B. Zalba, J.M. Marin, L.F. Cabeza, and H. Mehling. Review on thermal energy storage with phase change: Materials, heat transfer analysis and applications. *Applied Thermal Engineering*, 23(3):251 – 283, 2003. ISSN 13594311.

[82] USCG. Formic acid chemical hazards response information system datasheet. Technical report, CAMEO Chemicals NOAA, 1999.

[83] D.W. Hawes, D. Feldman, and D. Banu. Latent heat storage in building materials. *Energy and Buildings*, 20(1):77 – 86, 1993. ISSN 03787788.

[84] A. Elgafy and K. Lafdi. Effect of carbon nanofiber additives on thermal behavior of phase change materials. *Carbon*, 43(15):3067 – 3074, 2005. ISSN 00086223.

[85] Y. Zhang, J. Ding, X. Wang, R. Yang, and K. Lin. Influence of additives on thermal conductivity of shape-stabilized phase change material. *Solar Energy Materials and Solar Cells*, 90(11):1692 – 1702, 2006. ISSN 09270248.

[86] Technology Applications Inc. TAI graphite fiber thermal straps. Web Based Portable Document Format, Accessed 08/03/2010. URL `http://www.techapps.com/images/GFTS info paper072104.pdf`.

[87] K Technology, a division of Thermacore. Thermal straps: Efficient cooling without structural loading. Website, Accessed 08/03/2010. URL `http://www.thermacore.com/products/thermal-straps.aspx`.

[88] C.R. Ortizlongo and S.L. Rickman. Method for the calculation of spacecraft umbra and penumbra shadow terminator points. Technical Report NASA-TP-3547, NASA Johnson Space Center, 1995.

[89] NASA. Hinode (Solar-B). website, Accessed Dec 2010. URL `http://solarb.msfc.nasa.gov/`.

[90] H. Kim, M. Park, and K. Hsieh. Fatigue fracture of embedded copper conductors in multifunctional composite structures. *Composites Science and Technology*, 66(7-8): 1010 – 1021, 2006. ISSN 02663538.

[91] D.M. Elzey, A.Y.N. Sofia, and H.N.G. Wadley. A shape memory-based multifunctional structural actuator panel. *International Journal of Solids and Structures*, 42(7):1943 – 1955, 2005. ISSN 00207683.

[92] G.G. Swinerd. SESA3005 astronautics, thermal control lectures. Lecture Notes, 2007.

[93] Frederic Kuznik, Joseph Virgone, and Jean Noel. Optimization of a phase change material wallboard for building use. *Applied Thermal Engineering*, 28(11-12):1291 – 1298, 2008. ISSN 13594311.

[94] R.D. Karam. *Satellite Thermal Control for Engineers*, volume 181. AIAA, 1st edition edition, 1998. ISBN 1-56347-276-7.

[95] Y. Chen and J.W. Evans. Thermal analysis of lithium polymer electrolyte batteries by a two dimensional model. thermal behaviour and design optimization. *Electrochimica Acta*, 39(4):517 – 526, 1994. ISSN 00134686.

[96] K. Takahata and I. Terasaki. Thermal conductivity of $AxBO_2$-type layered oxides $Na_0 \cdot 77\,MnO_2$ and $LiCoO_2$. *Japanese Journal of Applied Physics, Part 1: Regular Papers and Short Notes and Review Papers*, 41(2 A):763 – 764, 2002. ISSN 00214922.

[97] J. Ying, C. Jiang, and C. Wan. Preparation and characterization of high-density spherical $LiCoO_2$ cathode material for lithium ion batteries. *Journal of Power Sources*, 129(2):264 – 269, 2004. ISSN 03787753.

[98] H. Kawaji, M. Takematsu, T. Tojo, T. Atake, A. Hirano, and R. Kanno. Low temperature heat capacity and thermodynamic functions of $LiCoO_2$. *Journal of Thermal Analysis and Calorimetry*, 68(3):833 – 839, 2002. ISSN 14182874.